THE ANALYSIS AND BEHAVIOUR OF COMPOSITE SPACE FRAMES WITH PROFILED STEEL SHEET FLOORS

A thesis submitted for the

Degree of Doctor of Philosophy

by

MAHMOOD M. A. KULEIB BSc MSc

Department of Civil Engineering

University of Salford

AUGUST, 1989

TABLE OF CONTENTS

LIST OF TABLES

LIST OF FIGURES

LIST OF PHOTOGRAPHIC PLATES

ACKNOWLEDGEMENTS

The author wishes to express his sincere appreciation and gratitude to Mr. D. C. O'Leary for his advice, supervision and guidance throughout this investigation.

Thanks are due to Mr. C. T. Duffy for his advice and help throughout the course of this work.

The author wishes also to express his gratitude to the members of the departmental laboratories and workshop staff, particularly Mr. K. Naylor, Mr. H. Naylor; and to Mr. C. Tivey for preparing the photographs.

Grateful thanks are also extended to Mr. S. Baird and Space Decks Limited for providing the units used in the experimental investigation, and for the experimental and computer information provided.

MAHMOOD M. A. KULEIB

AUGUST, 1989

DECLARATION

None of the material in this thesis has been submitted in support of an application for another degree or qualification in this or any other university or institution of learning.

MAHMOOD M. A. KULEIB

AUGUST, 1989

ABSTRACT

The objective of this research was to analyse and investigate the behaviour of a composite space frame. The space frame is assembled from individual inverted square-based pyramids. Each pyramid consists of a steel-angle section top-tray and diagonals. When the top trays are connected together , they form the top-chord members of a double-angle section connected back to back.

The investigation is primarily concerned with the composite section within the space frame system which comprises the top chord members, profiled steel sheeting and a concrete slab. This composite section is also assumed to work as a system of intersecting composite T-beams. Each composite T-beam comprises of a top chord member, a certain width of profiled steel sheet and a concrete slab. The composite action is ensured by a series of self-tapping screws.

The experimental work is based on two-unit space frame specimens. Each specimen represents two adjacent units with their top chord member which carries the highest compressive axial load in the real structure. Each unit is tested in a situation which simulates its position and loading within the real structure. In addition to the composite T-beams being tested, steel struts composed of the top chord member double-angles

were tested.

In the theoretical section, the real structure is analysed as composite beam elements and thin steel plate elements which all represent the top composite T-beams. The diagonals and the ties were considered as truss elements. A successful method of analysis was developed using matrix and finite element methods resulting in the force distribution and deformations for a full composite space frame. Additionally, the experimental work yielded useful information on the behaviour of composite struts of this type. Recommendations for future work are made.

The investigation of the behaviour of the composite T-beams with different locations and numbers of shear connectors together with the analysis of the structure comprise the main part of this work.

LIST OF MAIN SYMBOLS

A - Cross sectional area

a - Side length of a plate element

C_x, C_y and C_z - Directional cosines

D_x and D_y - Flexural rigidities in x- and y-directions

D_{xy} - Torsional rigidity

E - Modulus of elasticity

F - Force

G - Shear modulus

h - Long side of the area considered for the cross section in the calculation of J.

I_x and I_y - Second moments of area

J - Torsional constant

L - Beam or truss element length

q - Wave length of one repeated corrugation

q - Uniform load on a plate

s - Arc length of one repeating corrugation

t - Plate thickness

t - Short side of the area considered for the cross section in the calculation of J.

v - Poison's ratio

w - Lateral deflection

[EK] - Element stiffness matrix

$[K_b]$ - Beam element stiffness matrix

$[K_g]$ - Grid element stiffness matrix

[Su] - Global unrestrained stiffness matrix

[T] - Transformation matrix

α - Angle of rotation

α_1-α_{12} - Unknown coefficients used in polynomial equations

CSFU - Composite space frame unit

CU - Composite unit

CS - Composite strut

f_y - Yield stress

f_t - Ultimate strength of steel

f_{cu} - Characteristic cube strength of concrete

H.L. - Applied horizontal load

V.L. - Applied vertical load

σ_1 - Experimental combined stress at the centreline of the composite T-section

σ_2 - Calculated (theoretical) combined stress at the centreline of the composite T-section

CHAPTER ONE

INTRODUCTION

1.1 General Introduction

Composite space frames are structures utilising a combination of composite steel deck/concrete slab and space frames. Both of these structural systems are relatively new in the field of construction, having been introduced in the last 40 years. Both systems have a rightful claim of efficiency, both in terms of speed of construction and economy of materials.

1.2 Composite Structures

The development of shear connectors in the early 1950s enabled the efficient connection of the concrete floor slab in a building to the supporting steel beam to be carried out. The T-beam action resulting from this connection enabled the use of composite behaviour in structures to be developed. Profiled steel sheet/concrete floor systems have been used in North America since the early 1950s, and more recently they have become common in the U.K. The profiled steel sheet acts as tensile reinforcement as well as permanent shuttering for the composite slab.

A large number of profiled steel sheets are available on the market which differ in height, thickness, pitch and shape (see Figure 1.1).

1.3 Advantages of Composite Floor Systems

The significant advantages of steel-concrete composite floor deck structures have been identified by Harding (1986), the following six being the most important (1):

(1) The steel deck acts as a permanent shuttering for the in-situ cast concrete slab. Thus there is no need to erect and remove forms and falsework, with a consequent saving in time and labour.

(2) The steel deck, once in position, immediately provides a platform to support construction loads and a safe sturdy working surface. Since supporting falsework is not required, finishing trades can operate on the floor immediately below the one being constructed; this obviously facilitates the construction programme.

(3) The steel decking acts as the tensile reinforcement, thereby eliminating the time-consuming placing and fixing of reinforcing bars for the slab.

(4) The steel deck geometry can result in a

reduction of about 30% in the amount of concrete fill required for the floor. The consequent significant reduction in dead weight leads to lighter superstructures and reduced foundation loads.

(5) The cellular geometry of the deck permits the formation of ducting cells within the floor so that services can be incorporated and distributed within the floor depth. This gives the possibility of increased headroom or a reduction in building height.

(6) Since the steel decks are formed from thin gauge sheet steel, they are extremely light, facilitating the handling and placing by site workers. Also, hundreds of square metres of decking can be transported to site by a single lorry.

1.4 Disadvantages of the system

Harding (1986) has also noted the following disadvantages which must be noted, although they are relatively minor occurring at the construction stage (1):

(1) In areas of concentrated traffic or storage, the upper surface of the steel decking must be protected against damage from high local loads.

(2) Prior to concreting, the surface of the decking

must be cleaned of all dirt, debris, water and any other foreign matter, to ensure proper bonding between steel and concrete.

(3) Steel decks serving as working platforms tend to be slippery to walk on.

(4) High winds during site construction may disrupt the laying and fixing of the light decking.

(5) The most important disadvantage arises from the difficulty in achieving an adequate fire rating. However, this is now largely being overcome as further fire test information becomes available.

1.5 Methods of Shear Connection

It is required that the composite structural elements (steel and concrete in the present case) work together as one material. This is achieved by the interaction between them and a transfer of shear at the connection by means of bond or the use of shear connectors.

1.5.1 Bond

With the use of profiled steel sheet,shear connection is provided by bond at the profiled steel sheet/concrete interface. It is also provided by pressed embossments which project from the sides of the profiled sheet ribs into the concrete. Theoretical techniques are not

available to predict the shear bond capacity of these slabs. It is difficult to predict such behaviour for several reasons such as the geometry, flexibility and the uniqueness of each type of profiled steel sheet. Many experimental studies, however, have identified the loss of shear bond as the primary mode of failure for most composite slabs (1).

1.5.2 Shear Connectors

Shear connectors are used to provide shear connection at the interface of the composite slab and the steel beam where a part of the connector projects into the concrete.

The most common form of shear connectors which is widely used is the welded stud. Shot-fired shear connectors have been developed during the last few years. These shot-fired connectors (such as the Hilti connector) have the advantage over the welded connectors in that they can be used in adverse weather conditions with lighter fixing apparatus (2,3). The present work makes use of this advantage with the use of self drilling and tapping screws. These connectors differ from others in that only their heads project into the concrete.

Shear connectors are of great importance in composite beams for the interaction between the concrete slab and the steel beam. They transfer shear between the

two materials limiting the longitudinal slip and preventing the uplift between the two materials at their interface.

Full interaction between the two materials is not achieved as some slip between them is inevitable. Newmark et al.(1951) developed an elastic analysis taking this slip into account assuming a linear load-slip relation. This analysis has been extended by Dai et al.(1970) where the nonlinear load-slip characteristics of shear connectors and the inelastic behaviour of steel and concrete were considered (1,4).

Johnson (1970,1975) developed the 'Linear partial interaction design' method of analysis for composite beams. The method assumes that additional strength and stiffness of the beam caused by connection of concrete to the steel varies linearly with the partial connection (4).

1.6 Space Frames

Conical or dome-shaped structures, that were built with the branches of trees, were the first skeletal structures built and used by primitive people, for example, the buffalo hide covered American Indian tepee and the African thatched round house. Due to the lack of materials to build a self-supporting skeletal structure of long span, the development of space structures was

slow until the production of steel took place in the early nineteenth century. However, the tedious calculation and design of the space structure was another reason for the slow development of these structures. This latter difficulty was overcome by the introduction of the electronic digital computers which are very powerful and enable rapid analysis of many forms of structure to be carried out (5).

The space frame considered in this work is one of several types of double-layer grids. Double-layer grids are space frames assembled from prefabricated units of standard size and shape (see Figure 1.2). The space frame (considered in this work),in its final shape, is composed of two layers, top and bottom, parallel to each other and connected by diagonal members. Such space frames may be referred to as flat double-layer grids. In addition to their high rigidity and stiffness, flat double-layer grids have an extra advantage in that they can be used for both roof and floor construction (3,4).

1.6.1 Advantages of Flat Double-layer Grids

Flat double-layer grids are claimed to have a number of advantages such as (6):

(1) They are typical examples of a three-dimensional structure, in which external loads are distributed omnidirectionally.

(2) As a rule, double-layer grids are highly

statically indeterminate and buckling of any compression member under a heavy concentrated load will not lead to a collapse of the whole structure.

(3) Their great rigidity leads to relatively small deflections.

(4) Analysis and tests show that double-layer grids have a much greater fire resistance than conventional systems.

(5) Double-layer grids can be assembled with a few prefabricated parts which are precisely made in jigs, ensuring accuracy and speed in erection. Several of the commercially available double-layer grid systems are truly self-aligning. The small size of the components greatly simplifies handling, transportation and erection.

(6) They are characterised by expandability, demountability and almost random location of supports. This allows the designer great flexibility in choosing the layout and the positioning of columns. It is possible for some columns to be removed or have their position modified without damaging the structural integrity of the frame.

(7) The space between the top and the bottom grids can be used for the installation and maintenance

of mechanical and electrical services, such as heating, cooling and ventilating.

(8) The dry method of construction allows the erection of a double-layer grid structure during virtually any type of weather.

(9) Experience shows that double-layer grids resist aerial or terrorist attacks and explosions much better than any other structural system. They also resist horizontal earthquake forces better.

(10) The regular pleasing pattern of double-layer grids provides an extremely attractive appearance which becomes a valuable feature in many architectural applications. This is also the reason why many architects do not use false ceilings and leave the under-side of the structures exposed in churches, assembly halls and exhibition centres.

1.7 Space Deck System

A remarkable number of different commercial systems of double-layer grids have been introduced and put on the market since 1942(6). Space Deck is one of these systems which was introduced in England some 30 years ago. All the present work considering space frames is related to this system, and it is useful to describe the system at this stage of the introduction, and it may summarised as follows (6,7).

The system is based on the use of factory made components assembled on site to form a flat double-layer grid. The components are described under the following headings.

1.7.1 Unit (see Plate 1.1 and Figure 1.3)

It is an inverted square-based pyramid consisting of four steel rolled angles welded together to form a square top chord frame (top-tray) and of four tubular or solid diagonal bars welded to the corners of the top-tray and to a central boss which is left- and right-hand threaded,male and female,to take four adjustable tie bars. Units are available in four overall depths of 1200 mm, 750 mm, 1500 mm or 2000 mm identified as 1212, 1209, 1515 and 2000 ranges (8). Three unit types are available in each depth which differ in the sections used for the top tray and diagonal members. The three units are; the lightest unit which consists of the top-tray angles of 50x40x6 and four tubular diagonals; the shear unit which consists of the top-tray angles 60x60x8 and four solid diagonals and the heavy shear unit which is similar to the shear unit but with a heavier diagonal.

1.7.2 Tie bars (see Figure 1.3)

Main and secondary tie bars of high tensile steel are connected to the units through their bosses. The

main tie bar screws directly in to the boss forging, and the secondary tie bar is attached to the cross stud by means of a tapped hexagonal coupler (see fig.1.3). Opposite ends of each tie are threaded left- and right-hand providing a turnbuckle facility to adjust the centre to centre dimension of adjacent bosses and to adjust for any required roof or floor camber.

1.7.3 System Assembly and Advantages

When the units are connected together by means of bolts through holes on the sides of the top-trays, and by means of the ties through the bosses, the top-trays form the top layer while the ties form the bottom layer of the grid connected by the diagonal members. By this connection, the flat double-layer grid of space deck system is formed (see Figure 1.4).

In addition to the advantages mentioned for the flat double-layer grids, the Space Deck system also claims to have the following advantages (8):

(1) Excellent span to depth ratio.

(2) No purlins are required where roof decking can be fixed directly to the space frame.

(3) Suitable for structures of irregular plan shape.

(4) Fully adjustable cambering facility.

(5) Ease of transportation, handling and stocking.

(6) Standard range of accessories are available.

Based on the above description, the Space Deck

system is economical in that it is composed of light materials where the dead load of the steel structure normally amounts to some 20-25 Kg/m² for spans up to 32.4 x 32.4 m. The maximum recorded unobstructed span is up to 50x50 m. Due to its lightness, the system is said to be economical in that it saves money and time. The system is also claimed to be of a remarkable strength (8).

1.8 Development of Space and Composite Space Frame

The system in its early years after its introduction in 1954 was used for single story buildings, but in the early 1960s it was considered for multi-story building applications(see Figure 1.5). For this latter case, the roof covering is replaced by a floor membrane either as pre-cast concrete supported off corners of the unit tray or as profiled steel sheeting and site-poured concrete (7).

1.9 Testing Work To Date

1.9.1 Space Decks Limited

Since the introduction of the system, a series of tests have been carried out on system components as well as on full scale system by Space Decks Limited(7). In order to test the components capacities, a two-unit

space frame (see Figure 1.6) was considered by Space Decks Limited (9,10). Testing the top chord capacity, vertical loads were placed on the top chord to give twice the local bending moment designed for, and the axial force was gradually increased to failure. For the 1212 two-unit specimen,which is composed of 60x60x8 angles top trays and 28 mm diameter diagonals,the average compressive force reached at failure was 358 kN., but a force of 318kN was calculated to be reached on top chords at the yield of the tie bar (10). Similar tests on other type units have also been carried out.

A computer analysis of an 8400mm x 8400mm space frame roof was prepared by Space Decks Limited. It was analysed as space truss so that loading was taken as vertical loads at the top joints of the truss. The vertical loading was assumed to represent a uniformly distributed load resulting from the weight of the composite concrete/steel deck floor in addition to the assumed live load.

Based on these tests,especially for the 1212 series, and on the results of the computer analysis, a feasibility report (11) was produced on the use of a composite concrete/profiled steel sheet floor with a space deck floor or roofing system of the 8400 x 8400 mm plan area. The combined bending and axial stresses on the top chord member (composed of two/60 x 60 x 8) were checked, and the member was satisfactory in both

construction stage and permanent state. It was concluded that if 50 x 60 x 6 angles were required to be used all round, a further analysis would probably show reasonable margins of safety. Diagonals and ties were also satisfactory. It was stated (11) that with partial shear connection, the top chord member designed as a simply supported composite beam, produced a section with an ultimate moment of approximately twice that of double angles acting alone.

1.9.2 Steel Strut Tests

Since the present work is concerned with the top-chords of the space frame (double angles connected back to back), some tests were designed to investigate the behaviour of steel double angle struts. H. W. Lee (12) carried out similar tests on different steel struts including double angle struts. When outlining his work, Lee (12) stated that since the start of the experimental investigation for double angle struts in 1972 by Kennedy and Murty (13), the information on this particular subject was limited. He investigated double angle struts with short and long legs connected back to back and produced some useful results. He stated that when thin walled members were loaded axially, they may fail due to flexural buckling, flexural-torsional buckling and local plate buckling. Provided the plate buckling load is not

reached, the buckling mode will be either flexural or flexural-torsional and will not be affected by change in effective length. He also stated that for double angle struts, flexural torsional buckling occurs only when r_x/r_y is greater than 1. When r_x/r_y is less than 1, flexural buckling is the mode of failure. For long leg connected double angle struts, the buckling mode is flexural-torsional while for the short leg connected double angle struts, the buckling mode is flexural.

Analysis of Composite Space Frames

Analysis of space frames by computers is fairly common using computer programs which are described in many books on structures. However, the analyses of composite space frames by computers is not well developed. There appears to be no programs devoted to this type of structure. This may be due the fact that this field is still relatively new as is explained earlier. Therefore, a program has been developed as part of the research by the author.

In fact, such structures may be solved using program packages. There is, however, some difficulty involved in representing the elements of the structure and modifying them. In addition to time needed to analyse the structure using such packages, they are not easily accessible. They have limited use for certain applications and they are very expensive. For these

reasons, it was decided to use space frames program and to develop other methods to analyse this kind of structure.

Space Decks Limited used a space frame program to analyse the present non-composite space frame considered in this work. This is discussed in later chapters. A recent paper (14) is an example of the simplified methods concerning the analysis of composite space frames. This paper suggested three ways to analyse the composite space frame. The first way was to use finite element and matrix displacement methods. It was stated that although this method is very complicated to use, it was considered the most efficient one. The second method was to use a simulation of a sandwich structure. The floor elements are considered as upper, middle and lower layers of a sandwich structure. Due to the difficulty of solving the the complex differential equation to find the stresses and displacements, this technique is limited. The last way suggested and described (14) was to use a displacement method for space trusses. Using this method, the top part of the composite truss was replaced by a truss system in one plane. Therefore, the structure was still considered as a space truss structure and current computer space frame and truss programs could be used. The description of the program developed in this work is contained in chapter 2.

1.10 Scope and Layout of the Thesis

1.10.1 Composite Space Frame

The main aim of this present work is to consider the system as a composite space frame. It considers the use of a composite concrete/profiled steel sheet slab with the Space Deck System.

In the composite space frame, the concrete slab, the profiled steel sheet and the shear connectors are considered to work compositely with the top chord members of the space frame. The work considers in detail the behaviour of the top part of the composite space frame. This top part includes the top chord members(steel double angles bolted back to back), steel sheet decking, shear connectors and concrete. The work is divided in to two parts comprising the analysis section and the experimental work. The analysis is based on the same space floor dimension as that analysed by Space Decks Limited (8400 mm x 8400 mm) as well as the testing work considering the light space units of 1212 range only.

Chapter 2 contains mainly the theoretical analysis of the composite space frame floor based on stiffness and finite element methods. The structure is solved as

thin plate elements (the profiled steel sheet),combined with steel top-chord angles and concrete sections (concrete flanges of effective width of 300 mm) to form composite beam elements and space truss elements (diagonals and ties).

The analysis of the composite beams considered the two materials fully attached (full-interaction) while in the real situation, this may not be completely true. In real situations, full-interaction can not be achieved in beams, but in columns end slip is prevented. However, for the structure studied, a partial-interaction theory is explained in chapter five.

The results of the present analysis found by the composite space frame program is not wholly comparable with the previous space frame program results. The present analysis results contain moments, axial and vertical forces appearing as end actions (see Appendix C) while those of the space frame program contain axial forces only.

Chapter 3 contains the experimental testing programme which describe the testing procedure, set-up, instrumentation, etc. It also includes a summary of the tests.

Chapter 4 includes the experimental observations and behaviour of the specimens tested prepared in

graphical and tabulated forms followed by short discussion for each case.

Chapter 5 includes the interpretation of the experimental results. The different cases of composite specimens are discussed and compared with each other where the effective width of the composite T-beam is found.

The last chapter includes the conclusions related to this present work. Recommendations for further research are discussed for both the analytical and the experimental parts.

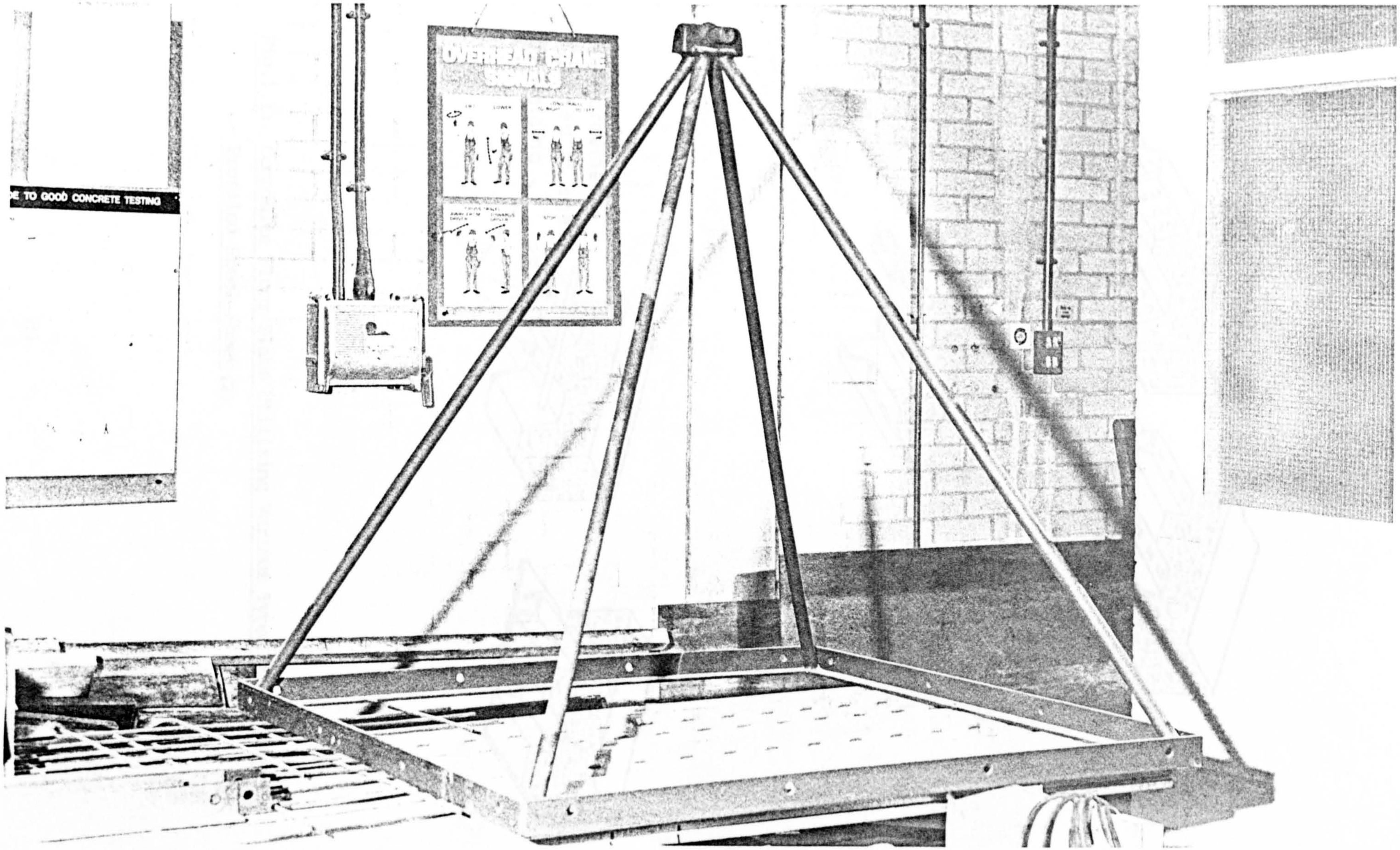

1.1 SPACE DECK UNIT (INVERTED)

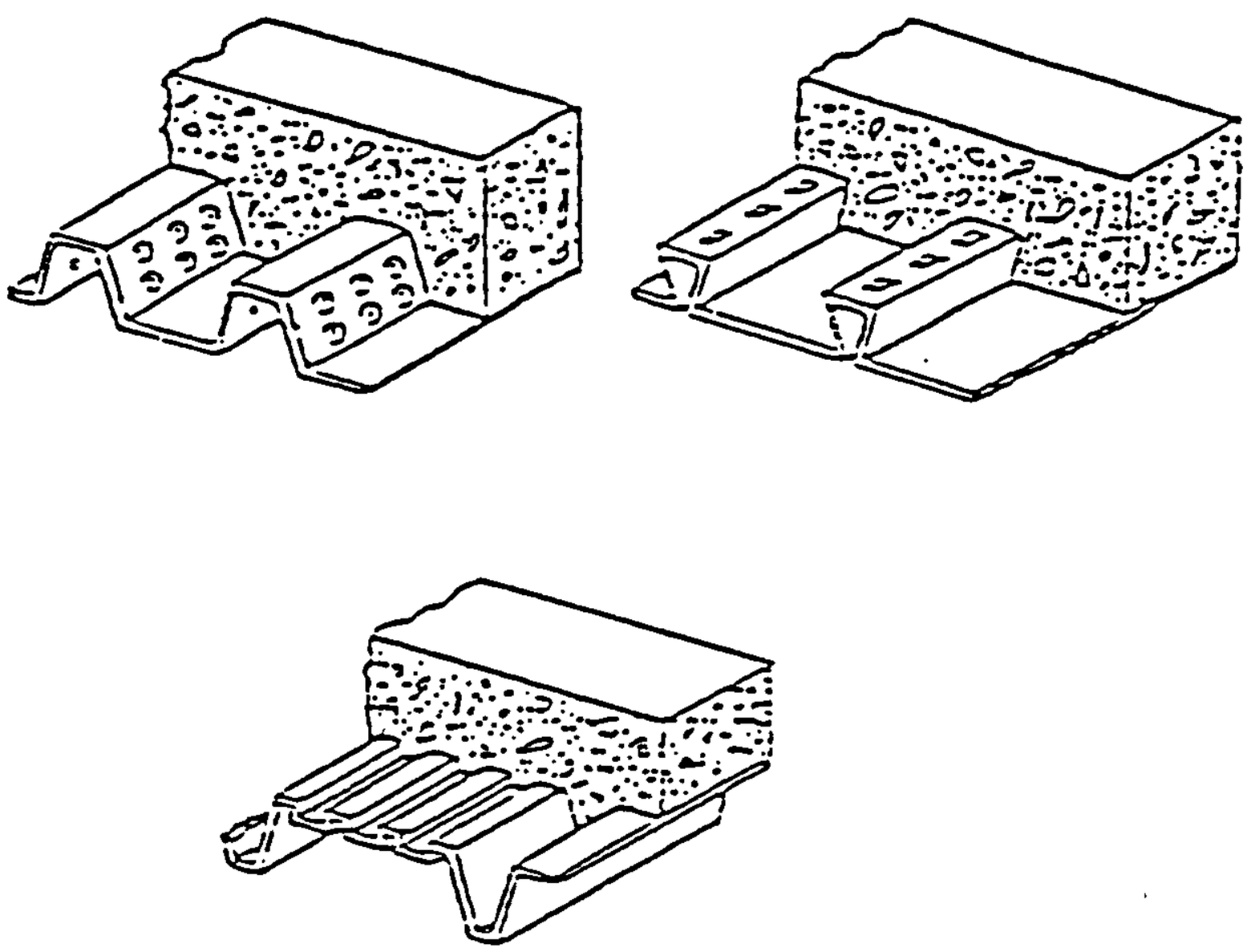

Fig.1.1: Composite Floor Slabs Utilizing Various Types of Profiled Steel Sheet (2)

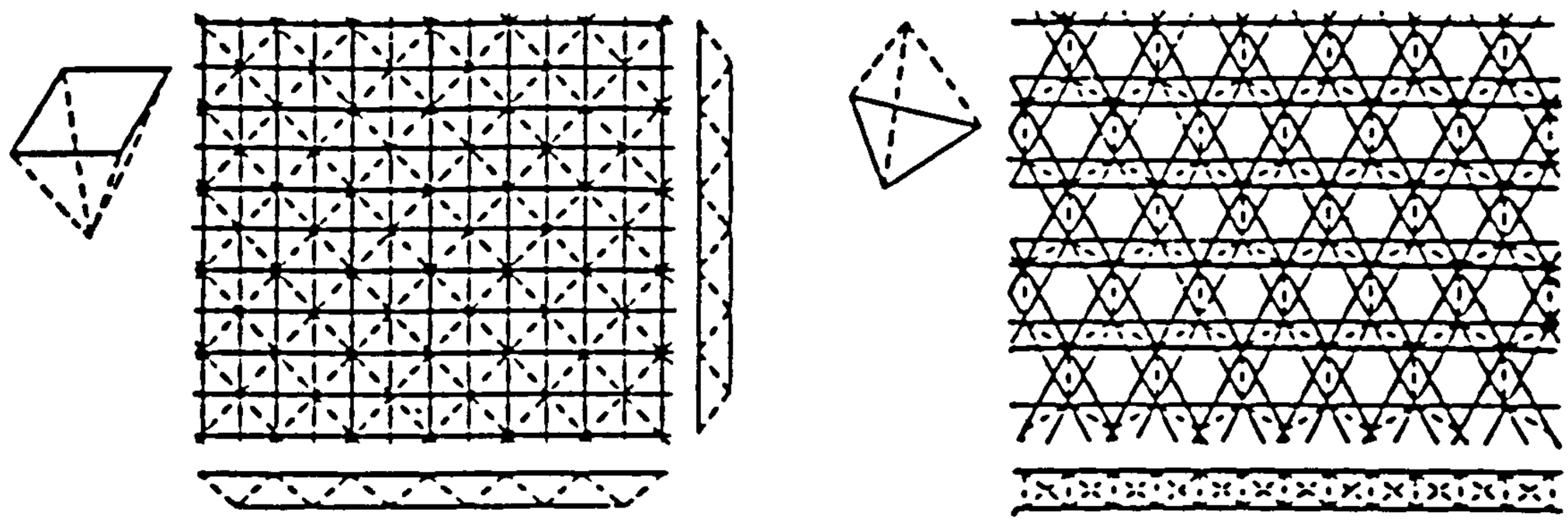

Fig.1.2: Main Types of Double-Layer Space Grids(6)

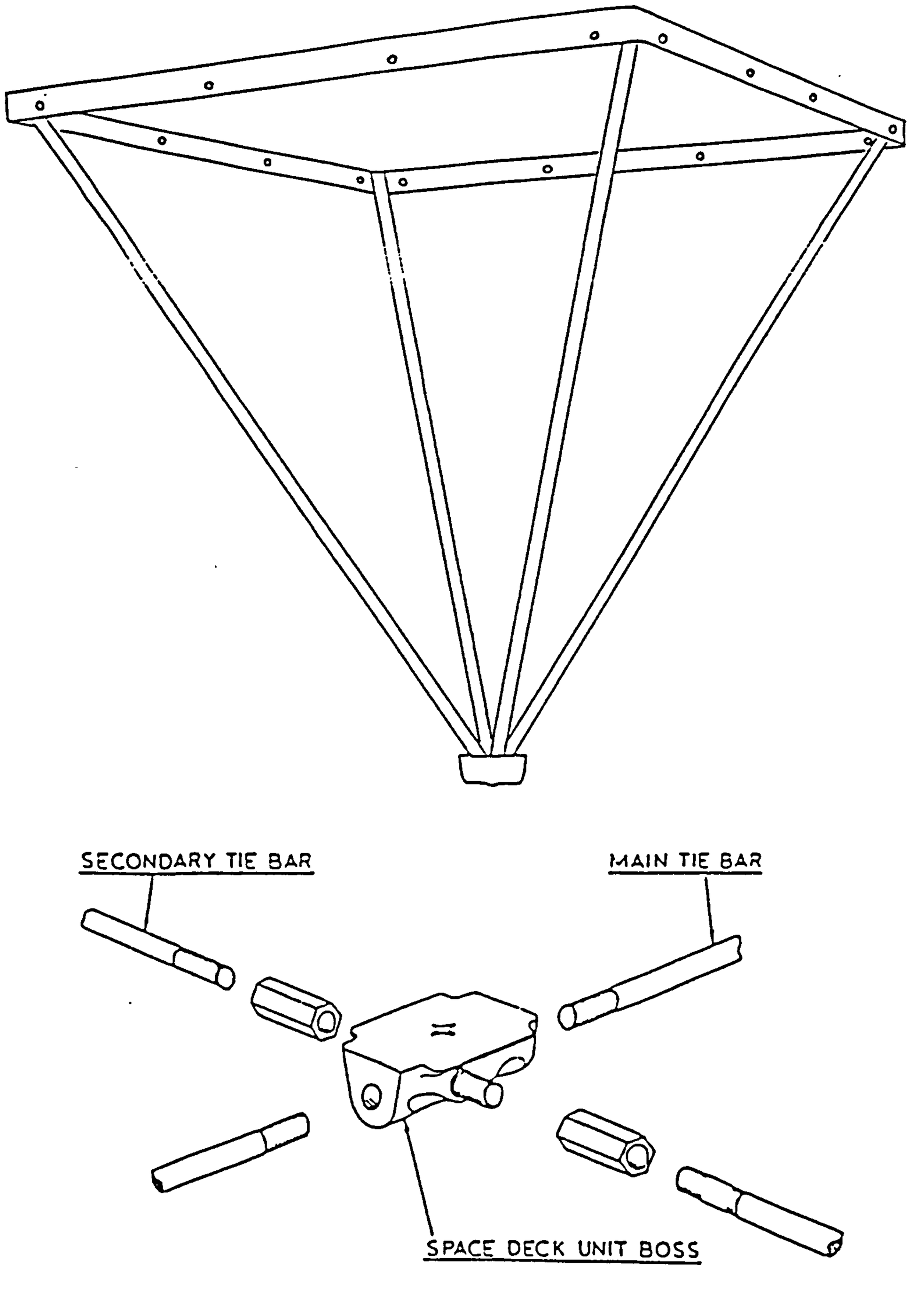

Fig.I.3: Space Deck Unit

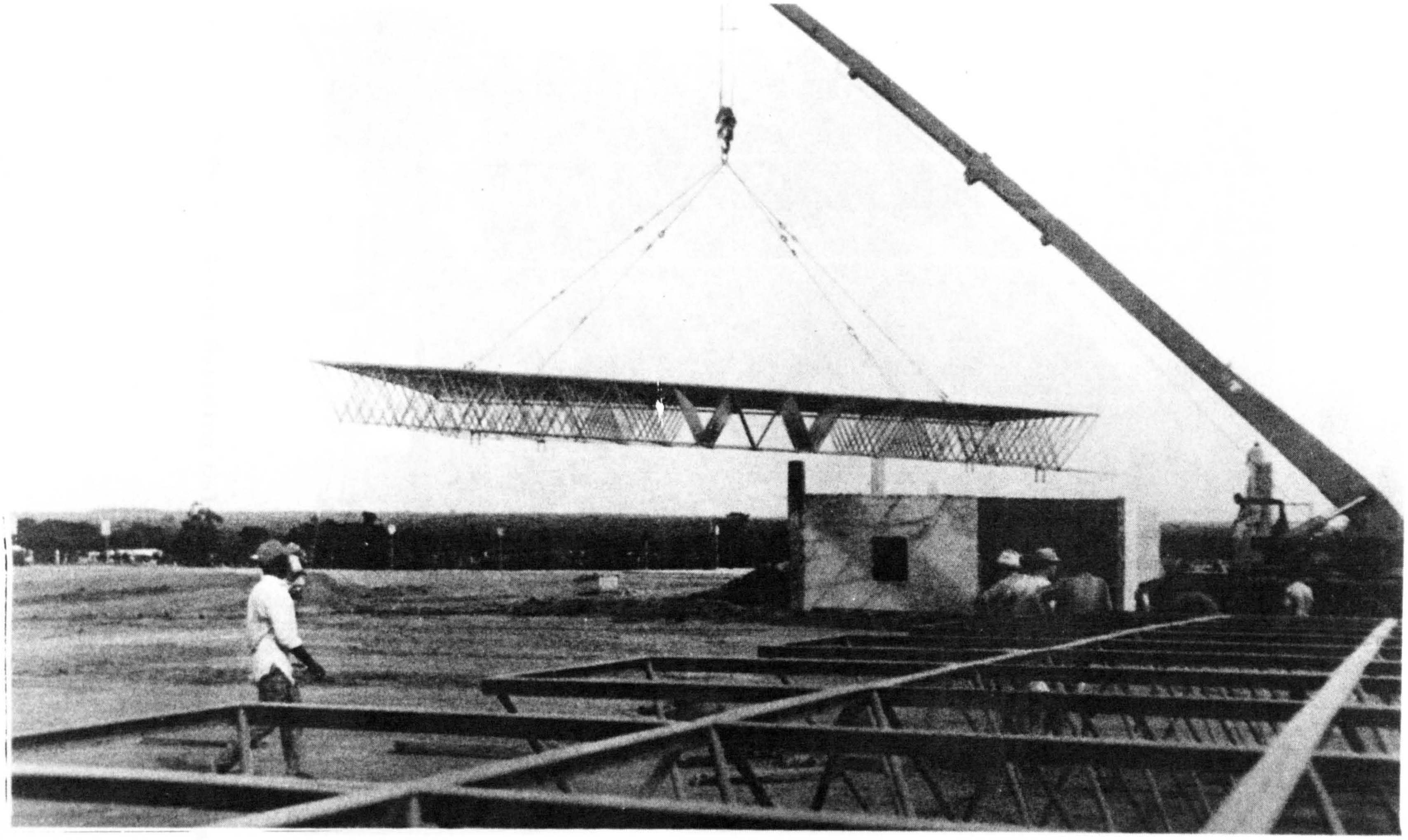

Fig. 1.4 Space Deck System Assembly

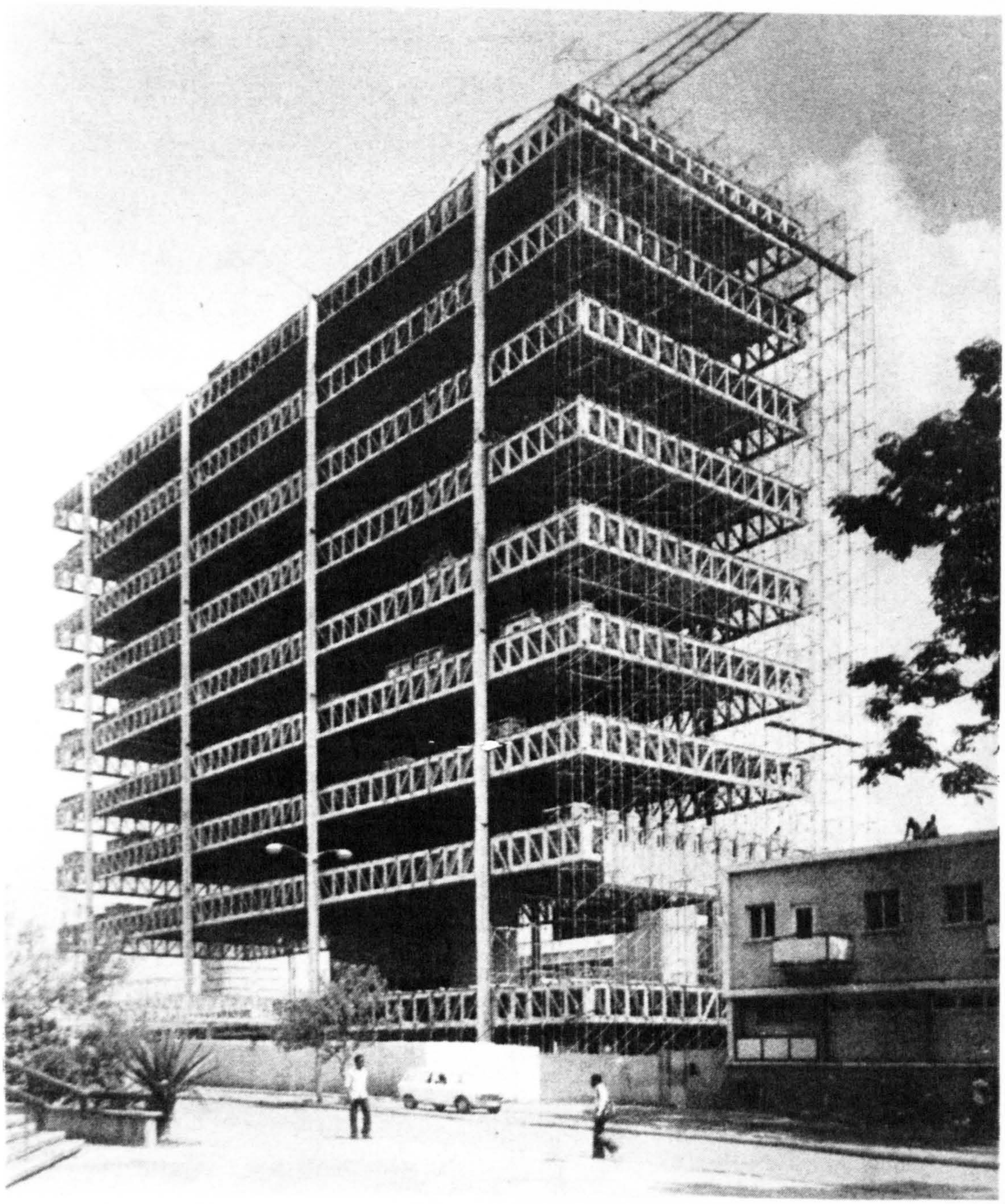

Fig. 1.5 A multi-storey Building Using the Space Deck System

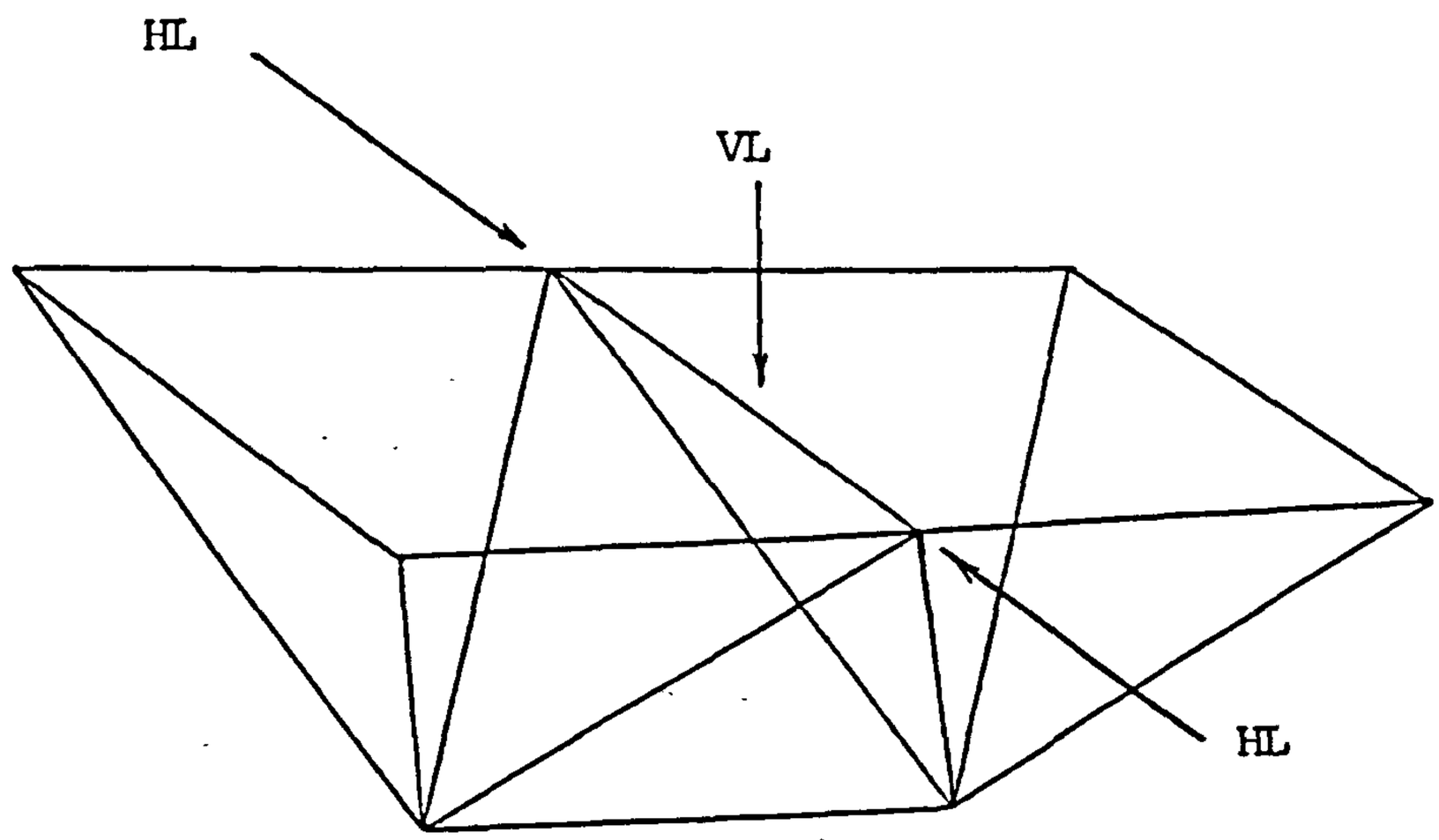

Fig.1.6: A Two-Unit Space Deck Used in the Tests

CHAPTER TWO

Theoretical Treatment Of Space Frames

2.1 Introduction

2.1.1 Space Frame Analysis

The analysis of the system by Space Decks Limited utilised a computer program which solved the space deck as a space truss structure. The loading was considered as vertical forces applied at the joints and, therefore, only axial forces and stresses in the member were produced by the analysis. The analysis of the structure in the feasibility study (11), mentioned in the introduction, was also based on the results of this program.

A similar space frame program (15) was considered in this work before the testing commenced. Although the axial forces found by such a program did not represent the real internal forces in the structure members, they were of great help at the beginning of this work. They were helpful in the testing of the first specimen which was tested as:

a) a double-unit non-composite space frame structure.

b) a double-unit composite space frame structure.

The structures were analysed with different axial and vertical loadings with different locations of strain measurements to provide initial information on the behaviour of such composite systems. The space frame computer program was useful in indicating which top chord members carried the maximum force so that the corresponding member or members could be investigated.

2.1.2 Composite Space Frame Analysis

It is clear that the space truss program is useful to a limited extent. It does not fully represent the composite space frame structure. The composite space frame is composed of plate and beam elements which carry axial force, vertical force and moment, and truss elements which carry only axial forces. The analysis presented in this chapter recognises this fact so that the results are closer to the actual behaviour.

The composite space frame is solved as composite sections which include the top chord angles, the profiled steel sheet and the concrete slab together with space truss member elements. The analysis is based on a Space Deck System roof with the dimension of 8400 x 8400 mm.

The composite cross-section is considered as a T-beam (see Figures 2.1 and 2.2). The first figure represents the cross section where the ribs of the profiled steel sheet are parallel to the steel beams while the other one represents the cross section where

the ribs of the profiled steel sheet are perpendicular to the steel beams. The effective width of both cross sections is taken as 300 mm which is found from the experimental work (the average effective width found by tests). This effective width was considered for the concrete section only. The width of 225 mm was considered for the profiled steel sheet which represents the repeated cross-section.

The composite section elements are considered as a plate element, representing the profiled sheet, in both flexure and for in plane forces, composite beam, representing the double angles back to back, and the concrete section. The profiled sheet is represented by a repeated cross-section for in and out of plane loadings. Stiffness matrices for plates in flexure and in plane forces are superimposed to form one stiffness matrix for both cases, and it is named [EK]. Similarly for the beam elements, the two cases of the composite beam according to its loading were considered, either loaded in plane (beam) or loaded normal to plane (grid). Stiffness matrices for both cases, grid and beam, are superimposed to form one stiffness matrix called a beam element stiffness matrix. The superimposed beam elements stiffness matrix is named [EK1]. The superposition of the different cases of one element such as the plate or the beam elements as explained above is also found in some references (16,17). The diagonals and ties are treated as space truss members and their transformed

stiffness matrix is named [EK2]. It should be noted that there are five deformations at each node of the plate element named and arranged as u, v, θ_x, θ_y and w which stand for linear deformations along and perpendicular to the member axis, rotations about the x- and the y-axes and lateral deflection in the z-direction respectively. The beam element has similar deformations at each of the two nodes, and they are u, v, θ_x, θ_y and w. The assembling of the unrestrained global stiffness matrix [SU] is, therefore, a direct operation for these elements. However, the space truss element has only linear deformations, i.e. no rotations about any axis. Therefore, blank rows and columns were considered within the truss stiffness matrix to match those corresponding to the two rotations of the plate and the beam elements. This is considered to ease the assembling of truss stiffness matrix in to the unrestrained global stiffness matrix [SU].

The computer program used to analyse this structure is based on the finite element approach. It has been based on a beam program, and developed to solve the present structure. Although the plate element dimensions are taken as 1200 mm x1200mm, and the beam element span is taken as 1200mm, it is possible to use smaller dimensions. For the present analysis, these dimensions have been considered so that the results could be compared with those of the space truss program. The dimensions are also considered reasonable when compared

to the real roof structure.

Due to the fact that the two cross sections are passing through each other, some parts of the concrete are taken twice. Moreover, other parts such as those beyond the effective width and those in the ribs perpendicular to the steel beams are excluded. This may result in some approximation within this solution.

2.2 Theoretical Treatment of Elements

2.2.1 Thin Plate Element

A rectangular plate element of sides a and b, and a thickness of t as shown in Figure 2.3 is taken for the analysis of both cases of plate in plane elasticity and in flexure. However, both sides are taken as the same length (a special case of a rectangular element). The plate which is considered throughout this analysis is a profiled steel sheet of a thickness of 1.2 mm which is accordingly a thin orthotropic plate element. The plate is thin compared to the other dimensions and this allows the plate to be analysed for the case of flexure according to the method described here.

The co-ordinate and the numbering system for a rectangular element considered throughout the analysis of thin plate in both flexure and in-plane forces is as shown in Figure 2.3 where the two axes x and y are parallel and perpendicular to the element sides.

a)Plate Element Loaded In-Plane:

The thin plate element in-plane has two degrees of freedom at each node so that eight unknown coefficients are to be involved in the polynomial representing the displacement pattern. Two suitable functions satisfy this requirement and they are (16):

$u=\alpha_1+\alpha_2 x+\alpha_3 y+\alpha_4 xy$

$v=\alpha_5+\alpha_6 x+\alpha_7 y+\alpha_8 xy$

where u and v are the displacements in the X- and and in the Y-directions. These displacements at each node of the plate element are shown in Figure 2.4.

The stiffness matrix of this case of rectangular plate element loaded in plane defined in Figure 2.3 and 2.4 is (16,17):

$$t/12.\begin{bmatrix}
4d_{11}+4d_{33} & & & & & & & \\
3d_{21}+3d_{33} & 4d_{22}+4d_{33} & & & & & & \\
2d_{33}-4d_{33} & 3d_{21}-3d_{33} & 4d_{11}+4d_{33} & & & & & \\
-3d_{21}+3d_{33} & -4d_{22}+2d_{33} & -3d_{21}-3d_{33} & 4d_{22}+4d_{33} & & & & \\
-4d_{11}+2d_{33} & -3d_{21}+3d_{33} & -2d_{11}-2d_{33} & 3d_{21}+3d_{33} & 4d_{11}+4d_{33} & & & \\
3d_{21}-3d_{33} & 2d_{22}-4d_{33} & 3d_{21}+3d_{33} & -2d_{22}-2d_{33} & -3d_{21}-3d_{33} & 4d_{22}+4d_{33} & & \\
-2d_{11}-2d_{33} & -3d_{21}-3d_{33} & -4d_{11}+2d_{33} & 3d_{21}-3d_{33} & 2d_{11}-4d_{33} & -3d_{21}+3d_{33} & 4d_{11}+4d_{33} & \\
-3d_{21}-3d_{33} & -2d_{22}-2d_{33} & -3d_{21}+3d_{33} & 2d_{22}-4d_{33} & 3d_{21}-3d_{33} & -4d_{22}+2d_{33} & 3d_{21}+3d_{33} & 4d_{22}+4d_{33}
\end{bmatrix}$$

SYMMETRIC

where for plane stress,

$d_{11}=d_{22}=E/1-v^2$

$d_{21}=d_{12}=vE/1-v^2$

$d_{33}=E/2(1+v)$

Provided that $E_x = E_y$ and $v_x = v_y$ for the profiled steel sheet.

b)Plate Element Loaded Normal To Plane:

The thin plate element loaded normal to its plane (plate in flexure) has three degrees of freedom at each

node, and the polynomial representing the lateral deflection is (16):

$$w=\alpha_1+\alpha_2x+\alpha_3y+\alpha_4x^2+\alpha_5xy+\alpha_6y^2+\alpha_7x^3+\alpha_8x^2y+\alpha_9xy^2+\alpha_{10}y^3 +\alpha_{11}x^3y+\alpha_{12}xy^3$$

The other two freedoms are related to this polynomial, and they are:

$$\theta_x=-\delta w/\delta y$$

$$\theta_y=\delta w/\delta x$$

where θ_x and θ_y are the rotations about the x-axis and the y-axis respectively. The end deformations at each node of the plate element are as shown in Figure 2.4.

The above equations are discussed in detail to derive the stiffness matrix applicable for orthotropic, thin and rectangular plate element in flexure (16). The plate element for this case is defined in Figure 2.3 and 2.4, and the stiffness matrix is:

$$
\begin{bmatrix}
KA & & & & & & & & & \\
-KB & KC & & & & & SYMMETRIC & & & \\
-KD & KE & KF & & & & & & & \\
KG & 0 & KH & KA & & & & & & \\
0 & KI & KL & KB & KC & & & & & \\
-KH & KL & KM & KD & KE & KF & & & & \\
KN & 0 & KO & KP & 0 & KQ & KA & & & \\
0 & KR & KS & 0 & KT & KU & KB & KC & & \\
KO & -KS & KX & -KQ & -KU & KY & -KD & -KE & KF & \\
KP & 0 & -KQ & KN & 0 & -KO & KG & 0 & KH & KA \\
0 & KT & KU & 0 & KR & KS & 0 & KI & -KL & -KP & KC \\
KQ & -KU & KY & -KO & -KS & KX & -KH & -KL & KM & KD & -KE & KF
\end{bmatrix}
$$

Where,

$KA=20a^2D_y+8b^2D_{xy}$

$KB=15abD_1$

$KC=20b^2D_x+8a^2D_{xy}$

$KD=30apD_y+15bD_1+6bD_{xy}$

$KE=30bp^{-1}D_x+15aD_1+6D_{xy}$

$KF=60p^{-2}D_x+60p^2D_y+30D_1+84D_{xy}$

$KG=10a^2D_y-2b^2D_{xy}$

$KH=-30apD_y-6bD_{xy}$

$KI=10b^2D_x-8a^2D_{xy}$

$KL=15bp^{-1}D_x-15aD_1-6aD_{xy}$

$KM=30p^{-2}D_x-60p^2D_y-30D_1-84D_{xy}$

$KN=10a^2D_y-8b^2D_{xy}$

$KO=-15paD_y+15bD_1+6bD_{XY}$

$KP=5a^2D_y+2b^2D_{xy}$

$KQ=15apD_y-6bD_{xy}$

$KR=10b^2D_x-2a^2D_{xy}$

$KS=30bp^{-1}D_x+6aD_{xy}$

$KT=5b^2D_x+2a^2D_{xy}$

$KU=15bp^{-1}D_x-6aD_{xy}$

$KX=-60p^{-2}D_x+30p^2D_y-30D_1-84D_{xy}$

$KY=-30p^{-2}D_x-30p^2D_y+30D^1+84D_{xy}$

Where for the profiled sheet(18),

$D_x=(q/s)Et^3/12(1-v^2)$

$D_y=EI_Y/q$

$D_{xy}=(s/q)Et^3/6(1+v)$

$D_1=0$

Where,

E=modulus of elasticity of the steel plate

t=thickness of the plate.

I_y=moment of inertia of one repeating cross section of the corrugation about its neutral axis.

s=the length of one repeating corrugation.

q=wave length of one repeated corrugation.

The calculation of these rigidities is based on a repeated cross-section shown in (Figure 2.5). D_x and D_y are the flexural rigidities in X and Y-directions, D_{xy} is the torsional rigidity and D_1 is$(v\sqrt{D_xD_y})$ which is taken as zero when $D_y>>D_x$, i.e. $D_y>50D_x$ (18).

The detailed formulation to construct the stiffness matrix for these cases of plates can be found in many references (16, 17, 19, 20 and 21).

It should be noted that the function representing the plate element of plane elasticity ensures full displacement continuity in the solution while for the function representing the plate element in flexure, this concept is not completely true. Along any edge , a discontinuity of the normal slope can exist (see Figure 2.6). Therefore, this function is called a 'non-conforming function' (16).

2.2.2 Beam Element

The co-ordinate and the numbering system for this element is as shown in Figure 2.7, where α is the angle which the element makes with the x-axis. The stiffness matrix of this element depends on the plane of loading either in the element plane or normal to it.

The beam element as a planar structure is either loaded in plane, which is plane XY in the present analysis, or normal to plane (grid structure). For the first case (loaded in plane), the possible joint displacements to be considered are u (axial translation), v (normal translation) and Θ_z (rotation about the Z-axis) as shown in Figure 2.8. However, for the second case (loaded normal to plane), the possible joint displacements to be considered are w (translation, or deflection in the present analysis, in the Z-direction), and two rotations Θ_x and Θ_y about X and Y-axes (see Figure 2.8). Therefore, each of the two cases (beam loaded in plane and grid loaded normal to plane)

produces its own stiffness matrix. Both stiffness matrices are defined below.

a)Beam Element Loaded In Plane

This element is defined as shown in Figures 2.7 and 2.8. The stiffness matrix $[K_b]$ as shown below (15).

$$\begin{bmatrix} AE/L & 0 & 0 & -AE/L & 0 & 0 \\ & 12EI/L^3 & 6EI/L^2 & 0 & -12EI/L^3 & 6EI/L^2 \\ & & 4EI/L & 0 & -6EI/L^2 & 2EI/L \\ & & & AE/L & 0 & 0 \\ & & & & 12EI/L^3 & -6EI/L^2 \\ & SYMMETRIC & & & & 4EI/L \end{bmatrix}$$

where,

A is the cross-sectional area of the element.

E is the modulus of elasticity.

I is the second moment area of the cross-section.

L is the element length.

In the present analysis, the rotation about the Z-axis has not been considered.

b)Beam Element Loaded Normal To Plane (Grid)

The stiffness matrix $[K_g]$ for this element defined as shown in Figure 2.7 and 2.8 is (15):

$$\begin{bmatrix} GJ/L & 0 & 0 & -GJ/L & 0 & 0 \\ & 4EI/L & 6EI/L^2 & 0 & 2EI/L & -6EI/L^2 \\ & & 12EI/L^3 & 0 & 6EI/L^2 & -12EI/L^3 \\ & & & GJ/L & 0 & 0 \\ & & & & 4EI/L & -6EI/L^2 \\ & \text{SYMMETRIC} & & & & 12EI/L^3 \end{bmatrix}$$

where,

G is the shear modulus [E/2(1+v)]

J is the torsional constant

If the section of a prismatic member is composed of slender rectangular areas (as that of the top chord angles) (see Figure 2.9a), the torsional constant for the section can be approximated by the expression ($J=1/3 \Sigma ht^3$) (15). This torsional constant for the concrete section being considered by this analysis can also be evaluated by the expression [$J=ht^3[1/3 - 0.21\ t/h\ (1 - t^4/12h^4)]$] (18). However, for a rectangular section with a large ratio of h/t, this expression reduces to ($J=ht^3/3$) (15) which is the case considered with the present analysis. In the first expression, h and t are the long and the short sides of each area. In the second and the third expression, h and t are the long and the short sides of the section which is taken as rectangular (see Figure 2.9b).

The transformation matrix of the beam element is defined below (15).

$$\begin{bmatrix} C_x & -C_y & 0 & 0 & 0 & 0 \\ C_y & C_x & 0 & 0 & 0 & 0 \\ 0 & 0 & 1 & 0 & 0 & 0 \\ 0 & 0 & 0 & C_x & -C_y & 0 \\ 0 & 0 & 0 & C_y & C_x & 0 \\ 0 & 0 & 0 & 0 & 0 & 1 \end{bmatrix}$$

where,

$C_x = \sin \alpha$

$C_y = \cos \alpha$

2.2.3 Space Truss Element

Space truss members are treated as beam elements, arbitrarily orientated in three dimensional space with an ideal spherical hinges at both ends (15)(see Figures 2.10 and 2.11). Therefore, there are three possible components of end displacement at each end to be considered. These end displacements are a displacement in the X direction δ_x, a displacement in the Y direction δ_y and a displacement in the Z direction δ_z. Considering the fact that a truss member can only resist axial deformations, the stiffness matrix of the truss member element is (15):

$$\begin{bmatrix} AE/L & 0 & 0 & -AE/L & 0 & 0 \\ 0 & 0 & 0 & 0 & 0 & 0 \\ 0 & 0 & 0 & 0 & 0 & 0 \\ -AE/L & 0 & 0 & AE/L & 0 & 0 \\ 0 & 0 & 0 & 0 & 0 & 0 \\ 0 & 0 & 0 & 0 & 0 & 0 \end{bmatrix}$$

Provided that the truss structure is loaded at its joints, and should the truss member have a constant cross-section over its length, the transformed stiffness matrix for a space truss member is (15):

$$AE/L \begin{bmatrix} C_x^2 & C_xC_y & C_xC_z & -C_x^2 & -C_xC_y & -C_{xy} \\ C_yC_x & C_y^2 & C_yC_z & -C_yC_x & -C_y^2 & -C_yC_z \\ C_zC_x & C_zC_y & C_z^2 & -C_zC_x & -C_zC_y & -C_z^2 \\ -C_x^2 & -C_xC_y & -C_xC_z & C_x^2 & C_xC_y & C_xC_z \\ -C_yC_x & -C_y^2 & -C_yC_z & C_yC_x & C_y^2 & C_yC_z \\ -C_zC_x & -C_zC_y & -C_z^2 & C_zC_x & C_zC_y & C_z^2 \end{bmatrix}$$

where,

C_x,C_y and C_z are direction cosines with respect to X,Y and Z axes.

A=cross sectional area

E=modulus of elasticity

L=member length

It is clear that the three axial displacements (δ_x,δ_y and δ_z) are similar to those u,v and w of the plate and the beam elements at any node of the

structure. Therefore, two (zero) deformations stand to match Θ_x and Θ_y of the plate and the beam elements at any node of the structure. Therefore, the third and the fourth rows and columns of the [EK3] are zeros.

2.3 Loading

The uniformly distributed loading applied on the plate is considered to be divided equally on the sub elements which in turn work as concentrated loads acting on the corners of the sub elements. As the structure is divided in to smaller elements, the loading becomes more representive of the actual uniformly distributed load.

2.4 Application

The program developed by the author, which was used to analyse the composite space frame structure, was originally a beam program for solving plane beam and truss elements (22). It has been developed here to solve some cases of plates in flexure with different boundary conditions. The results are listed in Tables 2.1, 2.2 and 2.3 for the cases of simply supported plate, clamped plate and plate supported at corners respectively. The program is also used to check plate bending with edge beam connection. The results are shown in Table 2.4. All the cases show that the program is working satisfactorily.

The solution of the system may be outlined as:

$$[SU]\ \{\delta\} = \{P\}$$

or,

$$\{\delta\} = [SU]^{-1}\{P\}$$

where,

$\{\delta\}$ is the deformation matrix of the structure.

$[SU]$ is the unrestrained global stiffness matrix of the whole structure.

$\{p\}$ is the load matrix of the structure.

and then,

$$[EK]_e\{\delta\}_e = [F]_e$$

where,

$[EK]_e$ is the matrix containing the element stiffness matrix.

$[\delta]_e$ is the matrix containing the element displacement matrix.

$[F]_e$ is the matrix containing the element end actions.

2.5 Composite Space Frame Worked Example

Having demonstrated that the program developed by the author worked satisfactorily for the cases referred to in section 2.4, it was then used for the analysis of the composite space frame considered by this work as follows.

Figures 2.12, 2.13 and 2.14 show the numbering of joints and elements of the composite space frame floor being solved by this analysis. Of the five deformations at each joint, only the unrestrained ones are numbered throughout all the joints of the space frame. The

restrained deformations are given the numbering of -1. This way of numbering is based on the local axes of the structure at each joint. They were transformed to the global axes in order to assemble the global unrestrained stiffness matrix for all the elements [SU]. This is necessary to solve for the structure joint deformations [δ] and then to calculate the end actions for each member [F] as is explained in section 2.4. The assemblage of the global unrestrained stiffness matrix is the result of the superposition of elements, that is adding beam and truss elements to the plate elements. This addition of elements which is followed here was first suggested by Zienkiewicz and Cheung (23). It is also discussed in reference 21. The computer program solves the structure for joint deformations and end actions for all the elements. The computer program is listed in Appendix c. The complete listing of the program, the data and the analysis results are presented in report (24). However, Tables 2.5 to 2.8 summarise some of the results of certain members. The maximum deflection found in the case of composite space frame is smaller than that found in the non composite case, and this is also true for all the joints (see Table 2.5). Referring to Tables 2.6 to 2.8, it is shown that all elements at the corner units are of smaller forces in the composite space frame case than in the space truss case. The vertical reactions are transferred into the supports through vertical shears in the case of the

composite space member rather than being transferred through the diagonals at the corners. For this reason, the axial forces in the corner diagonals are less in the composite space frame analysis. These observations are to be expected with the composite analysis.

With the results of the present analysis, the composite members could be designed more accurately since all the possible deformations and forces are considered. In addition to the axial loads which occur in the case of the non-composite space frame, there are moments and vertical forces as explained before, and they are shown in the results list. More accurate results are obtainable using this analysis considering the following comments.

2.5.1 Comments on the Analysis:

There are some assumptions taken with the present analysis which are to be considered in future development of the composite space frame program. These assumptions are as follows:

1. The rotated stiffness matrix of the truss element was taken as a special case as is stated earlier in section 2.2.3.
2. With the present loading case, no fixed end moments are considered in beam elements. Each beam element of the length of 1200 mm is considered individually as a complete beam

loaded at its ends, i.e. the whole span of the structure being analysed is considered to involve seven beams. If a whole span is to be taken as one beam loaded along its span, fixed end moments should be included.

3. If the structure is to be treated as considered by the present program (except the loads are to be applied within the 1200 mm) both remarks in 1 and 2 apply. The rotated stiffness matrix should be changed to the general case and the fixed end moments should be included.

4. The data preparation for the present analysis would take a significantly longer time in preparation if smaller elements are used. Therefore, it is recommended that a better form of data representation be developed and used in a future amendment of the program.

Although the result of the analysis can not to be directly compared to the experimental results, the maximum theoretical forces in the members, due to the ultimate loads, are well below the capacity of the section. For example, the maximum theoretical axial force is 86 kN for a vertical load of 3.40 kN which produces a moment (M_y) of nearly 1.0 kN-m for a composite member at the middle of an edge span (see list of results for beam element 60 and plate element 22). This compares to 500 kN (axial capacity) for a 45 kN lateral load (22.5 kN per node) which produced a

moment of 12.1 kN-m before failure of the composite space frame unit 3 (see Table 5.1). These results show that the structure is safe considering the ''light'' units only (the units of the smallest sizes of both top-chord angle components and diagonals as defined in chapter one).

It may also be concluded at the end of this chapter that other geometries and spans could be investigated in the future to possibly optimize the shape of the composite space frame for particular loadings and spans.

TABLE 2.1 SIMPLY SUPPORTED ISOTROPIC SQUARE PLATE UNDER UNIFORM LOAD

Work	Elements	Lateral Deflection	$M_x = M_y$
Author	6 x 6	0.00401	0.0483
Refs.19& 20	6 x 6	0.00401	0.0483
Ref. 25	(Exact)	0.004062	0.0479
Multiplier		qL^4/D	qL^2

TABLE 2.2 CLAMPED ISOTROPIC SQUARE PLATE UNDER UNIFORM LOAD

Work	Elements	Lateral Deflection	Maximum Negative M	Maximum Positive M
Author	6 x 6	0.00133	-0.0496	0.02496
Refs.19& 20	6 x 6	0.00133	-0.0496	0.0249
Ref.25	(Exact)	0.00127	-0.0513	0.0213
Multiplier		qL^4/D	qL^2	qL^2

TABLE 2.3 ISOTROPIC SQUARE PLATE SUPPORTED AT CORNERS UNDER UNIFORM LOAD

Work	Finite Element	point (1)		Point (2)	
		Lat. Def.	Moment	Lat. Def	Moment
Author	6 x 6	0.0171	0.149	0.0245	0.111
Refs. 23&26	6 x 6	0.0173	0.150	0.0244	0.109
Ref.27		0.0170	0.140	0.0265	0.109
Multiplier		qL^4/D	qL^2	qL^4/D	qL^2

Point (1):centre of side, and
Point (2):centre of plate.

TABLE 2.4 ISOTROPIC SQUARE PLATE WITH EDGE BEAMS SUPPORTED AT CORNERS UNDER UNIFORM LOAD

Work	Finite Element	point (1)		Point (2)	
		Lat. Def.	Moment	Lat. Def	Moment
Author	6 x 6	0.0037	0.0334	0.0084	0.0618
Ref.23	6 x 6	0.0037	0.0332	0.0083	0.0611
Ref.25				0.0087	0.0601
Multiplier		qL^4/D	qL^2	qL^4/D	qL^2

Point (1):centre of side, and
Point (2):centre of plate.

TABLE 2.5 COMPARISON OF NODAL DEFLECTIONS IN SPACE FRAME WITH CORRESPONDING NODAL DEFLECTIONS IN COMPOSITE SPACE FRAME

Node No.	C. 1. Deflection (mm)		% of Difference
	Space Frame *	Comp. Space Frame	
65	9.17	7.57	21
72	15.3	12.7	20
79	18.8	15.8	19
86	20.0	16.8	19
87	20.5	17.4	18
88	21.0	17.9	17
89	21.2 *	18.1	17

* These deflection values are found with all the internal and the external members of the space frame are double angles back to back. If the external members considered of only one angle, the deflections of all the joints increase, and the maximum deflection would be, for example, 23.5.

TABLE 2.6 COMPARISON OF AXIAL FORCES IN SPACE FRAME TOP-CHORDS WITH CORRESPONDING COMPOSITE MEMBERS IN COMPOSITE SPACE FRAME

Member No.	Axial Force (kN)		Rem.
	Space Frame	Comp. Space Frame	
57	42.25	39.76	
58	71.66	70.37	
59	83.04	83.48	
60	86.06	87.01	
64	1.76	0.06	Tension
65	22.70	21.83	
66	36.89	34.62	
67	41.26	39.83	
22	1.76	1.70	Tension
23	1.05	0.82	=
24	2.03	1.94	
25	3.69	3.41	

TABLE 2.7 COMPARISON OF AXIAL FORCES IN SPACE FRAME DIAGONALS WITH CORRESPONDING DIAGONALS IN COMPOSITE SPACE FRAME

Member No.	Axial Force (kN)		Rem.
	Space Frame	Comp. Space Frame	
1	101.14	95.18	Tension
2	26.51	21.60	
3	37.32	36.60	
4	37.31	36.98	
29	33.10	36.31	Tension
30	10.39	8.33	
31	6.99	9.72	
32	15.72	18.26	
33	32.05	30.65	Tension
34	10.46	8.63	
36	10.80	11.09	
57	11.51	13.13	Tension
58	3.55	3.17	
59	2.23	3.67	
60	5.72	6.27	
61	15.0	14.9	Tension
62	5.38	4.84	
63	3.72	4.20	
64	5.90	5.86	
65	9.47	9.44	Tension
66	3.96	3.66	
68	2.75	2.96	
85	1.51	2.21	Tension
87	1.51	2.19	
89	2.53	2.62	Tension
91	2.53	2.63	
93	2.23	2.11	Tension
95	2.23	2.11	
97	0.0	0.057	

TABLE 2.8 COMPARISON OF AXIAL FORCES IN SPACE FRAME TIES WITH CORRESPONDING TIES IN COMPOSITE SPACE FRAME

Member No.	Axial Force (kN)		Rem.
	Space Frame	Comp. Space Frame	
239	53.32	48.63	Tension
240	75.13	71.18	=
241	82.88	79.07	=
245	14.52	15.22	=
246	32.27	31.69	=
247	41.69	40.63	=
215	2.52	3.72	=
216	6.74	8.20	=
217	10.47	11.82	=

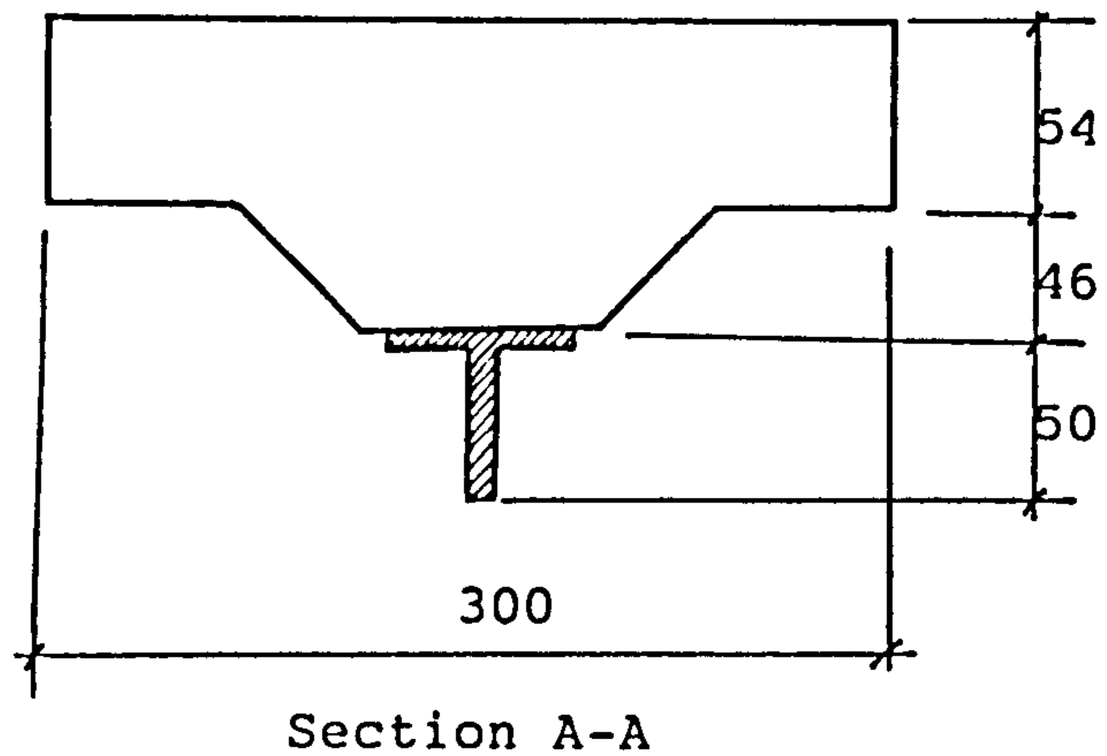

Section A-A

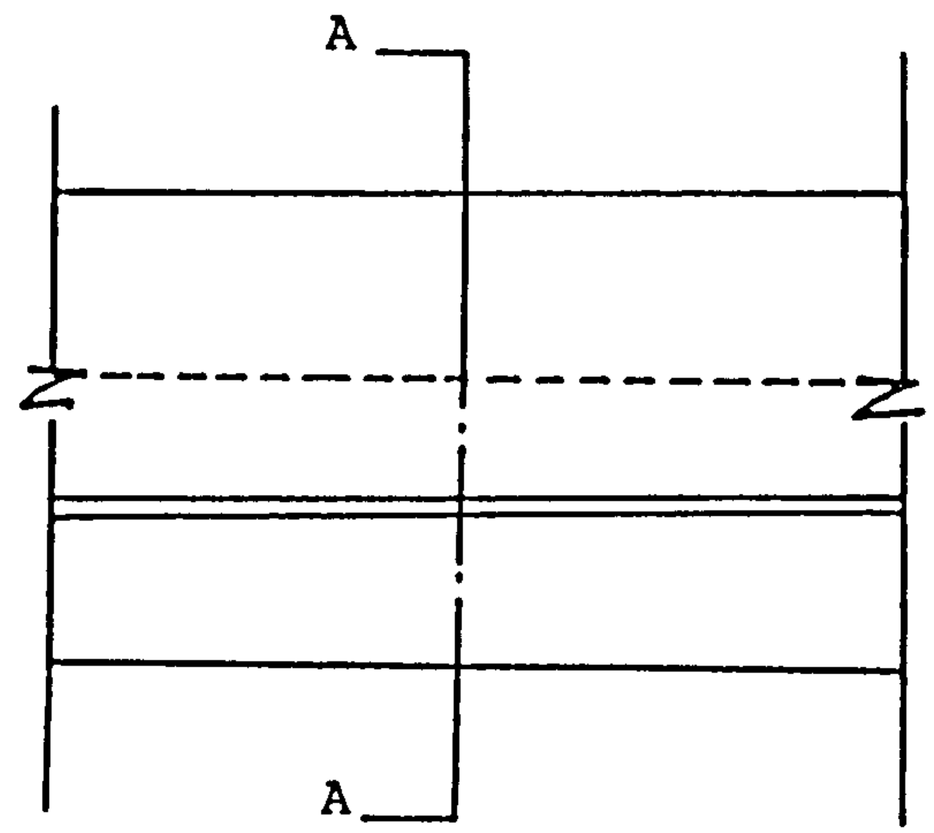

Fig. 2.1 Composite Beams with sheets parallel to them

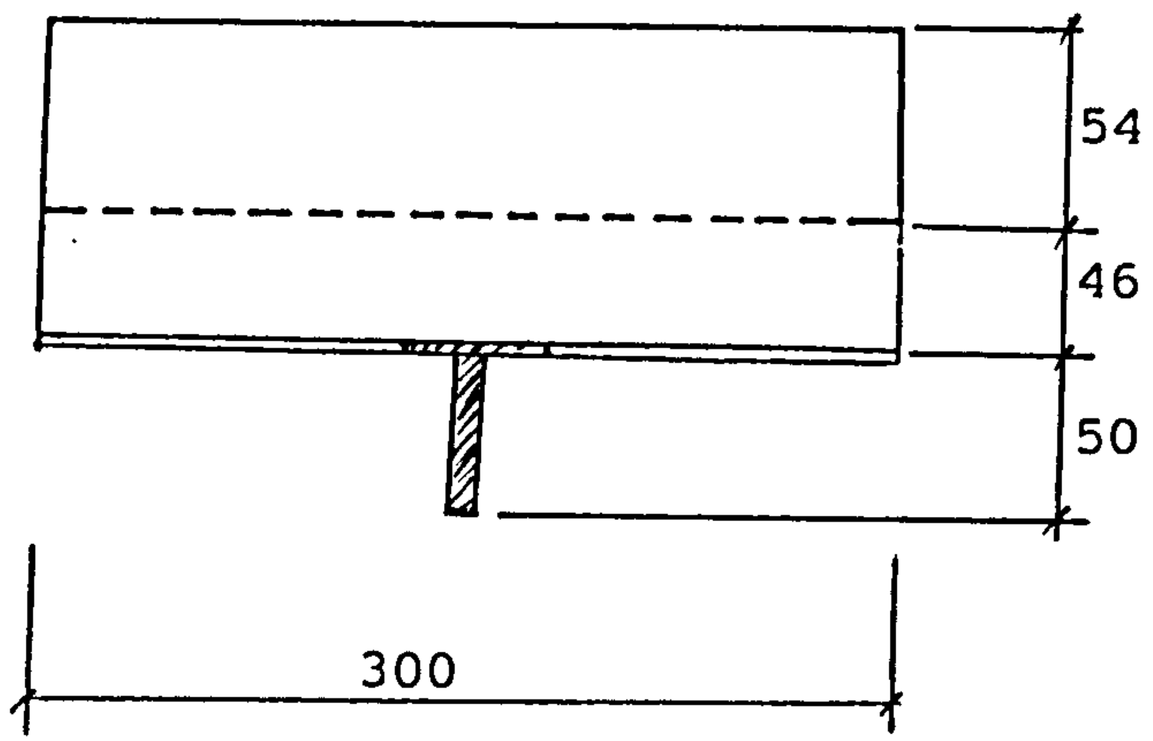

Section B-B

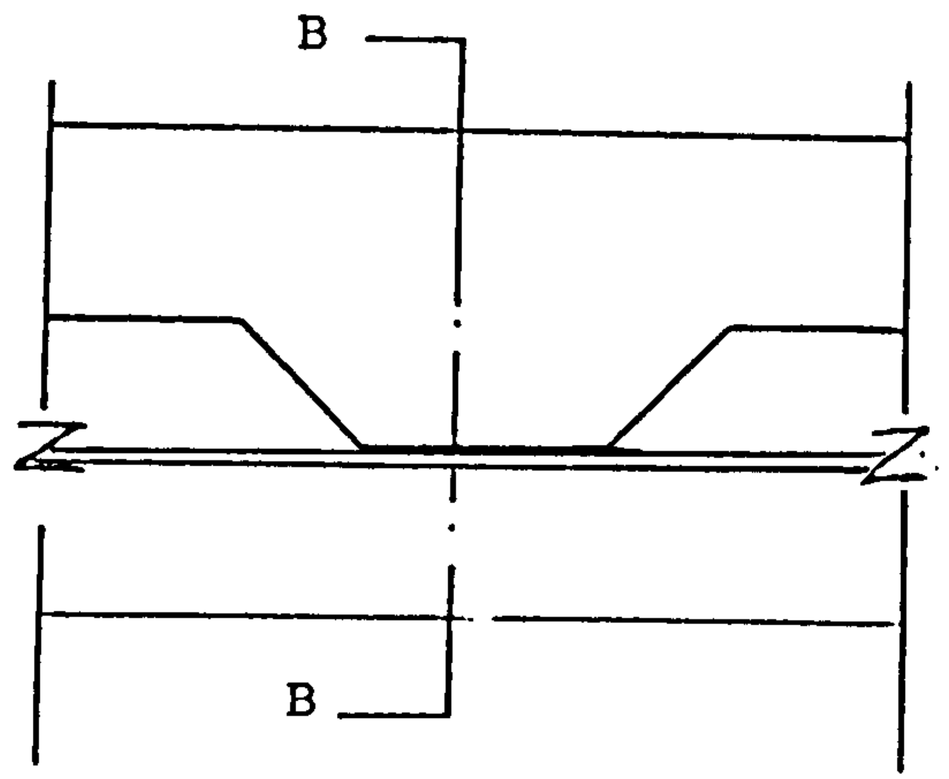

Fig. 2.2 Composite Beams with sheets running perpendicular to them

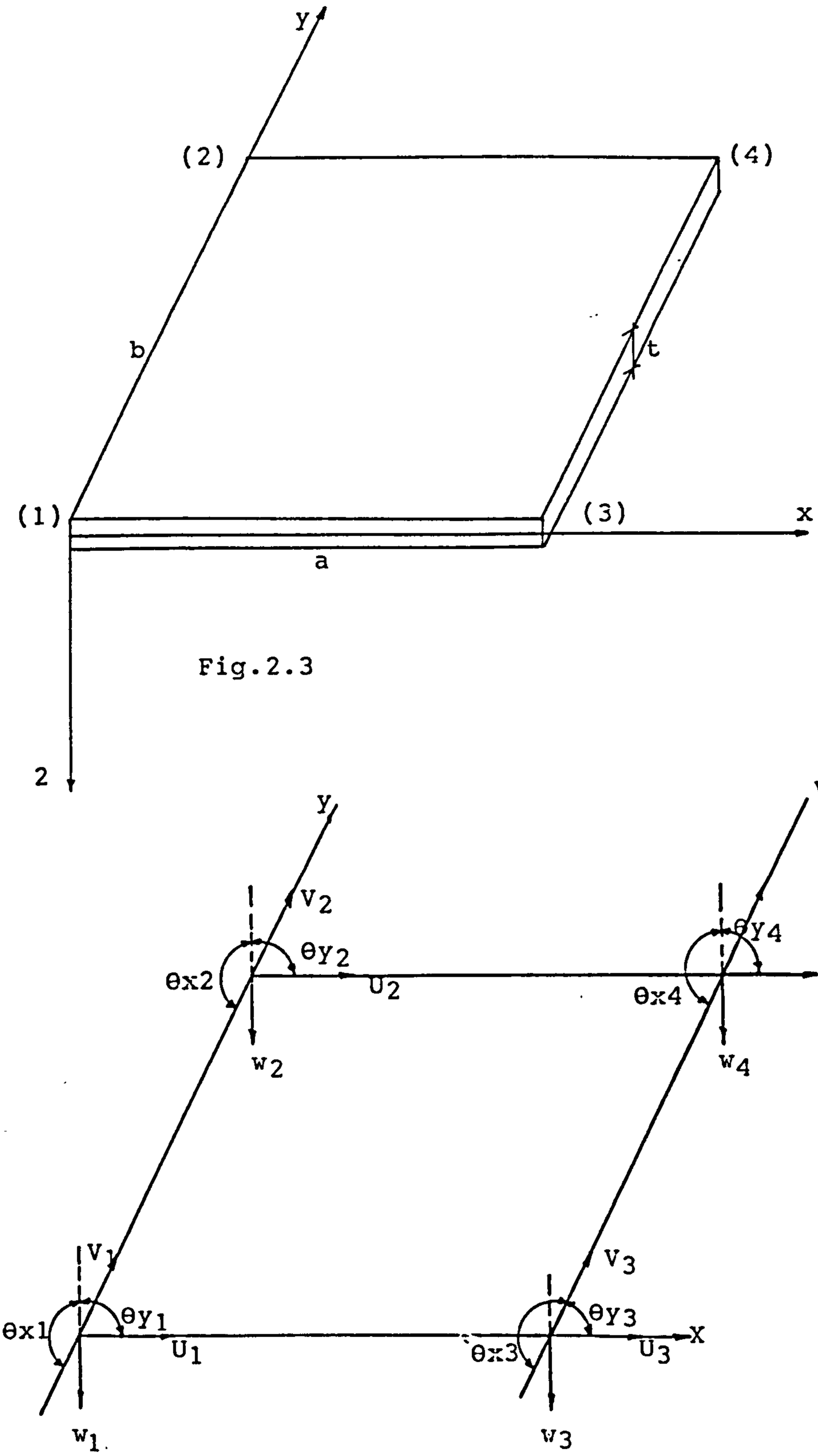

Fig.2.3

Fig. 2.4

Fig. 2.3 Plate Element co-ordinate numbering and dimensions

Fig. 2.4 Plate Element Nodal Displacements (Freedoms)

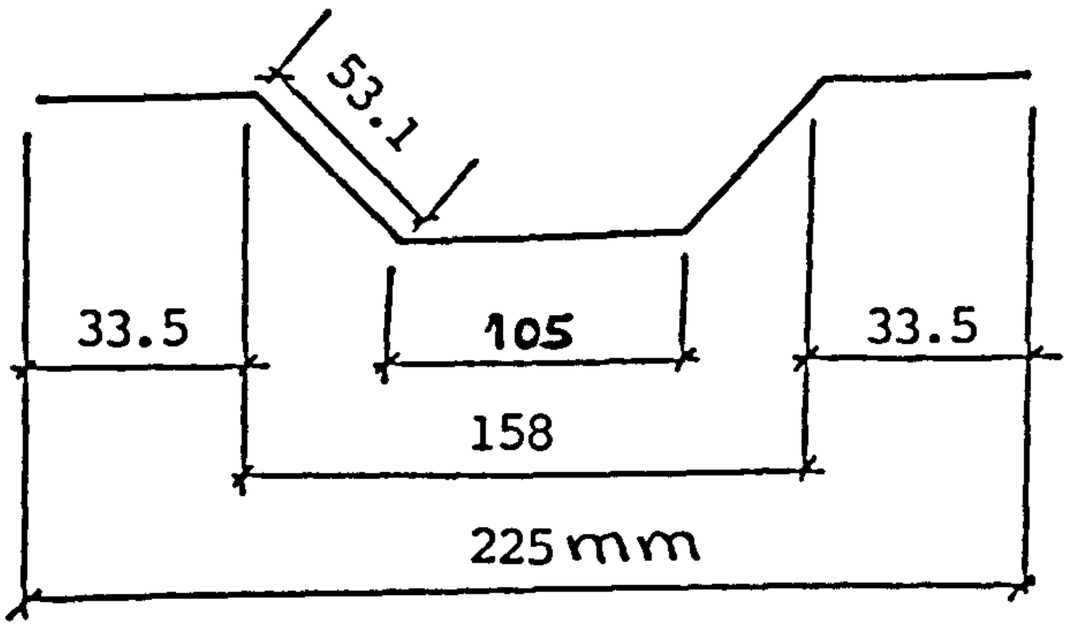

Fig.2.5: A Repeated Section of the Profiled Sheet

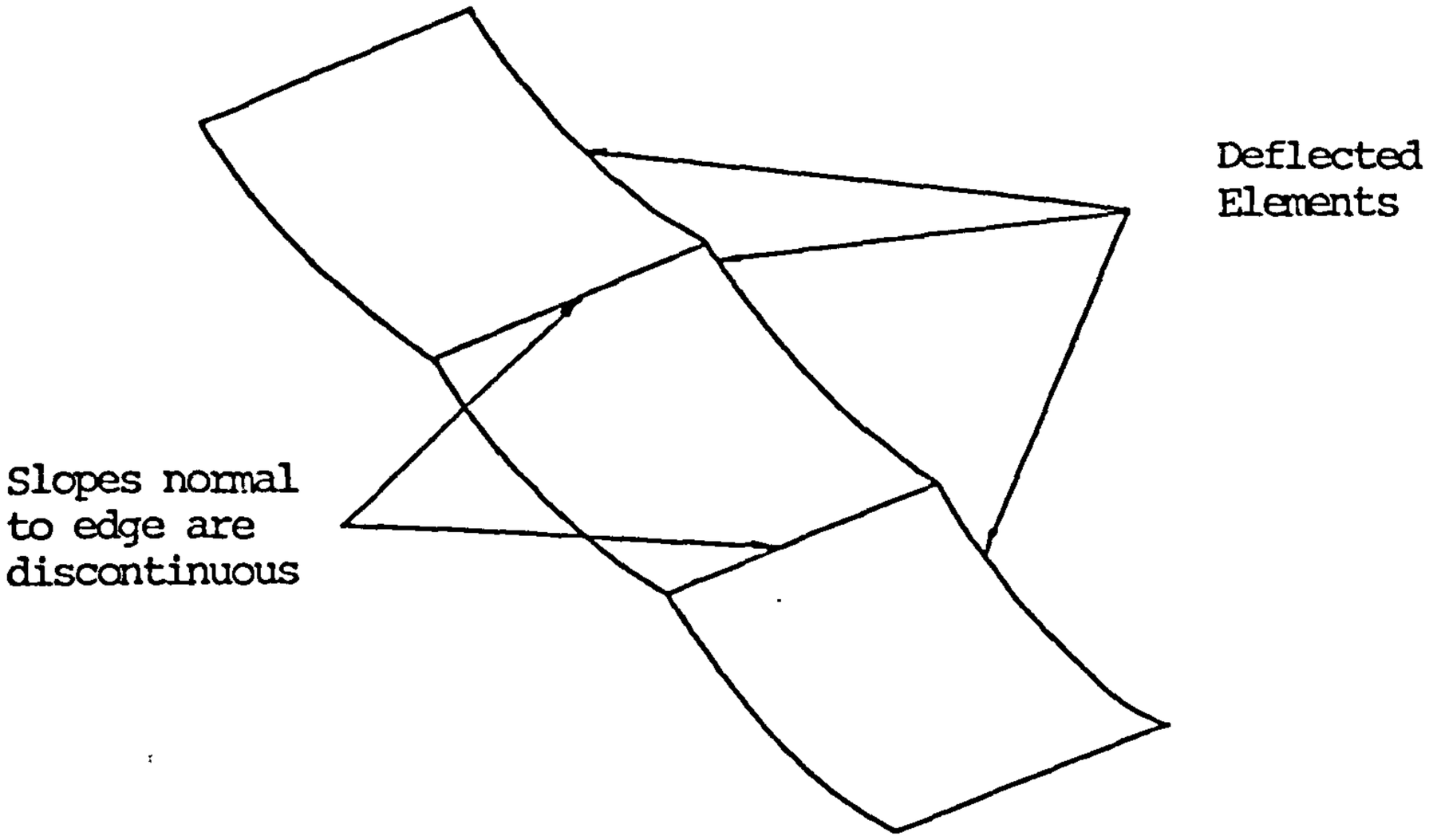

Fig.2.6: Discontinuity of Normal Slope

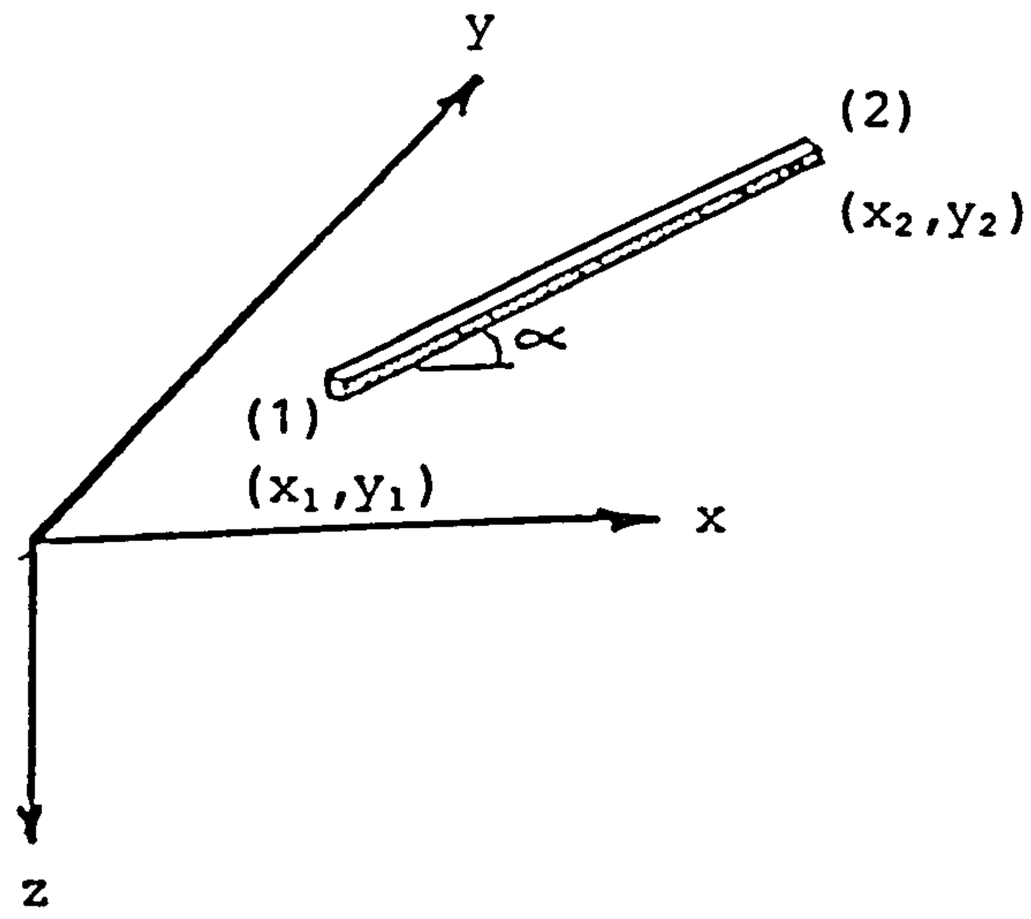

Fig.2.7: Beam Element Co-ordinates - Location and Numbering System

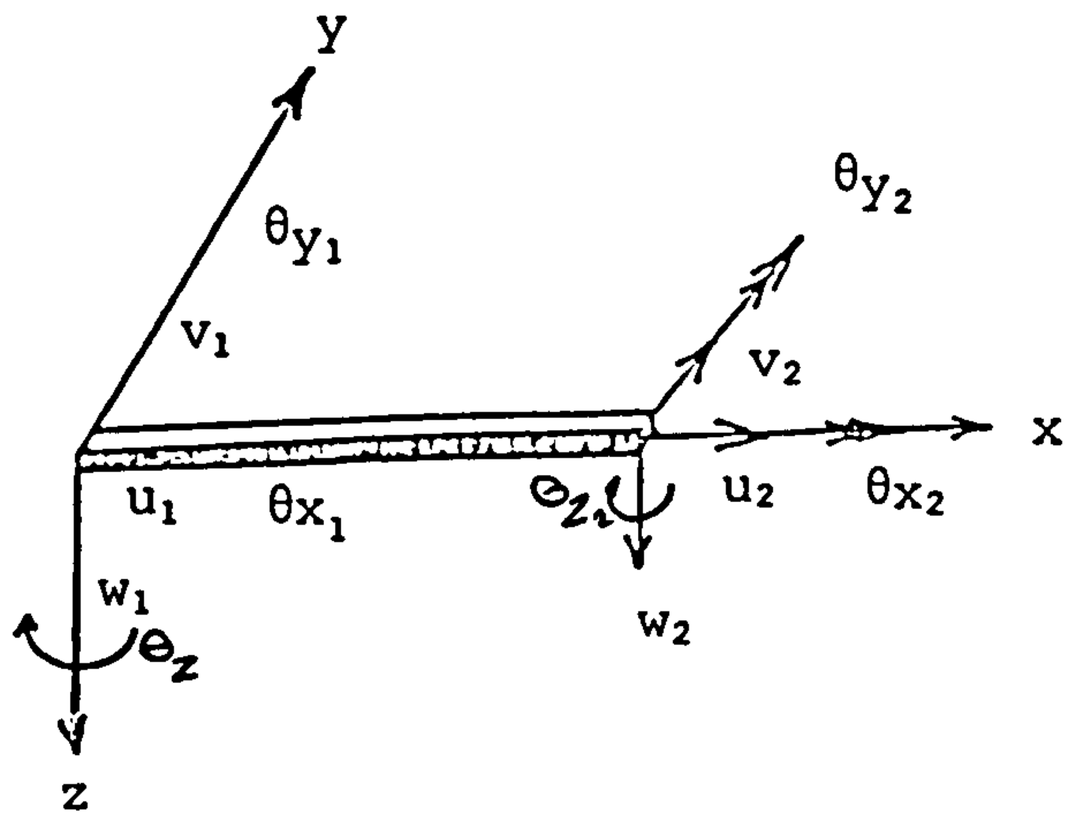

Fig.2.8: Beam Element Nodal Freedoms

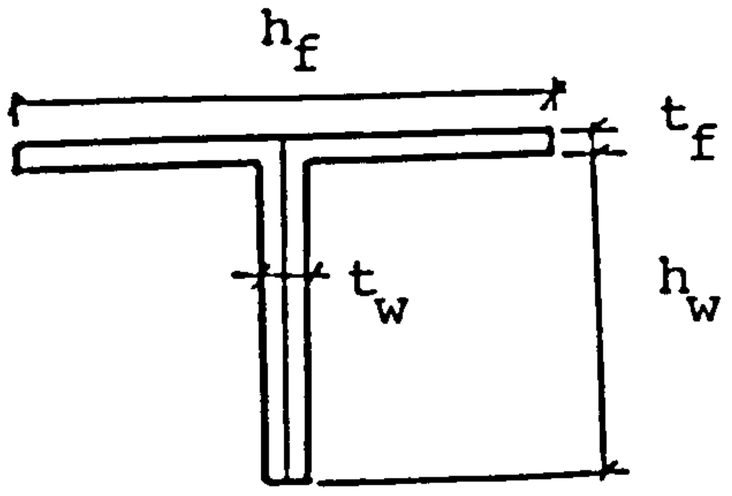

Fig.2.9a: Steel Cross Section

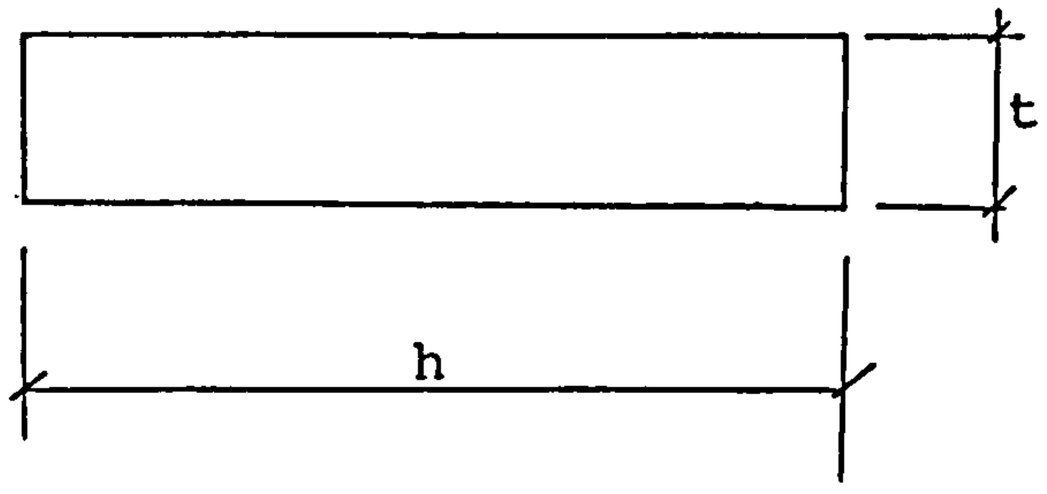

Fig.2.9b: Concrete Cross Section

(Used for Calculation of Torsional Constant)

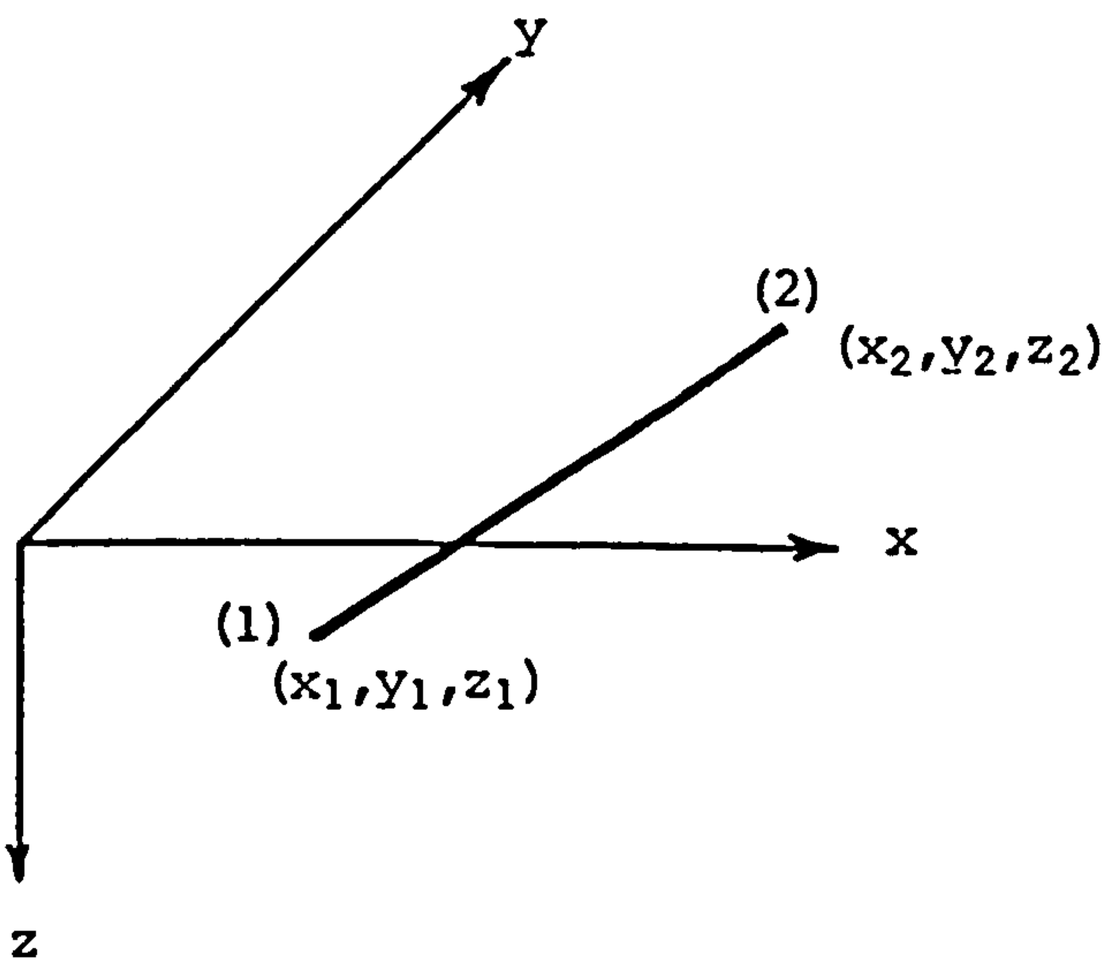

Fig.2.10: Truss Element Co-ordinates, Location and Numbering System

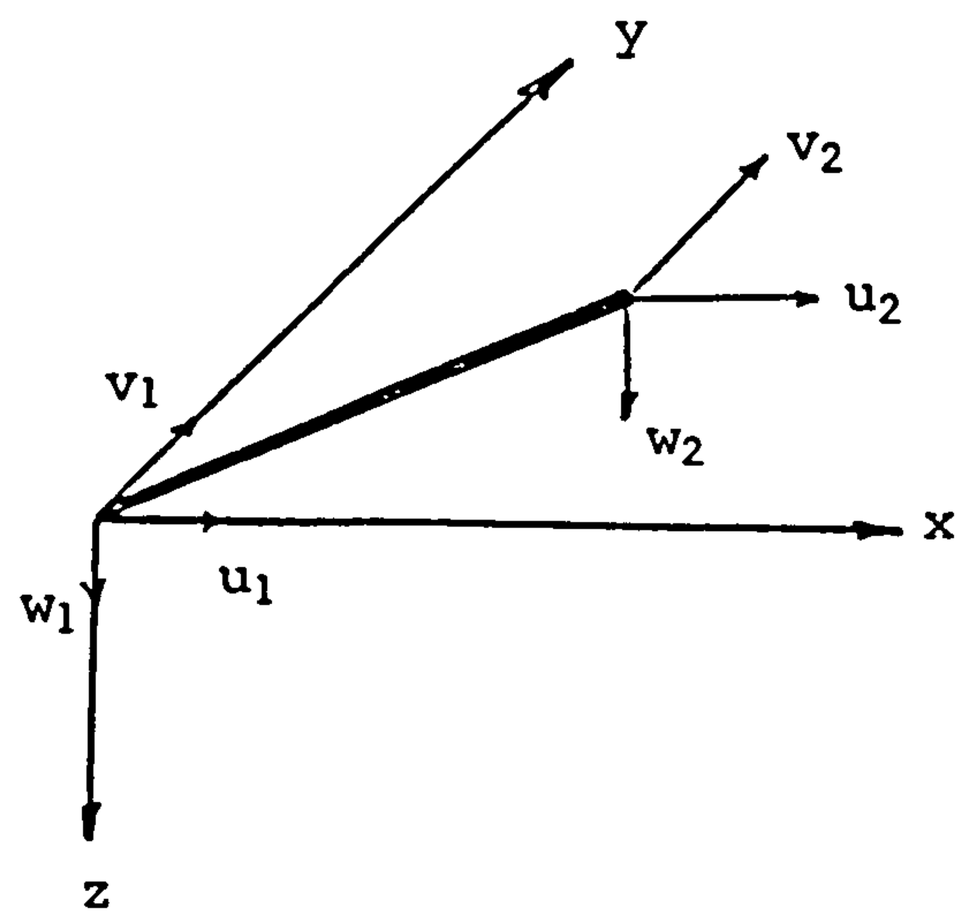

Fig.2.11: Truss Element Nodal Freedoms

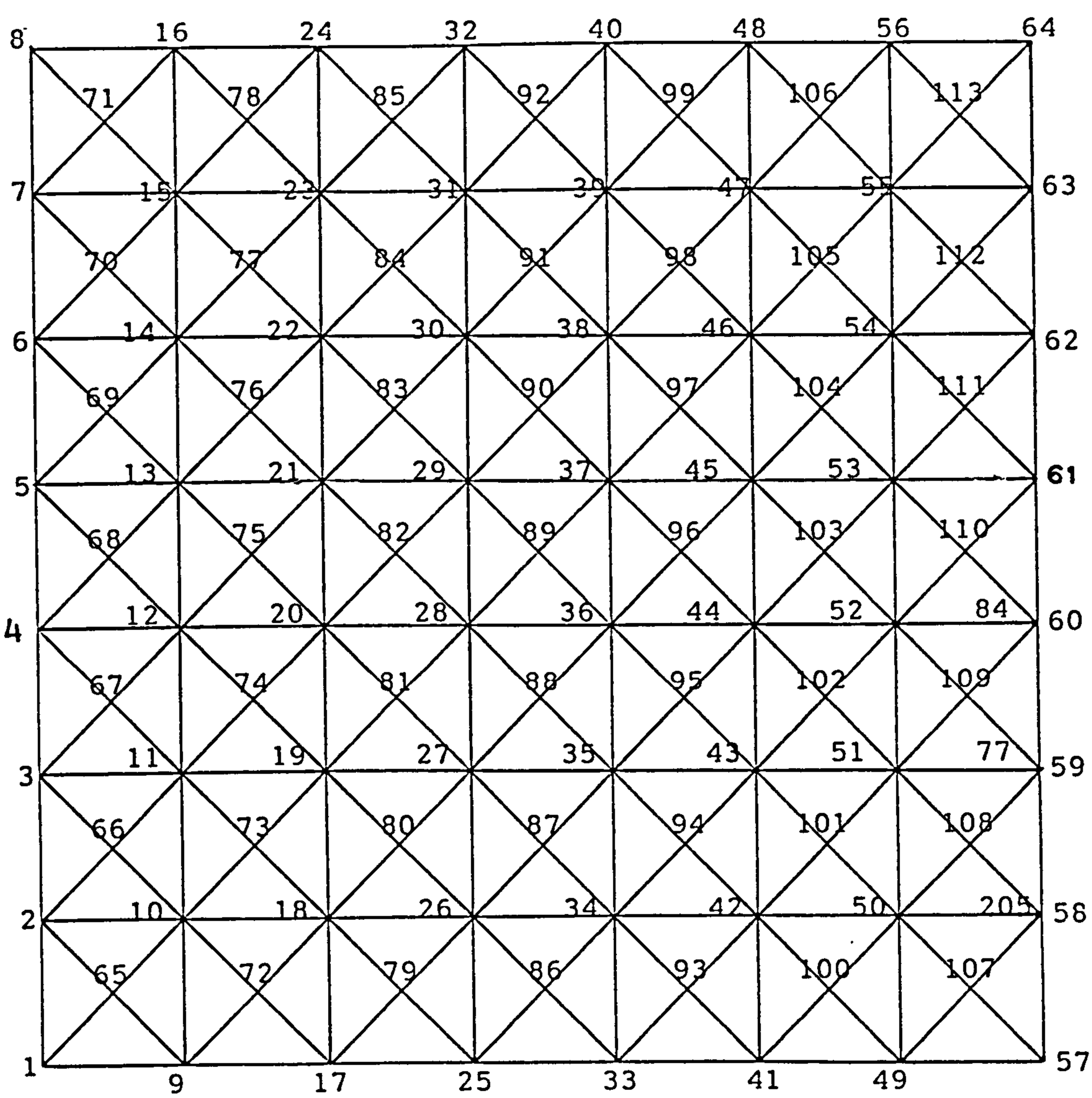

7 @ 1200 = 8400 mm

Fig. 2.12 Structure Dimensions & Node numbering

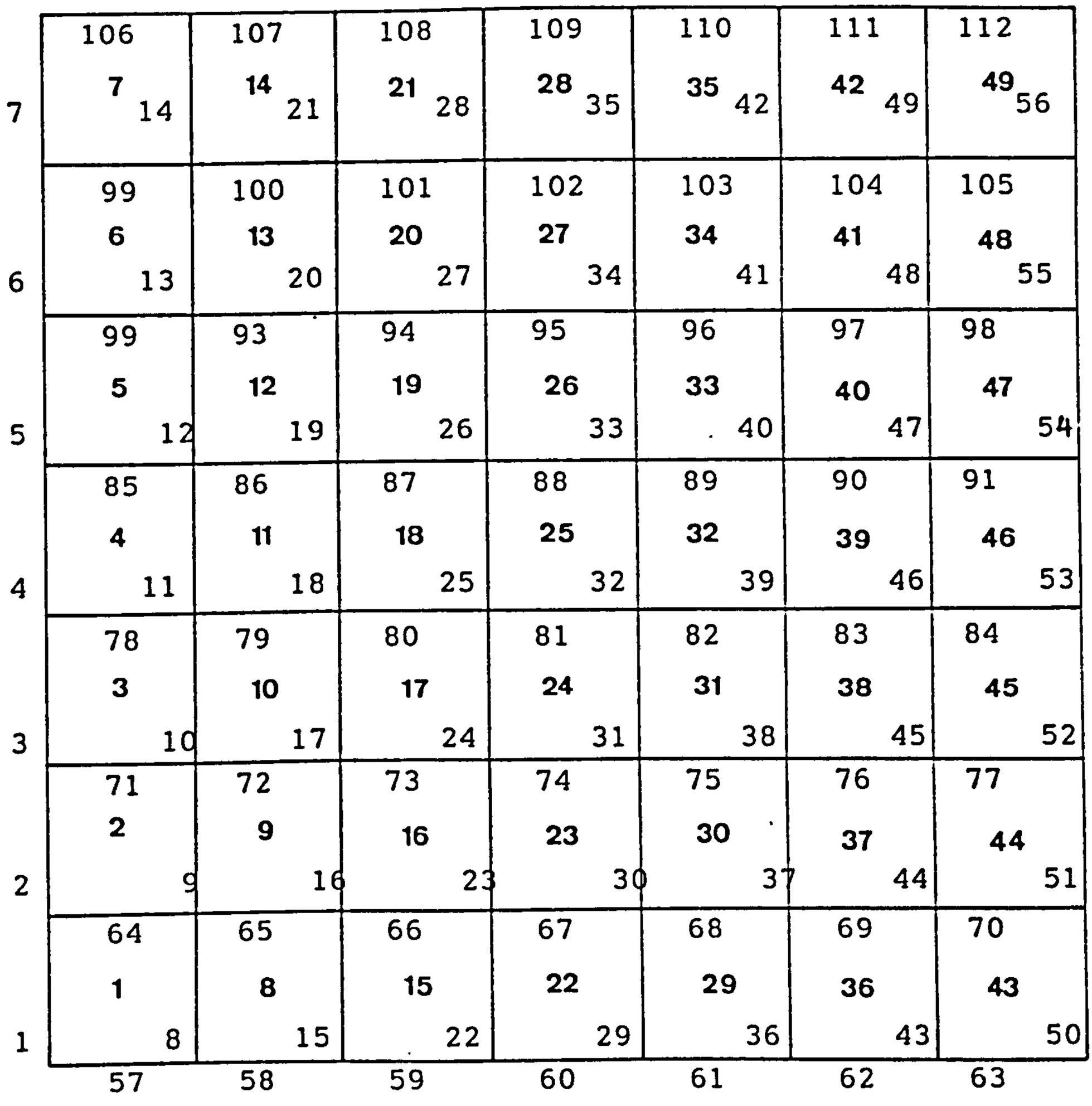

Fig. 2.13 Plate and Beam Elements Numbering

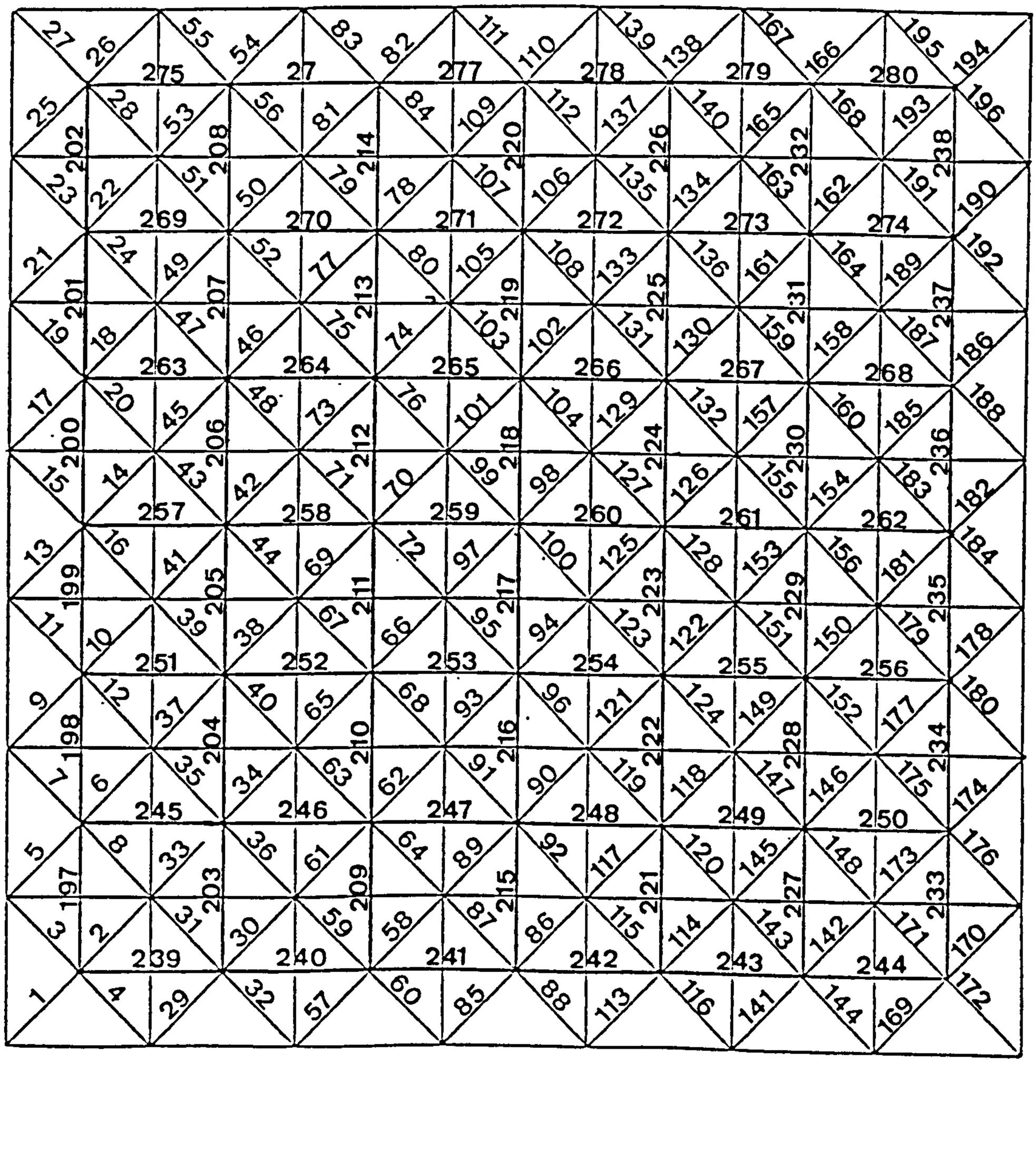

Fig. 2.14 Space Truss Elements Numbering

CHAPTER THREE

Testing Programme

3.1 Introduction

This chapter outlines the experimental work which includes the types of tests, the loading rig, test set-up, test objectives and descriptions.

The experimental programme consisted of different types of tests which are all related to the behaviour of composite T-beam. The programme was designed to provide information on:

(a) the effective width of the section as a T-beam which may be used as a guide in the theoretical work,

(b) the load carried by the composite section and

(c) the strain variation within the composite section, along and parallel to its centreline.

In all the tests, load versus deflection was recorded, and in most cases load versus strain was also recorded.

3.2 Loading Tests

3.2.1 Instrumentation

The strains and deflections of the top chord were measured for the test specimens by acoustic strain gauges and dial gauges respectively.

3.2.1.1 Strain measurements

Acoustic strain gauges (see Plate 3.1a and 3.1b) were used to measure strains in certain regions of the concrete slabs, the cold-formed steel profiles and steel double angles. Each acoustic gauge (vibrating wire gauge) comprises a steel wire inside a steel tube situated between two fixed steel blocks. The setting-up of the gauge required pretensioning the steel wire to a vibration value after having fixed the two steel blocks at ends to the required gauge length. When the specimen is subjected to load and a reading required, the tension wire is excited by a device fixed at the centre of the gauge, and signals are sent to the data logging equipment (see Plate 3.1b) to record it as the strain value at that certain applied load. Two gauge lengths of 2.5 and 5.0 inches were used throughout. The same acoustic gauges have been used successfully in similar work.

3.2.1.2 Deflection Measurements

Dial gauges reading to 0.01mm were used to read deflections at mid span and at span/4 from the ends of the top chord (the T-beam).

3.2.2 Test-Loading Rig

The test loading rig (see Plates 3.2a and 3.2b) was similar to the one used in Space Deck Limited series tests mentioned in the introduction. The two rigs only differ in either shape or size of the members used to construct them. The Salford rig comprises universal columns (204x204x73) and beams (203x133x73), and two angles (100x100x6) used for the purpose of squaring the rig base. All the elements were connected together by high strength bolts to produce a frame which supported horizontal and vertical jacks of 500 and 200 kN capacities respectively. The horizontal jack was bolted through its base and a bearing plate to one of the frame columns. Its weight was supported by a timber packing which maintained the jack horizontally. The timber packing was smooth so minimising any friction when the jack was operating. Because the jack had ball seats, the front end of the jack passed through a steel guide box to prevent it sliding to either side or jerking upwards during the test. The vertical jack was bolted to the top beam of the rig frame through its base and a bearing

plate, and was left to hang vertically. The horizontal jack could be adjusted in a way that the centroid of the jack coincided with that of the test unit. The vertical jack was already in position such that its centroidal axis was passing through the mid-span of the T-beam. The two jacks, which could be operated separately or simultaneously, were controlled by a Denison Console. The rig is, therefore, a self-straining frame, such that all the applied loads are taken by its members.

3.3 Test Set-up

Each one of the two individual units, which formed the space frame unit, was raised by the crane at each side of the mid-beam of the rig. The adjacent angles, which formed the top chord member, were bolted together. The two bosses of the individual units were also connected to each other by a horizontal tie in one direction while in the other direction (the perpendicular direction), each tie was located through holes made in the two base beams for this purpose. These latter ties were bolted at one side and left free at the other side. The dimensions of the tie spanning between the two bosses, was carefully measured. Each of the two ties spanning between the boss at one end and the hole, where the other end was bolted, was also carefully measured before tighting all the bolts. This ensured that the test specimen was horizontal and correctly positioned prior to testing (see Plates 3.3a

and 3.3b).

The test unit with this arrangement was assumed to represent two adjacent units of the actual structure where the top chord was mainly under axial compression due to loading. Several forms of test unit were used to simulate this situation of the the top chord within the rig. The top chord of these test units were simply supported at ends. The support near the horizontal jack was constructed as a roller. Hence, the vertical loading was applied at half the distance from the axis of the T-beam to the edges of the unit in the cases of the composite space frame units and the composite slab (see Figures 3.1a, 3.1b and 3.1c).

For the cases of the composite struts, the vertical loading was applied along the axis of the T-beam itself at L/4 from both ends. The axial loading for both cases was applied along the member at the centroid. The four corners of the composite slab rested on four I-sections to eliminate any interference in the deflection of the top chord. In other words, if the vertical load forced the end chords of the space frame unit to deflect, they in turn, would force the tie bar between the two bosses to shorten (to deflect upward) which would affect the deflection of the top chord considered. Therefore, the deflection of the top chord either in the upward or in the downward direction was mainly due to its characteristics and loading. This arrangement made it easy to place the steel profiles and to fix them to the

top-tray. Subsequently, the concrete slab was cast in place.

This arrangement also facilitated the testing of the top chord as a non-composite or a composite T-beam within the test unit and the replacement of one test unit with the next. Dial gauges, held by steel channels supported in a way not to be affected by the rig movement, were also easily placed at the required positions. The dial gauges were held in a way not to be affected by rig movement; however, there may be small effects due to support movement. This theoretical movement would be subtracted from or added to the deflection measured as described. However, this movement was assumed to be small and, therefore, neglected. Acoustic gauges were also attached at sections where strains were required and recorded on a data logger placed near to the rig itself.

3.4 Shear Connector Arrangement

With several different types of test, shear connectors were connected at positions on the basis of the lateral restraint of the top-chord, and three arrangements were considered. It was found that at least one lateral restraint was required within the top-chord length (1200 mm) as is shown in appendix A. It was then decided to attach the shear connectors:

(a) at L/4 from ends (see Figure 3.2a).

(b) at the centreline and at ends (see Figure 3.2b).

(c) at each rib of the profiled steel sheet (see Figure 3.2c).

The first arrangement considered the continuation of the top-chords in the actual structure so that the lateral restraints would be 600 mm apart. The second arrangement was similar except that the restraints were displaced towards the centreline and the ends of the top-chord. The two arrangements were assumed to satisfy the requirement of placing one lateral restraint within the top-chord length. The third arrangement was recommended by the feasibility study (11) mentioned in the introduction which was designed to give higher interaction between the composite slab and the top-chord members.

The composite space frame units 1 and 2, the composite unit and the composite strut (see Table 3.1) utilised the arrangement (a). Each had two connectors placed at each quarter span point except the composite space frame unit 2 which had four connectors at the quarter span point. Composite space frame unit 3 followed arrangement (c), with two connectors in each rib. Composite space frame unit 4 was constructed with arrangement (b) having four connectors placed in the two ribs on both sides of the composite T-section mid-span. They were placed as close as possible to the mid-span itself. In all the cases, the connectors were placed along the composite T-section as shown in Figures 3.2a, 3.2b and 3.2c. Moreover, one additional connector was

placed for each 1200 mm along the edges of the units.

3.5 Preliminary Tests

3.5.1 Non-composite Stage

At the beginning of testing it was found that the top chord member deflected upward when loaded with horizontal load alone or when loaded simultaneously with vertical and horizontal loads as will be discussed later. This feature was not considered to be a normal behaviour for the system, but it was found later that it was the normal response to the horizontal loading applied along the top chord member of the test unit.

The first preliminary test carried out on the test unit with no sheeting or concrete was to insure that all the axial load was transferred through the test member and was not transferred into the frame by another route. Constant vertical load (either 6, 8 or 10 kN) were applied simultaneously with a horizontal load being increased in increments of 10 kN (see Figure 3.3 and Plate 3.2a).

Centreline deflections at each horizontal load increment were recorded. This first test was arranged with acoustic gauges placed at the centre of the top chord (the double angles) to read the strains at each axial load increment. With the aid of these strains, which were recorded by a data logger, the corresponding loads were calculated at the top chord mid-span. These calculated loads were compared to the applied ones and

it was found that the correlation was acceptable for all load increments from zero to 100 kN. However, with some composite units tested later, two load cells (see Plate 3.1b) were also used to check if all the applied load transferred from one end of the member where it was applied to the other end of the composite T-beam. Again, it was found that the two loads were similar. The rest of the preliminary tests of the test unit with no sheeting or concrete were carried out to find the capacity of the top chord as a strut according to the Southwell method (28) . These preliminary tests, with their results are shown in appendix A. It should be mentioned here that the deflections with these preliminary tests did not show clearly any inversion from the downward to the upward direction, and that might be due to the fact that the test horizontal loading at that stage was not more than 150 kN.

3.5.2 Composite Stage

The composite specimens were tested in order to investigate the effect of loading on strains in areas along, near to and far from the composite T-section axes. Acoustic gauges were used, recording longitudinal and transverse strains along and parallel to both the longitudinal and the transverse axes of the composite T-section. Dial gauges also gave information on deflections at locations along the longitudinal axis of the composite T-section. Up to 23 acoustic gauges were

used in some runs to read strains at different locations when testing the first composite space frame unit.

At this stage, of the preliminary tests, the set-up for the testing work was considered to be acceptable to carry on the testing of the composite space frame specimens.

3.6 Summary Of Testing

Several different types of composite specimens were investigated in this work. They are listed and illustrated in Table 3.1. They are defined as follows:-

Preliminary (Group 1)	- Two space Deck units with no concrete or profiled steel sheet.
Composite Space Frame Unit (Groups 2 & 5)	-Four composite slabs with two top-trays, diagonals and ties.
Composite Unit (Group 3)	-A composite slab attached to two top-trays with no diagonals or ties.
Composite Struts (Group 4)	-Composite T-beams comprising top-trays and various widths of concrete flange and flat steel sheet.
Steel Struts (group 5)	-Two groups of steel struts formed from the top-tray angles.

When the first space frame unit was tested, upward deflection of the composite T-beam was observed at some stages of the axial loading. Using the different types of tests mentioned in Table 3.1 and the accompanying Figure, an investigation and a confirmation of this behaviour within the unit was carried out. A summary of these tests is to follow.

A composite steel/concrete slab attached to the top-trays of the unit with no diagonals and ties (a composite unit) was tested in the same way as the first composite space frame unit, and a similar deflection behaviour was found. The deflection was downwards at first, due to the vertical load, but at a certain value of the axial load it began to reverse and go upwards with the axial load increment until failure. Four composite struts cut out of eight trays were tested in two groups of two differing from each other in width of concrete flange. The same behaviour was again found for the deflection direction for all the eight composite struts. All the above tests were carried out with the same rig.

Ten steel angle struts cut out of ten trays were prepared for testing in compression with Losenhausenwerk testing machine in two groups of five. The two groups differed in the length of legs bolted back to back. The two groups also differed from each other in length. When they were cut out of the top-trays, one group was cut with the full length of the tray (1200 mm) while the

other group had a length of 1120 mm. Each strut of the first group composed of two angles connected with the two long legs back to back which was the actual connection of the top chords in the actual structure. The angles of the second group were connected with the short legs back to back. The steel struts were prepared with plates welded at their ends so that the load was applied axially at the centroid. The first group buckled to the side (the side of the top chord in its actual situation in the actual structure) at failure while the second group buckled to the downward direction. At this stage, the testing of the rest of space composite units continued with the acceptance of the reversed deflection to be related to the T-section within the unit.

The composite space frame units were the same except in the number and/or the spacing of shear connectors used to attach the profiled steel sheet to the top chord member as explained above in 3.4. All the four composite struts where also similarly prepared with the same number and spacing as that of the first composite space frame unit; however, they differ in that they had a flat galvanised steel sheet instead of a profiled steel sheet.

In all the composite space frame units tested, the profiled steel sheet was running perpendicular to the composite struts which is the critical case.

3.6.1 Composite Space Frame Unit 1 (CSFU1):

The space frame, analysed by the space frame program, was assumed to be loaded at the joints which represented external loading and the program gave the internal axial forces in the members due to these applied joint loads. Based on these values, a sequence of tests (up to ten runs) was carried out. The dead load, which represented the weight of the structural elements on the truss floor, was considered together with the live load as a vertical applied load on the top joints of the truss. The space frame program was used for this step (the beginning of the first test). The applied forces (loads) are entered in to the program as data while the internal axial forces are produced as results. The structure was analysed for several cases of different applied loads, and in each case, the composite space frame unit was tested in the way that the vertical jack exerted a constant vertical load on the specimen, equal to that entered as data, while the horizontal jack exerted horizontal load in increments up to the maximum value of the internal axial force found by the program for the critical top-chord member. Table 3.2 shows the sequence of the ten cycles where the applied vertical and horizontal loads are shown for each run.

The first value of the live load considered was 4 kN/node, that is 8 kN for the specimen comprising two units. This was the force which the vertical jack was to

apply at first. It should be noted here that the dead load was already applied (the composite slab weight) which is different from the case analysed by the space frame program which assumes the live and the dead loads applied as joint loads. With this sequence of testing, a large amount of information was gathered from the first composite space frame unit, before the final test to failure. The information gathered in this way was helpful in the testing of the rest of the specimens. It should be noted that the critical top-chord member considered was the one identified as carrying the maximum internal axial force found by the space frame program (the middle edge member).

21 acoustic gauges were used in one arrangement to read strains at different locations on the steel top chord and on the concrete. Four other arrangements of acoustic gauges (up to 23 gauges) were also used with this composite space frame unit. Three dial gauges were placed below the composite section along its longitudinal axis to read the deflections at the mid-span and at the distances of L/4 from each of the two ends (see Figure 3.4).

3.6.2 Further Composite Frame Specimens:

The rest of the composite frame units were tested using up to 16 acoustic gauges and three dial gauges. The composite unit (the composite slab which was attached only to top-chords without diagonals) was

tested in a similar way. The centreline deflection and the longitudinal and the transverse strains along the longitudinal and the transverse axes of the T-beam were measured. The rest of the composite space frame units (composite slabs attached to space frame top-chords, diagonals and ties) were tested considering the centreline deflection and strains along the longitudinal and the transverse axes within a T-beam width up to 800 mm (400 mm to each side of the longitudinal axis). The four composite struts were tested considering the measurement of the centreline deflection and the longitudinal strains along the longitudinal axis.

All the composite specimens were of a total slab depth of 100 mm. They were also tested when the concrete strength was more than 25 kN/mm^2, generally achieved after approximately two weeks.

3.6.3 Steel Struts

The steel struts were tested in compression. The deflections either downwards or upwards and to the side of each strut were measured. Two dial gauges were used to measure deflection at the centreline relative to the two major axes which represent downwards or upwards and to either of the sides of the double angles in the actual structure. The set-up for these tests is shown in Plate 3.4.

3.7 Loading

The vertical loading was first applied, and it was kept constant through the test. For the cases of the composite slabs, it was distributed by two timber beams. The two beams were laid parallel to the longitudinal axis of the T-beam at distances of 600 mm to each side of the longitudinal axis. Each beam was placed on four timber spacers which ensured the load was distributed along the the two main axes of the two timber beams. The horizontal load was applied in increments at the centroid of the T-beam. A steel plate of the same width of the column of the rig, and of the same depth of the composite slab was used to distribute the horizontal load on to the end of the specimen. The same idea was followed in testing the composite struts except that the vertical load was half of that of the composite slab cases, and it was directly applied on the longitudinal axis of the T-beam at L/4 from each end.

3.8 Materials And Material Control Tests

3.8.1 Profiled Steel Sheet

PMF C46 steel sheets of trapezoidal profile (see Figure 3.5) were used throughout the experimental work except for the cases of composite struts where flat steel sheets were used. A total of 56 tensile specimens cut longitudinally along the ribs of one of this type of profile sheet were tested, and the tests results summary

is shown in Table 3.3.

3.8.2 Flat Galvanised Steel Sheet

Z28 galvanised steel sheets of characteristic yield strength of 280 kN/mm² and of the thickness of 1 mm was used with the four composite struts.

3.8.3 Steel Angles

Four tensile specimens were taken from four steel angles of one tray and tested. The results of these tests are shown in Table 3.4.

BS18 (29,30) was observed in testing all steel specimens.

3.8.4 Shear Connectors

The connectors which were used through out all the experimental work were of the self tapping and screw type (see Plate 3.5). The connectors were fixed using an electric drill.

3.8.5 Concrete

Ordinary Portland Cement and crushed gravel aggregate of maximum size of 10 mm was used to produce normal concrete mixes of good workability and with a nominal characteristic strength of 30 N/mm² at 28 days. The concrete mix proportions were 1: 2 : 4 that is cement: fine and coarse aggregates respectively with the W/C of 0.60. The concrete, which was mixed using a

horizontal pan-type mixer, was poured in to the slab mould placed where the slab was to be subsequently tested. The concrete slab together with the control specimens were left to to cure in the laboratory environment. The concrete control specimens consisted of 100 mm standard cubes, 150 x 300 mm cylinders and 100 x 100 x 500 mm beams and all the specimens were trowel finished. BS1881 (31) was observed in making and testing concrete. Table 3.5 shows the properties of the concrete control specimens. It should be noted that the sides used during the casting of the composite units were left on except for composite struts and CSFU4, It was assumed that this would have little influence the strength of the units tested.

3.8.6 Steel mesh

Anti-crack steel mesh (A142) was used in the top of all the composite slabs and struts (cover distance = 25mm).

TABLE 3.1 TEST TYPES *

Group No	Test Type	Test description
1	Preliminary	A two-unit steel specimen was tested according to Southwell method.
2	Composite Space Frame Unit.	The above Test Unit was tested with a composite steel/ concrete slab attached to it .
3	Composite Unit.	The unit was tested similar to the previous case, but no ties and diagonals were attached to the composite slab.
4	Composite Struts.	Two groups of composite struts cut out of the top-trays were tested. The two groups differ in their widths.
5	Composite Space Frame Units.	Another three complete composite units were tested.
6	Steel struts	Two groups of steel struts cut out of the the top-trays were tested. The two groups were mainly differ in the length of the two legs connected back to back.

* see Figure 3.6

TABLE 3.2 SEQUENCE OF TESTS FOR GROUP TWO (TABLE 3.1)

Run No.	Vertical Load (kN)	Axial load in the top chord (kN)
1	8.00 (working load)	80.00 (working axial)
2	8.00	80.00x1.5
3	8.00x1.5 (ultimate vertical)	120.0 (ultimate axial)
4	12.00	120.0x1.5
5	12.0x1.5	180.0
6	18.00	230.0
7	18.0x1.5	280.0
8	27.00	300.0
9	27.00	350.0
10	40.00	350.0

TABLE 3.3 COMPOSITE SLAB - STEEL DECK PROPERTIES

Specimen No.	Gross Thickness	Core Thickness	Yield Load kN	Yield stress N/mm²	Ultimate Load kN	Ultimate stress N/mm²
1	1.167	1.121	3.99	284.9	5.24	374.2
2	1.161	1.121	4.02	287.1	5.23	373.0
3	1.157	1.122	3.95	282.1	5.21	371.8
4	1.167	1.122	3.97	283.4	5.20	370.6
5	1.167	1.126	4.02	286.2	5.25	373.3
6	1.171	1.134	3.98	280.8	5.22	368.5
7	1.166	1.128	4.06	287.7	5.30	375.8
8	1.171	1.129	3.97	281.8	5.28	374.3

* All the values shown in the table are the average of seven samples.

TABLE 3.4 TENSILE PROPERTIES OF STEEL ANGLES

Specimen No.	Thickness mm	Yield Load kN	Yield Stress N/mm^2	Ultimate Load kN	Ultimate Stress N/mm^2	M.O.E kN/mm^2
1	6	48	320.0	76	506.7	217
2	6	46	306.7	69	460.0	207
3	6	48	320.0	72	480.0	216
4	6	50	333.3	75	500.0	214

Average Yield Stress f_y=320 N/mm^2

Average Ultimate Tensile Strength f_t=487 N/mm^2

Average Modulus Of Elasticity E=214 kN/mm^2

TABLE 3.5 PROPERTIES OF CONCRETE CONTROL TESTS

Test specimen	Slump (mm) *	Cube Strength f_{cu} (N/mm^2)		Properties at the time of tests			
		7 days	28 days	Age Of Slab(Days)	Cube Strength f_{cu}(N/mm^2)	Young's Modulus E_c(kN/mm^2)	Modulus Of Rupture (N/mm^2)
CSFU1	27	26.7	—	—	37.3	33.4	2.51
CU		24.0	—	—	31.3	27.6	2.38
CS1/CS2		25.2	33.1	30,37	35.6,36.3	23.4	2.50
CS3/CS4		23.9	32.4	18,21	26.3,29.8	24.9	2.26
CSFU2		26.4	36.4	20	32.0	28.6	2.43
CSFU3		31.0	37.3	16	35.4	32.0	2.56
CSFU4		29.0	35.6	18	32.9	30.3	2.51

CSFU1 to CSFU4- Composite space frame units 1,2,3 and 4.

CU - A composite unit.

CS1 to CS4 - Composite struts 1,2,3 and 4.

Average Modulus of Elasticity E_C= 28.6 kN/mm^2.

* Slump is the average of all the mixes.

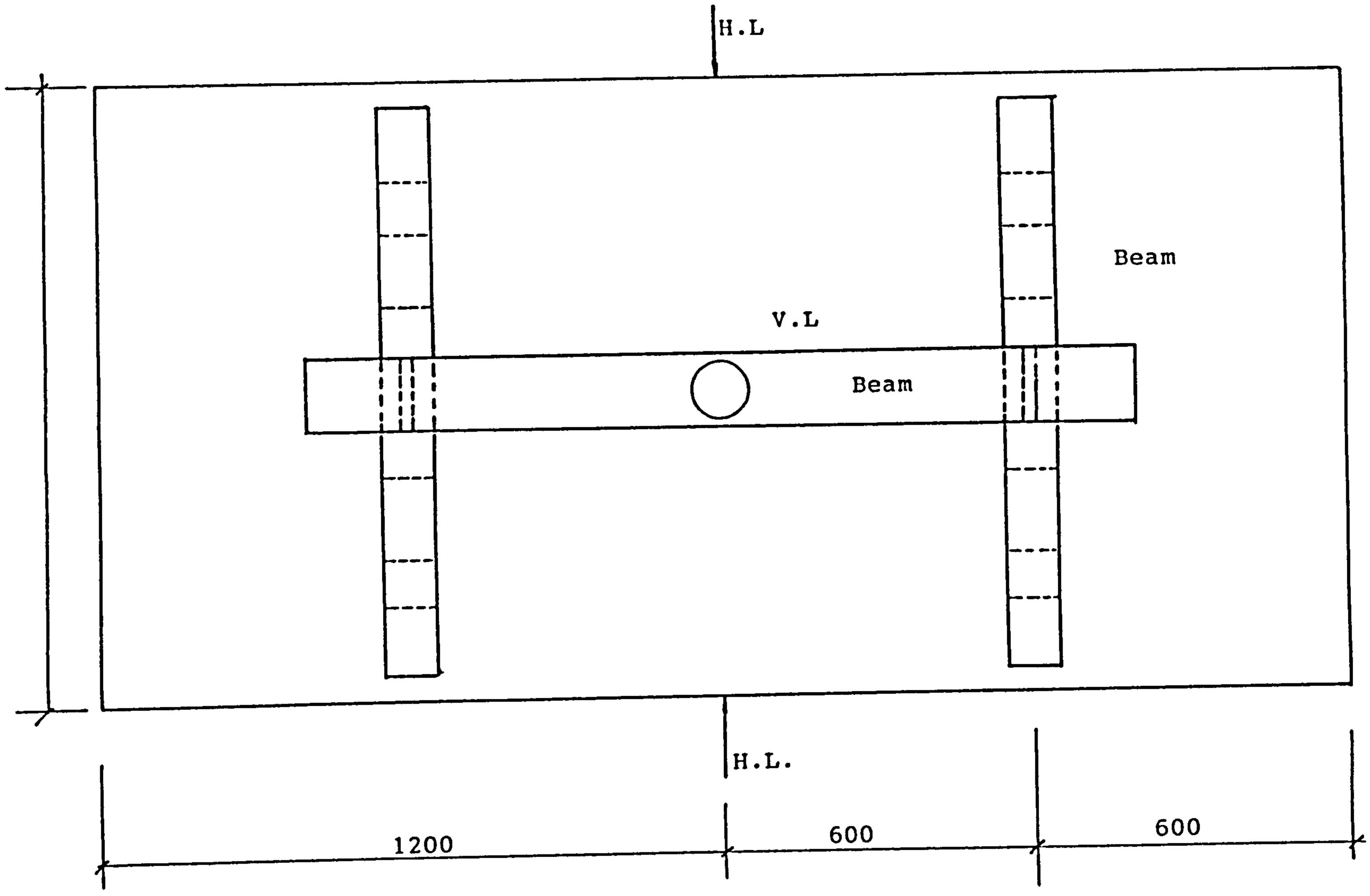

Fig. 3.1a Composite Space Frame Unit (plan)

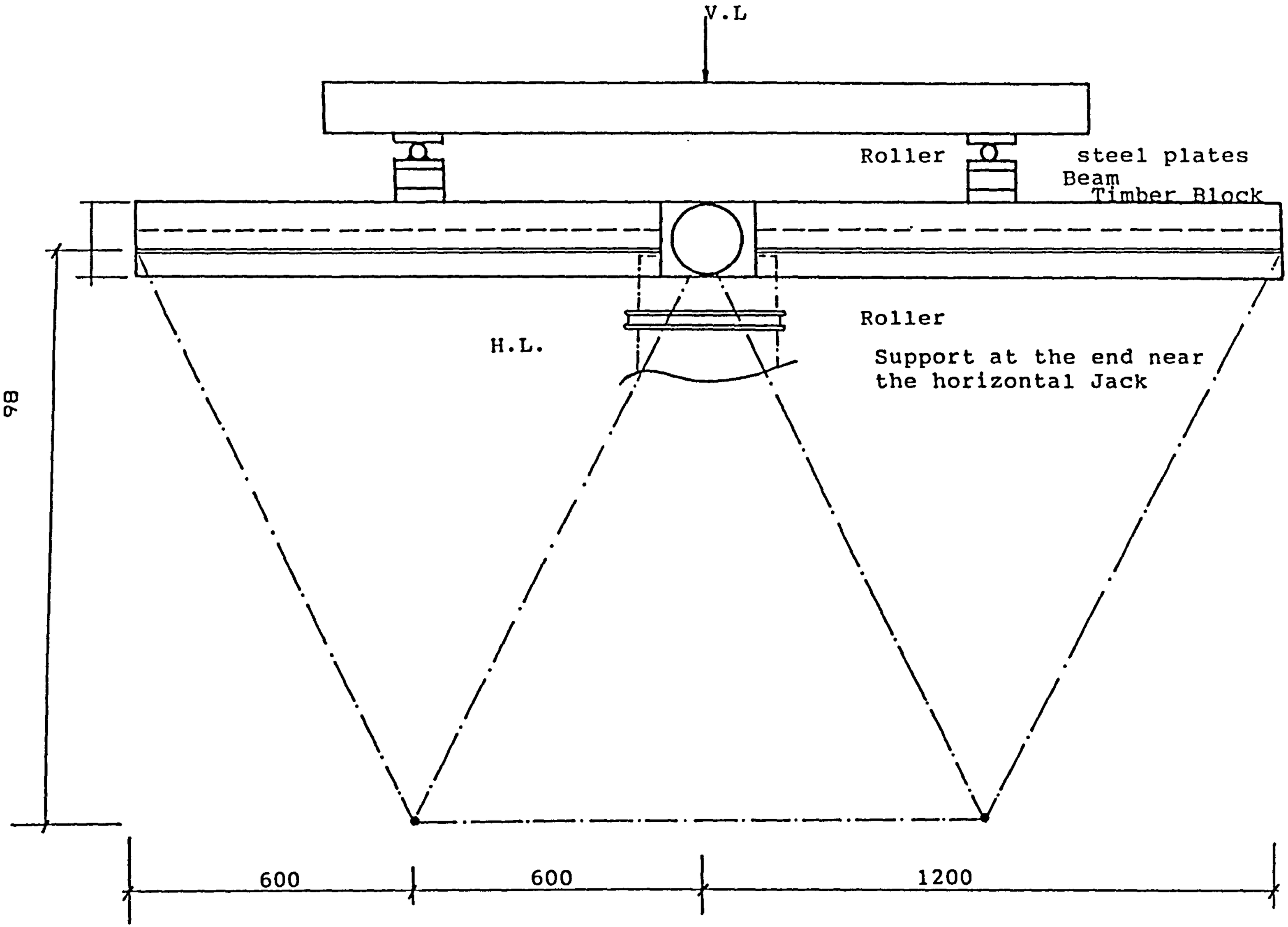

Fig. 3.1b Composite Space Frame Unit (side view)

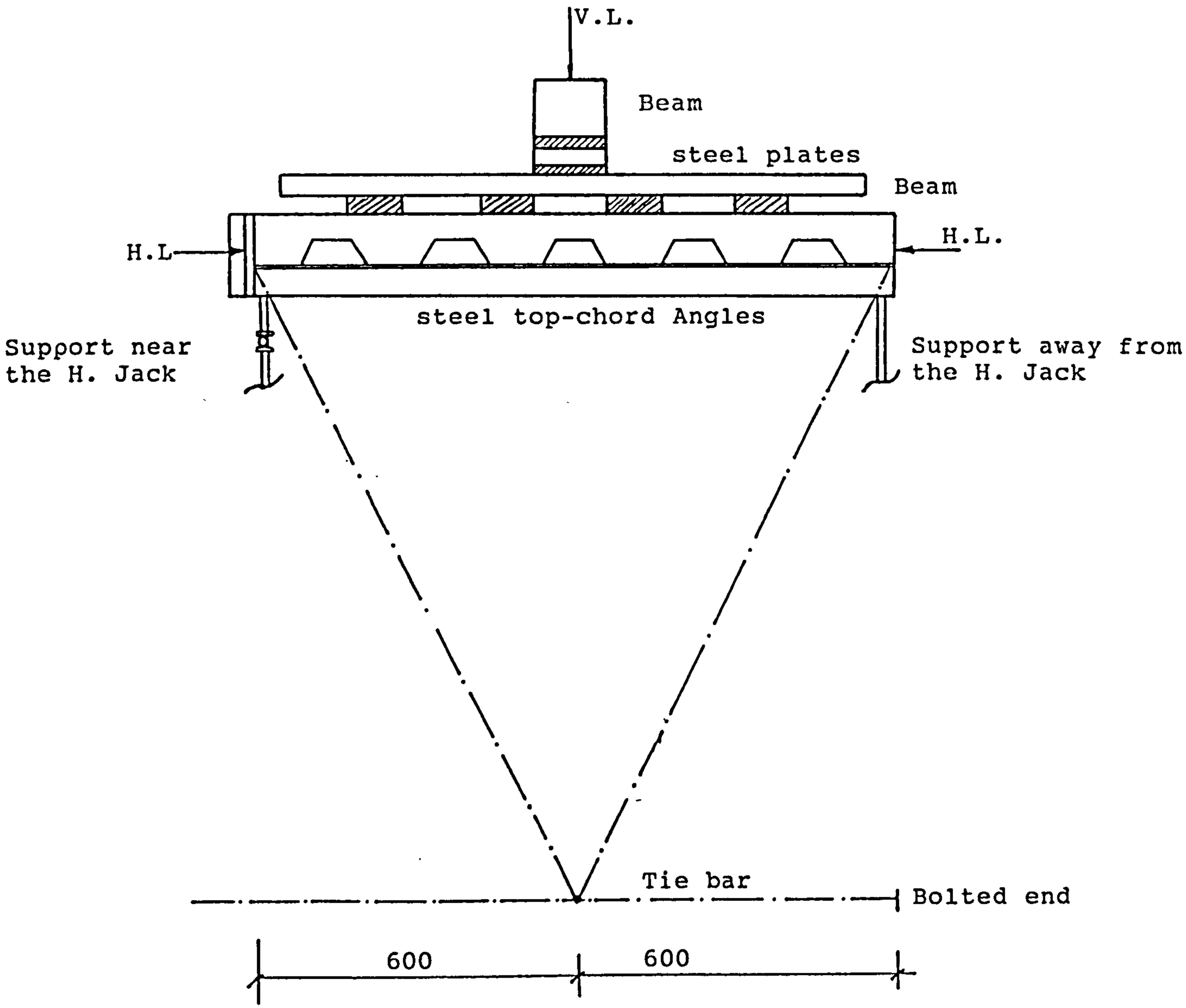

Fig 3.1c Composite Space Frame Unit (Front View)

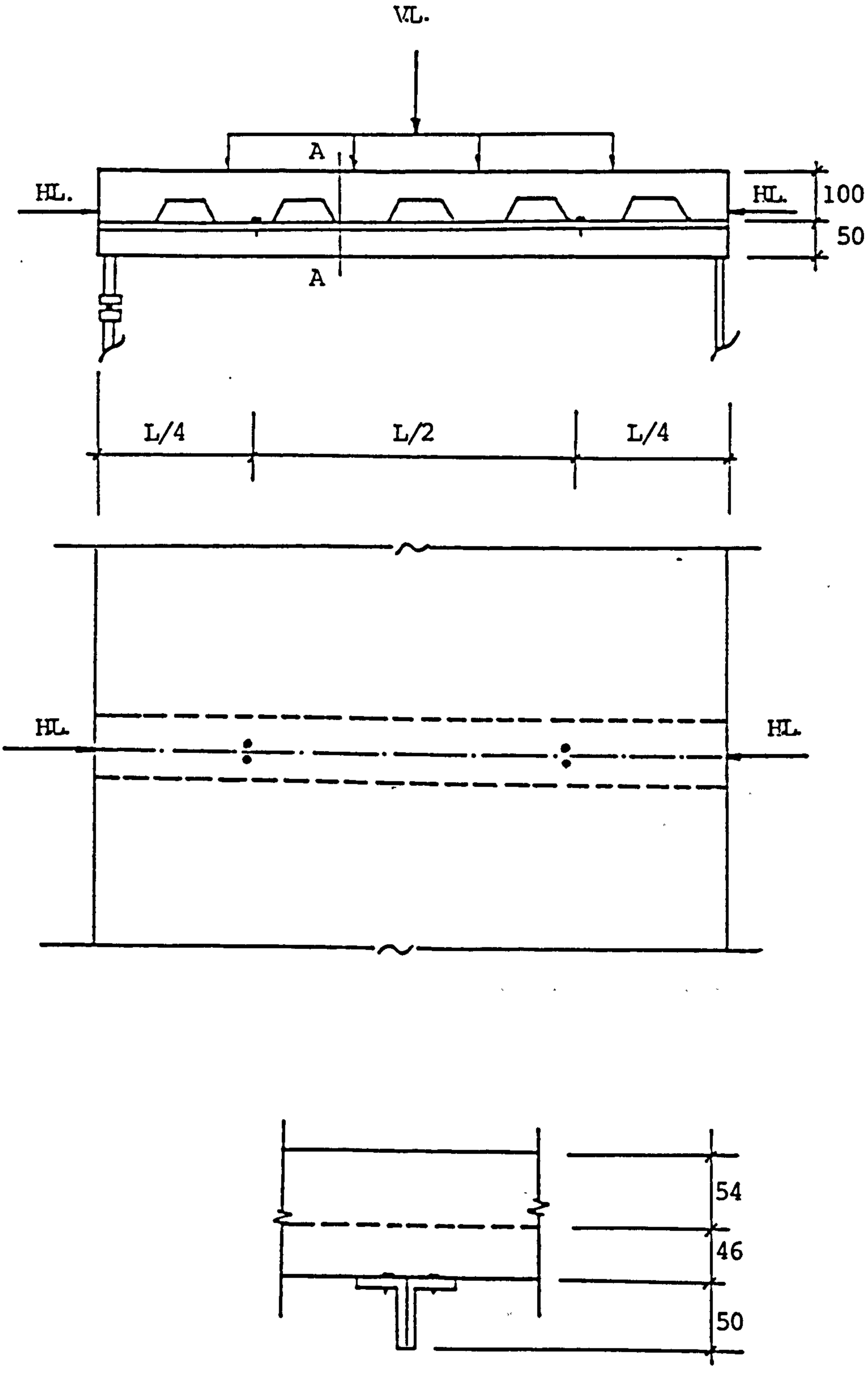

Section A-A

Fig.3.2a: Composite T-Beam with 2 Connectors at L/4

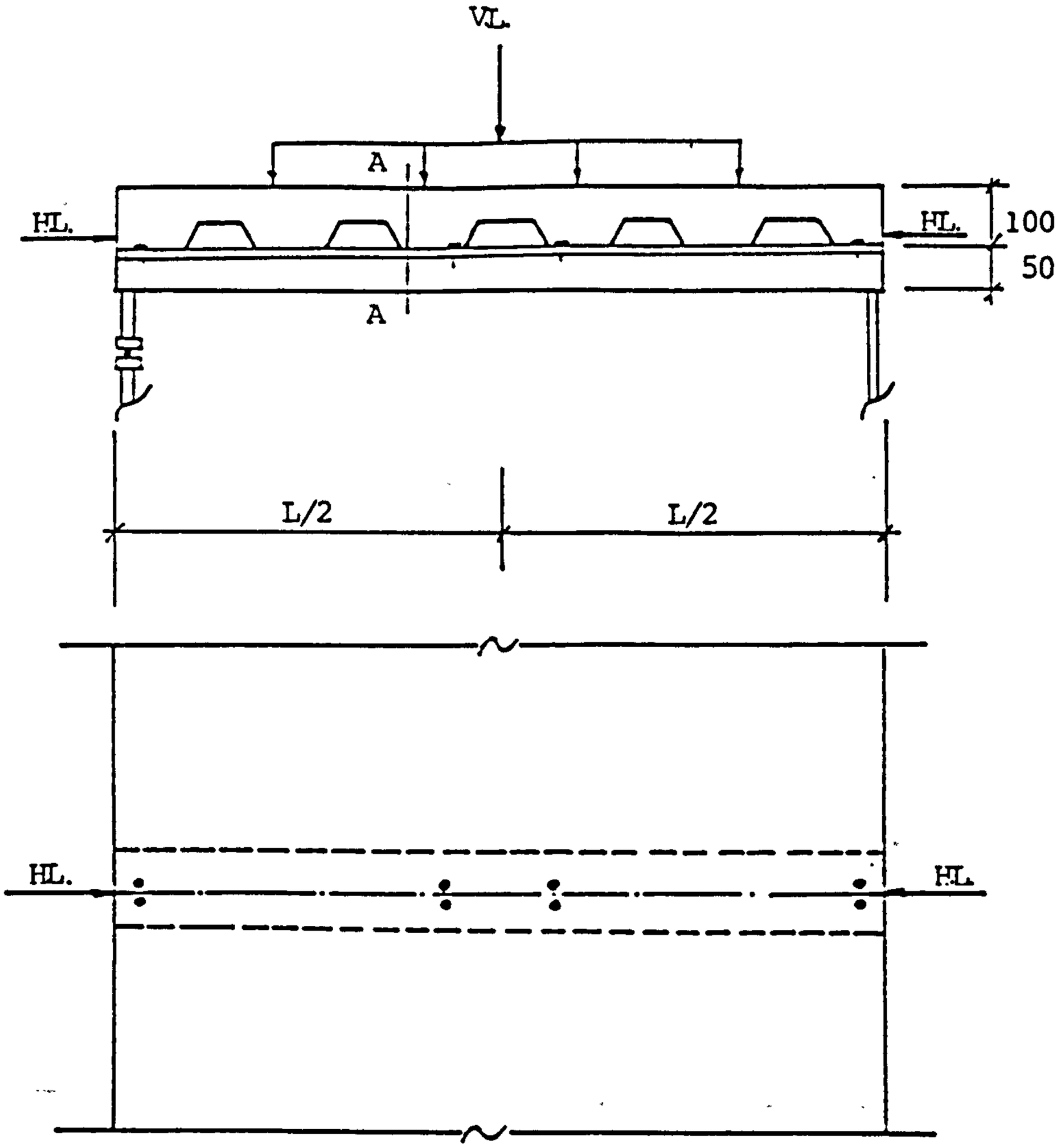

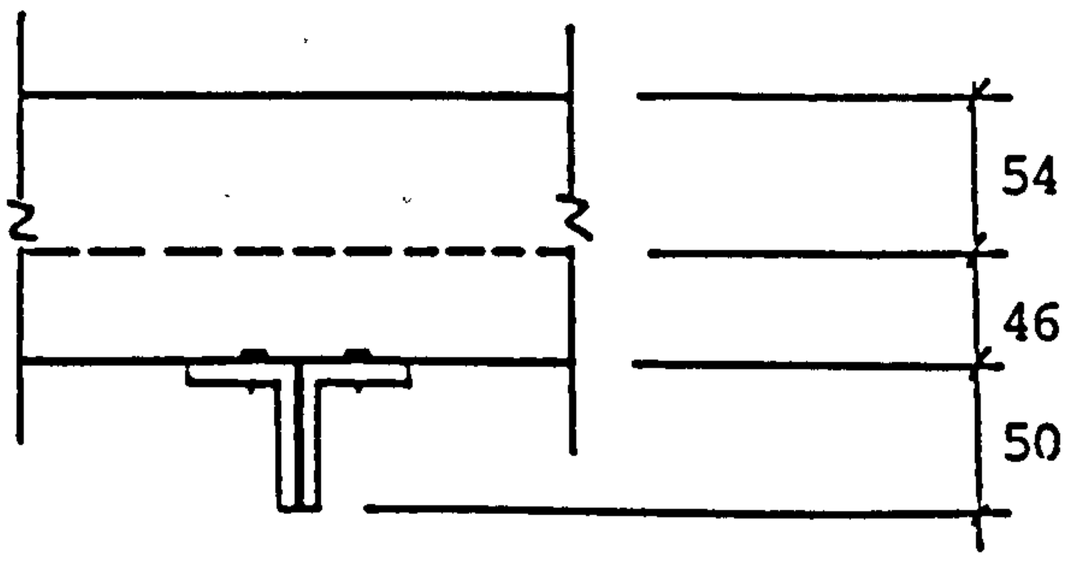

Section A-A

Fig.3.2b: Composite T-Beam with 4 Connectors at Mid-Span and 2 Connectors at End

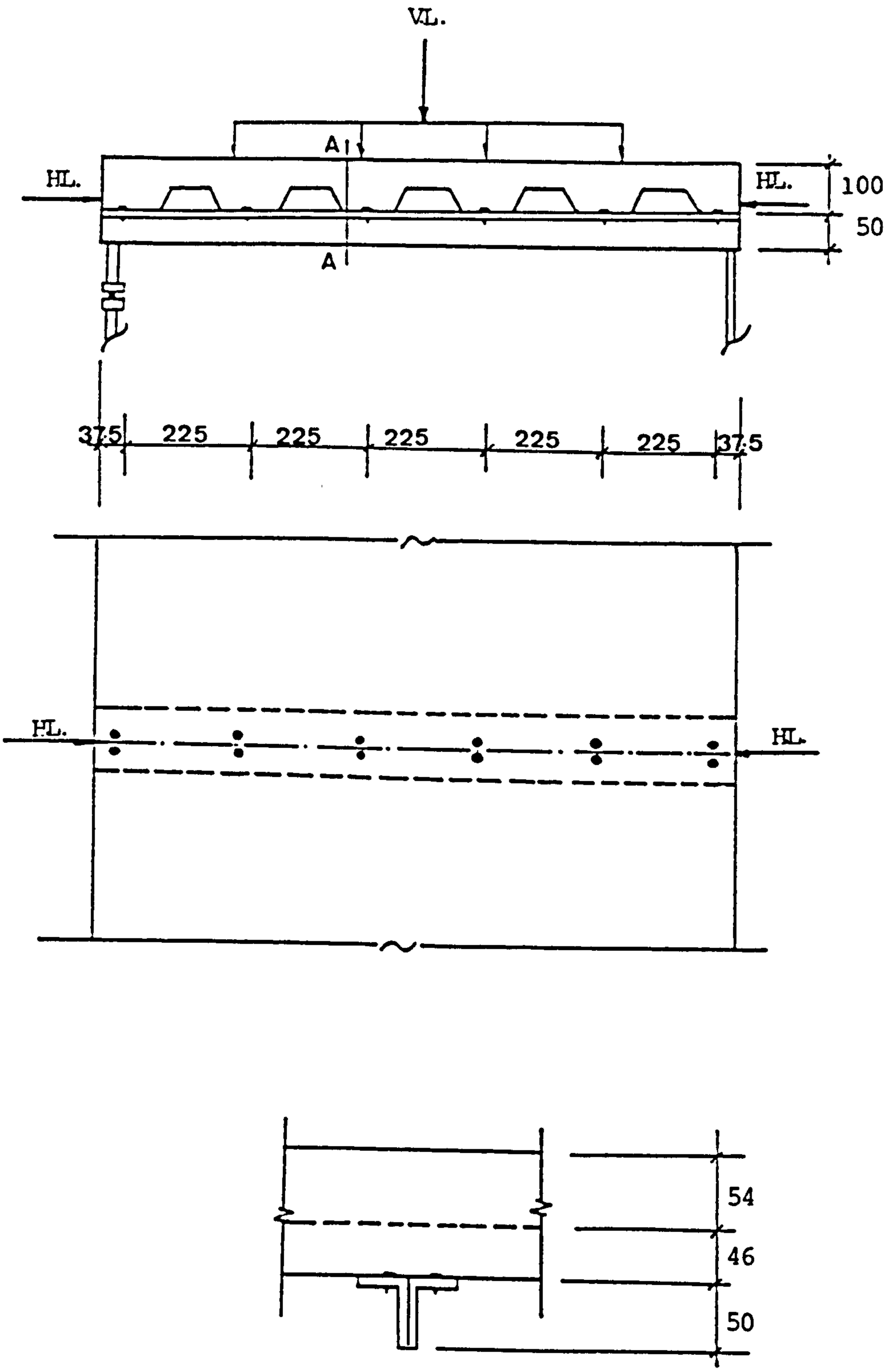

Fig.3.2c: Composite T-Beam with 2 Connectors Per Rib

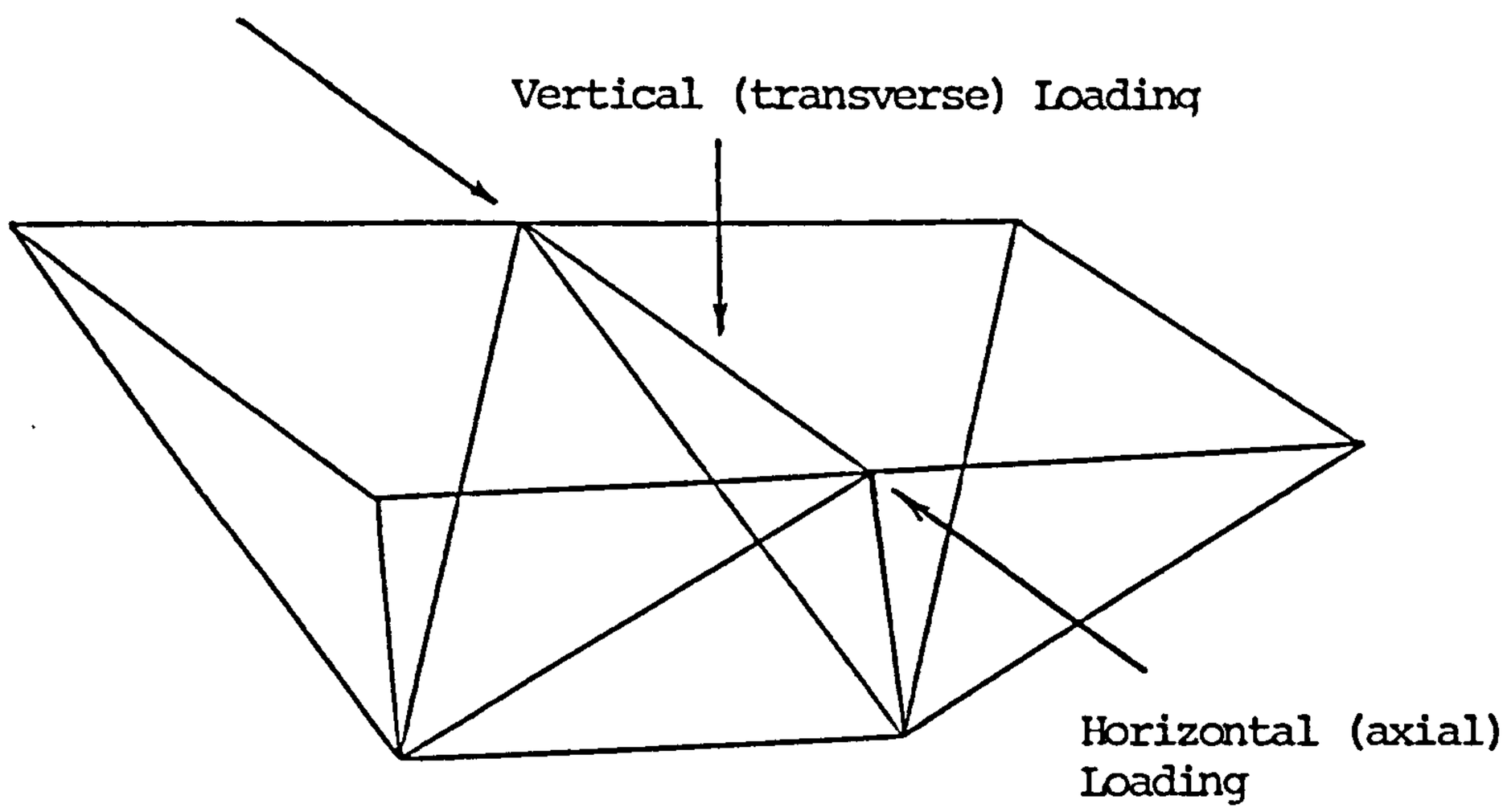

Fig.3.3: A Two-Unit Space Deck: Preliminary Test

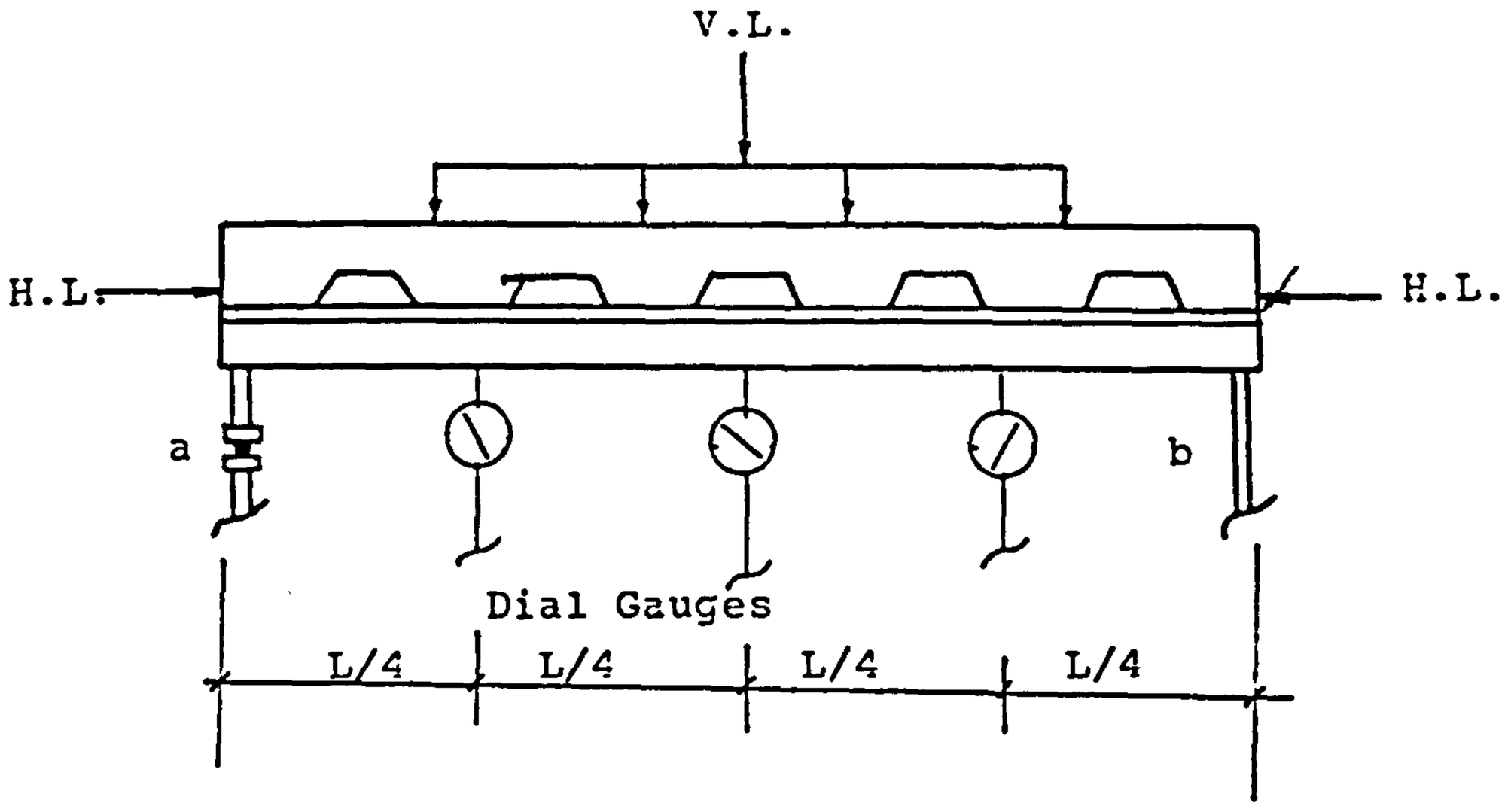

- Supports a and b are bolted to the mid-beam of the Rig
- The dial gauges were placed on steel channels to record deflection w.r.t. the lab floor

Fig 3.4 Composite T - beam set-up

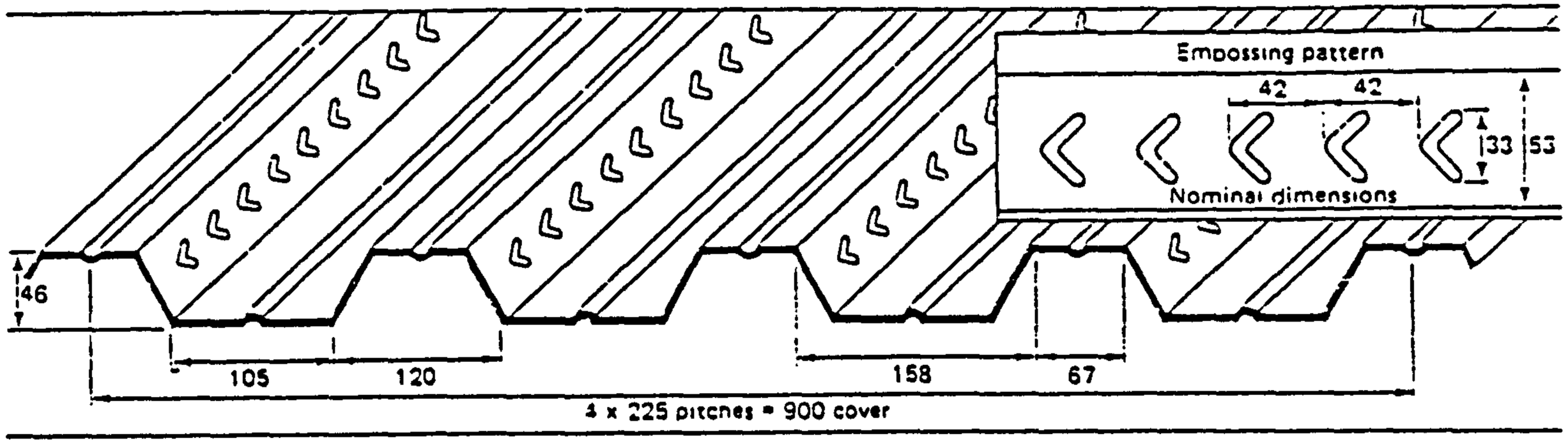

Section properties

Nominal thickness	Design thickness	Weight	Moment of inertia	Net steel area	Characteristic moment capacity (ultimate) kNm/m	
mm	mm	kN/m²	cm⁴/m	cm²/m	Positive	Negative
0.9	0.85	0.083	41.5	10.80	4.41	4.49
1.2	1.15	0.112	53.0	14.59	5.73	5.87

Fig. 3.5 PMF C46 Profiled Steel Sheet

Group 1

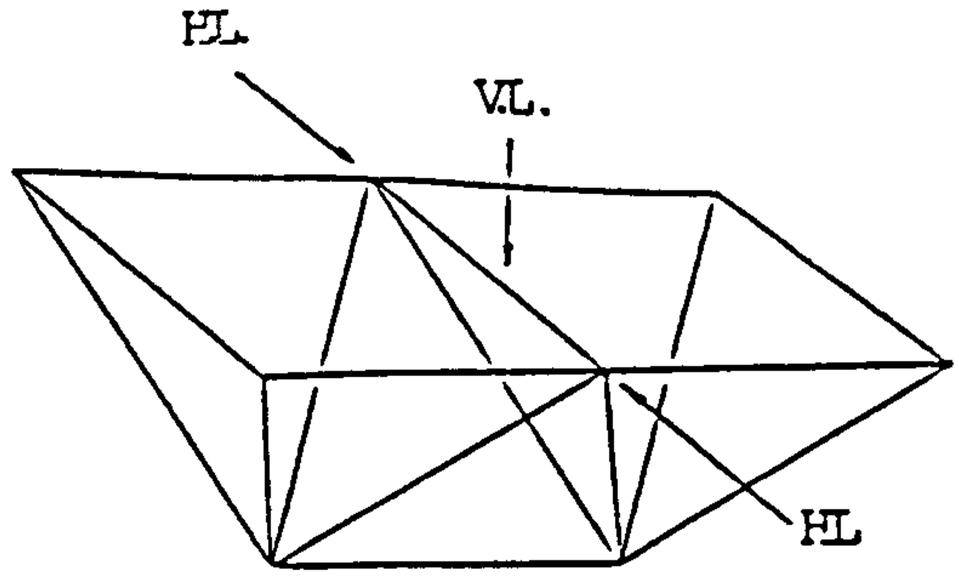

Groups 2 & 5

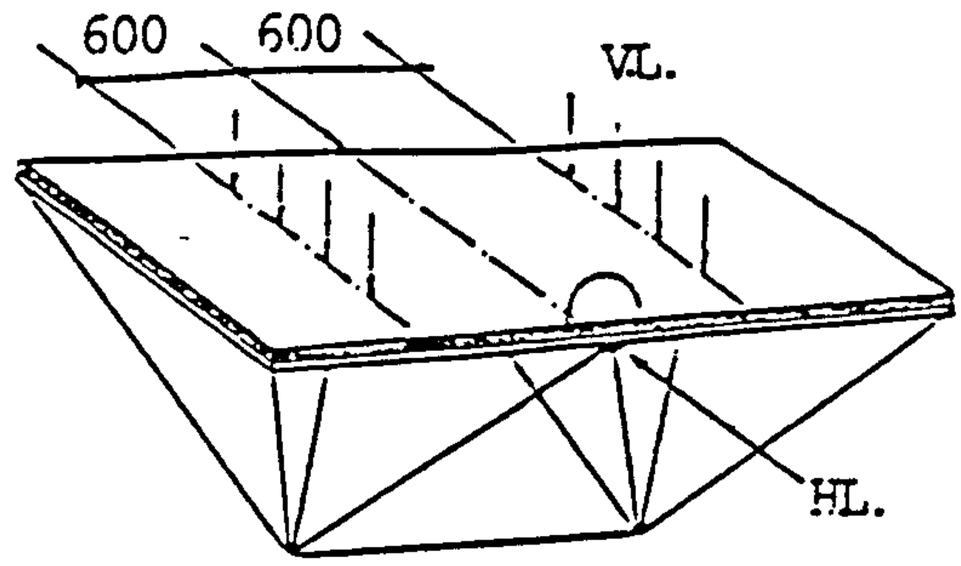

Group 3

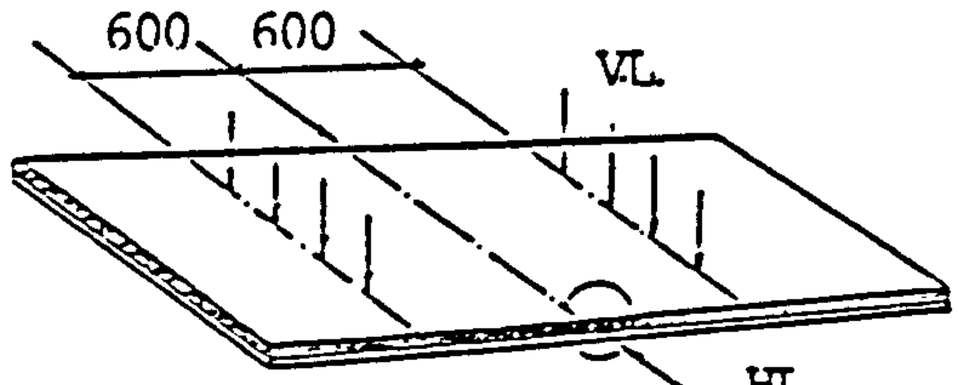

Group 4

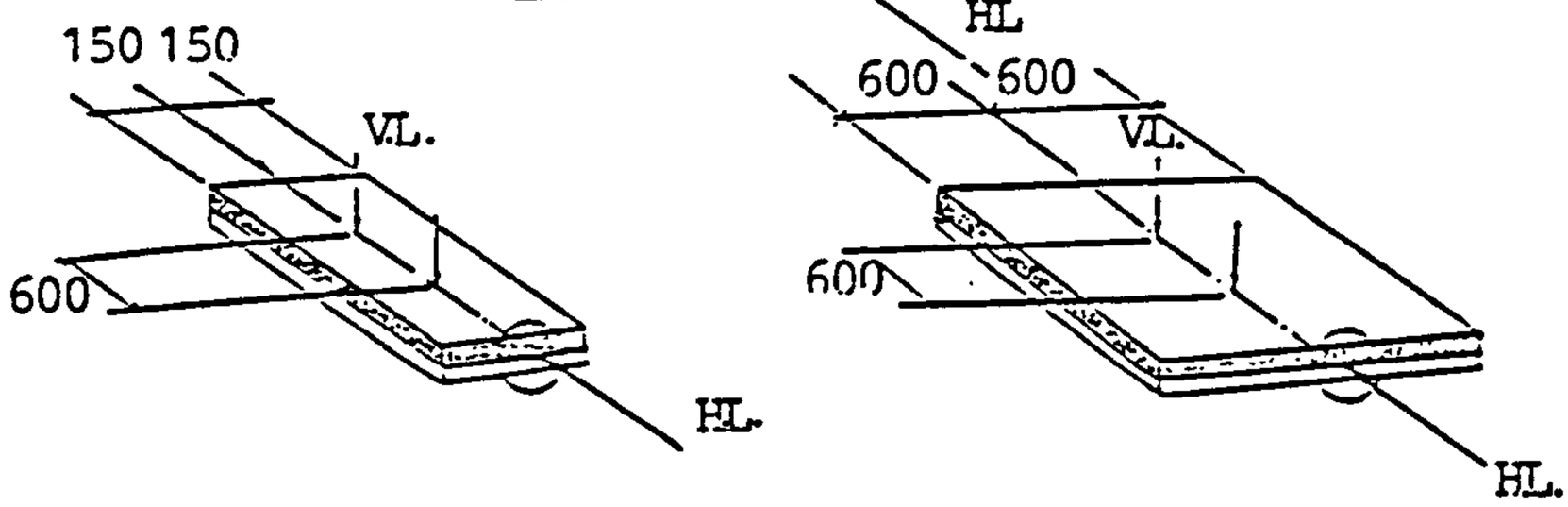

Group 6

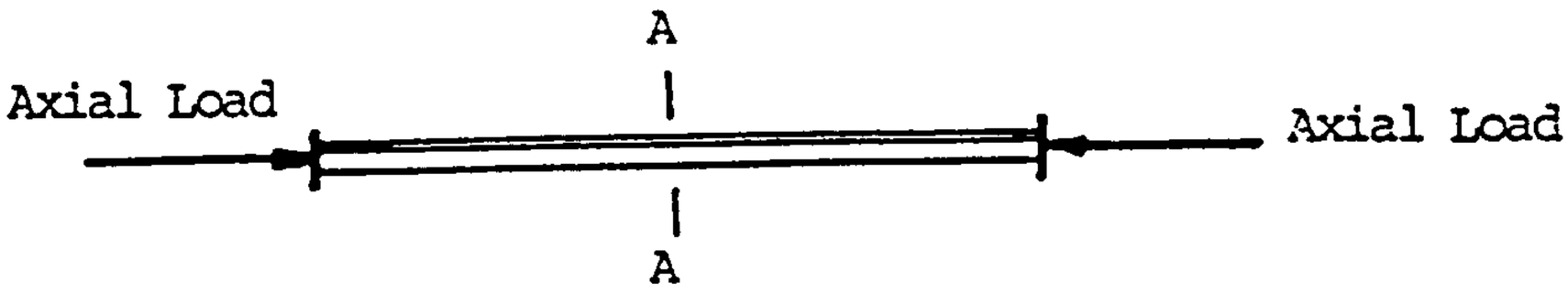

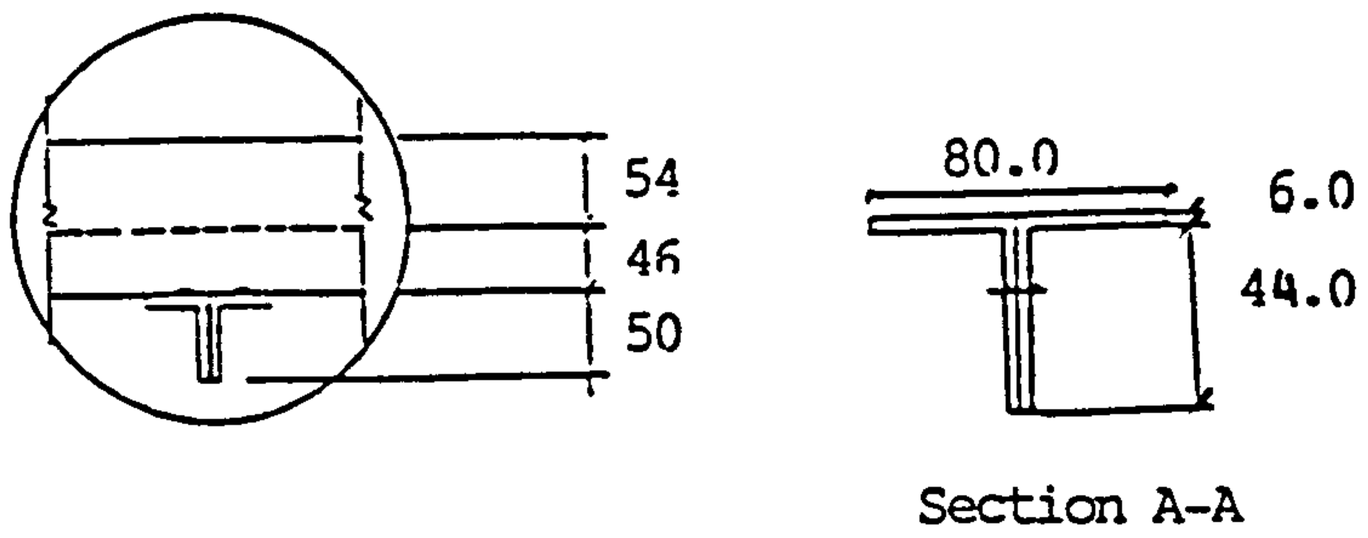

Fig. 3.6 Groups of Test Specimens

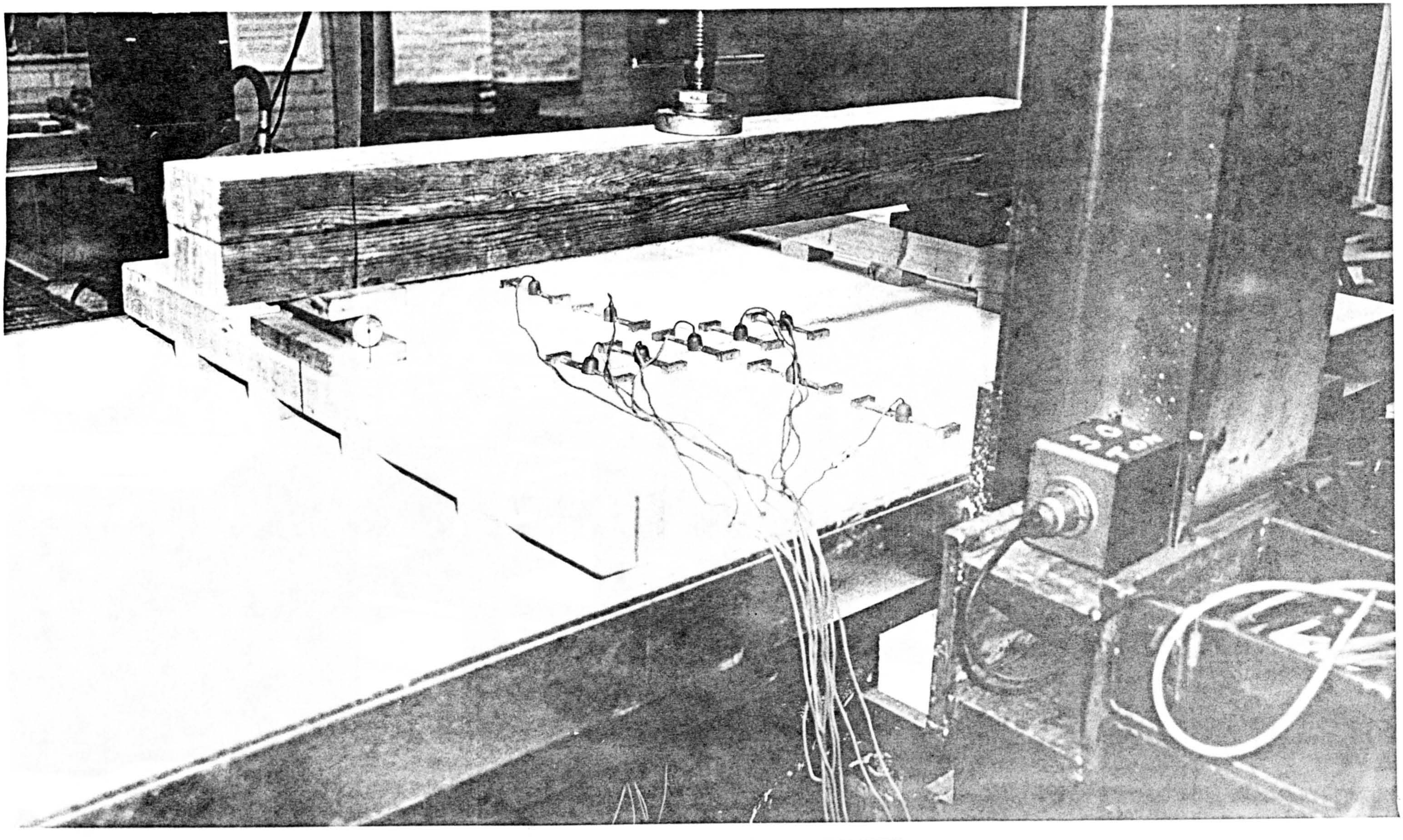

3.1a ACOUSTIC STRAIN GAUGES

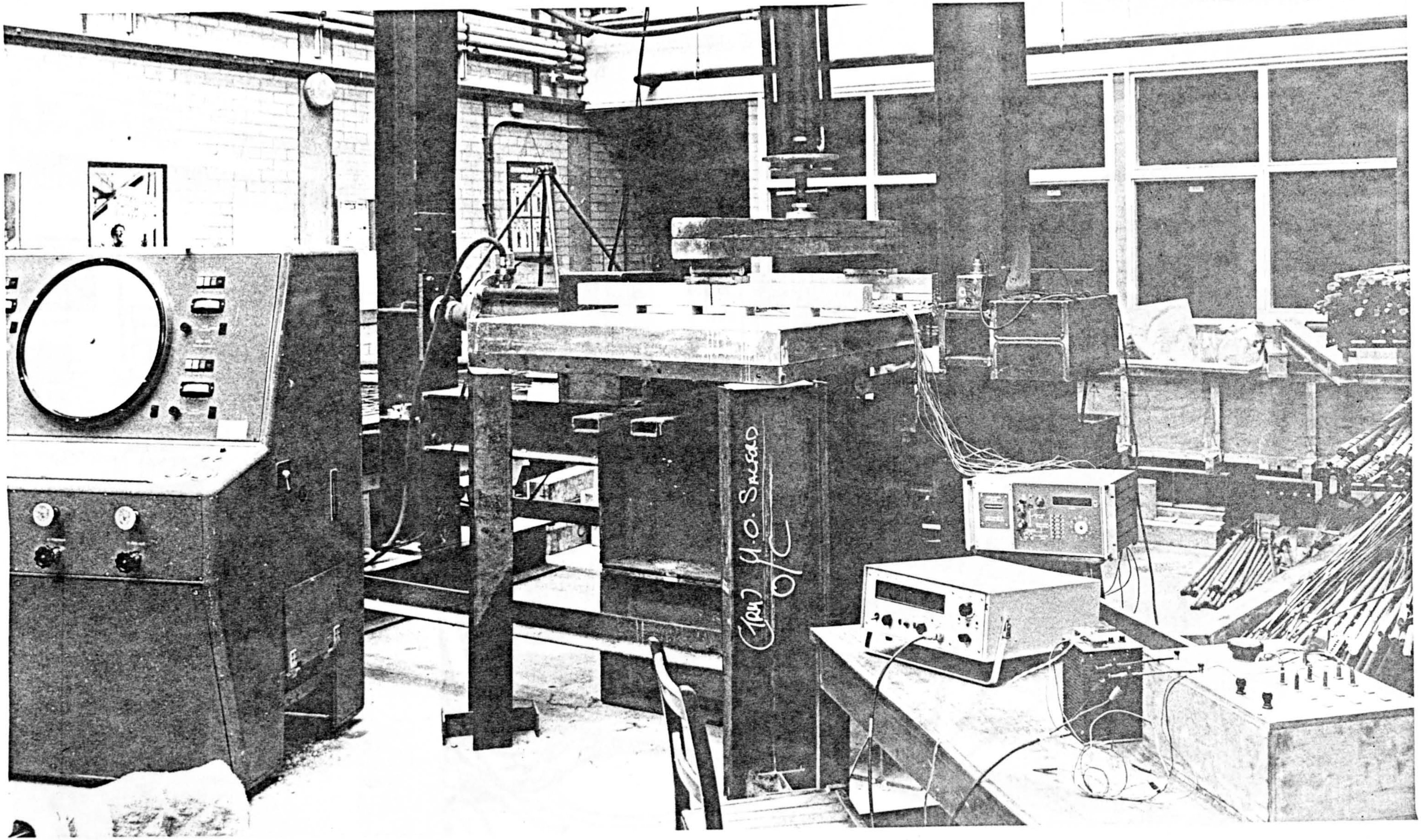

3.1b TYPICAL INSTRUMENTATION

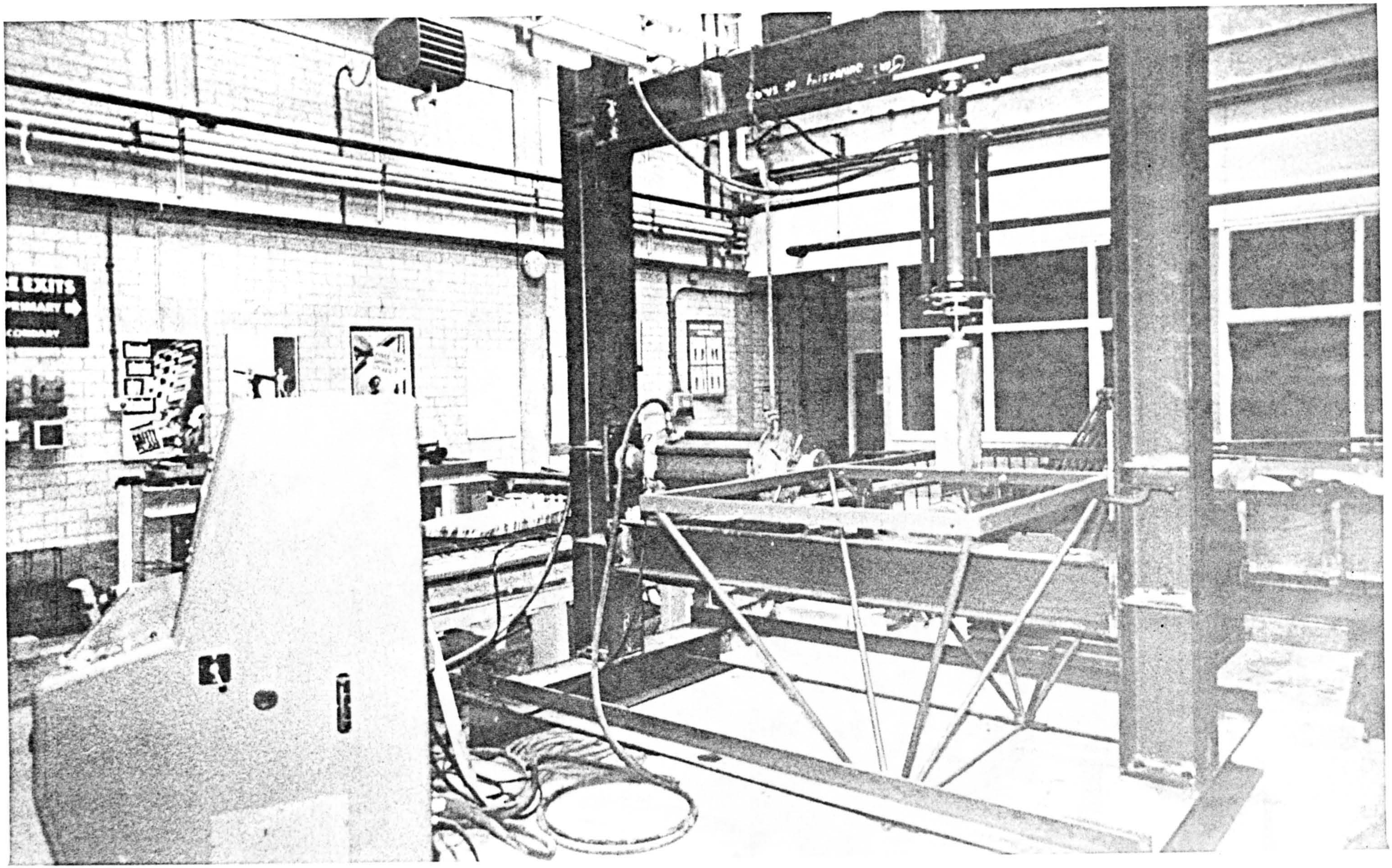

3.2a A TWO-UNIT SPACE DECK WITHIN THE TEST-LOADING RIG

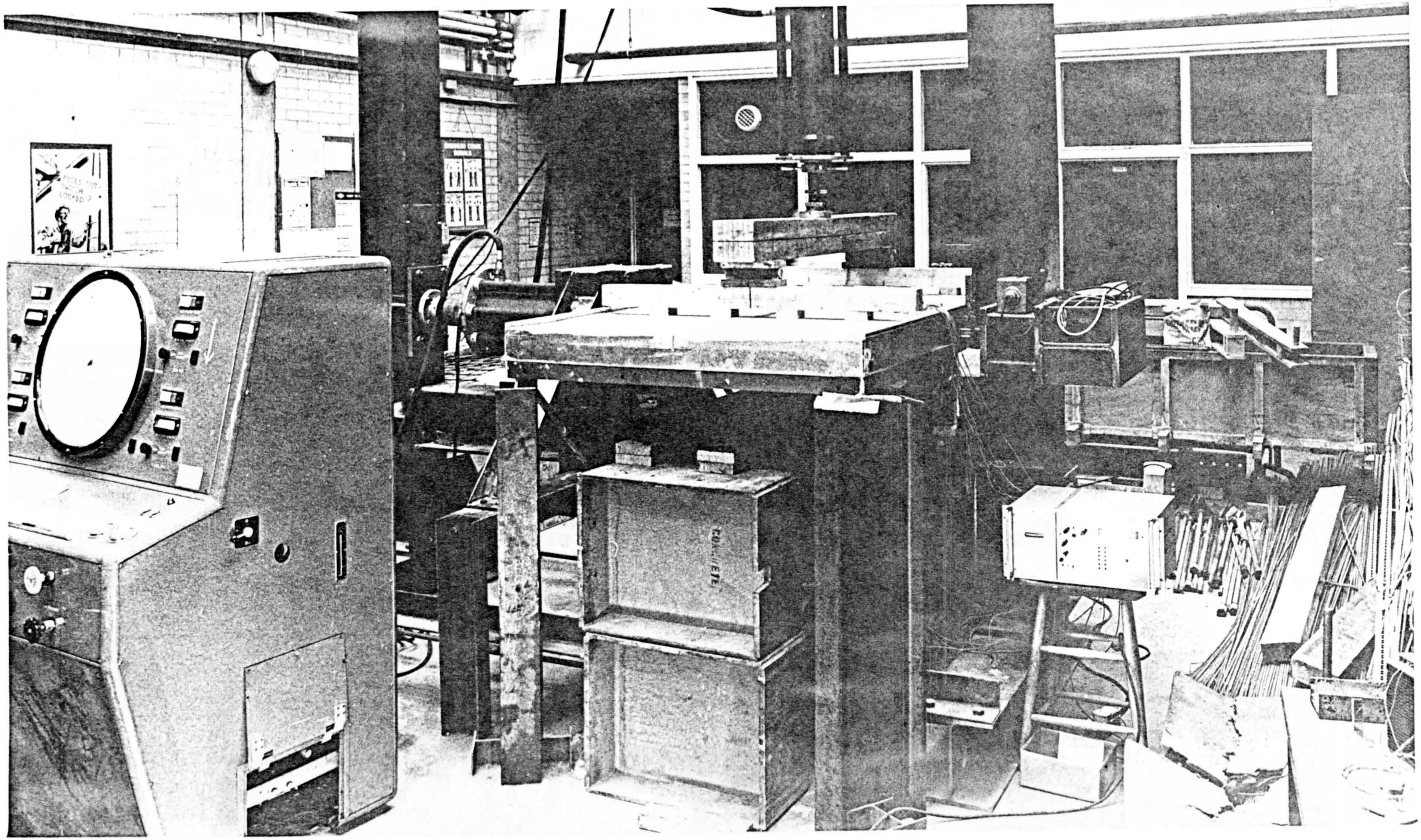

3.2b TEST - LOADING RIG

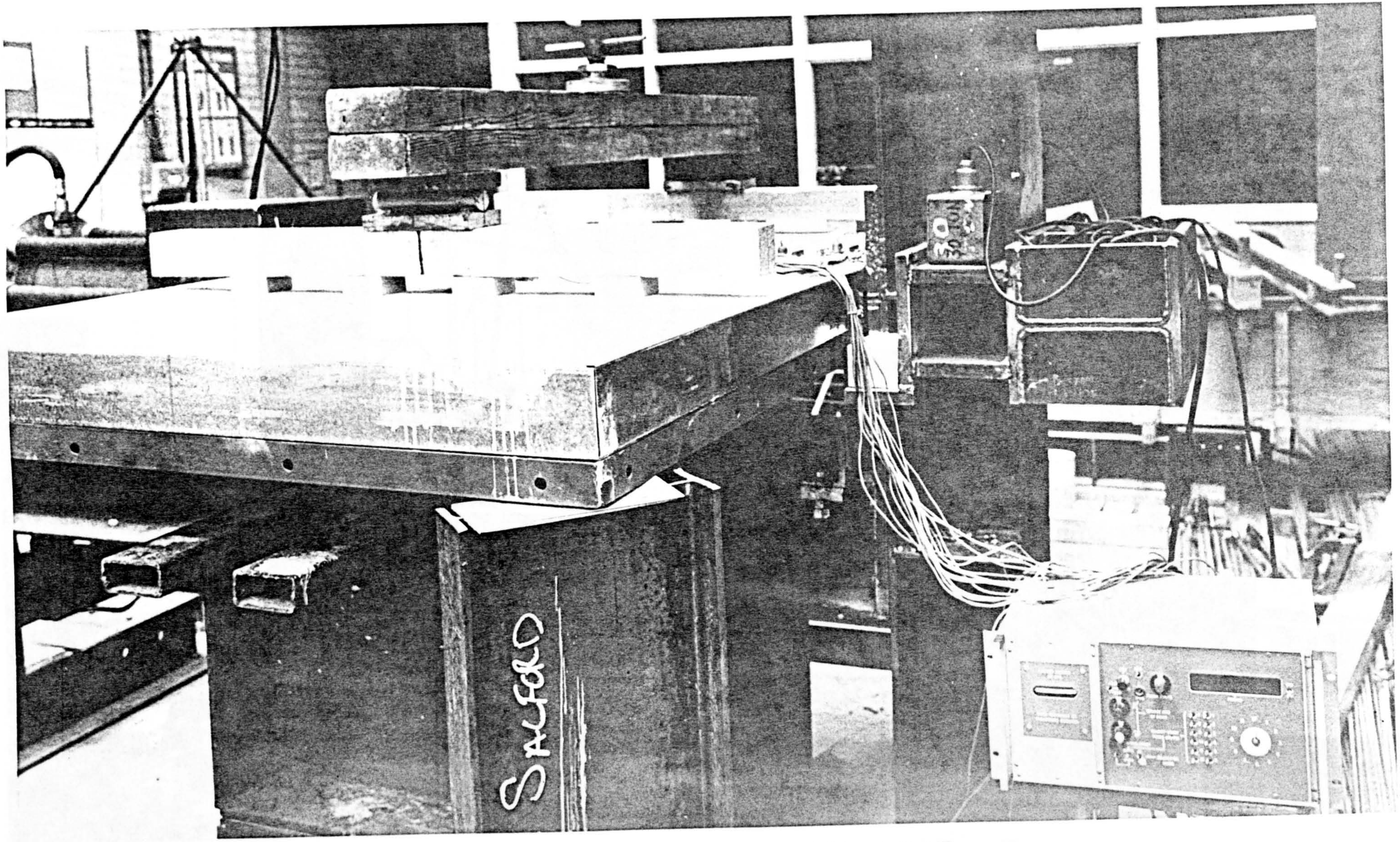

3.3a COMPOSITE UNIT SET-UP

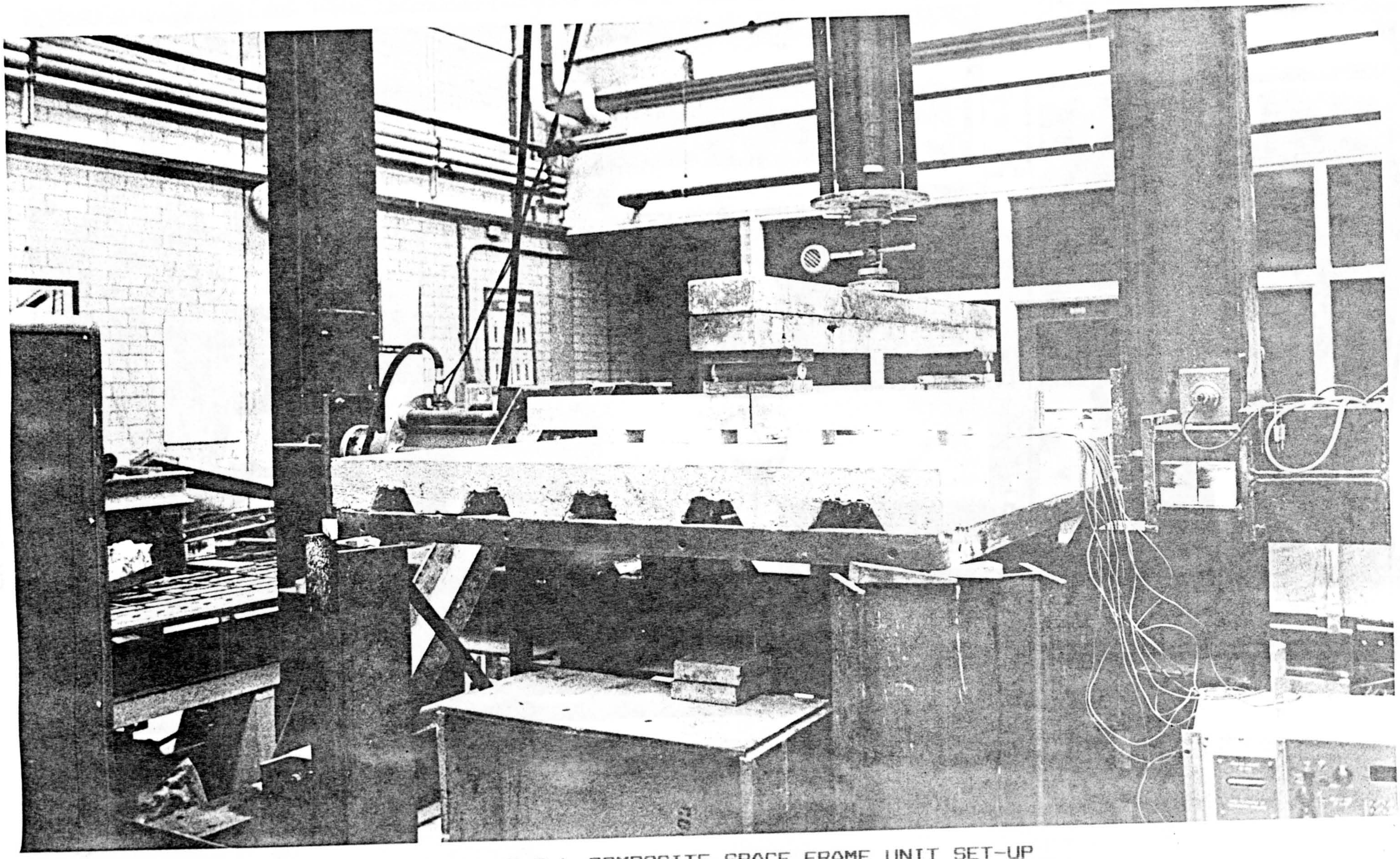

3.3 b COMPOSITE SPACE FRAME UNIT SET-UP

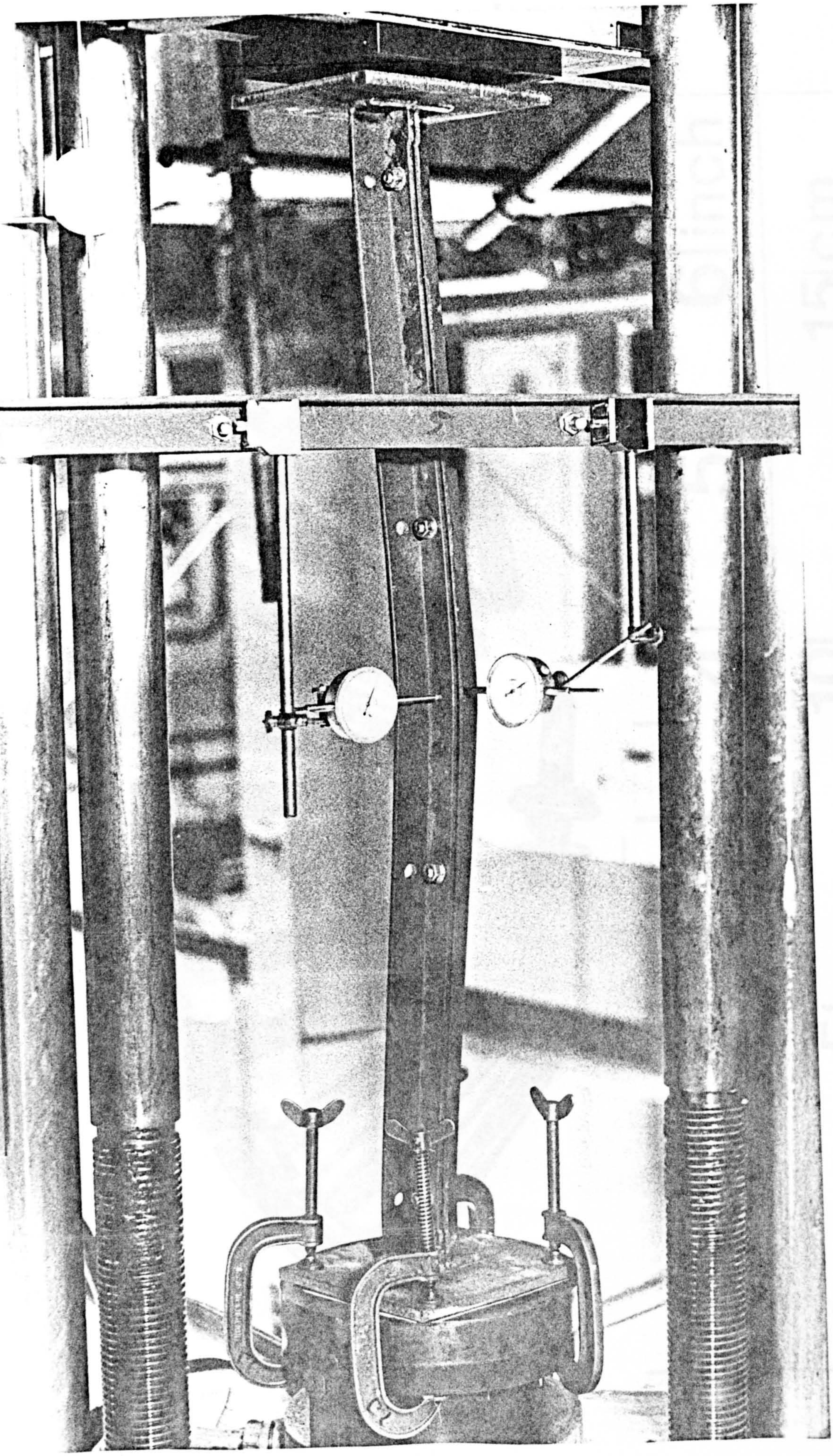

3.4 STEEL STRUT SET-UP

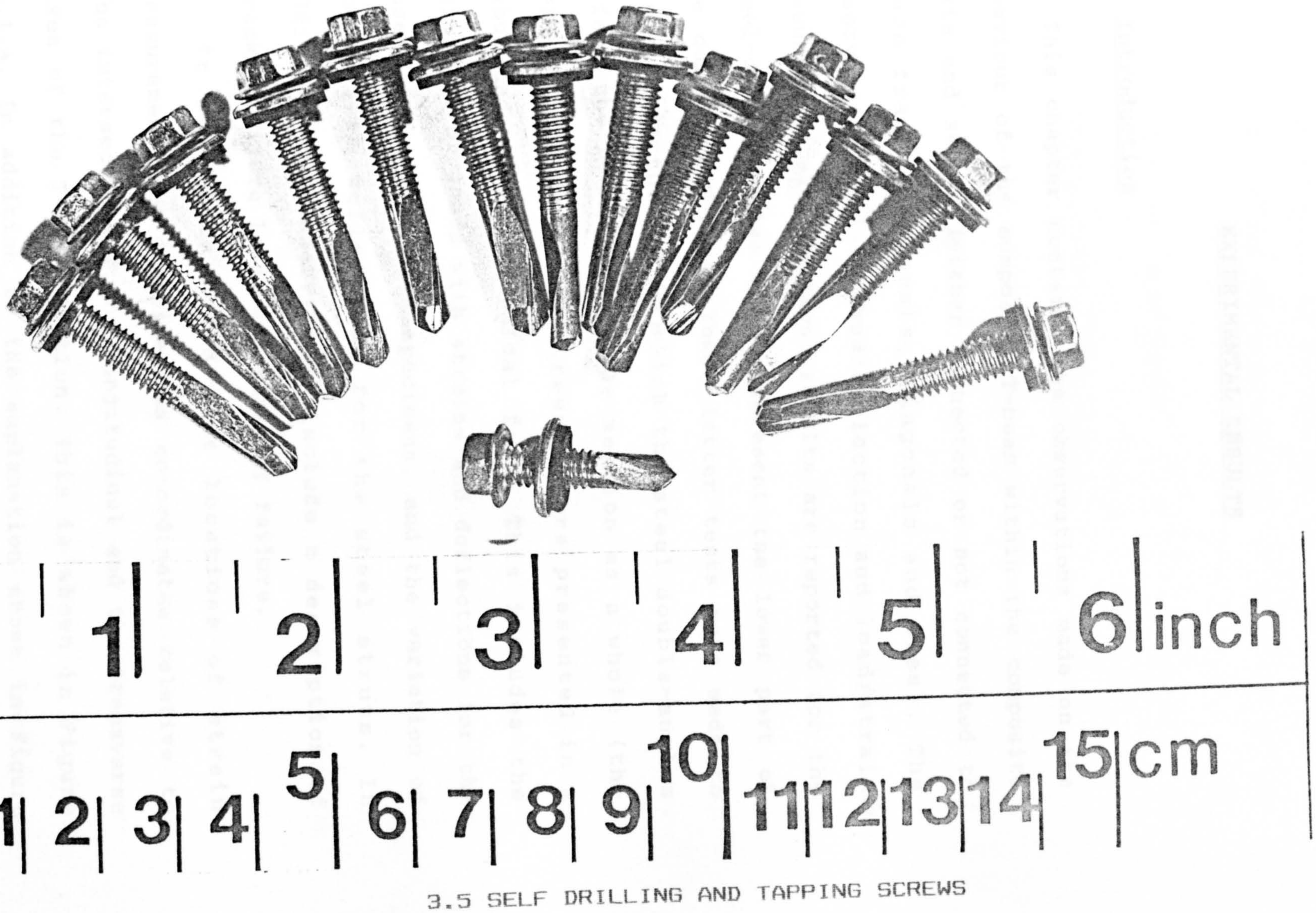

3.5 SELF DRILLING AND TAPPING SCREWS

CHAPTER FOUR

EXPERIMENTAL RESULTS

4.1 Introduction

This chapter contains the observations made on the behaviour of the composite T-beam within the composite units and struts (either connected or not connected to space frame components, diagonals and ties). The observations include load/deflection and load/strain measurements. In addition, results are reported for the steel-double angles which represent the lower part of the composite T-beam. These latter tests were made to investigate the way in which the steel double-angles affect the behaviour of the section as a whole (the composite T-beam). The results are presented in a tabulated and/or graphical form. This includes the variation of loads with strains and deflections for the cases of the composite specimens, and the variation of loads with deflections for the steel struts. In addition, the observations include a description of cracks, failure loads and modes of failure.

It should be noted that locations of strain measurement are described as co-ordinates relative to the intersection of the longitudinal and the transverse axes of the T-beam section. This is shown in Figure 4.1.a. In addition to the explanation shown in Figure

4.1.a, Figures 4.1.b to 4.1.e are produced to show the arrangement of acoustic gauges for the loading runs of CSFU1. This assists the explanation of the rest of the test units.

4.2 Composite Specimens Tests

4.2.1 Composite Space Frame Unit 1:

The first composite space frame unit was tested following the sequence mentioned in Table 4.8 (Table 3.1 repeated). Runs one and two (see Table 4.8) were different to the other runs in the arrangement of the acoustic gauges. In addition to measuring strains along the longitudinal and the transverse axes, strains were also measured along axes parallel to the main axes. Run one is described in more detail in this chapter (see Table 4.1.1 showing loads and strain variations). Seven other tests shown in Table 4.8 are also included. They are the third, the fifth, the sixth, the seventh, the eighth, the ninth and the tenth runs. The detailed results of these are shown in Tables 4.1.2 to 4.1.5, and are summarised in Tables 4.1.6.1 to 4.1.14.2.

Referring to run one (see Table 4.1.1), it can be seen that the transverse strains along the longitudinal axis measured at (0,300) are higher than those along the transverse axis measured at (300,0). Transverse strains along the longitudinal axis measured at (0,300) are also higher than those along the axis parallel to it which were measured at (300,300). This latter observation is

also true for the longitudinal strains along the longitudinal axis and the axis parallel to it (see strains measured at (0,150) and (300,150)). The difference between the transverse strains along the transverse axis measured at (300,0) and along the axis parallel to it measured at (300,300) is small, and this is assumed to be true for the longitudinal strains also. Therefore, for further runs only the strains along the longitudinal and the transverse axes of the composite T-section were measured,i.e. no strains along the axes paralel to these.

The strains were symmetrical along each of the two axes. The strains along the longitudinal axis for similar distances from the centreline towards the composite T-section ends were approximately equal. This was also the case for strains measured along the transverse axis. This symmetry allowed the measurement of strains at closer to or the same distances from the centreline along the required axis to be made. This is shown with longitudinal strains measured at (0,280) and at (0,300) along the longitudinal axis (see Tables 4.1.6.1 to 4.1.9.1 and 4.1.11.1), and for longitudinal and transverse strains measured at the same points along the transverse axis (see Tables 4.1.2). Due to this symmetry, the strain variation for these units may be represented in one quadrant.

Referring to all the runs of this first unit, it can be seen that strains, both longitudinal and transverse,

vary with distance from the centreline to the ends of both axes. Tables 4.1.6.1 to 4.1.12.2 show this variation along both axes. In addition to the effect of the distance from the centreline to the ends of the two axes, the variation of strains is also affected by the value of the applied vertical loading as it is clear in Tables 4.1.13.1 to 4.1.14.2. Moreover, the variation of strains along the longitudinal axis are also affected by the presence and the arrangement of the shear connectors as will be seen later.

The variation of both longitudinal and transverse strains along the transverse axis was inversely proportional to the distance from the centreline to the ends of the transverse axis. The values of the strains beyond a certain width were found to be small compared to those within that width. According to the results in the tables, this width was between 200mm and 400mm which was found to be the case for all the runs of the first composite space frame unit, with the different arrangements of acoustic gauges. The strain variation along the longitudinal axis itself was different to the transverse axis. For example, run one showed that transverse strains on the concrete surface at the centreline were nearly equal to those at the quarter points of the composite T-section (see Table 4.1.1 for strains measured at (0,0) and (0,300)). However, longitudinal strains along this longitudinal axis were found to increase from the quarter points towards the

supports, and decrease from the quarter points towards the centreline. Longitudinal strains on the stem of the steel double angles measured at the quarter points were found higher than those at the centreline of the composite T-beam. These observations were also true for the other runs of the first unit (see Tables 4.1.2 to 4.1.5).

It can be seen that at the distance of 300 mm, the strains were higher than those at 280 mm (see Tables 4.1.6.1 to 4.1.11.1) along the longitudinal axis. From the quarter points (where the shear connectors were attached) to the supports, the strains are higher than those from the quarter points to the centreline. It may be concluded that for the units with the sheets attached at the quarter points, the strain variation followed the pattern described above. From the quarter points to the supports there was only connection through the sheet (in its 'weak' direction) while from the quarter points the shear connectors provided mechanical connection . Thus, the presence of the shear connectors at the quarter points, for this particular test, causes the transfer of load between the steel and the concrete section. It appears that the load was carried mainly by the steel section between the quarter points and the supports even though the load was applied through a steel plate. This point will be discussed later with other units.

At higher loads, cracks began to appear along two lines nearly parallel to the longitudinal axis of the T-

beam on both of its sides. This took place at a horizontal load of 340 kN. However, the test was stopped at the next load increment which was 350 kN. This was to check whether the upward deflection (see Figure 4.2), which caused the cracks in the concrete, was due to the horizontal load being applied below the calculated centroid of the composite section. The unit was re-tested with the horizontal load axis well above the centroid of the composite section. As a result, the axis of the applied horizontal load was found to have no effect on the deflection when it again reversed from the downwards direction to the upwards direction with this arrangement. This latter test was stopped again at the horizontal load of 300 kN, and it was re-tested with the horizontal load applied at the calculated centroid of the composite section. It failed this time, but at a smaller horizontal load which was 280 kN. The failure took place when the concrete at the section adjacent to the horizontal jack crushed. In addition to the crushing of concrete at that section, the steel profile buckled, and started to pull away from the shear connectors along the longitudinal axis, and those along the sides of the unit. The characteristics of the failure mode for the profiled steel sheet are shown in Plates 4.1a, 4.1b and 4.1c. However, the failure mode of the concrete section was similar to the rest of the composite units.

The load-deflection curve of Run 10 (the run of the highest horizontal and vertical loads of the first test)

is shown in Figure 4.2. According to the figure, the load of the 350 kN at which the test was stopped (Run 10), was considered as the lower bound for the potential strength of the unit. Any development of increasing deflection at high load being restrained by the vertical loading.

It is considered that the previous sequence of loading up to run 10 may have caused the unit to fail at a lower load. Thus, only the earlier load runs were considered to investigate the load/strain behaviour, and run 10 was considered for load/deflection observations.

4.2.2 Composite Unit (Composite Slab with no diagonals and Ties):

This case (composite unit) was similar to that of the first composite space frame unit in the number and the spacing of connectors. The difference for this arrangement was that it was not attached to the space frame diagonal and tie members. Longitudinal and transverse strains for this case are shown in Tables 4.2.1 and 4.2.2 respectively.

Transverse tensile strains along the longitudinal axis were generally lower than the longitudinal compressive strains at the same points relative to the centreline of the composite unit (see Tables 4.2.1 and 4.2.2 for strains measured at (0,200) and (0,400)). This observation confirmed the conclusion in the previous test. At the same distance from the centreline, the

longitudinal compressive strains were always higher than the transverse tensile strains along both the longitudinal and the transverse axes.

For both the transverse and the longitudinal strains, along the longitudinal axis, the highest strains appeared to be those at the distance of 400 mm from the centreline (see Tables 4.2.1 and 4.2.2). The lowest strains appeared to be those at the distance of 200 mm from the centreline (see Tables 4.2.1 and 4.2.2).

The longitudinal strains at the distance of 200 mm along the longitudinal axis were less than half those at 400 mm from the centreline at higher loads (see Table 4.2.1).

Therefore, in a similar manner to the previous test, it may be concluded that longitudinal strains near the connectors towards the centreline were significantly lower than longitudinal strains from the quarter points towards the supports.

Strain variations along the transverse axis were similar to those in the first composite space frame unit; they were inversely proportional to the distance from the centreline away to the ends of the axis (see Tables 4.2.1 and 4.2.2). Transverse strains along this axis were different at the two locations where they were measured (100mm and 200mm from the centreline) as is shown Table 4.2.2.

The central deflection (see Figure 4.3) shows the same initial behaviour as that of the previous case. It

deflected downwards first due to the vertical load (oa). The horizontal load had then its influence on the deflection in that it decreased the effect of the vertical load directly at its first application up to certain value (ab). It then deflected upwards with each horizontal load increment (bc). After that, it can be seen that the deflection was mainly influenced by the horizontal load when it continued to deflect upwards to failure (cd).

Cracks began to be visible to the naked eye at a horizontal load of 330 kN near the ends of the composite T-beam section and parallel to its longitudinal axis. Failure occurred at a load of 390 kN when concrete at the end of the composite T-section, away from the horizontal jack, crushed (see Plate 4.2). The crack pattern, the load at which cracks appeared and the failure mode were similar to that of the first composite space frame unit. The failure load for this case was higher than that of the previous test which supports the view that the previous unit may not have failed at the lower load had it not been weakened by the series of runs of loading and re-loading.

This case had two characteristics which differentiated it from the previous test. The first, was the high transverse strains which were, in some cases, nearly equal to the longitudinal strains measured at similar locations (see Tables 4.2.1 and 4.2.2). The second, the failure load of 390 kN (with V.L. 8kN)

compared to the lower bound load of 350 kN (with V.L. 45kN) of the previous specimen. Longitudinal strains measured at the same points, relative to the centreline of the composite unit, along the longitudinal and the transverse axes appeared to be nearly equal (see Table 4.2.1 and Figure 5.7 for strains measured at (0,200) and at (200,0)). Since only one composite unit of this type was tested, this conclusion requires further experimental evidence. However, for this work, the indication of certain similar behaviour to that of the first test, such as the deflection downwards then upwards, strain values near and away from connectors and the load at which cracks appeared, was considered sufficient.

As a result of the previous CSFU1 and this composite unit, only the longitudinal strains were measured along the longitudinal and the transverse axes in the remainder of the tests.

4.2.3 Composite Struts:

Two composite struts of width of 1200 mm were tested first. They had the same number and spacing of connectors as the previous two test units, but they were prepared with flat steel sheets. At a horizontal load of 380 kN, the first strut failed by a sudden shearing of connectors. This might have been due to a slight horizontal deviation between the applied horizontal load and the longitudinal axis of the composite strut. The

third and the fourth composite struts were of width of 300 mm. They were prepared with the same flat steel sheets and the same number and arrangement of connectors. They were tested similarly to the previous two tests. These two struts failed at the horizontal loads of 270 kN and 310 kN with crushing of concrete away from and near the end of the horizontal jack respectively. In both cases, the steel sheet buckled at that section (see Figure 4.4). The loss of bond between the concrete and the galvanised sheet and the strength of concrete (26.3 and 29.8 N/mm^2) for these two composite struts (compared to the other composite units) were assumed to influence the failure at these loads. However, the second composite strut (1200 mm wide) was loaded up to 500 kN horizontally and no failure occurred. Neither cracks nor loss of bond between the concrete and the galvanised sheet being seen at this load. This composite strut was re-tested with horizontal load of up to 200 kN. It was then re-tested with a vertical load of up to 50 kN when it failed. Its failure was characterised by cracking along the transverse axis together with obvious separation between the galvanised steel sheet and the concrete (see Plate 4.3).

Only the longitudinal strains along the longitudinal axis were considered for the composite struts. The minimum and the maximum measured strains were found to be those at the distances 200 mm and 400 mm from the centreline respectively, that is 100 mm from the

connectors towards the centreline and 100 mm from the connectors towards the end of the strut (see Table 4.3).

Load-deflection curves are shown for the second composite strut in Figures 4.5 to 4.7. With the presence of both vertical and horizontal loads, all the load-deflection graphs show the same feature as the previous composite space frame unit and the composite unit. The deflection went down at first, but reversed to the upward direction later. The load-deflection behaviour of the second strut displayed the tendency of the composite T-beam section to go upward from the first application of the horizontal load.

4.2.4 Composite Space Frame Unit 2:

This unit was similar to the previous composite space frame unit 1 except that it had double the number of connectors. According to results in Table 4.4, the following load/strain behaviour were observed. The longitudinal strain just before failure of the unit at 100 mm from the connectors towards the centreline of the unit was found to be -245.0×10^{-6}. It was $+90.75 \times 10^{-6}$ at 100 mm from the connectors towards the end of the composite T-beam section. Therefore, it may be concluded that the minimum strain was at or close to the location of the connectors. Tensile longitudinal strains along the longitudinal axis appear between the quarter points and the supports as is shown in Table 4.4 for strains at (0,400). This observation confirms the conclusion

mentioned in section 4.2.1; however, the use of more connectors in this case makes it clearer. As stated in section 4.2.1, the section between the quarter points and the supports had no shear connectors. As a result, a significant part of the load is carried by the steel section from the supports up to the quarter points. The presence of shear connectors at the quarter points enables load to be transferred to the concrete between the two quarter points. This transfer appears to be the reason for concrete tensile stresses being developed in this case between the quarter point and the support. Along the transverse axis, the longitudinal strain before failure at the distances of 100 mm and 200 mm were -226×10^{-6} and $+15.1 \times 10^{-6}$ respectively. Therefore, the minimum strain occurs between the two points.

At the centreline, the longitudinal strains (before failure) on the concrete surface, the profiled sheet and the stem of the double angles are -176, -393 and -882 micro strain respectively.

The load-deflection curve (see Figure 4.8) shows that the deflection of the composite T-beam went down first due to the applied vertical load, but it reversed to the upward direction directly with the first increment of the applied horizontal load. It continued to deflect upwards until the unit failed at the maximum horizontal load of 470 kN. Failure was observed with concrete crushing at the end near to the horizontal jack

(see Plates 4.4a, 4.4b and 4.4c).

4.2.5 Composite Space Frame Unit 3:

This unit was different from the previous types in the number and spacing of connectors. It was prepared with two connectors in each trough. The following observations were based on results shown in Table 4.5.

Along the longitudinal axis, at the centreline, the longitudinal strains were found to be the highest at the greatest distance from the connectors. At a horizontal load of 500 kN, the strain at the centreline was -339 x 10^{-6} where the nearest connectors being 112.5 mm away. However, the longitudinal strain at the same horizontal loading, at a distance of 200 mm from the centreline is lower (-287 x 10^{-6}), and the distance to the nearest connectors is shorter (87.5 mm) than those at the centreline. The longitudinal strain at the same load along the same axis was found to be the lowest (-154 x 10^{-6}) at a distance of 400 mm from the centreline and at a distance to the nearest connectors which is the shortest (62.5 mm). Therefore, it may be concluded for this case that strains were proportional to distance from the connectors along the longitudinal axis.

Along the transverse axis, the strains reduced with distance away from the centreline. At the same horizontal loading (500 kN), the strains at the centreline and at 100 mm, 200 mm and 400 mm from it were -339, -46, -48 and +21 micro strain respectively.

At the centreline, at the same loading, the strain at the middle of the stem of the double angles is -990 x 10^{-6} which was nearly 3 times that on the concrete surface (-339 x 10^{-6}).

Load-deflection curve (see Figure 4.9) shows that the deflection went down at first due the applied vertical load. It reversed to the upward direction from the first increment of the applied horizontal load. Cracks first appeared at the horizontal load of 370 kN parallel to the longitudinal axis and around the two ends of the T-beam section.

The unit had not failed up to a horizontal load of 500 kN with the same constant vertical load applied on all the test units (8 kN). The vertical load increased in steps up to 45 kN while the horizontal load kept constant at 500 kN and no failure took place. The horizontal load was then kept constant at 370 kN, that was the load when the first crack appeared, and the vertical load applied directly on the longitudinal axis at the centreline in increments. Failure took place at the maximum horizontal load of 370 kN and the maximum vertical load of 168 kN. Failure took place with crushing of the concrete and bending of the double angles below the vertical load. The concrete crushed almost all the way along the longitudinal axis. This failure mode is shown in Plates 4.5a, 4.5b and 4.5c.

4.2.6 Composite Space Frame Unit 4:

The composite slab of this unit had a different connector arrangement to the others. Two connectors were attached in each of the two ribs to the sides of the centreline and two at each end of the composite T-beam. This arrangement is assumed to follow arrangement b mentioned in chapter 3 (section 3.4). Although it was not possible to place the connectors exactly at the centreline, those connectors placed in the two ribs adjacent to it were assumed to represent this case. The following observations are based on results shown in Table 4.6.

Along the longitudinal axis, the lowest strains were those at the centreline between the four connectors located in the two adjacent ribs. The strains were low at the ends near the two end connectors. The highest strains were at points furthest from the connectors. Before failure, the strains at the centreline, at 200 mm and 500 mm from the centreline were -318, -2112 and -1515 micro strain respectively.

Along the transverse axis, the strains at the centreline were higher than all the previous tests irrespective of the connector placement. Before failure, at the same load, the strains at the centreline and at 100 mm, 200mm and 400 mm from the centreline are -318, -181, -209 and -79 micro strain respectively.

Before failure also, the strain at the centreline on

the concrete surface, on the profiled sheet and on the stem of the steel double angles are -318, -1032 and -618 micro strain respectively. The lowest strain was that on the concrete surface, and the maximum strain was on the profiled steel sheet.

The load-deflection curve (see Figure 4.10) shows that deflection went down first under the applied vertical load similar to the previous cases. It also reversed to the upward direction directly with the application of first increment of the horizontal load. Cracks appeared at a horizontal load of 320 kN parallel to the longitudinal axis and around the two ends of the T-beam section. Failure took place at a maximum horizontal load of 500 kN and a constant vertical load of 8 kN. Failure was recognised for this case with crushing of the concrete at the end of the composite T-beam near the horizontal jack (see Plate 4.6a and 4.6b).

4.2.7 Effective Width Results

Generally, as stated before, it was found that longitudinal strain decreases as the distance increases from the mid-span to the ends of the transverse axis. However, with CSFU1 (run 6), the strain measurement at (200,0) was higher than that at (100,0). The same thing is true with the same unit (run 10) where the strain measurement at (300,0) was higher than that at (200,0). On the other hand, strains at (100,0) and (200,0) are nearly equal in the case of CSFU3 (-45.6 and -48.4

microstrain). This may be due to misleading readings from the acoustic gauges at some of these locations and/or the effect of vertical loading covering a significant area along the transverse axis in the cases of CSFUs. This produces local strains masking the overall strut effect. The strain reading at (100,0) for CSFU1, run 6 (mentioned above) is the only reading which does not agree with the general observation. If this reading is excluded, the strain readings at (0,0), (200,0) and (400,0) follow the general assumption. This is also supported by the corresponding strain measurements for the case of CSFU1 (run9) where all strains including that at (100,0) agree with the hypothesis.

Observations opposite to that generally assumed were seen in the cases of CSFU2 and CSFU3. It is seen that longitudinal strains at (0,400) were decreasing at certain loadings. A lack of continuity may be the reason behind this behaviour.

4.3 Steel Struts:

A group of steel double-angle struts with the short legs connected back to back was tested first. A load-deflection curve for one of the struts of this group is shown in Figure 4.11. The curve represents the deflection in the plane and to the direction of the final deformation of the strut after failure. All the five steel struts of this group deflected to the side

representing the downward direction of the top chord in the actual structure. The maximum loads reached at failure of all the struts of this group are shown in Table 4.7. The other group of the steel struts with the long legs of angles were connected back to back were tested in the same way. It was found that all the struts of this group deflected to the side which represented the side direction of the top chord in the actual structure. The load-deflection curve for one of these struts is shown in Figure 4.12. The maximum loads reached at failure of the struts in this group are also shown in Table 4.7. Figure 4.13 shows the relation between the downward and the sideward deflections. Plates 4.7 and 4.8 shows the failure of the two groups of the steel struts.

4.3.1 Non-composite and Composite struts

For the elastic buckling of slender members, the Euler formula $P_{cr}=\pi^2EI/L^2$ can be applied provided the slenderness ratio $(L/r)_{lim} \geq \sqrt{2\pi^2E/F_y}$. In other cases, the buckling load does not follow Euler formula, and the compression member may undergo inelastic buckling (12). For the two-angle strut tested, L/r = 769.0, and $\sqrt{2\pi^2E/F_y}$ = 114.0 so the Euler formula is applicable. The Euler load is 351 kN if the strut is assumed pin-ended. It would be higher if some degree of fixity at the supports is assumed. However, experimental results showed that failure load was less than this. The top-

chord member within the unit failed at 254 kN (Space Decks Limited) (10). When the top-chord was tested as steel struts, the average failure load was 202 kN as explained in appendix A. The lower experimental value for these struts may be explained by lack of straightness and eccentricity of the applied load which is supported by the Southwell determination (27) of the buckling load for the CSFUs.

When the top-chord is considered as a composite section, the Euler formula is not applicable and, therefore, the member may undergo inelastic buckling. However, experimentally, the concrete section failed before reaching this stage.

TABLE 4.1.1 VARIATION OF STRAINS WITH LOADS FOR CSFU1 (RUN 1)

Vertical Load (kN)	Horizontal Load (kN)	Strain x 10^{-6}							
		Transverse on the Concrete Surface at (mm)				Longitudinal on steel Angle Stems at (mm)		Longitudinal on Concrete Surface at (mm)	
		(0,0)	(300,300)	(0,300)	(300,0)	(0,0)	(0,300)	(0,150)	(300,150)
0.0	0.0	0.0	0.0	0.0	0.0	0.0	0.0	0.0	0.0
8.0	10.0	+24.2	+9.08	+24.2	+6.05	+11.9	+5.0	-18.8	-8.13
	20.0	+27.2	+9.08	+28.7	+6.05	-4.67	-11.9	-27.5	-12.5
	30.0	+28.0	+9.08	+30.3	+9.08	-9.07	-23.9	-31.3	-16.9
	40.0	+30.3	+9.08	+30.3	+9.08	-22.8	-42.8	-34.4	-16.9
	50.0	+30.3	+9.08	+30.3	+9.08	-40.7	-66.3	-37.5	-16.9
	60.0	+33.3	+12.1	+33.3	+9.08	-57.8	-91.0	-40.0	-20.0
	70.0	+33.3	+12.1	+33.3	+9.08	-76.0	-110.3	-43.1	-21.9
	80.0	+39.3	+15.1	+33.3	+12.1	-77.2	-136.0	-46.9	-24.4

Sign convention: +ve Tensile
-ve Compression

TABLE 4.1.2 VARIATION OF STRAINS WITH LOADS FOR CSFU1 (RUN 3)

Vertical Load (kN)	Horizontal Load (kN)	Strain x 10^{-6}								
		Longitudinal on the Concrete Surface at (mm)						Transverse on the Concrete Surface at (mm)		
		(0,0)	(0,280)	(0,300)	(1000,0)	(800,0)	(400,0)	(1000,0)	(800,0)	(400,0)
0.0	0.0	0.0	0.0	0.0	0.0	0.0	0.0	0.0	0.0	0.0
12.0	10.0	-60.6	-33.3	-35.0	-15.1	-21.2	-30.3	0.0	0.0	+15.1
	20.0	-69.4	-36.9	-40.6	-15.1	-21.2	-33.3	+3.03	0.0	+15.1
	40.0	-73.8	-41.3	-47.5	-15.1	-21.2	-36.3	+3.03	0.0	+21.2
	60.0	-78.8	-48.8	-52.5	-15.1	-18.2	-39.3	+3.03	0.0	+21.2
	80.0	-86.9	-55.0	-63.8	-15.1	-21.2	-42.4	+3.03	0.0	+24.2
	100.0	-91.9	-61.9	-73.1	-15.1	-21.2	-45.4	+3.03	0.0	+15.1
	120.0	-104.4	-71.9	-90.0	-15.1	-21.2	-51.4	+3.03	-1.25	+21.2

TABLE 4.1.3 VARIATION OF STRAINS WITH LOADS FOR CSFU1 (RUN 6)

Vertical Load (kN)	Horizontal Load (kN)	Strains on the Concrete Surface x 10^{-6}							
		Longitudinal at (mm)							Transv. at (mm)
		(0.,0.)	(0.,280)	(0.,300)	(0.,450)	(100,0.)	(200,0.)	(400,0.)	(0.,80)
0.0	0.0	0.0	0.0	0.0	0.0	0.0	0.0	0.0	0.0
18.0	10.0	-92.5	-48.1	-46.9	-84.4	—	-63.5	-39.3	+42.4
	20.0	-93.8	-51.3	-49.4	-57.5	—	-66.6	-39.3	+45.4
	40.0	-101.3	-55.6	-60.6	-93.8	-8.75	-72.6	-45.4	+51.4
	60.0	-106.3	-62.5	-65.0	-118.0	-8.75	-66.6	-51.4	+51.4
	80.0	—	-71.9	-73.8	-142.2	-15.6	-84.7	-48.4	+51.4
	100.0	-119.4	-81.9	-83.1	-166.4	-16.3	-90.9	-54.5	+54.5
	120.0	-127.5	-91.3	-91.9	-187.6	-27.5	-99.9	-54.5	+54.5
	140.0	-135.6	-98.1	-102.5	-217.6	-35.6	-102.9	-60.5	+60.5
	160.0	-141.9	-108.1	-117.5	-242.0	-38.8	-108.9	-60.5	+54.5
	180.0	-151.3	-119.4	-128.1	-272.3	-46.9	-118.0	-72.6	+57.5
	200.0	-158.1	-128.8	-140.0	-296.5	-54.4	-124.0	-72.6	+57.5
	220.0	-164.4	-138.8	-150.0	-317.6	-61.9	-127.1	-72.6	+57.5
	230.0	-167.5	-149.4	-153.8	-326.7	-65.6	-127.1	-75.6	+57.5

TABLE 4.1.4 VARIATION OF STRAINS WITH LOADS FOR CSFU1 (RUN 9)

Vertical Load (kN)	Horizontal Load (kN)	Strain x 10^{-6}								
		Longitudinal on the Concrete Surface at (mm)							Transverse on the Concrete Surface at (mm)	
		(0.,0.)	(0,280)	(0.,300)	(0.,450)	(100,0)	(200,0	(400,0)	(0,80)	(300,0)
0.0	0.0	0.0	0.0	0.0	0.0	0.0	0.0	0.0	0.0	0.0
27.0	10.0	-132.5	-66.9	-56.9	——	-106.3	——	-63.5	+57.5	+36.9
	50.0	-145.0	-82.5	-72.5	——	-115.6	——	-72.6	+57.5	+36.9
	100.0	-160.0	-109.4	-89.4	-15.1	-131.9	-133.1	-81.7	+57.5	+40.6
	150.0	-161.9	-140.6	-115.0	-84.7	——	-145.2	——	——	+45.0
	200.0	-195.0	-160.0	-145.6	-136.1	-157.5	-154.3	-93.8	+75.6	+48.8
	250.0	-209.4	-178.1	-170.0	-190.6	-170.6	——	-99.8	+93.8	+51.9
	280.0	-217.5	-188.1	-185.6	-220.8	-168.1	——	-105.9	+84.7	+54.4
	290.0	-223.1	-193.1	-193.8	——	-181.3	——	-105.9	+84.7	+56.3
	300.0	-225.6	-198.1	-200.0	-242.0	-183.8	-172.4	-108.9	+84.7	+54.4
	310.0	-230.6	-201.3	-207.5	-251.1	-183.8	-175.5	-108.9	+84.7	+55.6
	320.0	-235.6	-208.8	-213.8	-263.2	-188.8	-178.5	-111.9	+84.7	+58.1
	330.0	-238.1	-209.4	-223.1	-266.2	-191.9	-184.5	-108.9	+84.7	+58.1
	340.0	-241.3	-216.9	-229.4	——	-194.4	-184.5	-118.0	+84.7	+59.4
	350.0	-245.6	-220.6	-237.5	-777.4	-196.6	-184.5	——	+84.7	+59.4

TABLE 4.1.5 VARIATION OF STRAINS WITH LOADS FOR CSFU1 (RUN 10)

Vertical Load (kN)	Horizontal Load (kN)	Strain x 10^{-6}								
		Longitudinal on Angles Stem at (mm)		Longitudinal on the Concrete Surface at (mm)						
		(0,0)	(0,300)	(0,0)	(0,100)	(0,270)	(0,500)	(200,0)	(300,0)	(400,0)
0.0	0.0	0.0	0.0	0.0	0.0	0.0	0.0	0.0	0.0	
40.0	50.0	-58.1	-82.5	-21.3	-21.9	-35.0	-211.8	——	-105.9	-9.1
	100.0	-99.7	-119.4	-27.5	-53.1	-65.6	-366.0	-27.2	-111.9	-9.1
	140.0	-120.9	-167.2	-43.8	-76.3	-88.8	-450.7	——	-105.9	-6.1
	160.0	-130.9	-180.0	——	-88.1	-96.9	-490.1	-33.3	——	-3.0
	180.0	-139.7	-202.5	-44.4	-100.0	-107.5	-523.3	-30.3	-111.9	-3.0
	200.0	-148.4	——	-55.0	-115.6	-122.5	-565.7	-39.3	-111.9	-3.0
	220.0	-150.3	-213.8	-58.8	-124.4	-128.1	-595.9	-42.4	-111.9	-3.0
	240.0	-160.9	-223.4	-65.0	-143.8	-145.0	-686.7	-45.4	-111.9	-3.0
	260.0	-172.2	-230.0	-65.0	-156.3	-152.5	-744.2	-45.4	-111.9	0.0
	280.0	-180.9	-239.7	-68.1	-168.1	-163.8	-822.8	-48.4	-111.9	0.0
	300.0	-190.0	-262.2	-74.4	-182.5	-176.9	-901.5	-51.4	-111.9	0.0
	320.0	-201.9	-267.9	-80.6	-198.1	-190.0	-986.2	-51.4	-111.9	——
	340.0	-218.8	-294.1	-86.3	-215.0	-205.6	-1073.9	-51.4	-111.9	——
	350.0	-236.3	-298.4	-92.5	-226.9	-216.3	-1131.4	-54.5	-115.0	——

TABLE 4.1.6.1 STRAIN VARIATION ALONG THE LONGITUDINAL AXIS ON CONCRETE SURFACE

Run No.	Distance From C.L. (mm)	Longitudinal Strain $\times 10^{-6}$	Transverse Strain $\times 10^{-6}$
3 V.L.=12kN H.L=120kN	0.0 280.0 300.0 ——	-104.4 -71.9 -90.0 ——	+48.4 at distance of 80.0 mm on both sides of the C.L.

V.L. - Vertical Load
H.L. - Horizontal Load

TABLE 4.1.6.2 STRAIN VARIATION ALONG THE TRANSVERSE AXIS ON CONCRETE SURFACE

Run No.	Distance From C.L. (mm)	Longitudinal Strain $\times 10^{-6}$	Transverse Strain $\times 10^{-6}$
3 V.L.=12kN H.L=120kN	0.0 400.0 800.0 1000.0	-104.4 -51.4 -21.2 -15.1	21.2,-1.3 and 3.0 at distances of 400, 800. and 1000 mm respectively.

TABLE 4.1.7.1 STRAIN VARIATION ALONG THE LONGITUDINAL AXIS ON CONCRETE SURFACE

Run No.	Distance From C.L. (mm)	Longitudinal Strain $\times 10^{-6}$	Transverse Strain $\times 10^{-6}$
5 V.L.=18kN H.L=180kN	0.0	-58.8	+75.6 at distances of 80. mm each side of the C.L.
	280.0	-116.3	
	300.0	-131.3	
	—	—	

TABLE 4.1.7.2 STRAIN VARIATION ALONG THE TRANSVERSE AXIS ON CONCRETE SURFACE

Run No.	Distance From C.L. (mm)	Longitudinal Strain $\times 10^{-6}$	Transverse Strain $\times 10^{-6}$
5 V.L.=18kN H.L=180kN	0.0	-58.8	+24.2,2.5 and 3.0 at distances 400., 800. and 1000 mm respectively.
	400.0	-75.6	
	800.0	-6.05	
	1000.0	-3.03	

TABLE 4.1.8.1 STRAIN VARIATION ALONG THE LONGITUDINAL AXIS ON CONCRETE SURFACE

Run No.	Distance From C.L. (mm)	Longitudinal Strain $\times 10^{-6}$	Transverse Strain $\times 10^{-6}$
6 V.L.=18kN H.L=230kN	0.0	-167.5	+63.5 at distance of 80.0 mm on both sides of the from the C.L.
	280.0	-149.4	
	300.0	-153.8	
	450.0	-326.7	

TABLE 4.1.8.2 STRAIN VARIATION ALONG THE TRANSVERSE AXIS ON CONCRETE SURFACE

Run No.	Distance From C.L. (mm)	Longitudinal Strain $\times 10^{-6}$	Transverse Strain $\times 10^{-6}$
6 V.L.=18kN H.L=230kN	0.0	-167.5	+50.0 at distance of 100. mm from the C.L.
	200.0	-127.1	
	300.0	-99.8	
	400.0	-75.6	

TABLE 4.1.9.1 STRAIN VARIATION ALONG THE LONGITUDINAL AXIS ON CONCRETE SURFACE

Run No.	Distance From C.L. (mm)	Longitudinal Strain $\times 10^{-6}$	Transverse Strain $\times 10^{-6}$
7 V.L.=27kN H.L=280kN	0.0	-103.1	+9.1 at distance of 80.0 mm on both sides of the from the C.L.
	280.0	-131.9	
	300.0	-133.8	
	450.0	-338.8	

TABLE 4.1.9.2 STRAIN VARIATION ALONG THE TRANSVERSE AXIS ON CONCRETE SURFACE

Run No.	Distance From C.L. (mm)	Longitudinal Strain $\times 10^{-6}$	Transverse Strain $\times 10^{-6}$
7 V.L.=27kN H.L=280kN	0.0	-103.1	———
	200.0	-81.7	
	300.0	-45.4	
	400.0	-3.03	

TABLE 4.1.10.1 STRAIN VARIATION ALONG THE LONGITUDINAL AXIS ON CONCRETE SURFACE

Run No.	Distance From C.L. (mm)	Longitudinal Strain $\times 10^{-6}$	Transverse Strain $\times 10^{-6}$
8 V.L.=27kN H.L=300kN	0.0	-198.1	+48.4 at distance of 80.0 mm from the C.L.
	270.0	-218.8	
	310.0	-273.1	
	450.0	——	

TABLE 4.1.10.2 STRAIN VARIATION ALONG THE TRANSVERSE AXIS ON CONCRETE SURFACE

Run No.	Distance From C.L. (mm)	Longitudinal Strain $\times 10^{-6}$	Transverse Strain $\times 10^{-6}$
8 V.L.=27kN H.L=300kN	0.0	-198.1	+26.9 at distance of 200. mm from the C.L.
	200.0	-124.0	
	300.0	——	
	400.0	-51.4	

TABLE 4.1.11.1 STRAIN VARIATION ALONG THE LONGITUDINAL AXIS ON CONCRETE SURFACE

Run No.	Distance From C.L. (mm)	Longitudinal Strain x 10^{-6}	Transverse Strain x 10^{-6}
9 V.L.=27kN H.L=350kN	0.0	-245.6	+87.7 at distance of 80.0 mm on both sides of the C.L.
	280.0	-220.6	
	300.0	-237.5	
	450.0	-777.4	

TABLE 4.1.11.2 STRAIN VARIATION ALONG THE TRANSVERSE AXIS ON CONCRETE SURFACE

Run No.	Distance From C.L. (mm)	Longitudinal Strain x 10^{-6}	Transverse Strain x 10^{-6}
9 V.L.=27kN H.L=350kN	0.0	-245.6	+59.4 at distance of 200. mm from the C.L.
	200.0	-184.5	
	300.0	-139.1	
	400.0	-118.0	

TABLE 4.1.12.1 STRAIN VARIATION ALONG THE LONGITUDINAL AXIS ON CONCRETE SURFACE

Run No.	Distance From C.L. (mm)	Longitudinal Strain $\times 10^{-6}$	Transverse Strain $\times 10^{-6}$
10 V.L.=40kN H.L=350kN	0.0	-92.5	+48.4 at distance of 80.0 mm from the C.L.
	100.0	-226.9	
	270.0	-216.3	
	500.0	-1131.4	

TABLE 4.1.12.2 STRAIN VARIATION ALONG THE TRANSVERSE AXIS ON CONCRETE SURFACE

Loading Case	Distance From C.L. (mm)	Longitudinal Strain $\times 10^{-6}$	Transverse Strain $\times 10^{-6}$
10 V.L.=40kN H.L=350kN	0.0	-92.5	+26.9 at distance of 200. mm from the C.L.
	100.0	-58.0	
	200.0	-54.5	
	300.0	-115.0	
	400.0	0.0	

TABLE 4.1.13.1 COMPARISON OF STRAINS AT SIMILAR HORIZONTAL LOADINGS AND DIFFERENT VERTICAL LOADINGS ALONG THE LONGITUDINAL AXIS ON CONCRETE SURFACE

Distance From C.L. (mm)	Longitudinal Strain at Horiz. Load=200 KN	
	(Run 6*) x 10^{-6}	(Run9**) x 10^{-6}
0.0	-158.1	-195.0
280.0	-140.0	-145.6
300.0	-128.8	-160.0
450.0	-296.5	-136.1

TABLE 4.1.13.2 COMPARISON OF STRAINS AT SIMILAR HORIZONTAL LOADINGS AND DIFFERENT VERTICAL LOADINGS ALONG THE TRANSVERSE AXIS ON CONCRETE SURFACE

Distance From C.L. (mm)	Longitudinal strain at Horiz. Load=200 KN	
	(Run 6*) x 10^{-6}	(Run9**) x 10^{-6}
0.0	-158.1	-195.0
200.0	-124.0	-145.2
300.0	-93.8	-124.0
400.0	-72.6	-93.8

* V.L.=18kN
** V.L.=27kN

TABLE 4.1.14.1 COMPARISON OF STRAINS AT SIMILAR HORIZONTAL LOADINGS AND DIFFERENT VERTICAL LOADINGS ALONG THE LONGITUDINAL AXIS ON CONCRETE SURFACE

Distance From C.L. (mm)	Transverse Strain at Horiz. Load=200. KN	
	(Run 6*) x 10^{-6}	(Run9**) x 10^{-6}
80.0	+66.6	+75.6

TABLE 4.1.14.2 COMPARISON OF STRAINS AT SIMILAR HORIZONTAL LOADINGS AND DIFFERENT VERTICAL LOADINGS ALONG THE TRANSVERSE AXIS ON CONCRETE SURFACE

Distance From C.L. (mm)	Transverse Strain at Horiz. Load=200. KN	
	(Run 6*) x 10^{-6}	(Run9**) x 10^{-6}
200.0	+46.9	+48.8

* V.L.=18kN
** V.L.=27kN

TABLE 4.2.1 VARIATION OF STRAINS WITH LOADS FOR COMPOSITE UNIT

Vertical Load (kN)	Horizontal Load (kN)	Strain x 10^{-6}. Longitudinal on the Concrete Surface at (mm)				
		(0,0)	(0,200)	(0,400)	(100,0)	(200,0)
0.0	0.0	0.0	0.0	0.0	0.0	0.0
8.0	10.0	-16.9	-16.9	-2.50	-18.8	-18.2
	40.0	-23.8	-27.5	——	-30.6	-24.2
	80.0	-42.5	-36.9	——	-41.9	-33.3
	120.0	-55.6	-49.4	-15.6	-53.8	-45.4
	160.0	-70.6	-57.5	-49.4	-67.5	-54.5
	180.0	-78.8	-62.5	-72.5	-73.1	-60.5
	200.0	-87.5	-65.0	-94.4	-79.4	-66.6
	220.0	-94.4	-68.1	-118.8	-83.8	-69.6
	240.0	-101.3	-68.1	-140.6	-89.4	-72.6
	260.0	-107.5	-69.4	-162.5	-91.3	-78.7
	280.0	-112.5	-67.5	-172.5	-91.9	-78.7
	300.0	-118.8	-69.4	-182.5	-93.8	-78.7
	310.0	-125.8	-70.0	-186.9	-95.6	-81.7
	320.0	-130.6	-70.0	-191.3	-98.1	——
	330.0	-136.3	-70.6	-194.4	-99.4	-81.7
	340.0	-141.9	-70.6	-206.3	-100.6	-84.7
	350.0	-150.0	-73.1	-213.1	-103.8	-84.7
	360.0	-160.0	-74.4	-218.1	-108.1	-87.7
	370.0	-165.0	-78.8	-246.3	-117.5	-87.7
	380.0	-172.5	-85.0	-275.6	-127.5	-87.7
	390.0	Failure				

TABLE 4.2.2 VARIATION OF STRAINS WITH LOADS FOR COMPOSITE UNIT

Vertical Load (kN)	Horizontal Load (kN)	Strain x 10^{-6}				
		Transverse on the Concrete Surface at (mm)				
		(0,100)	(0,200)	(0,400)	(100,0)	(200,0)
0.0	0.0	0.0	0.0	0.0	0.0	0.0
8.0	10.0	+6.05	+6.05	+6.05	+18.8	+1.88
	40.0	+3.03	——	+6.05	+20.0	-0.625
	80.0	+12.1	+9.09	+18.2	+29.4	-3.75
	120.0	——	+15.1	+27.2	+41.3	-6.25
	160.0	+9.09	+15.1	+30.3	+53.1	-9.38
	180.0	——	+15.1	+33.3	*	-7.50
	200.0	——	+18.2	+36.3		-7.50
	220.0	+9.09	+18.2	+54.5		-8.75
	240.0	+12.1	+21.2	+60.5		-7.50
	260.0	+15.1	+24.2	+72.6		-8.75
	280.0	——	+30.3	+84.7		-7.50
	300.0	+27.2	+36.3	+96.8		-5.00
	310.0	+27.2	+48.4	+105.9		-5.00
	320.0	——	+54.5	+108.9		-3.75
	330.0	+39.3	+54.5	+115.0		-3.13
	340.0	——	+60.5	+127.1		-0.625
	350.0	+57.5	+60.5	+133.1		-0.625
	360.0	+63.5	+60.5	+139.2		-0.625
	370.0	+66.6	+60.5	+151.3		+1.88
	380.0	+69.6	+60.5	+257.1		+3.13
	390.0	Failure				

* The gauge came off at this load.

TABLE 4.3 VARIATION OF STRAINS WITH LOADS FOR COMPOSITE STRUT(2)

Vertical Load (kN)	Horizontal Load (kN)	Strain x 10^{-6}		
		Longitudinal on the Concrete Surface at (mm)		
		(0,0)	(0,200)	(0,400)
0.0	0.0	0.0	0.0	0.0
4.0	10.0	-13.1	-21.2	-21.2
	40.0	-24.4	-36.3	-33.3
	80.0	-37.5	-48.4	-54.5
	100.0	-43.8	-54.5	-60.5
	120.0	-50.0	-60.5	-66.6
	150.0	-60.0	-72.6	-78.7
	200.0	-82.5	-81.7	-66.6
	250.0	-94.4	-90.8	-108.9
	300.0	-114.4	-105.9	-130.1
	320.0	-116.3	-108.9	-136.1
	340.0	-125.0	-121.0	-145.2
	360.0	-143.4	-127.1	-151.3
	380.0	-142.5	-136.1	-157.3
	400.0	-148.8	-142.2	-163.4
	420.0	-157.5	-151.3	-178.5
	440.0	-157.5	-157.3	-184.5
	460.0	-174.4	-163.4	-187.6
	480.0	-183.8	-178.4	-196.6
	500.0	-191.3	-184.5	-202.7

TABLE 4.4 VARIATION OF STRAINS WITH LOADS FOR CSFU2

Vertical Load (kN)	Horizontal Load (kN)	Strain x 10^{-6}						
		Longitudinal on the Concrete Surface at (mm)					Longitudinal on the sheet & stem at (mm)	
		(0,0)	(0,200)	(0,400)	(100,0)	(200,0)	(0,0)	(0,0)
0.0	0.0	0.0	0.0	0.0	0.0	0.0	0.0	0.0
8.0	10.0	-27.2	-21.2	-18.2	-163.4	-30.3	+6.88	+15.6
	40.0	-33.3	-33.3	-6.05	-166.4	-30.3	+5.00	-6.25
	80.0	-30.3	-42.4	+12.1	-166.4	-30.3	+1.88	-31.3
	100.0	-30.3	-42.4	+27.2	-166.4	-30.3	-1.25	-37.5
	120.0	-36.3	-48.4	+33.3	-169.4	-30.3	-1.25	-53.1
	140.0	-42.4	-48.4	+57.5	-175.5	-30.3	-1.25	-71.3
	160.0	-45.4	-48.4	+72.6	-175.5	-24.2	-1.88	-98.1
	180.0	-48.4	-57.5	+90.8	-178.5	-24.2	——	-120.6
	200.0	-51.4	-69.6	——	-166.4	-24.2	-3.75	-179.4
	220.0	-39.3	-78.7	+124.0	-166.4	-24.2	-6.88	-192.5
	240.0	-45.4	-87.7	+130.1	-172.4	-24.2	-8.75	-237.5
	260.0	-51.4	-93.8	+130.1	-175.5	-24.2	-10.0	-301.9
	280.0	-54.5	-102.9	+136.1	-175.5	0.0	-17.5	-346.9
	300.0	-63.5	-111.9	+136.1	-181.5	+3.03	-41.3	-429.4
	320.0	-69.6	-121.0	+181.5	-184.5	+18.2	-218.3	-503.8
	340.0	-75.6	-133.1	+187.6	-187.6	+24.2	-256.9	-556.9
	360.0	-87.7	-148.2	+187.6	-187.6	+27.2	-290.6	-602.5
	380.0	-96.8	-163.4	+184.5	-193.6	+27.2	-503.8	-646.3
	400.0	-105.9	-175.5	+178.5	-199.7	+33.3	-630.0	-693.1
	420.0	-124.0	-196.6	+163.4	-208.7	+30.3	-546.9	-743.8
	440.0	-142.2	-217.8	+133.1	-220.8	+24.2	-460.6	-803.1
	460.0	-175.5	-245.0	+90.75	-226.9	+15.1	-392.5	-881.9
	470.0	Failure						

TABLE 4.5 VARIATION OF STRAINS WITH LOADS FOR CSFU3

Vertical Load (kN)	Horizontal Load (kN)	Strain x 10^{-6}						
		Longitudinal on the Concrete Surface at (mm)						Longit. on Stem at (mm)
		(0,0)	(0,200)	(0,400)	(100,0)	(200,0)	(400,0)	(0,0)
0.0	0.0	0.0	0.0	0.0	0.0	0.0	0.0	0.0
8.0	10.0	-245.0	-187.6	-142.2	-56.9	-51.4	-42.4	-46.9
	40.0	-254.1	-199.7	-163.4	-60.0	-60.5	-48.4	-70.6
	80.0	-263.2	-214.8	-193.6	-76.9	-69.6	-60.5	-72.5
	100.0	-272.3	-226.9	-211.8	-83.1	-81.6	-66.6	-89.4
	140.0	-275.3	-236.0	-242.0	-80.6	-78.7	-63.5	-151.9
	180.0	-272.3	-239.0	-260.2	-76.9	-75.6	-51.4	-214.4
	200.0	-272.3	-236.0	-260.2	-71.9	-69.6	-42.4	-240.6
	220.0	-272.3	-236.0	-260.2	-66.3	-63.5	-39.3	-274.4
	240.0	-269.2	-236.0	-242.0	-60.0	-63.5	-27.2	-310.0
	260.0	-272.3	-232.9	-254.1	-56.9	-54.5	-21.2	-349.4
	280.0	-272.3	-226.9	-217.8	-55.0	-54.5	-15.1	-391.3
	300.0	-272.3	-217.8	-193.6	-48.1	-54.5	-60.5	-441.3
	320.0	-272.3	-223.9	-190.6	-45.0	-60.5	——	-493.8
	340.0	-275.3	——	-184.6	-37.5	-45.4	+9.08	-499.4
	360.0	-281.3	-232.9	-178.5	-34.4	-39.3	+12.1	-618.8
	380.0	-287.4	-236.0	-160.3	-33.1	-39.3	+18.2	-675.0
	400.0	-284.4	-236.0	-139.2	-28.1	-33.3	+27.2	-730.0
	420.0	-302.5	——	-136.1	-31.3	-39.3	+21.2	-760.6
	440.0	-311.6	-251.1	-133.1	-35.0	-39.3	+21.2	-810.6
	460.0	-317.6	-257.1	-105.9	-36.3	-39.3	+27.2	-862.5
	480.0	-323.7	-269.2	-127.1	-38.8	-48.4	+27.2	-920.6
	500.0	-338.8	-287.4	-154.3	-45.6	-48.4	+21.2	-990.6

TABLE 4.6 VARIATION OF STRAINS WITH LOADS FOR CSFU4

Vertical Load (kN)	Horizontal Load (kN)	Strain x 10^{-6}							
		Longitudinal on the Concrete Surface at (mm)						Longit. on Sheet and Angles Stem at (mm)	
		(0,0)	(0,200)	(0,500)	(100,0)	(200,0)	(400,0)	(0,0)	(0,0)
0.0	0.0	0.0	0.0	0.0	0.0	0.0	0.0	0.0	0.0
8.0	10.0	-39.3	-54.5	+6.05	-44.4	-42.4	+78.6	+11.3	+0.625
	40.0	-54.5	-60.5	0.0	-58.8	-54.5	-39.3	+8.75	-65.6
	80.0	-69.6	-72.6	-18.2	-68.8	-63.5	-39.3	+6.88	-138.1
	100.0	-78.7	-81.7	-21.2	-79.4	-66.6	-45.4	+6.88	-176.3
	140.0	-105.9	-105.9	-27.2	-90.0	-87.7	-51.4	+6.88	-221.9
	180.0	-121.0	-127.1	-78.7	-98.1	-99.8	-45.4	-2.50	-249.4
	200.0	-130.1	-130.1	-105.9	-101.3	-105.9	-54.5	-2.50	-261.3
	220.0	-142.2	-142.2	——	-106.3	-118.0	-54.5	-18.8	-264.4
	240.0	——	-151.3	-172.4	-106.3	-118.0	-51.4	——	-270.6
	260.0	-157.3	-160.3	-214.8	-104.4	-127.1	-54.5	——	-279.4
	280.0	-175.5	-160.3	——	-90.0	-127.1	-51.4	——	-288.8
	300.0	-199.7	-142.2	——	-80.6	-124.0	-45.5	-81.8	-297.5
	320.0	-217.8	-396.3	-523.3	-79.4	-127.1	-51.5	-231.9	-305.0
	340.0	-226.9	-1697.0	——	-95.0	-139.2	——	-267.5	-320.6
	360.0	-239.0	-1751.5	-701.8	-103.8	-148.2	-51.4	-295.0	-350.0
	380.0	-254.1	——	-789.5	-112.5	-154.3	-51.4	-377.5	-370.6
	400.0	-263.2	——	——	-121.9	-163.4	-51.4	-505.6	-391.3
	420.0	-272.3	-1923.9	-1031.5	-130.0	-172.4	-45.4	-666.3	-415.0
	440.0	-284.4	-1987.4	-1179.8	-141.9	-181.5	-51.4	-798.8	-453.8
	460.0	-296.5	-2044.9	-1312.9	-155.0	-190.6	-66.6	-956.3	-503.8
	480.0	-305.5	-2111.5	-1461.1	-171.6	-202.7	-75.6	-1031.9	-503.1
	490.0	-317.6	——	-1515.5	-181.3	-208.7	-78.7	——	-617.5
	500.0	Failure							

TABLE 4.7 FAILURE LOADS OF STEEL STRUTS

Strut No.	Failure Load (kN)
a) Long legs b.t.b	
1	190.0
2	210.0
3	210.0
4	200.0
5	200.0
b) Short legs b.t.b.	
1	270.0
2	250.0
3	270.0
4	250.0
5	230.0

TABLE 4.8 TEST TYPES *

Group No	Test Type	Test description
1	Preliminary	A two-unit steel specimen was tested according to Southwell method.
2	Composite Space Frame Unit.	The above Test Unit was tested with a composite steel/ concrete slab attached to it .
3	Composite Unit.	The unit was tested similar to the previous case, but no ties and diagonals were attached to the composite slab.
4	Composite Struts.	Two groups of composite struts cut out of the top-trays were tested. The two groups differ in their widths.
5	Composite Space Frame Units.	Another three complete composite units were tested.
6	Steel struts	Two groups of steel struts cut out of the the top-trays were tested. The two groups were mainly differ in the length of the two legs connected back to back.

* Table 3.1 (repeated)

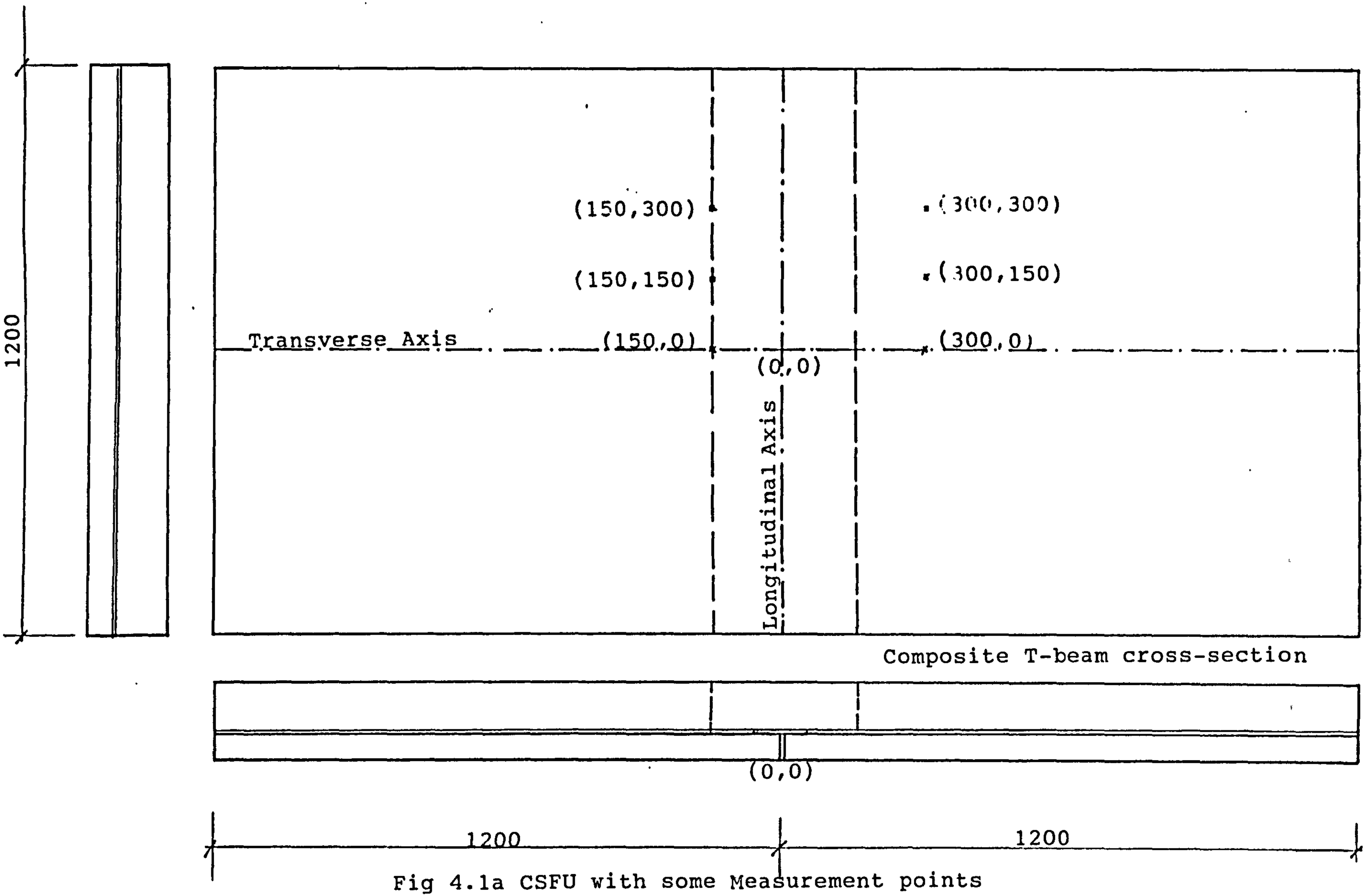

Fig 4.1a CSFU with some Measurement points

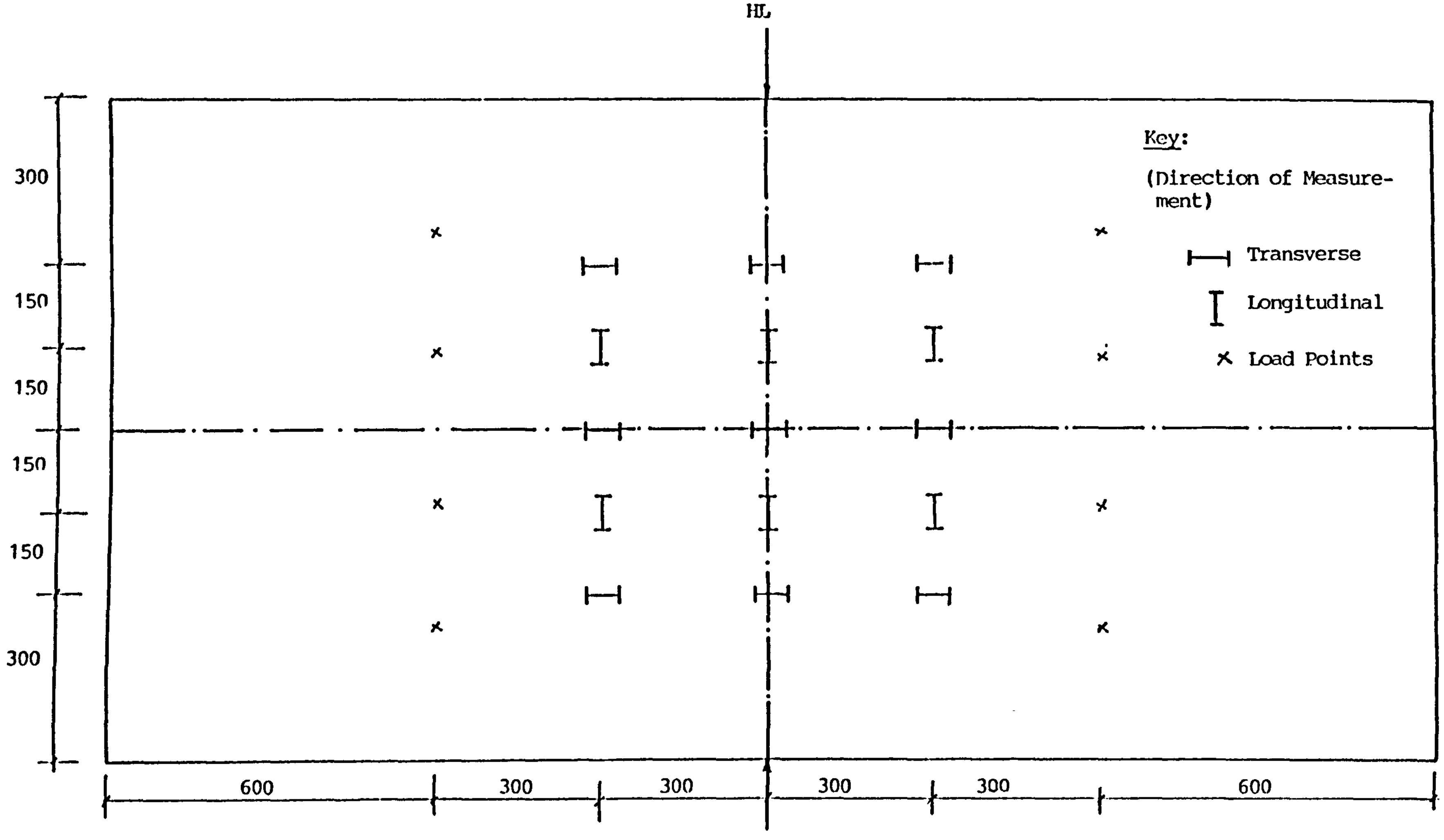

Fig.4.1b: Acoustic Gauges Arrangement for CSFUI (Runs 1 and 2)

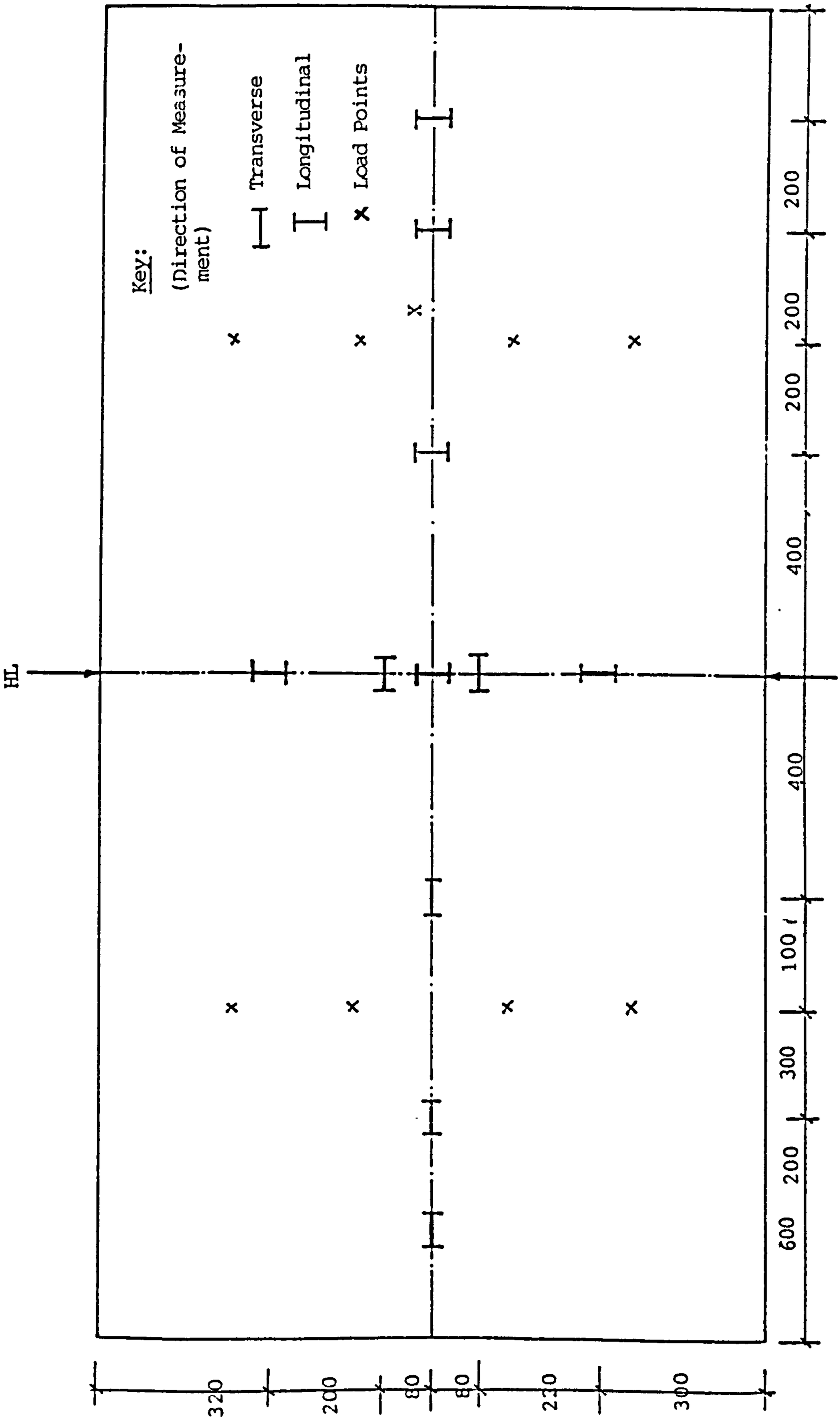

Fig. 4.1c Acoustic Gauges arrangement for CSFU1 (Runs 3and5)

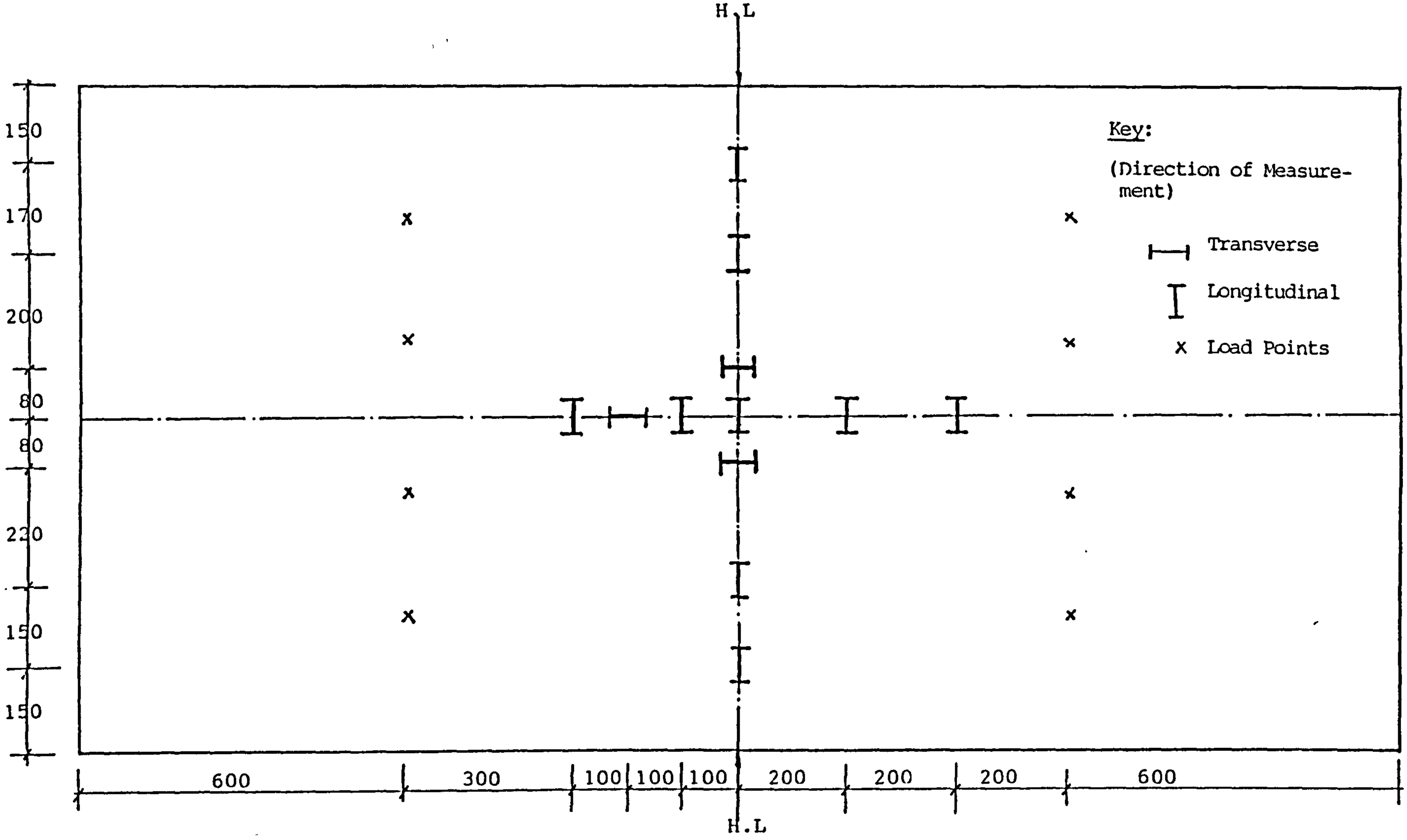

Fig. 4.1d Acoustic Gauges Arrangement for CSFU 1 (Runs 6,7 and 9)

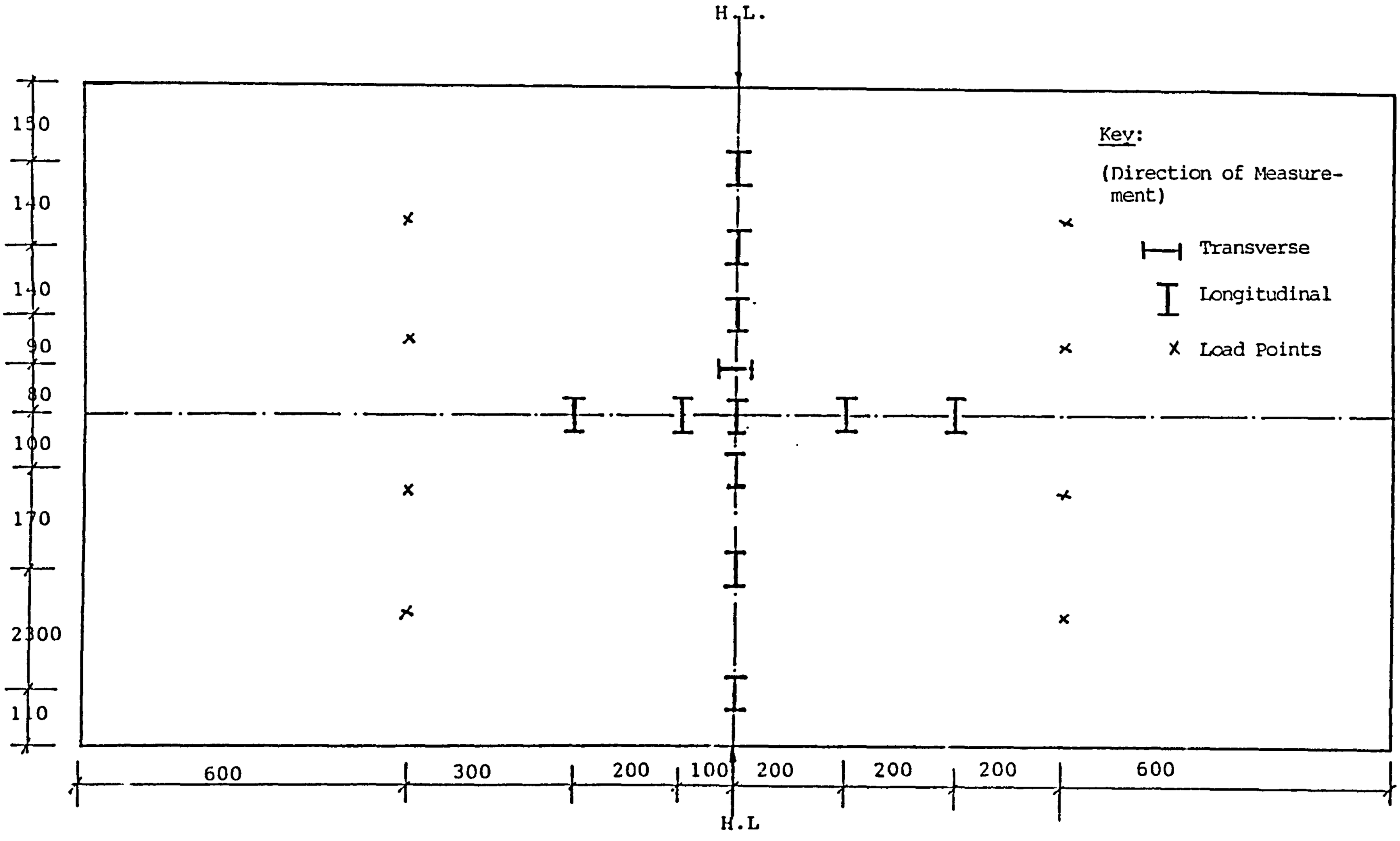

Fig. 4.1e Acoustic Gauges Arrangement for CSFU 1 (Runs 8 and 10)

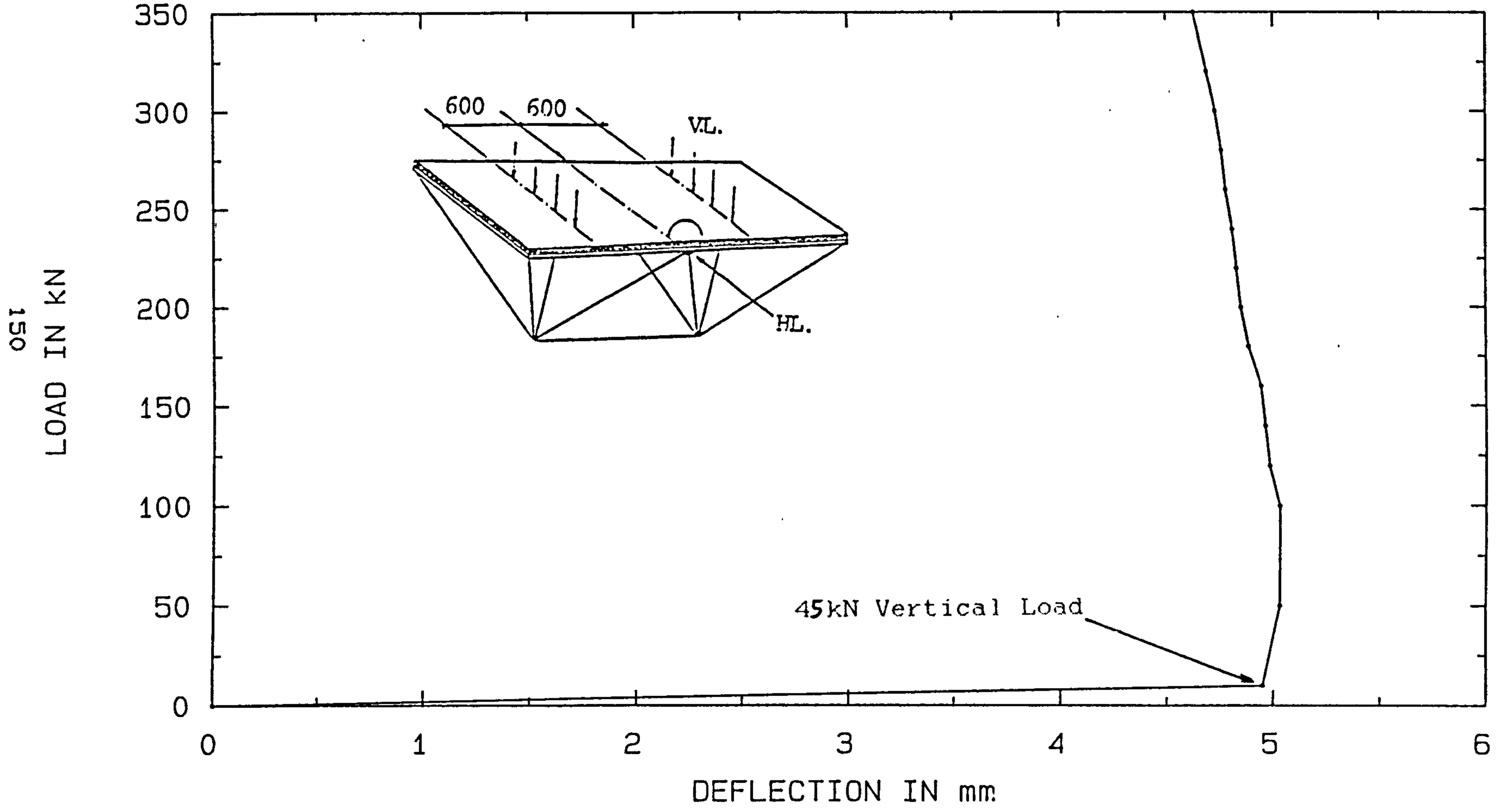

FIG.4.2 C.L. DEFLECTION OF THE COMPOSITE SPACE FRAME UNIT 1

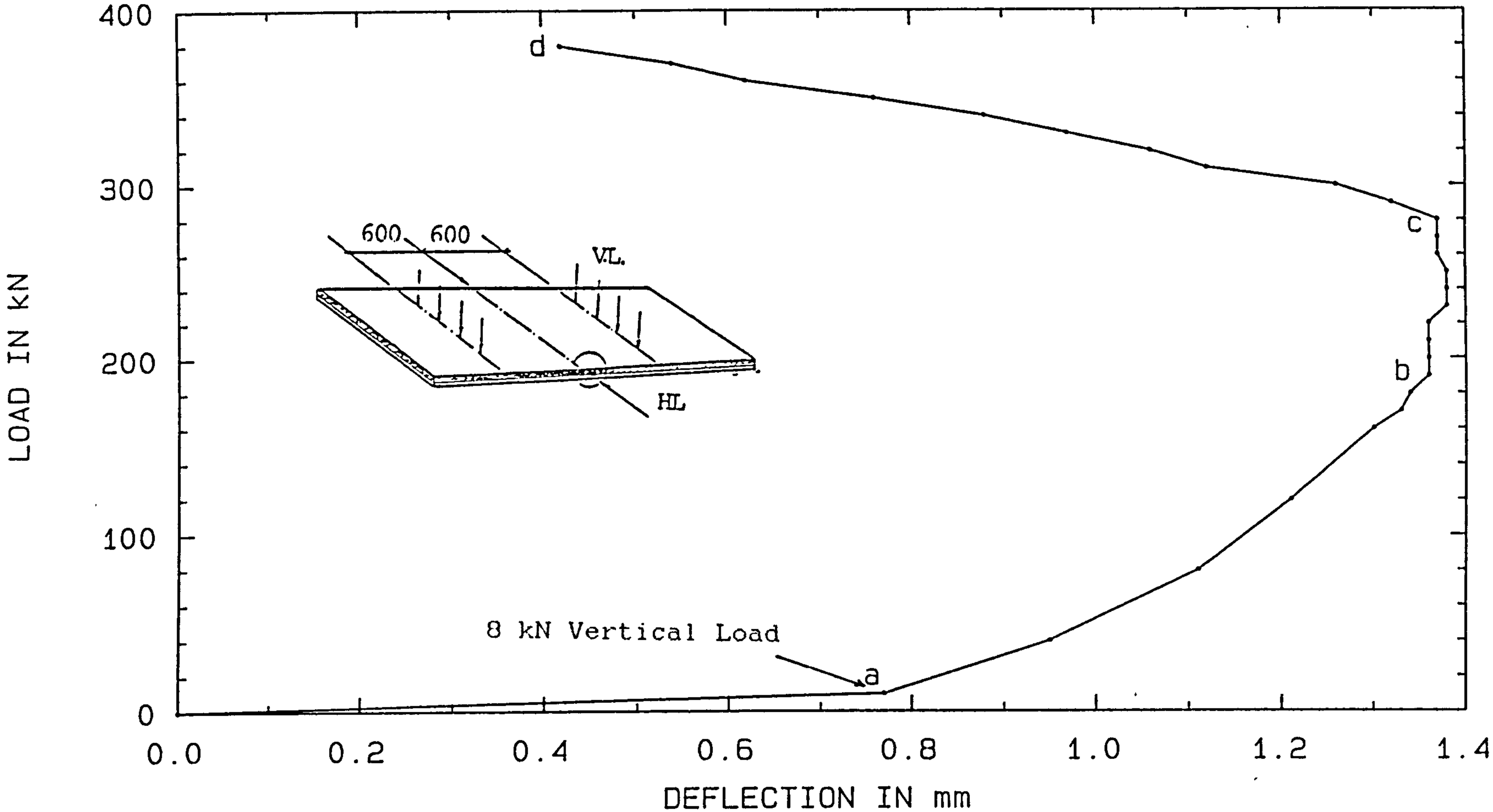

FIG.4.3 C.L. DEFLECTION OF THE COMPOSITE UNIT

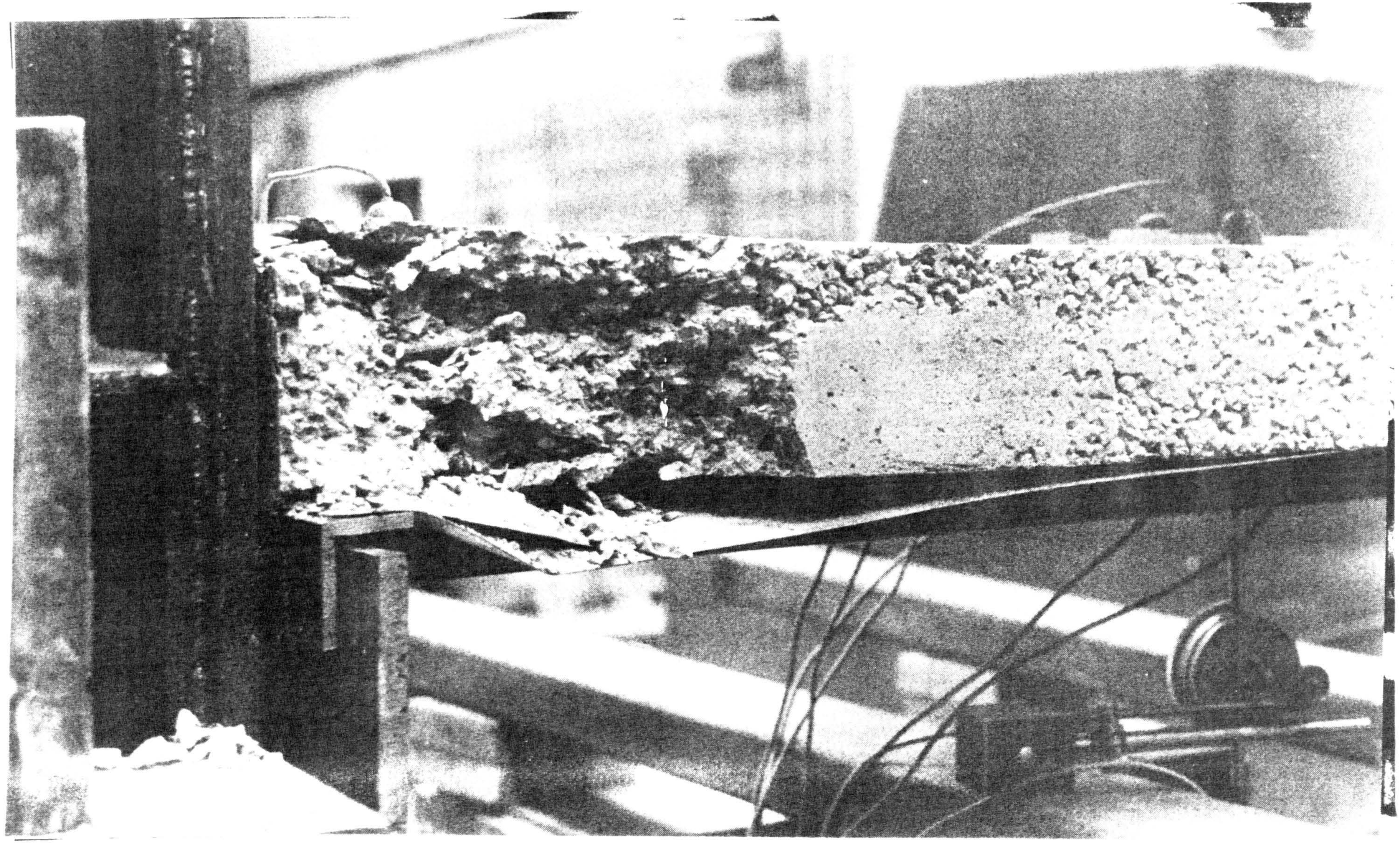

Fig. 4.4 Failure mode of composite strut 3

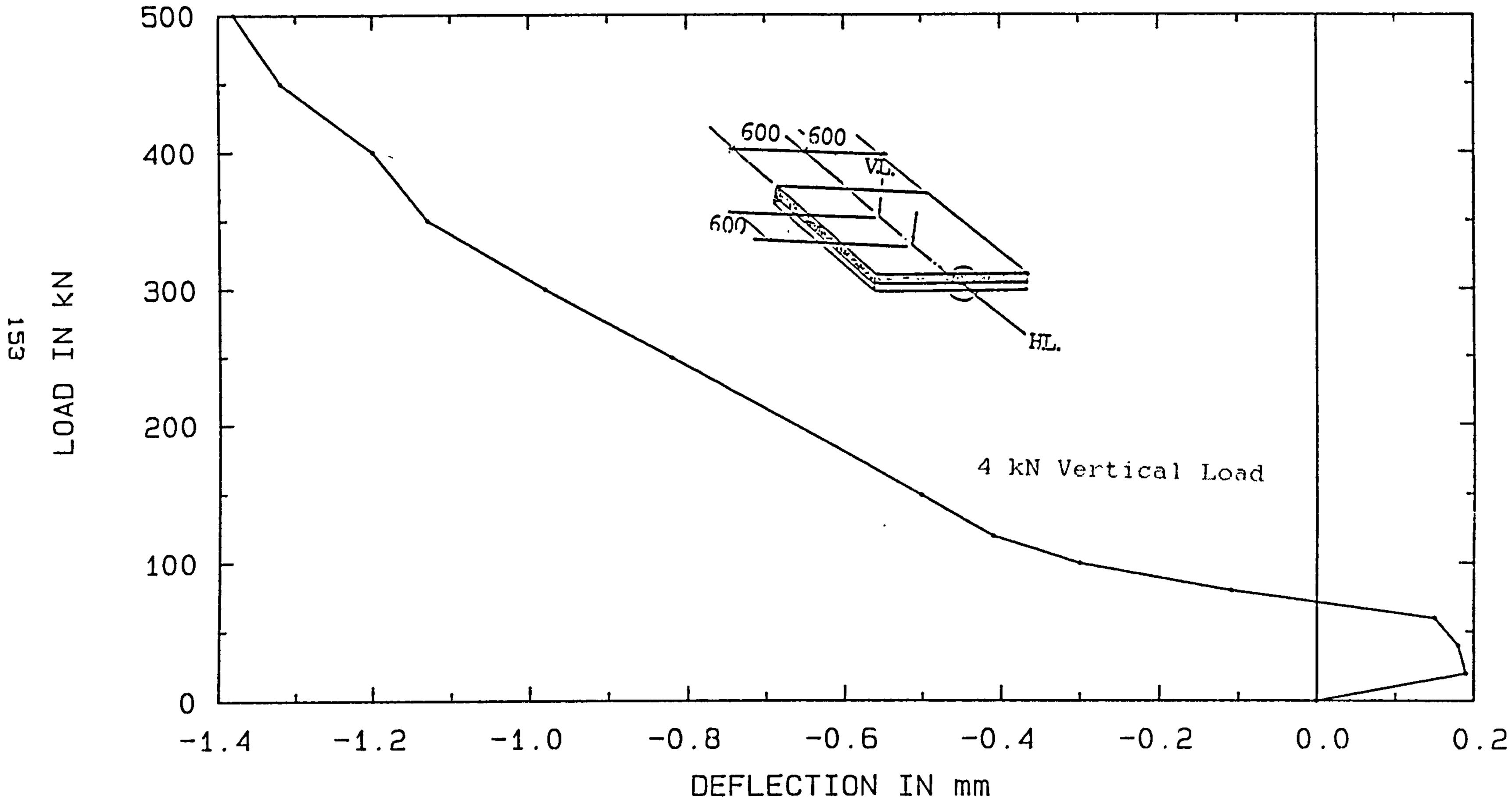

FIG.4.5 C.L. DEFLECTION OF THE COMPOSITE STRUT 2

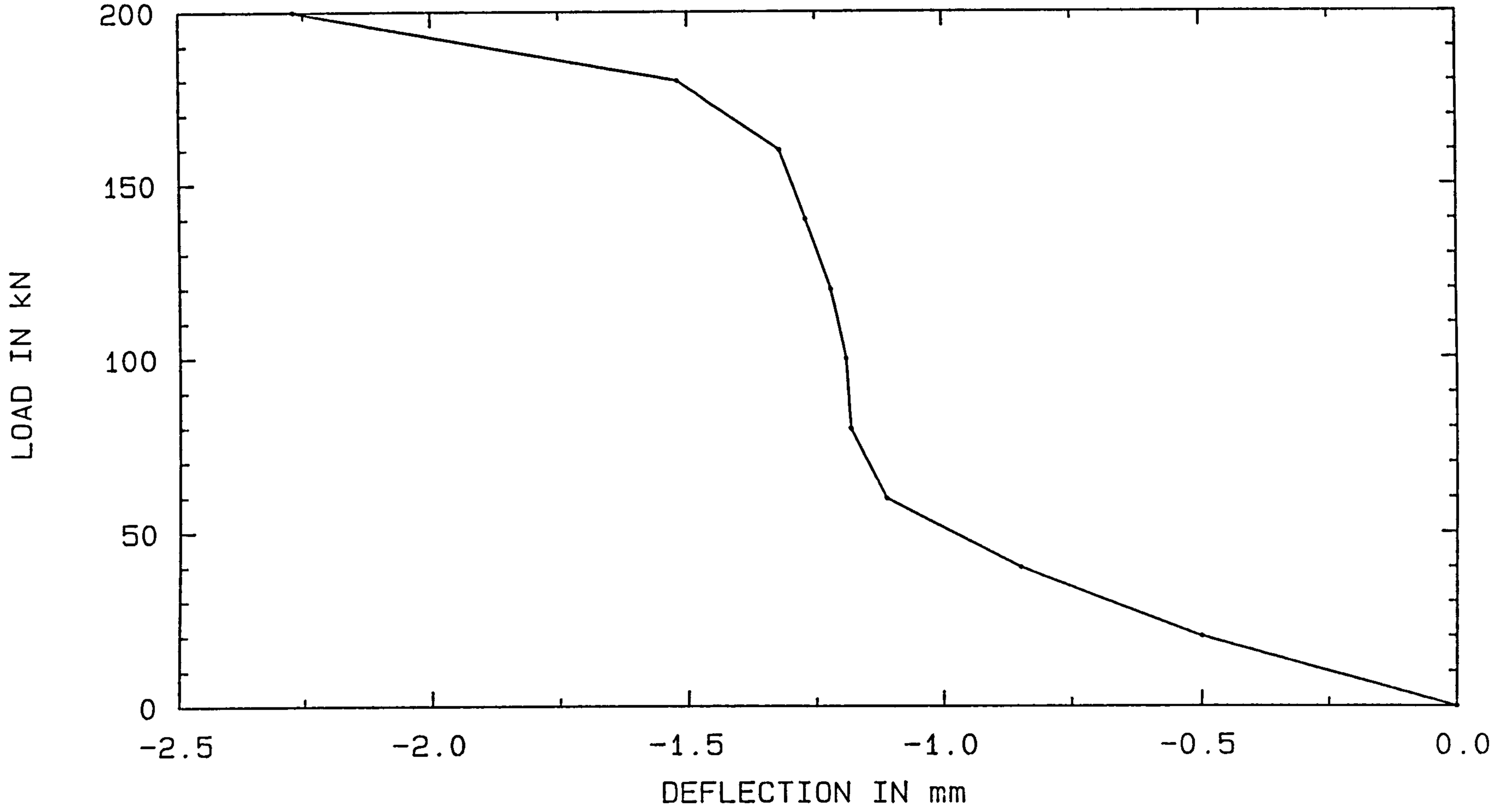

FIG.4.6 C.L. DEFLECTION OF THE COMPOSITE STRUT 2 DUE TO H.LOAD ONLY

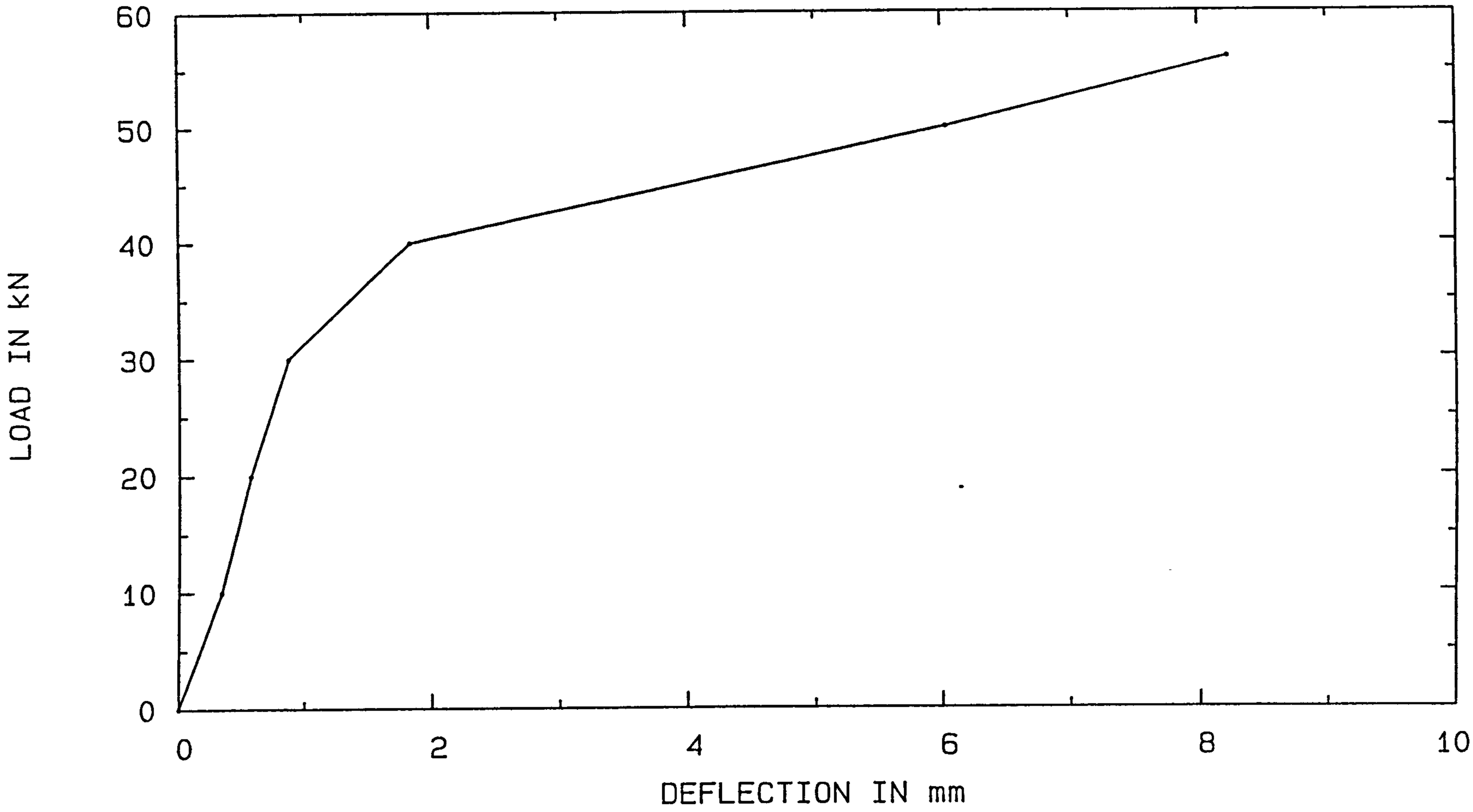

FIG.4.7 C.L. DEFLECTION OF THE COMPOSITE STRUT 2 DUE TO V.LOAD ONLY

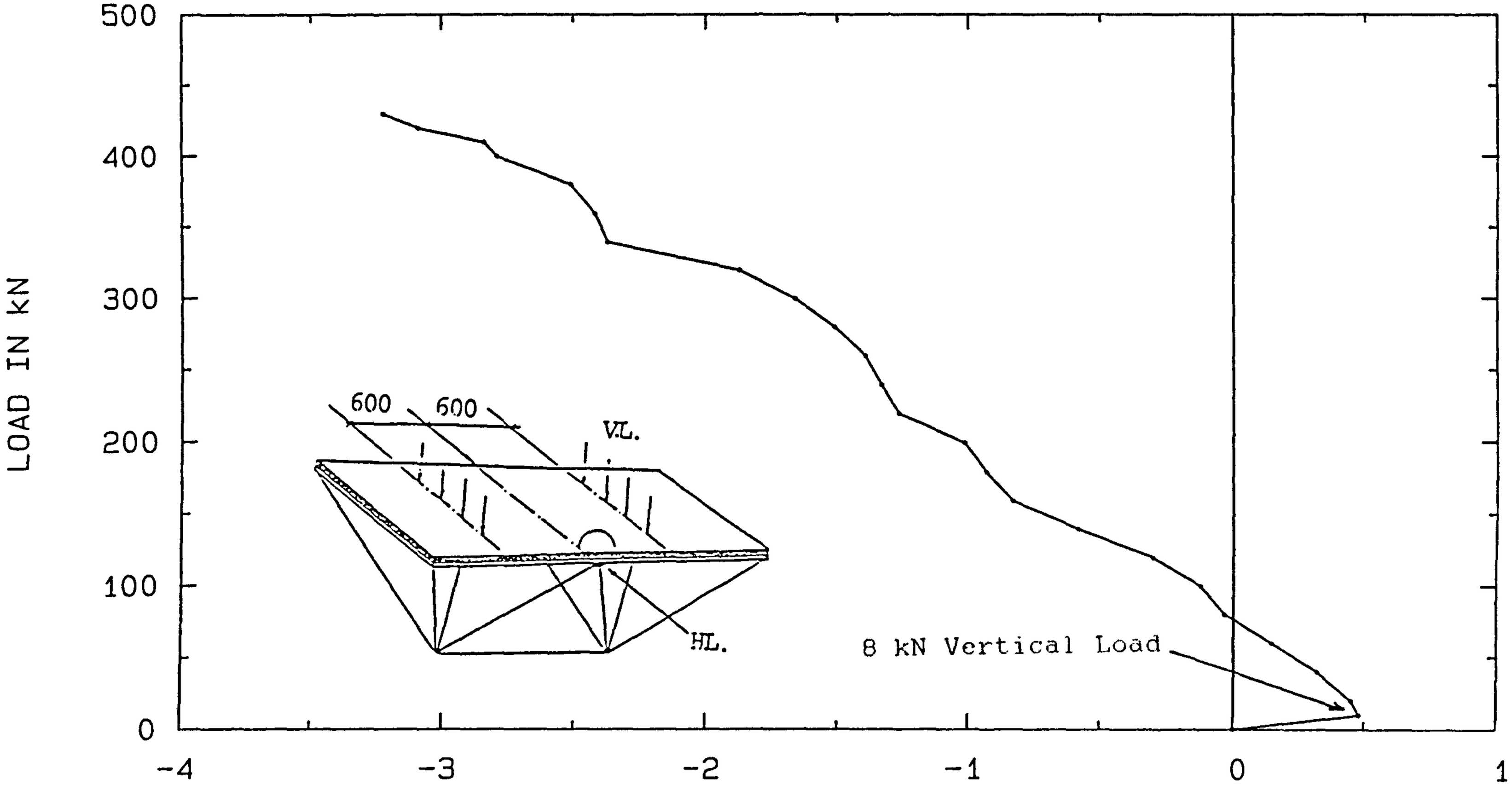

FIG.4.8 C.L. DEFLECTION OF THE COMPOSITE SPACE FRAME UNIT 2

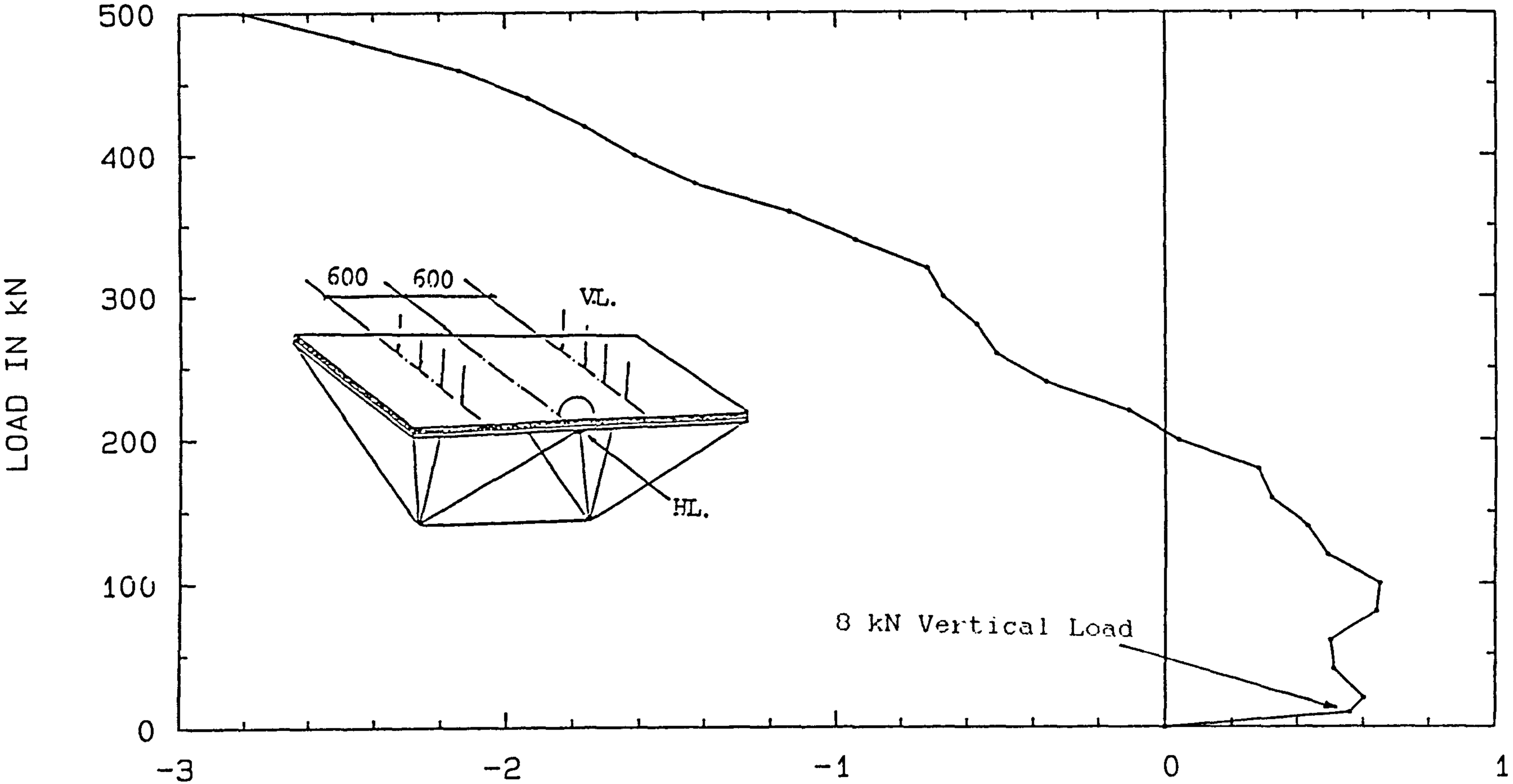

FIG.4.9 C.L. DEFLECTION OF THE COMPOSITE SPACE FRAME UNIT 3

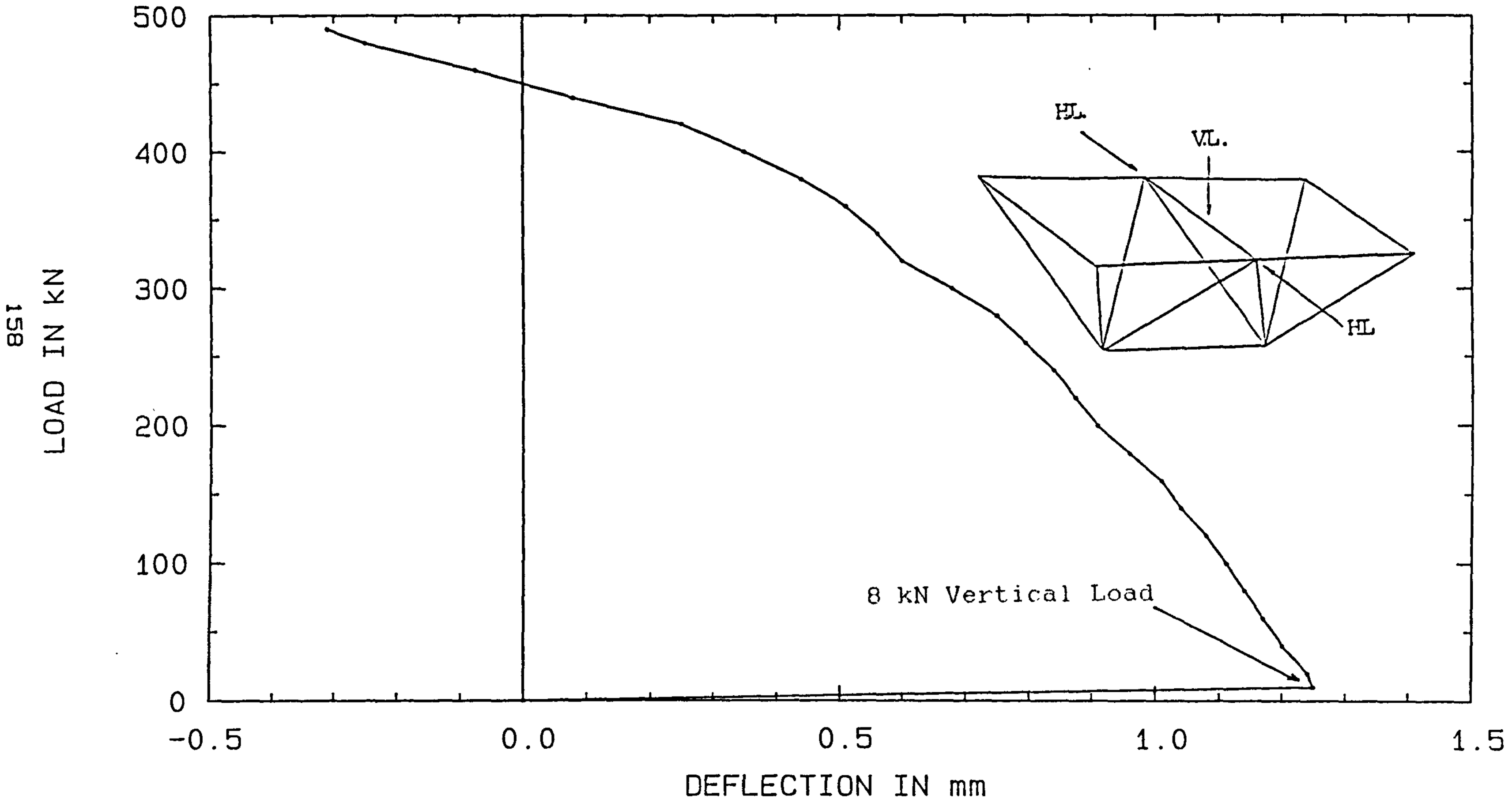

FIG.4.10 C.L. DEFLECTION OF THE COMPOSITE SPACE FRAME UNIT 4

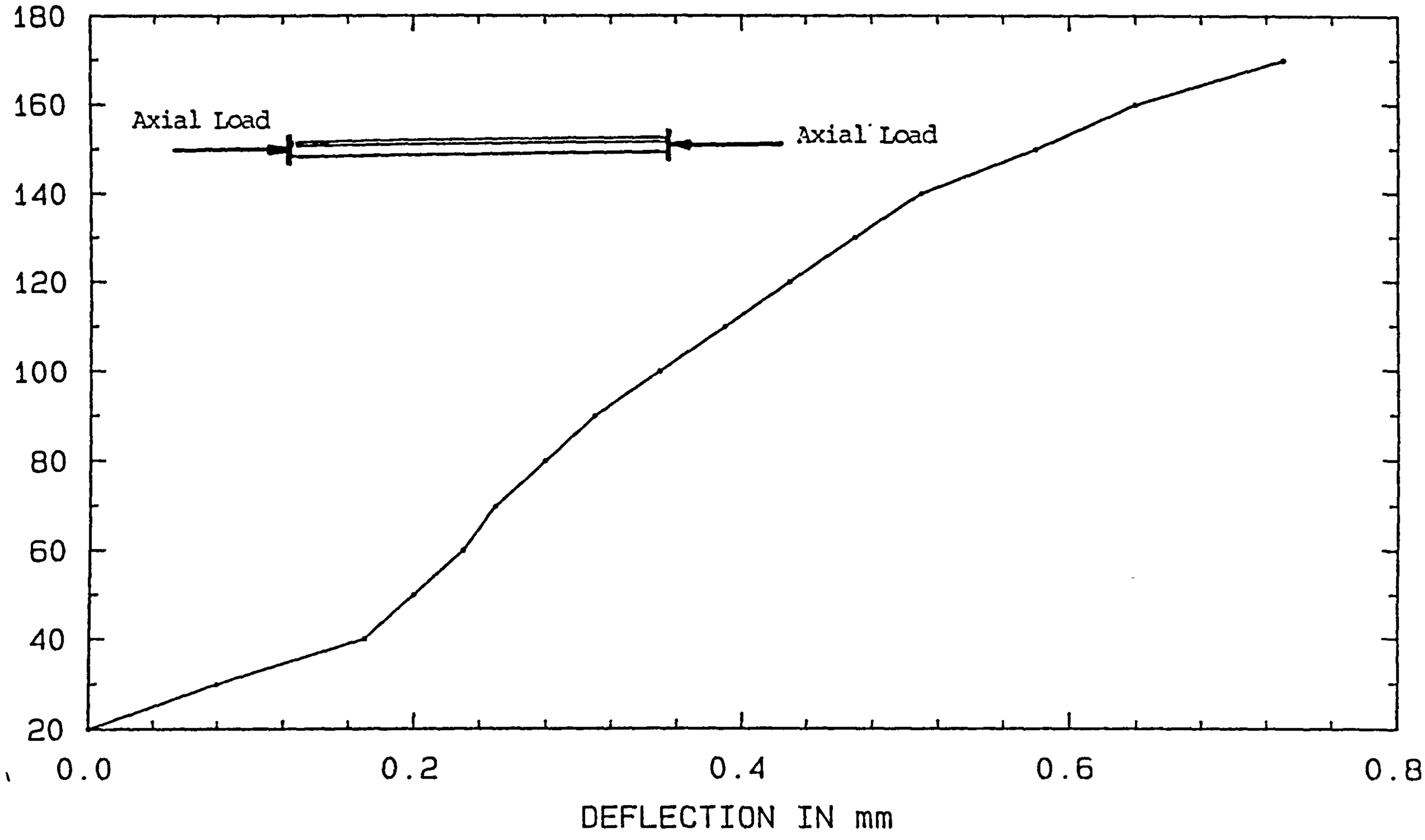

FIG.4.11 C.L. DEFLECTION FOR STEEL DOUBLE ANGLE STRUT
(W/SHORT LEGS CONNECTED B.T.B.)

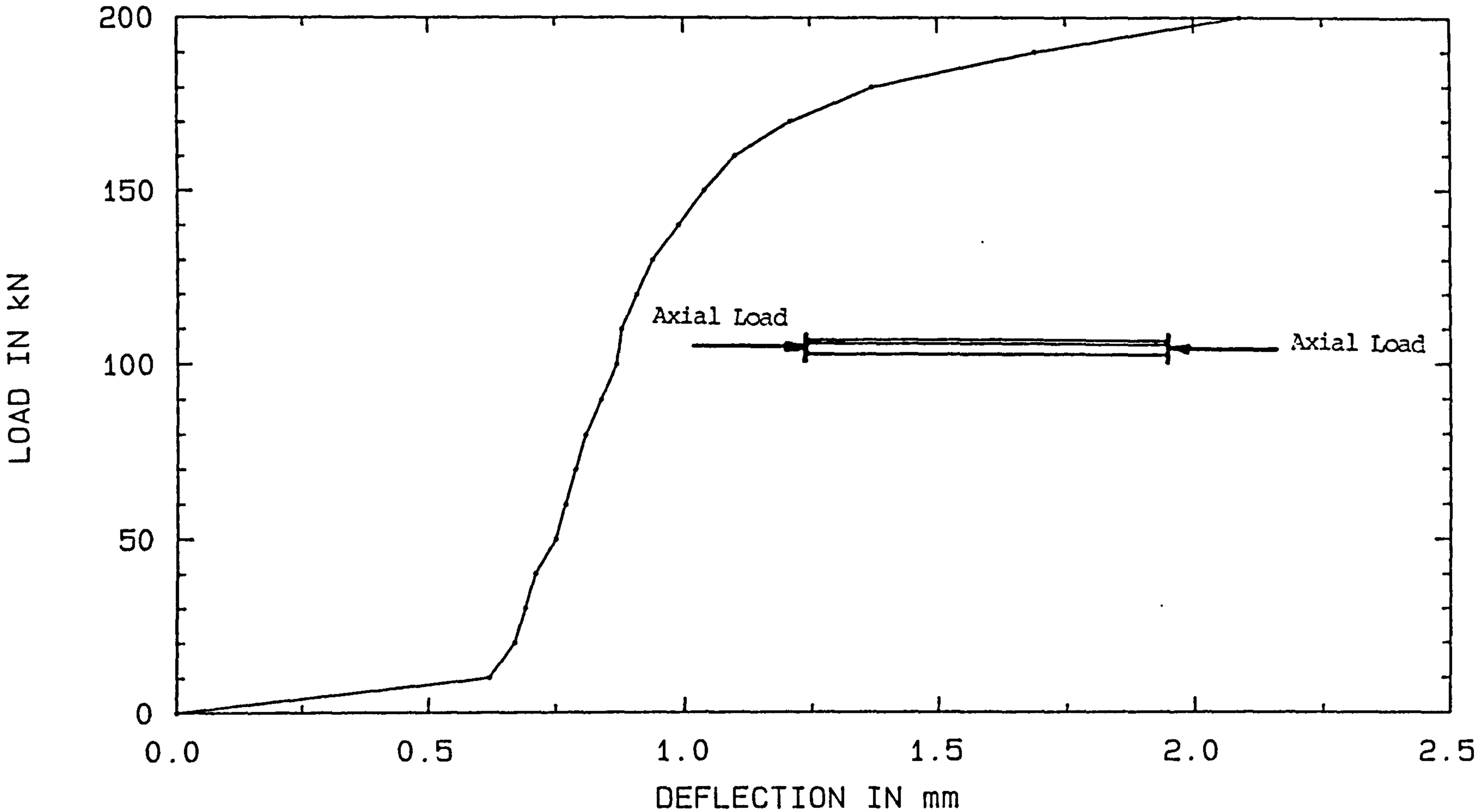

FIG.4.12 C.L. DEFLECTION OF STEEL DOUBLE ANGLE STRUT
(W/LONG LEGS CONNECTED B.T.B.)

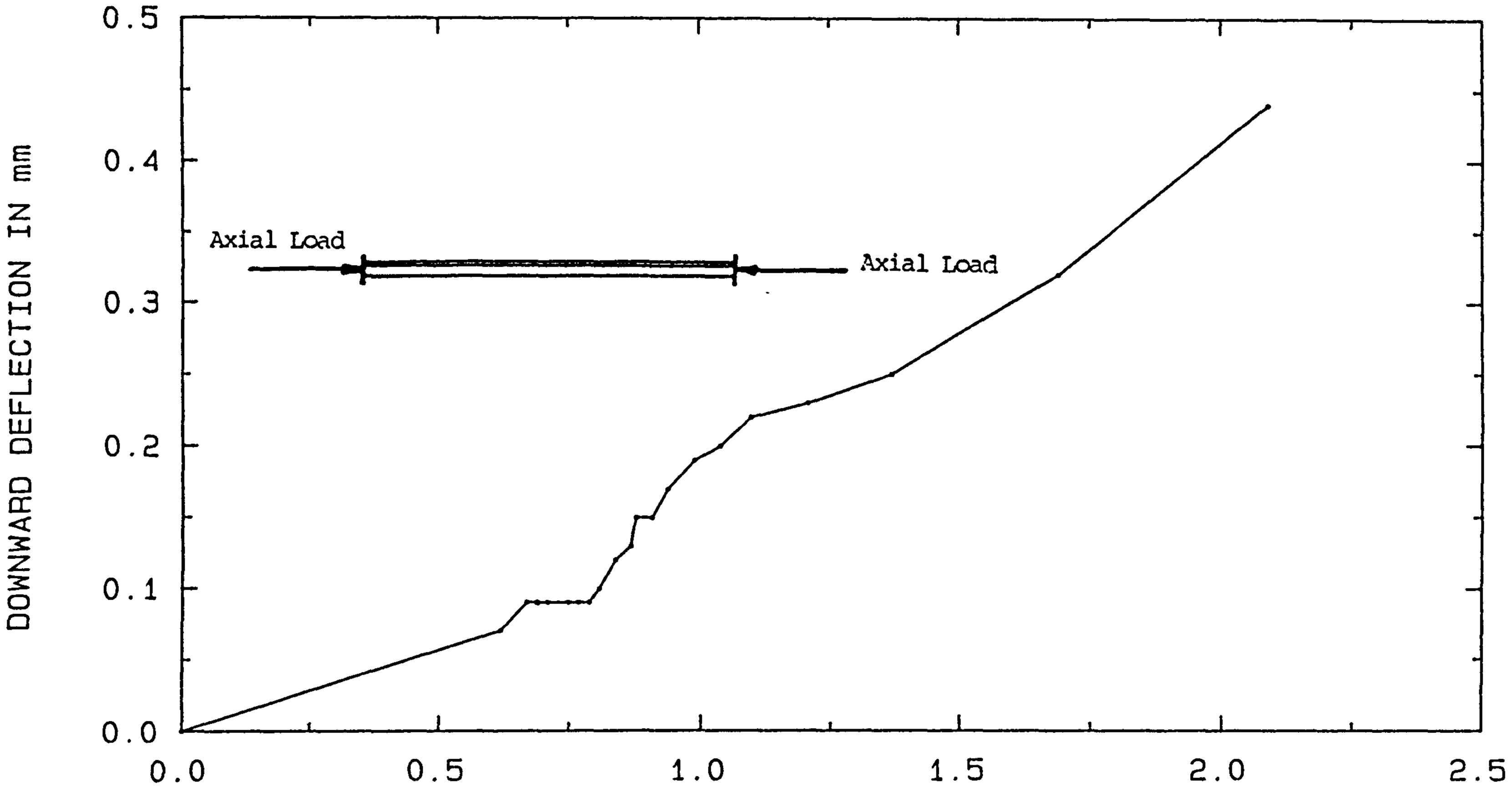

FIG.4.13 C.L. DEFLECTIONS OF THE STEEL DOUBLE ANGLE STRUT

(W/LONG LEGS CONNECTED B.T.B.)

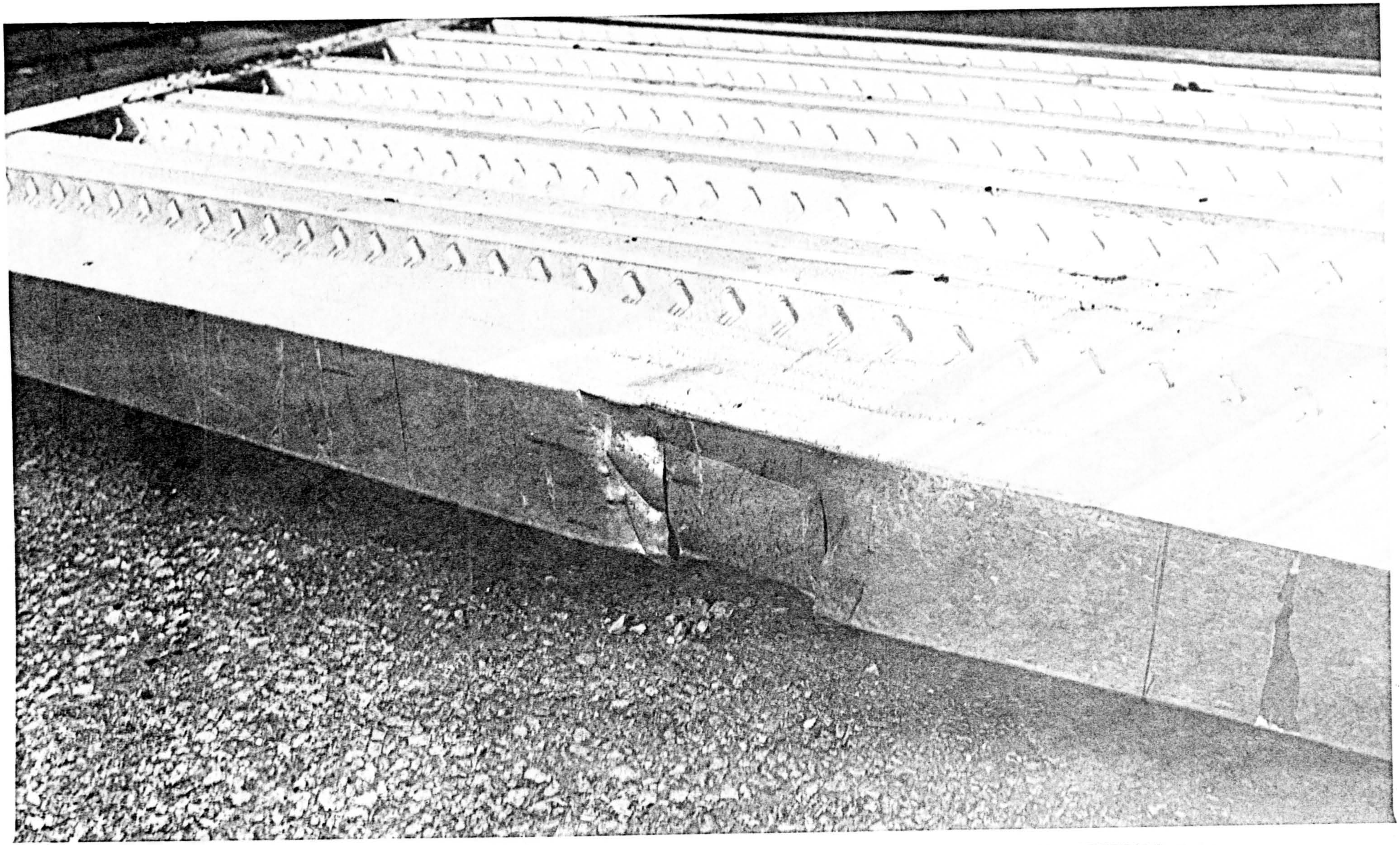

4.1a FAILURE OF THE PROFILED STEEL SHEET NEAR TO THE H.JACK (CSFU1)

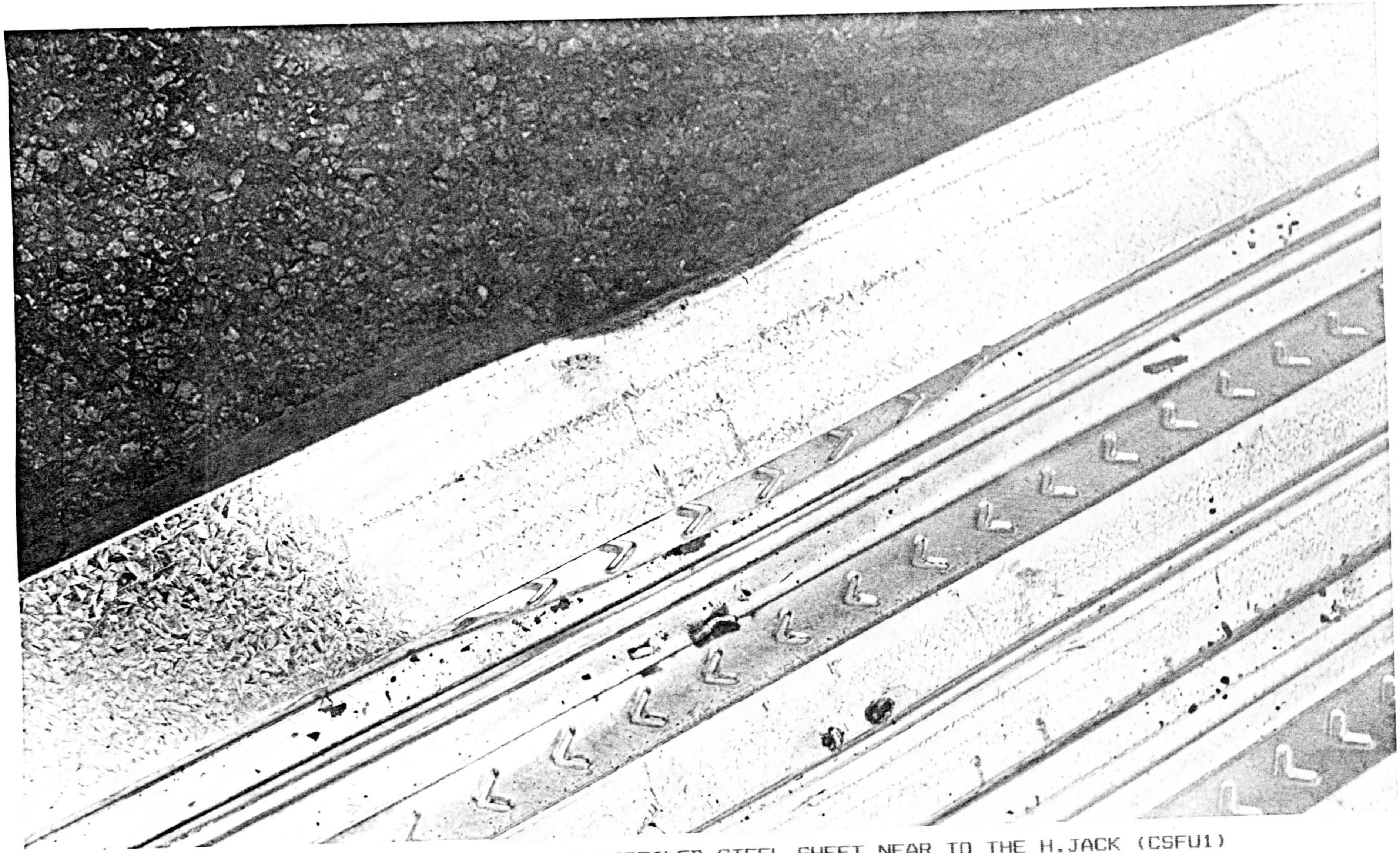

4.1b BUCKLING OF THE PROFILED STEEL SHEET NEAR TO THE H.JACK (CSFU1)

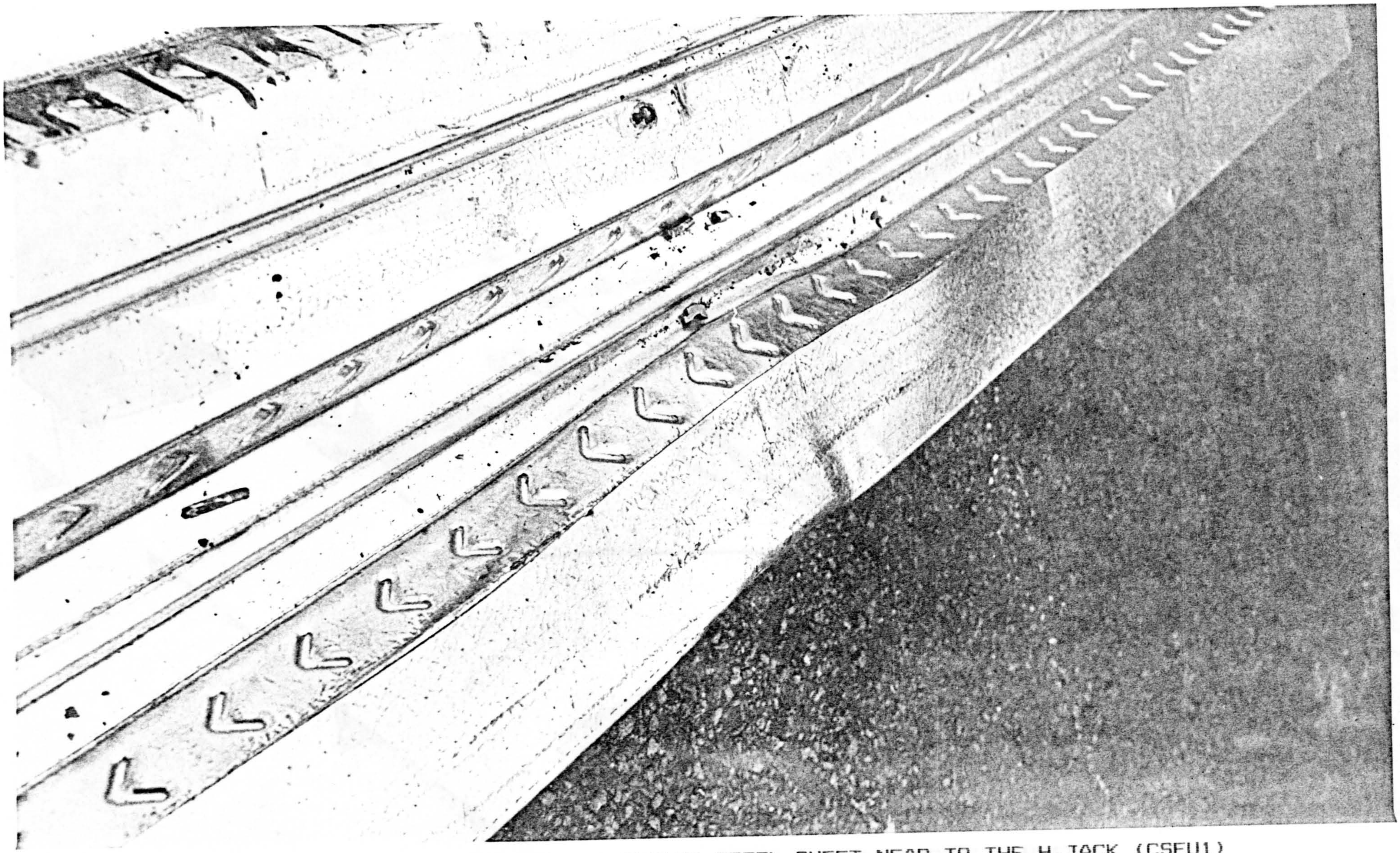

4.1c BUCKLING OF THE PROFILED STEEL SHEET NEAR TO THE H.JACK (CSFU1)

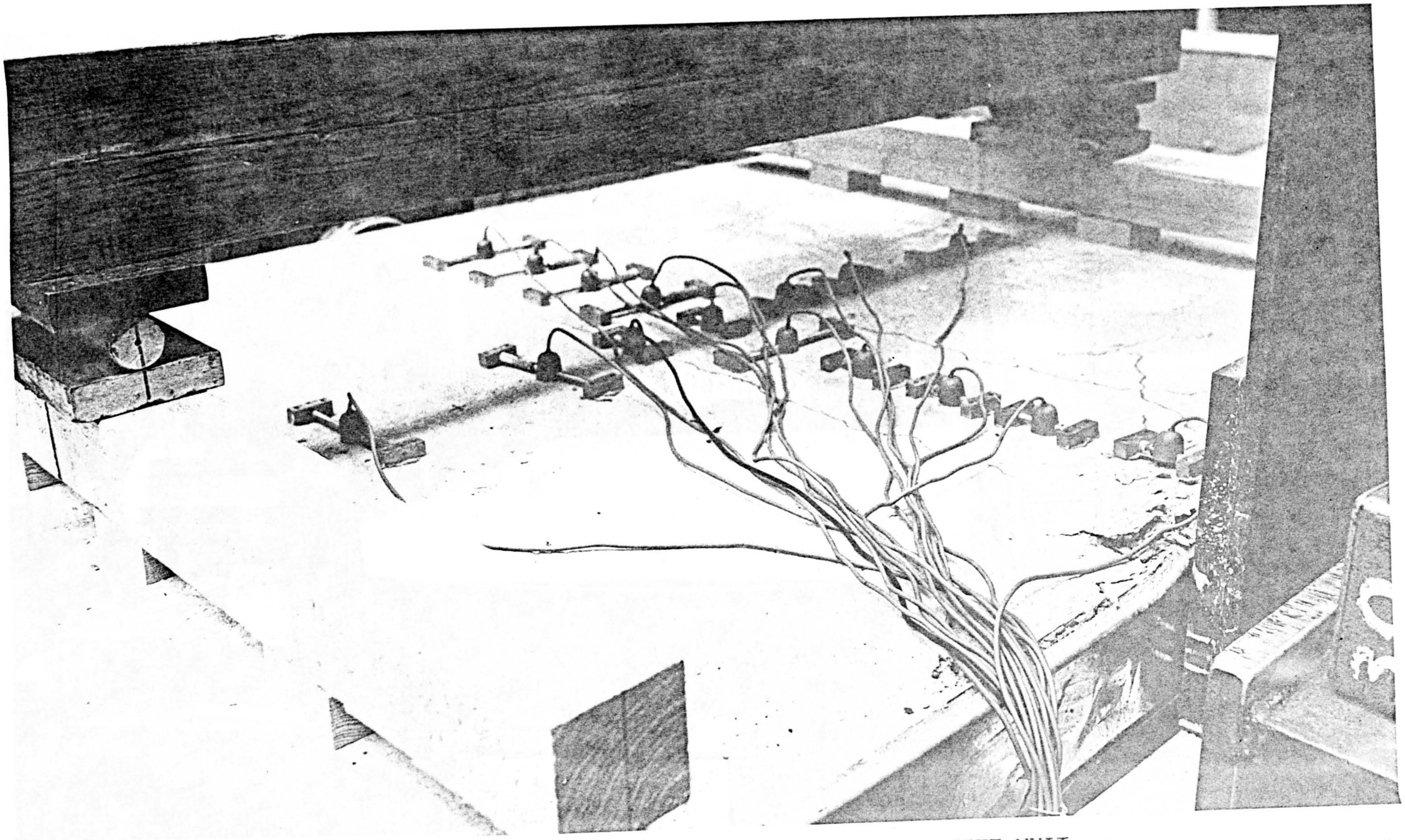

4.2 TYPICAL FAILURE MODE OF THE COMPOSITE UNIT

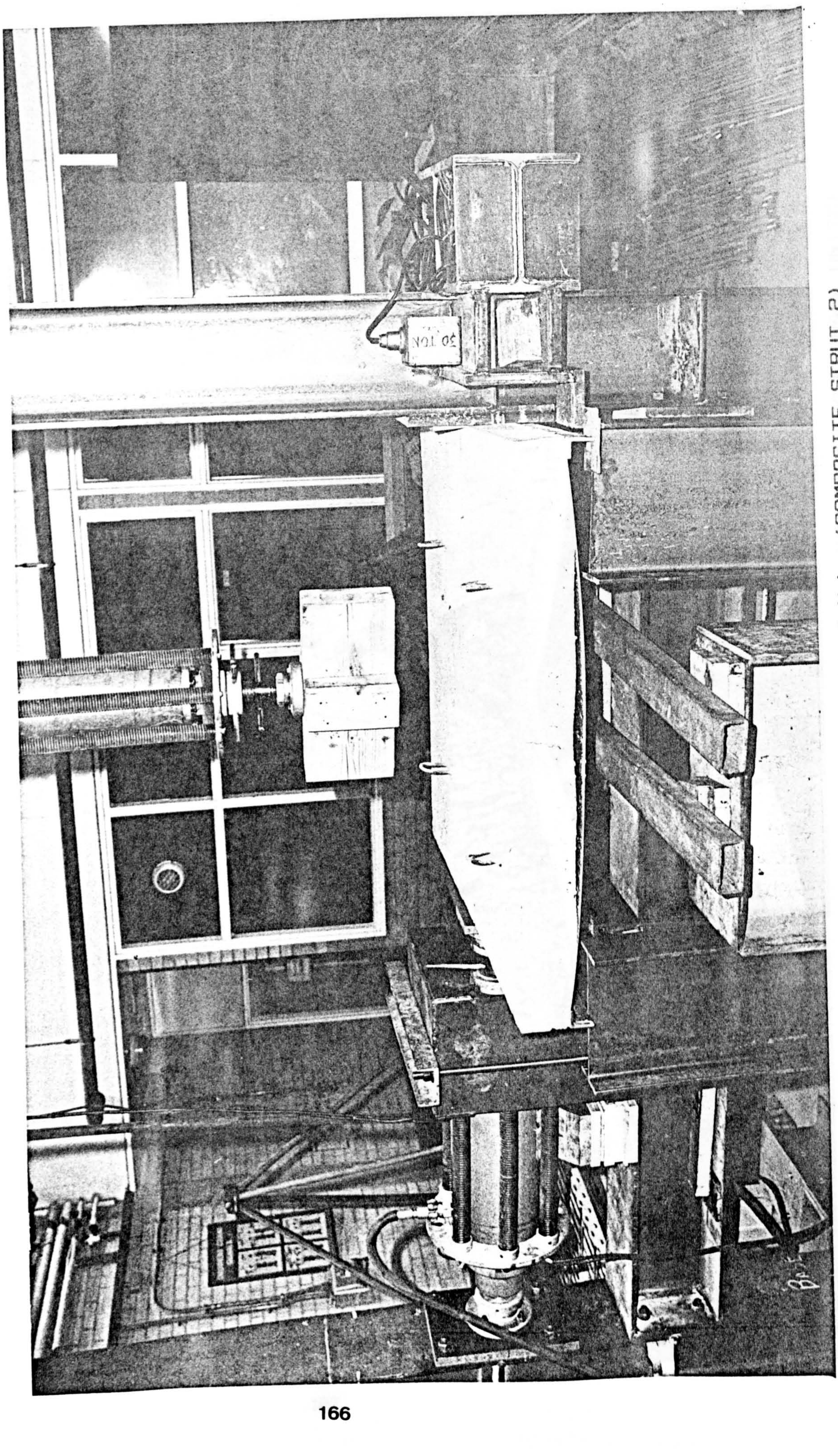

4.3 FLEXURAL FAILURE DUE TO V.L. (COMPOSITE STRUT

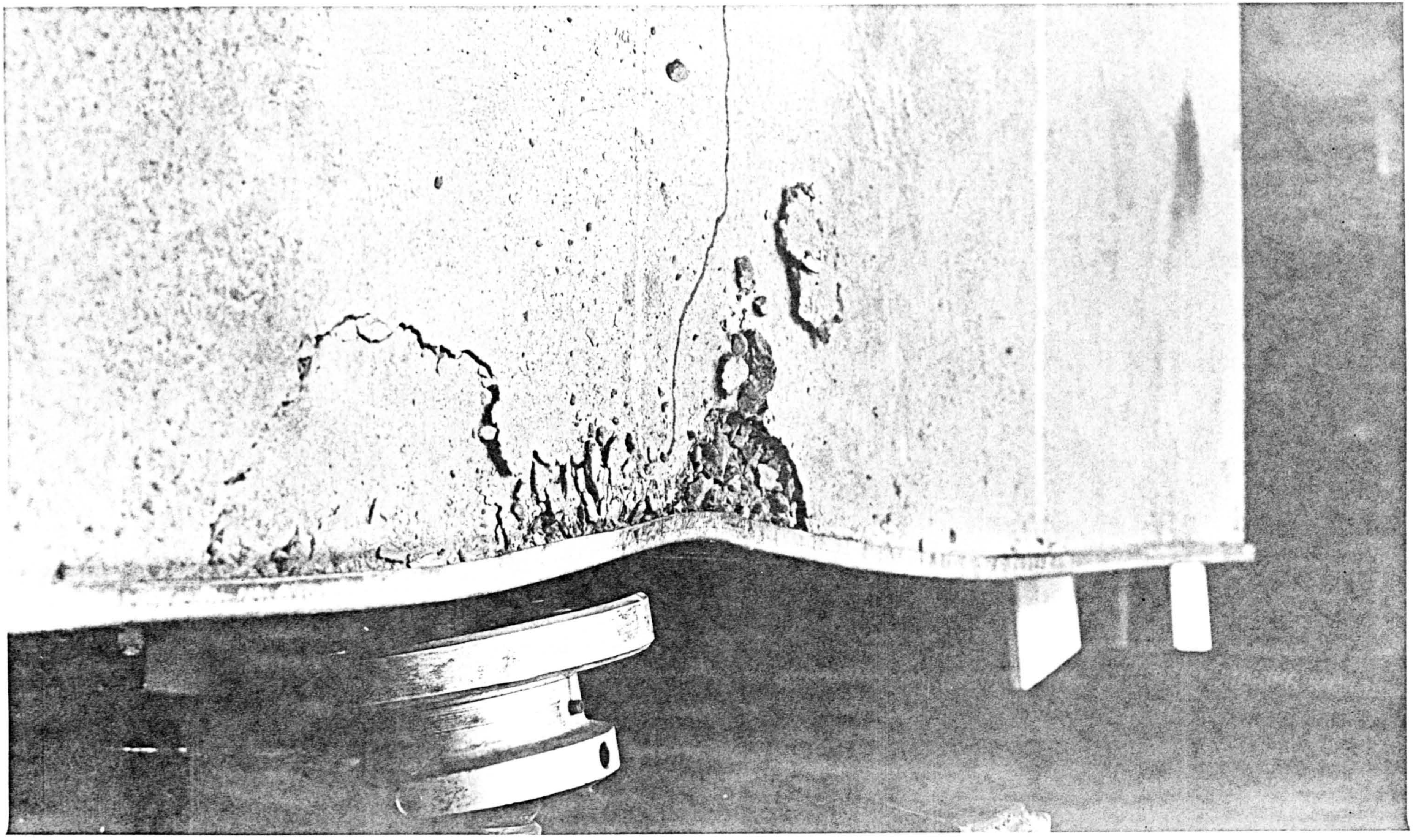

4.4a FAILURE OF CSFU2 (TYPICAL FOR ALL COMPOSITE SPACE FRAME UNITS)

4.4b LONG. CRACK ACCOMPANYING FAILURE OF CSFU2 (TYPICAL FOR ALL CSFUS)

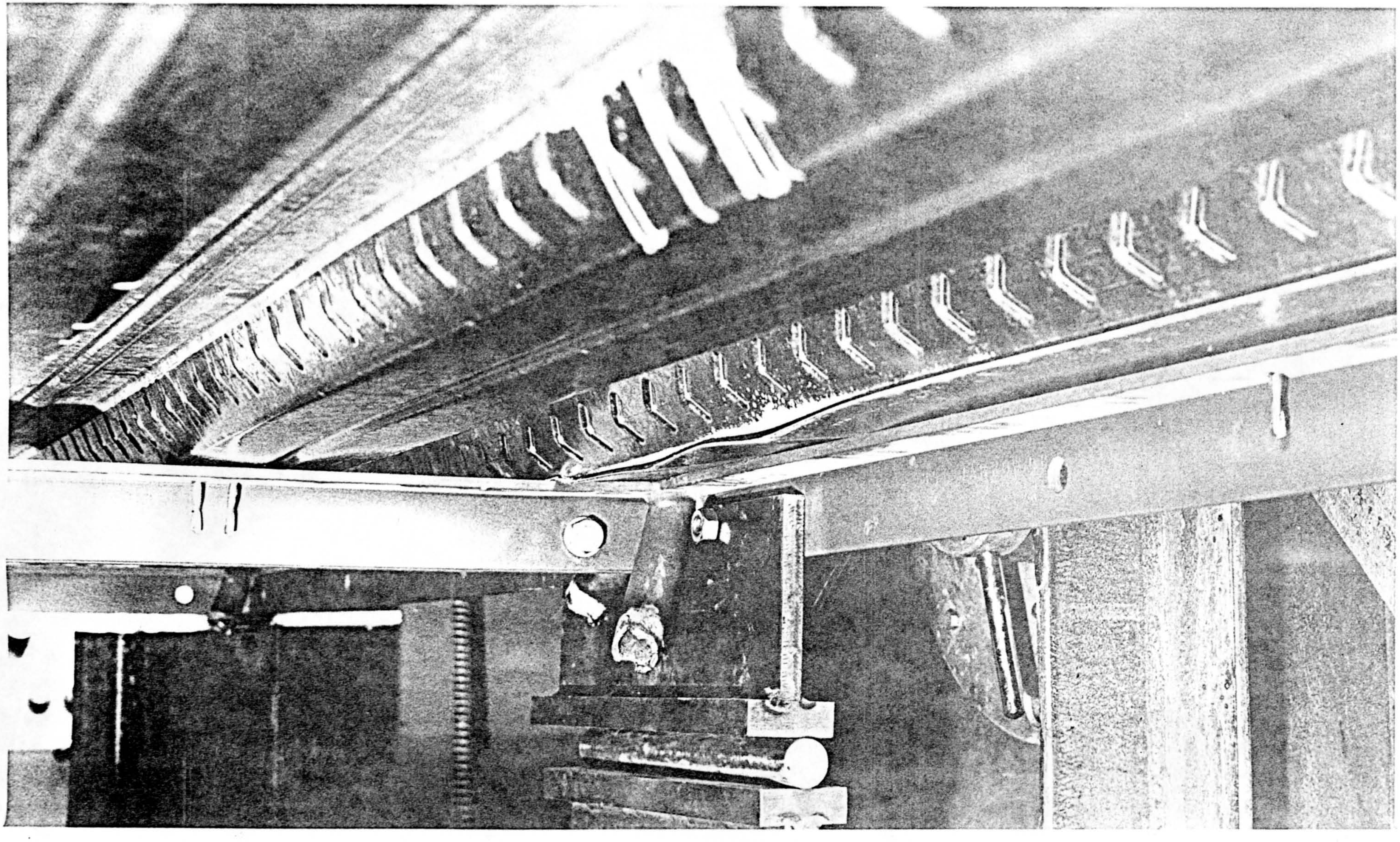

4.4c BUCKLING OF THE PROFILED STEEL SHEET (CSFU2)

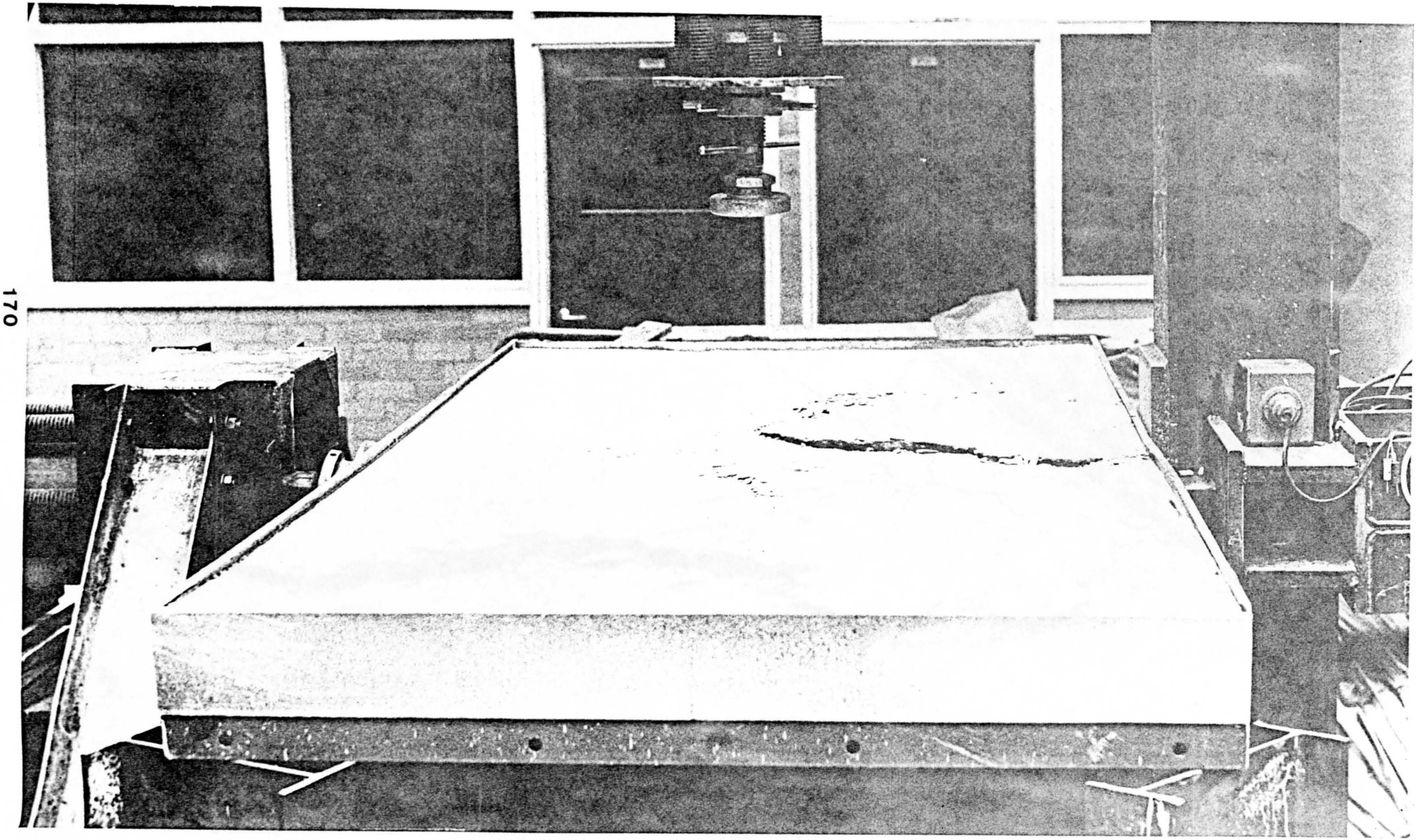

4.5a CONCRETE FAILURE OF CSFU3

4.5b CONCRETE FAILURE OF CSFU3

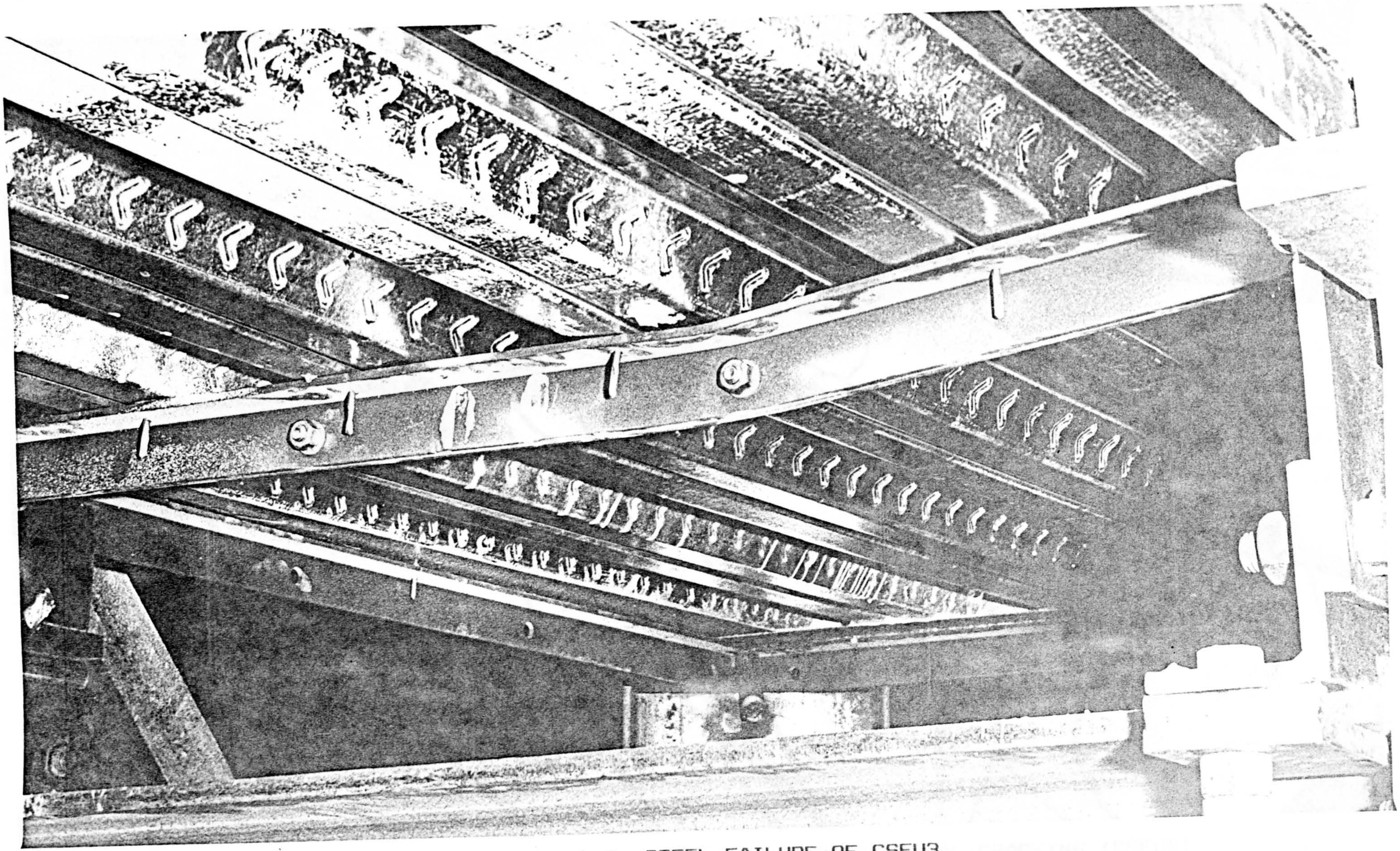

4.5c STEEL FAILURE OF CSFU3

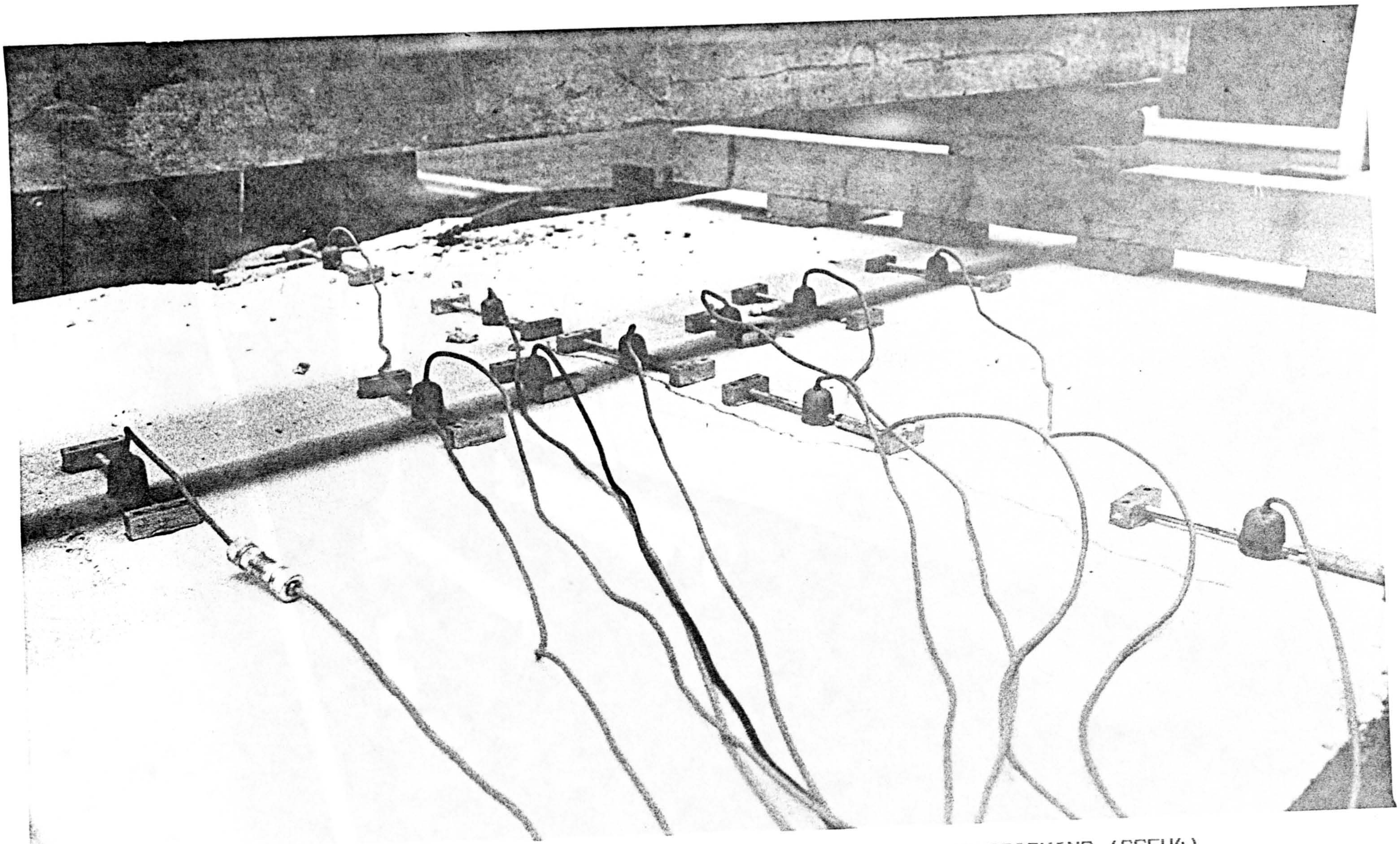

4.6a TYPICAL CONCRETE CRUSHING WITH LONGITUDINAL CRACKING (CSFU4)

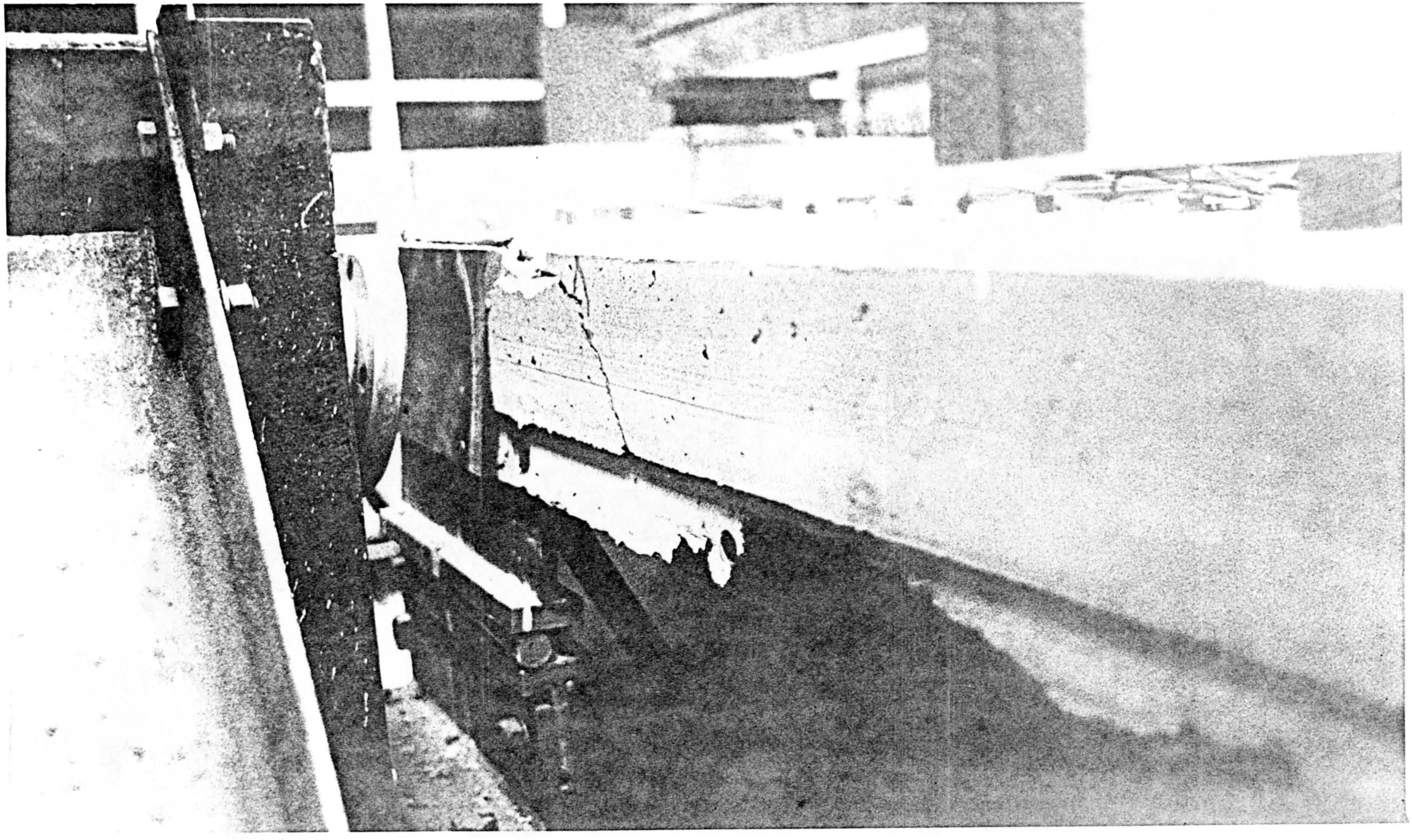

4.6b FAILURE MODE AT THE SUPPORT (CSFU3)

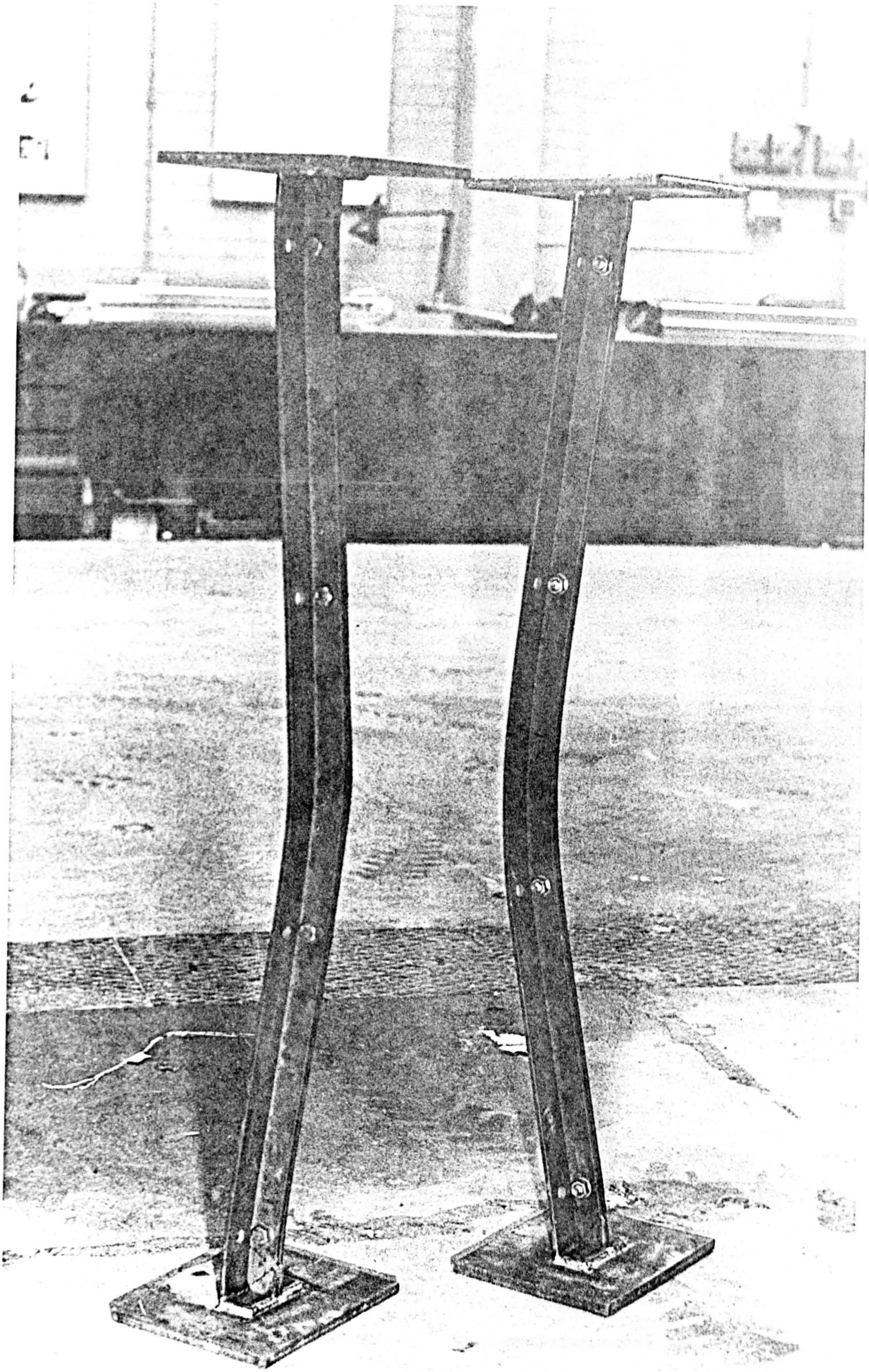

7 TYPICAL MODE OF FAILURE OF STEEL STRUTS(W/SHORT LEGS B.T.B.)

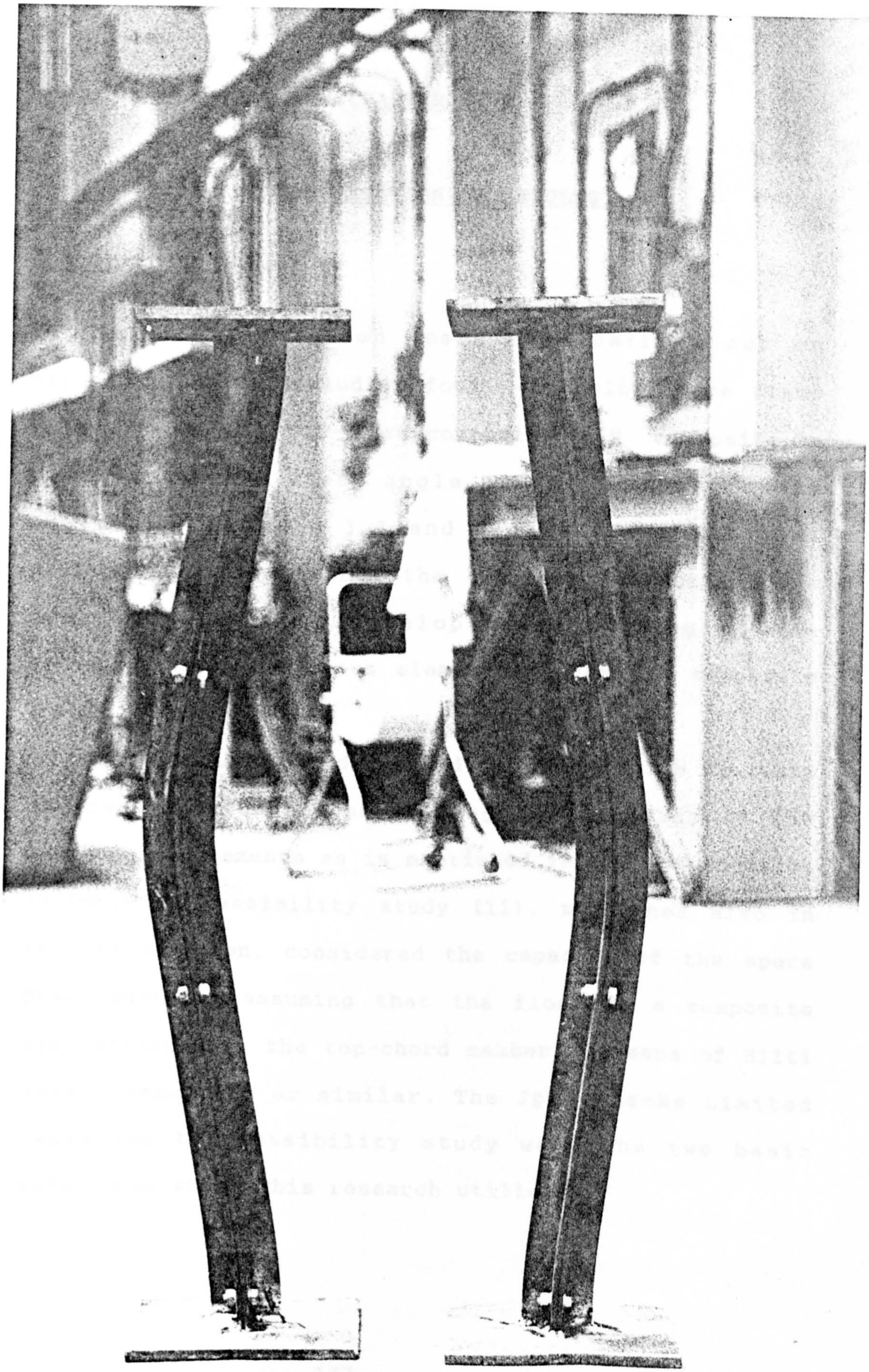

8 TYPICAL MODE OF FAILURE OF STEEL STRUTS(W/LONG LEGS B.T.B.)

CHAPTER FIVE

INTERPRETATION OF RESULTS

5.1 Introduction:

In total, nineteen tests were carried out on structural units including four composite space frame units, a two-unit top-chord composite unit, composite T-beam struts and steel angle struts (as previously described in Table 3.1 and Figure 3.6). The test programme developed from the original composite space deck unit tests to develop understanding of the behaviour of the various elements within the composite T-beam.

Space Decks Limited carried out three kinds of tests on space deck units considering the capacity of the space frame elements as is mentioned in the introduction (9,10). The feasibility study (11), mentioned also in the introduction, considered the capacity of the space frame elements assuming that the floor is a composite slab attached to the top-chord member by means of Hilti shear connectors or similar. The Space Decks Limited tests and the feasibility study were the two basic references which this research utilises.

5.2 Load Carrying Capacity:

5.2.1 Space Decks Limited Tests

Space Decks Limited have performed a series of tests to establish the ultimate strength of the various elements of the units as is mentioned in the introduction. To test the top-chord, it was subjected to vertical loading which resulted in a bending moment which was double that from the anticipated serviceability top-chord loading. In addition, axial load was gradually applied via a horizontal jack. At regular intervals, the dial gauge readings and the corresponding jack forces were recorded (9).

From these tests, the top chord members of the space frame unit (similar in all members to those considered in this work) failed at a maximum horizontal force of 240 kN in addition to a maximum vertical force of 1.88 kN per 1200 bay (10).

5.2.2 Salford Results

The top-chord member was tested as outlined in chapter three. The horizontal load was applied similarly to that described above while vertical load was applied by a vertical jack. Moreover, the top-chord was modelled in several different ways. It was considered as a steel strut only (Group 6, Table 3.1) with long legs and with short legs connected back to back. It was also loaded as a non-composite strut within the double-unit (not to

failure) according to the Southwell method (27) (Group 1, Table 3.1). It was finally investigated as a composite strut separately (Group 4, Table 3.1) and a composite strut within the double-unit (Groups 2 and 5, Table 3.1).

The top chord member tested as a double-angle strut failed at an average maximum axial load of 225 kN. However, the composite struts, the composite unit and the composite space frame units resisted higher loads, generally in the range 280-500 kN in addition to the vertical loads applied. Moreover, failure did not occur in some of these cases until higher vertical loads were applied to the unit. For example, in the case of composite space frame unit 3 (CSFU3), with 22.5 kN/node vertical load, the maximum horizontal load of 500 kN was applied without failure. It failed later at a maximum vertical load of 168 kN concentrated load on the mid-span of the composite T-section together with the maximum horizontal load of 370 kN. Composite strut 2 failed at maximum vertical concentrated loads of 25 kN at the quarter span points of the composite T-section. Table 5.1 summarises the maximum loads reached for each of the cases tested.

5.3 Load-Deflection Behaviour:

The trends for all the composite units was the same as previously noted. Initially the members deflected downward under the influence of the vertical load

followed by reversal of deflection at each increment of the horizontal load.

In order to make the behaviour of the composite units clear, it is useful to begin with the behaviour of the steel struts as they represent the steel part of the composite T-section.

5.3.1 Steel Struts (group No. 6, Table 3.1)

The load-deflection curves of the steel struts tested and mentioned in the earlier chapters show that the plane and the direction of deflection depend on the side length of the two angles connected back to back (see plates 4.12 and 4.13).

Referring to the load-deflection curves of the steel struts, it can be concluded that the top-chord member in its actual position within the test unit (the long legs were connected back to back) tends to deflect to its side due to the applied axial load. When, however, it is incorporated within the composite T-beam, the top chord member is restrained by the slab through the shear connectors which prevents this movement. The degree of restraint depends on the number and spacing of these shear connectors as shown earlier.

S. Kitipornchai and H. W. Lee (32) stated that the number of bolts which are used to connect a two-angle strut (the top chord member in the present work) has little or no influence on the ultimate capacity of the strut.

The two groups of steel struts deflected differently, and it may be concluded that the number of bolts used to connect the two angles to form the top-chord has no effect on the direction of deflection.

5.3.2 Composite Specimens (Groups 2-5, Table 3.1)

All the composite units utilised the arrangement of shear connectors described in chapter 3 (section 3.4), and they were tested as mentioned in chapter 4.

The deflection behaviour of the various composite units are summarised in Figures 5.1 and 5.2. The slopes of the composite strut 2, the composite space frames 2 and 3 are similar initially, but as load increased, the composite strut stiffened slightly. The composite unit (Group 3) and the composite space frame 4 together with the composite space frame unit 1 had similar slopes and the trend indicates that the ultimate failure load generally assumed of 500 kN is lower bound value (which could not be exceeded due to the jack capacity).

The slight changes of slopes at A, B, C, D and E are associated with concrete cracks as previously mentioned in chapter four.

As the vertical displacement of the composite T-section increased, the vertical load registered by the jack also increased. This load increase resulted from the vertical jacking system which was restraining the vertical movement. Therefore, the vertical load was checked at every horizontal load increment and adjusted

if necessary to keep it constant.

5.3.2.1 Analogy With Beams

Partial interaction theory developed by Newmark et al. (1952) showed that fairly large variations in the value of shear connector modulus affected the deflections considerably. Johnson (1975) showed that the effects of slip on deflection of composite beam are less than the theoretical calculations due to higher connector modulus and the presence of bond in actual construction (4).

In practice, it is often advantageous to use fewer connectors than the number required for full interaction for cases where the stiffness and strength of the composite member is sufficient for the design requirement (33). Johnson and May (33) also stated that a partial-connection design method can also be useful when the concrete flange of a composite beam is cast with corrugations running across the flange of the steel beam. The voids under the corrugations limit the amount of shear that can be transferred from the slab to the beam, and may make full-interaction design difficult. The composite T-beams struts described in the present experimental work may be considered as partially connected when acting as beams alone.

The degree of shear connection used appears to produce deflections which are consistent with partial interaction theory. It is shown that the T-beams with

the higher degree of shear connection deflect less than those with a lower degree. It may be added that from the results for the deflection of the composite T-beam that it is not only the number of connectors that affect the deflection, but also their arrangement along the member. It is shown that the T-beam with two shear connectors in each rib (composite space frame unit 3) deflected downwards slightly more than the T-beam with four shear connectors placed at the quarter points (composite space frame unit 2). However, the total deflection of composite space frame unit 3 was less. This latter point is explained later. There is evidence for composite columns, that the position of connectors may be more important than for beams.

5.3.2.2 Flexural Stiffness

In the tests where initially only vertical load was applied, a displacement resulted in the direction of the load. Its value depended on the value of the vertical load and the number and arrangement of shear connectors. This is in accordance with established theory for composite beams with partial interaction; the greater the degree of interaction, the higher the flexural rigidity of the beam.

Figure 5.1 shows this, the largest downward deflection was associated with composite space frame unit 1 and composite unit (Group 3) which had the lowest degree of shear connection.

In the experimental programme, the deflections of the chords acting as beams (T-beam struts) are generally similar to those predicted by Johnson's formula (34) although the values are small. These deflection calculations are shown in appendix B.

5.3.3 Deflection Under Axial Load

The upward deflection (above that at zero loading) appears to have no direct effect on the composite specimen failure at test. This is clear with those specimens which deflected downwards the greatest amount. When the deflection reversed, either it did not return to zero (composite test unit) or had just exceeded it (composite space frame unit 4) at the time of failure. The cases of the space frame units 2 and 3 and that of the composite strut (representing the four composite struts) confirmed this. They had deflected in a net upwards direction before failure took place. Certainly, the amount of the downward deflection affects the total deflection. When the downward deflection, caused by the vertical load, is high, the counter balancing effect of the horizontal load does not, in every case, produce a net upward deflection before failure.

Allowing for the differences in deflection of each of units due to horizontal load, the slopes of the vertical load/deflection curves are similar. No firm conclusions can be drawn apart from the case of

composite space frame units 2 and 3 where the greater degree of composite action in 3 may have produced the greater axial load capacity

Downward deflection under vertical load is considered normal for the actual structure. However, in an actual frame, it would be of interest to check chord behaviour between nodes under very high axial loads and relatively small vertical loads.

With orthotropic sandwich plates, it was found experimentally and theoretically that the maximum deflection of an orthotropic plate subject to a transverse uniform load does not necessarily occur at the centre of the plate and an upward deflection at some points on the plate surface may occur for a concentrated downward load (35,36).

5.4 Load-Strain Behaviour:

The strains in concrete and steel were measured as outlined in chapter 3 (section 3.2.1.1).

For the concrete surface both the longitudinal and the transverse strains were measured as mentioned in the previous chapter. It is also noted that longitudinal strains are considered primarily because they relate to the composite behaviour. They were, of course, considerably higher and more responsive to loading than the transverse strains. However, the hogging over the composite T-beam caused by the vertical loading may affect the behaviour of the unit as well as the

transverse strains. The discussion of load-strain behaviour in this chapter considers the longitudinal strains.

It was found that the longitudinal strains at the mid-span on the stem of the top-chord angles are higher than those at mid-span on the concrete surface as shown in Table 4.1.5 (see also Figures 5.3 to 5.6 and 5.9 to 5.11). Moreover, Figures 5.3 to 5.11 for the load-strain relation show the increase of strain towards the maximum load. Longitudinal strain profiles for the top (concrete) and bottom (steel) of the composite T-beam at the centreline are shown in figures 5.9, 5.10 and 5.11 for CSFU2, CSFU3 and CSFU4 respectively. They show, that at low horizontal loads when the deflection is downwards, the steel strain is tensile. As the horizontal load increases and the deflection reverses, the concrete strain at the top of the slab is a combination of tensile strain from deflection and compressive from the vertical load. Also, the steel angles are in compression from the vertical load and the bending. With shear connectors placed at the quarter points, strains are small along the section from the quarter points towards the centreline on the concrete surface. The opposite is true for concrete strains along the sections from the quarter points towards the supports of the composite T-beam (see Tables 4.1 to 4.4). This is clearer for the case where higher numbers of shear connectors are used at these locations

(see Table 4.4). It may be concluded that within the actual structure, with this arrangement, additional connectors may need to be placed along the edges to minimise the strains there and to reduce the possibility of slip. Figures 5.12 to 5.16 show strain distribution along the longitudinal and the transverse axes for runs one, three, six, nine and ten of CSFU1. The figures comprises also strain profiles at the maximum load of each run at two sections on both steel and concrete. Figure 5.16 shows that the concrete strains are high between the quarter points and the supports and that they are smaller from the quarter points to the centreline of the composite T-beam of CSFU1. Figure 5.17 for CSFU2 shows this latter characteristic too.

With shear connectors placed in all the ribs of the profiled steel sheet (CSFU3), the strains along the composite T-beam on the concrete surface are more uniform and relatively smaller close to the supports than CSFU1 and CSFU4(see Table 4.5 and Figure 5.18).

With shear connectors placed at the centre and near the supports of the composite T-beam of CSFU4 (see Table 4.6), the maximum concrete strains occurred not at but between the supports and the centreline. Strains close to the supports were also high. With this arrangement, the concrete strains along the composite T-beam were relatively high compared to the other two arrangements (see Table 4.6 and Figure 5.19).

When shear connectors were used at the ends, only in

the case where shear connectors were placed in all the ribs were the strains close to supports relatively small. This, in part, explains why the composite space frame unit 3 did not fail at high loads. On the other hand, high strains at the ends may also explain why for all the other units failure was always characterised with concrete crushing at the supports despite the upward deflection at the centreline.

Generally, in all the cases, strains at or near the locations of shear connectors are usually small. This is obvious when high number of connectors are used. In the case of CSFU2, the smallest concrete strain is close to the shear connector locations (at the quarter points), and of CSFU4, the smallest concrete strain is at the centreline which is approximately the location of the shear connectors.

Longitudinal strains on steel stem at the centreline and at the quarter points increase with increasing load as is shown for CSFU1 (runs 1, 3, 6 and 9). However, run 10 is opposite when compared to run 9. Both runs were of the same horizontal load, but run 10 had a higher vertical load. The higher vertical load in the case of run 10 made the strains on steel lower compared to the previous run. The longitudinal strain on the concrete surface close to the support, together with the low strain on steel, may indicate a loss of shear connection between the two materials. This loss of connection may have taken place as a result of either a partial

shearing of the connectors or slip.

Finally, with the strain measurement using acoustic strain gauges, one point should be mentioned here. The presence of shear connectors near the stems of the double angle top-chord at a section made it difficult to attach the acoustic gauges at that section (on the stem of the double angles). Moreover, due to the acoustic gauge size, it was found difficult to attach it to the flange of the double angle top-chord without damaging it. It may be useful to use electrical strain gauges at the section required along the top-chord to measure strains there in future similar work.

5.5 Flow of Load

The partial interaction theory mentioned in 1.5.2 and 5.3.2.2, stated also that the value of shear connector modulus (K) affected to a large degree the elastic strains and stresses. In the present work, it was found that strains on the concrete surface were high at the ends of the T-beam, and they decreased at or near shear connectors. Generally it may be seen that when a large number of shear connectors were used, the strains were smaller. This was found with the two cases where four and two connectors placed at the quarter points respectively. Shear connectors being placed at each rib made the strains on the concrete surface small at the ends and nearly uniform along the composite T-beam. The cases mentioned showed that the greater the numbers of

shear connectors at locations along the composite T-beam, the more effective was the T-beam composite action. From these observations, it can be seen how vital the presence of shear connectors is in the distribution of load in the elements of a composite member. However, the shear connectors used did not project in to the concrete by more than their heads.

5.5.1 Effective Width of the Composite Section

Results of the composite space frame unit 2 (see Table 4.4) show that strains were zero between 100 mm and 200 mm from the centreline along the transverse axis of the T-beam. Although the zero strains for the composite space frame unit 3 is shown to be between 200 mm and 400 mm from the centreline along the transverse axis, the strains at the distances 100 mm and 200 are nearly constant and are considerably smaller compared to that at the mid-span. For the case of the composite unit, the strain at the distance of 200 mm from the centreline along the transverse axis is half of that at the centreline. It is, therefore, considered that the effective width of the composite T-beam within the composite space frame structure could be taken from the mid-span up to 150 mm to each of the sides, that is 300 mm i.e. span/4 which compares reasonably with span/3 or span/5 normally used for composite beams. The load is applied to various elements of the composite space frame at the joint (the end of the T-beam) through a

plate 224 mm width x 100 mm depth x 18 mm thickness. The load is then distributed along the composite T-beam as is shown in Figure 5.20.

For the composite struts, the lower failure loads for the 300 mm wide specimens indicates that the assumption of the effective width of 300 mm is not fully supportable from the CSFUs failure loads. It may be, therefore, said that the effective width may be taken as greater than that assumed here as noted in chapter 4 (section 4.2.7).

5.6 Overall Discussion on Experimental Results:

The top-trays are, as explained in the introduction, composed of angles. Each one was constructed of 4 angles welded at their ends. These top-trays when connected together formed the top-chord members. The top-chord member considered during the experimental work was welded at each end to the perpendicular top-chords which met at those ends. The steel struts, cut of the top-chords were welded at the ends to steel plates. One set of struts of 1200 mm length included a small section from the angle running at 90 degrees to the strut. When these steel struts were tested in compression, their deflected shapes showed the effect of this welding that ends are fixed. This situation may be assumed to produce end moments in the composite beams tested. The high strains measured close to the ends (at 500 mm from the centreline) may be in part result from these moments.

This is clear when reference is made to both run 10 of CSFU1 and the last test (CSFU4). Although the highest strains were away from shear connectors as was the case with all the composite specimens, the strain at the ends were still high despite the presence of shear connectors there (-1516 microstrain at 500 mm from the centreline along the longitudinal axis for the case of CSFU4).

The inflection points observed during the steel struts failure in compression (see Figure 5.21), may explain the efficiency of the shear connectors located at the quarter points of the composite T-beam tested for all the composite specimens. The presence of the shear connectors there appears to reduce vertical deflections which are similar to the others specimens which have a different arrangement of shear connectors (see Figs. 5.1 and 5.2). This feature provides the composite T-beam with high stiffness. However, the presence of shear connectors at every rib which covers this arrangement produces both smaller deflections and higher strength.

Before failure occurred, the upward deflection increased rapidly as seen by the dial gauges. This was not represented in the load deflection figures because in all the cases the dial gauges were removed before failure to prevent damage. The failure in all cases occurred with crushing of the concrete at one of the ends The steel did not reach its yield stress. This type of failure was semi-ductile.

5.6.1 Correlation of Results

The provision of two connectors in each rib in the case of composite space frame unit 3 made the elements of the composite T-beam behave with a higher degree of interaction than the other composite T-beams. It had the highest vertical and horizontal load capacity. Moreover, cracks appeared at a higher horizontal load compared to the other test specimens. These points are discussed in this section where the last three composite space frame units are compared.

The discussion of these points is presented in the correlation of the experimental results (strains, stresses and deflections) together with the applied loads. Loads versus mid-span deflections and strains are shown in Tables 5.2 to 5.4.

Before going in the details of the correlation, it is useful to restate here the deflection behaviour of the composite T-beam. This is important because it is relevant to this correlation as will be seen.

It is mentioned earlier that the composite T-beams deflected first downwards due to the applied vertical load. As the horizontal load is applied, the composite T-beam deflection reversed to the upward direction.

The concrete slab would either deflect downwards or upwards about its weak axis. It is unlikely, then, that the composite slab follows the double angle top-chord which tends to deflect to the side. It will not deflect to the side either as the provision of shear connectors

prevents this happening. In fact, the top-chord is likely to follow the deflection of the concrete slab. The centroid of the two materials of the composite T-beam is located below that of the concrete element. This may explain to some degree the tendency of the composite T-beam to deflect upwards under the effect of the horizontal loading.

The main stresses (on the top and bottom of the T-beam section) measured by the acoustic gauges at the mid-span of the composite T-section are found to be compressive stresses. They resulted, of course, from the application of the horizontal load. The flexural stresses resulted from both vertical and horizontal loads. These stresses are calculated as shown in Tables 5.5 to 5.7. In each Table, two stresses σ_1 and σ_2 for both the top (concrete surface) and bottom (top-chord steel angles stem) of the composite T-beam section at mid-span are included. The stress σ_1 represents the internal stress which is calculated from strains measured by the acoustic gauges. However, the stress σ_2 represents the stresses due to the external loads.

The calculation of σ_2 is considered with the composite T-beam cross-section mentioned in 5.4.1, being transformed for this purpose (see Figure 5.22).

As mentioned earlier, the vertical load forced the T-beam to deflect downwards which is opposite to the deflection due to the horizontal load. Therefore, flexural stresses due to each the loads are of different

sense. They are compressive at the top and tensile at the bottom of the section due to the vertical load. They are tensile at the top and compressive at the bottom of the section due to the horizontal load. Since the effect of the horizontal load is to reverse deflection initially created by the vertical load, stresses due to the horizontal load are taken opposite to those due to the vertical load when the composite T-beam was deflecting downwards. That is also true for the stresses due to the vertical load when the composite T-beam was deflecting upwards. The calculations are illustrated in appendix B.

Referring to Tables 5.5 to 5.7, it may be seen that the T-beams considered with composite frame units 2 and 3 show similar stresses (σ_1 and σ_2) on the steel section for certain values of loading. The stresses are closer in composite space frame unit 3 than those in composite space frame unit 2; however, there is poor correlation in the case of composite space frame unit 4. For this unit, at a certain load before the deflection reversed to the upward direction, the two stresses (σ_1 and σ_2) on the steel section are close which is similar to the previous two cases. However, at the load just before the appearance of cracks on the concrete surface (300 kN), the two stresses diverge and continue diverging for the rest of loading which is different than the previous two cases. This may be due to the fact that the interaction between the steel and concrete had weakened more than

the other two cases so that the interaction assumed in the analysis was not now valid. However, it reached a maximum failure load as high as those of the other cases.

These stress results confirm the previous three assumptions discussed earlier in this chapter. These are that the effective width of the T-beam cross-section which was found to be 300 mm was satisfactory, that the complete restraint case performed most effectively and that the presence of shear connectors at the quarter points improves the composite behaviour of the system. The three assumptions are reasonable because all the stress calculations are based on the cross-section effective width of 300 mm. The experimental and theoretical stresses show the best similarity with the case of composite space frame unit 3 which had 2 connectors per rib and the experimental stresses appeared more uniform with this case also.

According to these assumptions, it may be also mentioned that all the applied loads are resisted by the composite T-beam as previously mentioned. Moreover, it may be concluded that the composite T-beam with connectors located at each rib is effective and any additional connectors should be placed at the quarter points.

TABLE 5.1 MAXIMUM AND FAILURE LOADS OF THE VARIOUS SPECIMENS

Test Specimen	Maximum Load (kN) (No Failure)		Failure Load (kN)	
	Vertical	Horizontal	Vertical	Horizontal
Composite Space Frame Unit 1	40	340	27	280
Composite Unit (Slab)	–	–	8	390
Composite Strut 1	–	–	4	380
Composite Strut 2	4	500	50	–
Composite Strut 3	–	–	4	270
Composite Strit 4	–	–	4	310
Composite Space Frame Unit 2	–	–	8	470
Composite Space Frame Unit 3	45	500	168	370
Composite Space Frame Unit 4	–	–	8	500
Steel Struts	–	–	–	225 Ave.

TABLE 5.2 LOAD VERSUS DEFLECTION AND STRAINS OF COMPOSITE SPACE FRAME UNIT (2) AT CENTRELINE

V. Load (kN)	H. Load (kN)	Centreline Deflection (mm)	Strain on Concrete Surface $\times 10^{-6}$	Strain on Top-chord Stem $\times 10^{-6}$
0.0	0.0	0.0	0.0	0.0
8.0	10.0	0.48	-27.2	+15.6
	40.0	0.32	-33.3	-6.25
	80.0	-0.03	-30.3	-31.3
	100.0	-0.12	-30.3	-37.5
	140.0	-0.58	-42.4	-71.3
	160.0	-0.83	-45.4	-98.1
	180.0	-0.93	-48.4	-120.6
	200.0	-1.01	-51.4	-179.4
	220.0	-1.26	-39.3	-192.5
	240.0	-1.33	-45.4	-237.5
	260.0	-1.39	-51.4	-301.9
	280.0	-1.51	-54.4	-346.9
	300.0	-1.66	-63.5	-429.4
	320.0	-1.87	-69.6	-503.8
	*340.0	-2.37	-75.6	-556.9
	360.0	-2.42	-87.7	-602.5
	380.0	-2.51	-96.8	-646.3
	400.0	-2.79	-105.9	-693.1
	420.0	-3.09	-124.0	-743.8
	440.0	-3.09	-142.2	-803.1
	460.0	—	-175.5	-881.9
	470.0	Failure		

* Cracks appeared at this loading.

TABLE 5.3 LOAD VERSUS DEFLECTION AND STRAINS OF COMPOSITE SPACE FRAME UNIT (3) AT CENTRELINE

V. Load (kN)	H. Load (kN)	Centreline Deflection (mm)	Strain on Concrete Surface $\times 10^{-6}$	Strain on Top-chord Stem $\times 10^{-6}$
0.0	0.0	0.0	0.0	0.0
8.0	10.0	0.56	-245.0	-46.9
	40.0	0.51	-254.1	-70.6
	80.0	0.64	-263.2	-72.5
	100.0	0.65	-272.3	-89.4
	180.0	0.28	-272.3	-214.4
	200.0	0.04	-272.3	-240.6
	220.0	-0.11	-272.3	-274.4
	240.0	-0.36	-269.2	-310.0
	260.0	-0.51	-272.3	-349.4
	280.0	-0.57	-272.3	-391.3
	300.0	-0.67	-272.3	-441.3
	320.0	-0.72	-272.3	-493.8
	340.0	-0.94	-275.3	-499.4
	360.0	-1.14	-281.3	-618.8
	*370.0	-1.21		
	380.0	-1.43	-287.4	-675.0
	400.0	-1.61	-284.4	-730.0
	420.0	-1.76	-302.5	-760.6
	440.0	-1.93	-311.6	-810.6
	460.0	-2.14	-317.6	-862.5
	480.0	-2.46	-323.7	-920.6
	500.0	-2.80	-338.8	-990.6

*Cracks appeared at this loading.

TABLE 5.4 LOAD VERSUS DEFLECTION AND STRAINS OF COMPOSITE SPACE FRAME UNIT (4) AT CENTRELINE

V. Load (kN)	H. Load (kN)	Centreline Deflection (mm)	Strain on Concrete Surface $\times 10^{-6}$	Strain on Top-chord Stem $\times 10^{-6}$
0.0	0.0	0.0	0.0	0.0
8.0	10.0	1.25	-39.3	+0.625
	40.0	1.20	-54.5	-65.6
	100.0	1.11	-69.6	-138.1
	160.0	1.04	-105.9	-221.9
	180.0	1.01	-121.0	-249.4
	200.0	0.96	-130.1	-261.3
	220.0	0.91	-142.2	-264.4
	240.0	0.88	-	-270.6
	260.0	0.84	-157.3	-279.4
	280.0	0.80	-175.5	-288.8
	300.0	0.75	-199.7	-297.5
	*320.0	0.68	-217.8	-305.0
	340.0	0.60	-226.9	-320.6
	360.0	0.56	-239.0	-350.0
	380.0	0.44	-254.1	-370.6
	400.0	0.35	-263.2	-391.3
	420.0	0.25	-272.3	-415.0
	440.0	0.08	-284.4	-453.8
	460.0	-0.08	-269.5	-503.8
	480.0	-0.25	-305.5	-583.1
	490.0	-0.31	-317.6	-617.5
	500.0	Failure		

*Cracks appeared at this loading.

TABLE 5.5 LOAD VERSUS STRESS AT CENTRELINE FOR COMPOSITE SPACE FRAME UNIT (2)

H. Load (kN)	Stress on Concrete Surface (N/mm²)		Stress on Top-chord Stem (N/mm²)	
	σ_1 (Experi.)	σ_2 (Theory)	σ_1 (Experi.)	σ_2 (Theory)
40.0	-7.07	-10.6	-1.31	-10.8
80.0	-6.37	-21.1	-6.57	-21.3
200.0	-10.8	-51.8	-37.7	-56.4
240.0	-22.2	-61.5	-49.9	-68.9
300.0	-13.4	-76.1	-90.2	-87.7
320.0	-14.6	-80.7	-105.8	-92.3
400.0	-22.3	-98.0	-145.5	-121.7

TABLE 5.6 LOAD VERSUS STRESS AT CENTRELINE FOR COMPOSITE SPACE FRAME UNIT (3)

H. Load (kN)	Stress on Concrete Surface (N/mm²)		Stress on Top-chord Stem (N/mm²)	
	σ_1 (Experi.)	σ_2 (Theory)	σ_1 (Experi.)	σ_2 (Theory)
40.0	-53.3	-10.5	-14.8	-11.0
180.0	-57.2	-47.6	-45.0	-48.7
200.0	-57.2	-53.3	-50.8	-53.4
220.0	-57.2	-58.5	-57.6	-59.0
280.0	-57.2	-73.4	-82.2	-77.1
300.0	-57.2	-78.4	-92.7	-83.1
320.0	-57.2	-83.5	-103.7	-88.9
360.0	-57.2	-89.6	-130.2	-102.3
370.0	-	-95.2	-	-105.5
380.0	-60.3	-97.1	-141.8	-109.7
400.0	-59.7	-101.7	-153.3	-116.6

TABLE 5.7 LOAD VERSUS STRESS AT CENTRELINE FOR COMPOSITE SPACE FRAME UNIT (4)

H. Load (kN)	Stress on Concrete Surface (N/mm²)		Stress on Top-chord Stem (N/mm²)	
	σ_1 (Experi.)	σ_2 (Theory)	σ_1 (Experi.)	σ_2 (Theory)
40.0	-11.5	-10.3	-13.8	-11.4
200.0	-27.3	-51.8	-54.9	-56.3
300.0	-41.9	-78.2	-62.5	-83.4
400.0	-55.3	-105.6	-82.2	-108.8
460.0	-62.3	-122.4	-105.8	-123.2

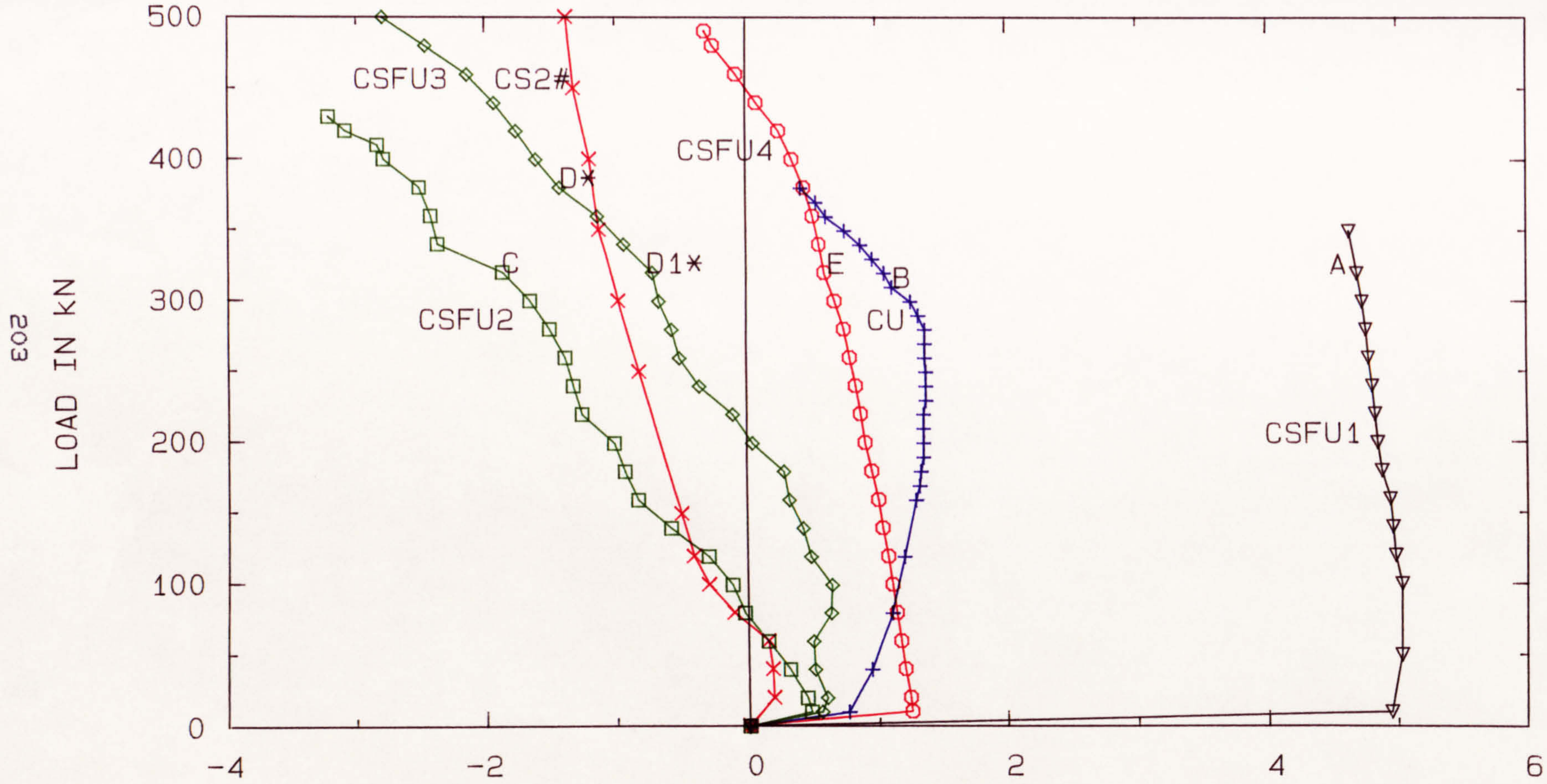

FIG.5.1 LOAD-DEFLECTION FOR THE COMPOSITE SPECIMENS

(#) No cracks appeared with this unit during the whole test.

(*) Probable interval where cracks appeared; they were first seen at D.

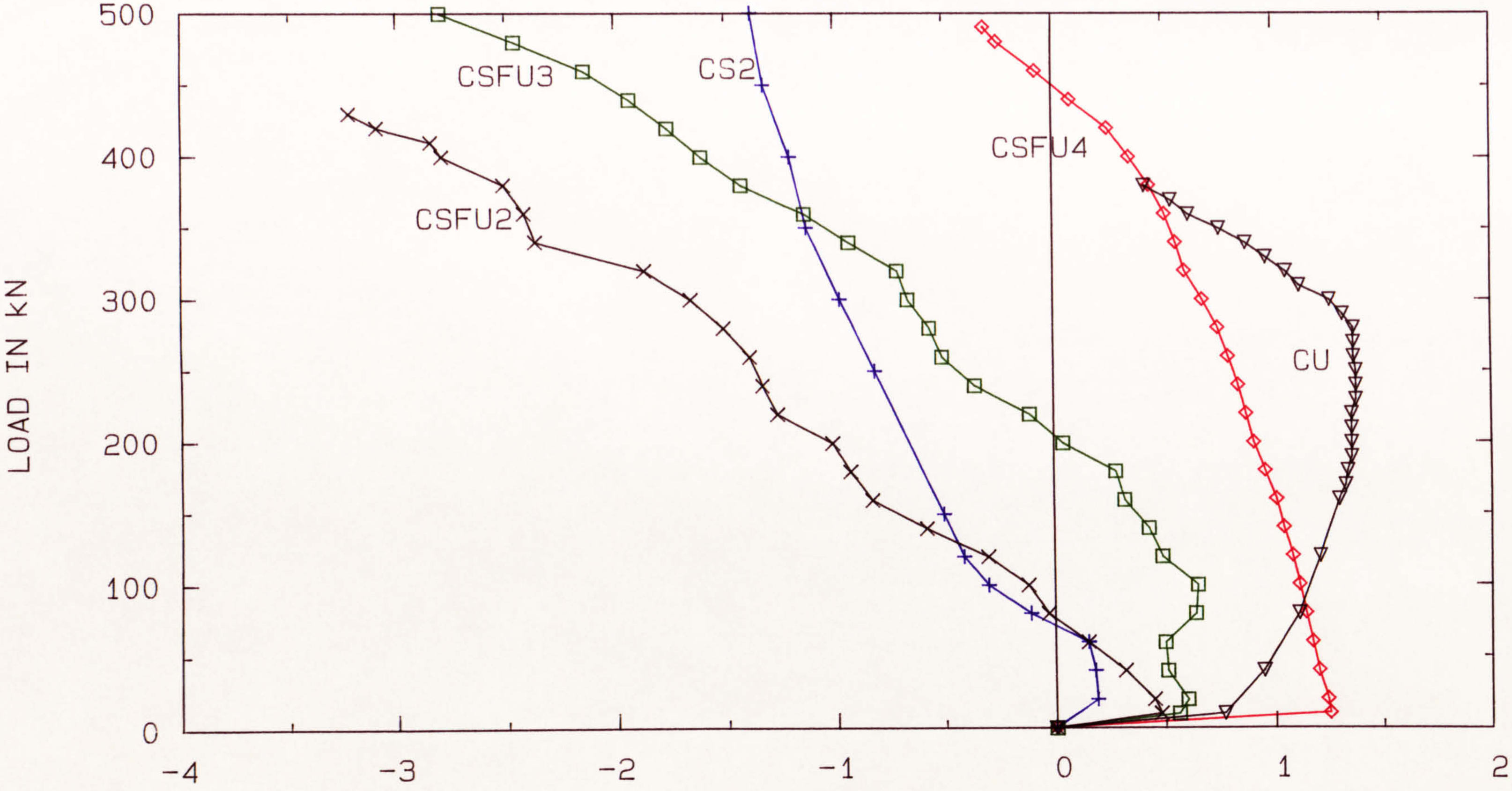

FIG.5.2 LOAD-DEFLECTION FOR THE COMPOSITE SPECIMENS

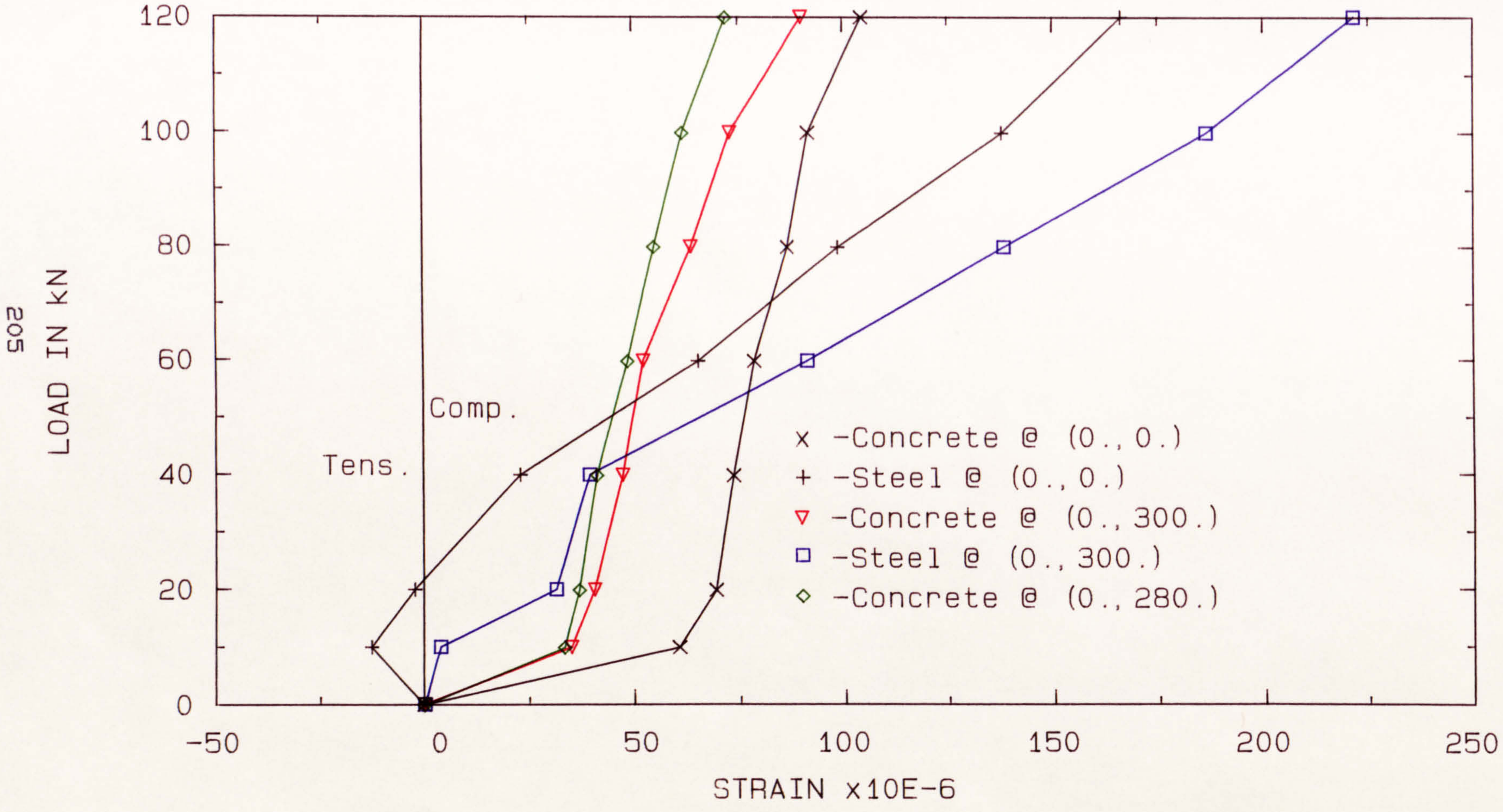

FIG.5.3 STRAIN VARIATION WITH HORIZONTAL LOAD (CSFU1/3)

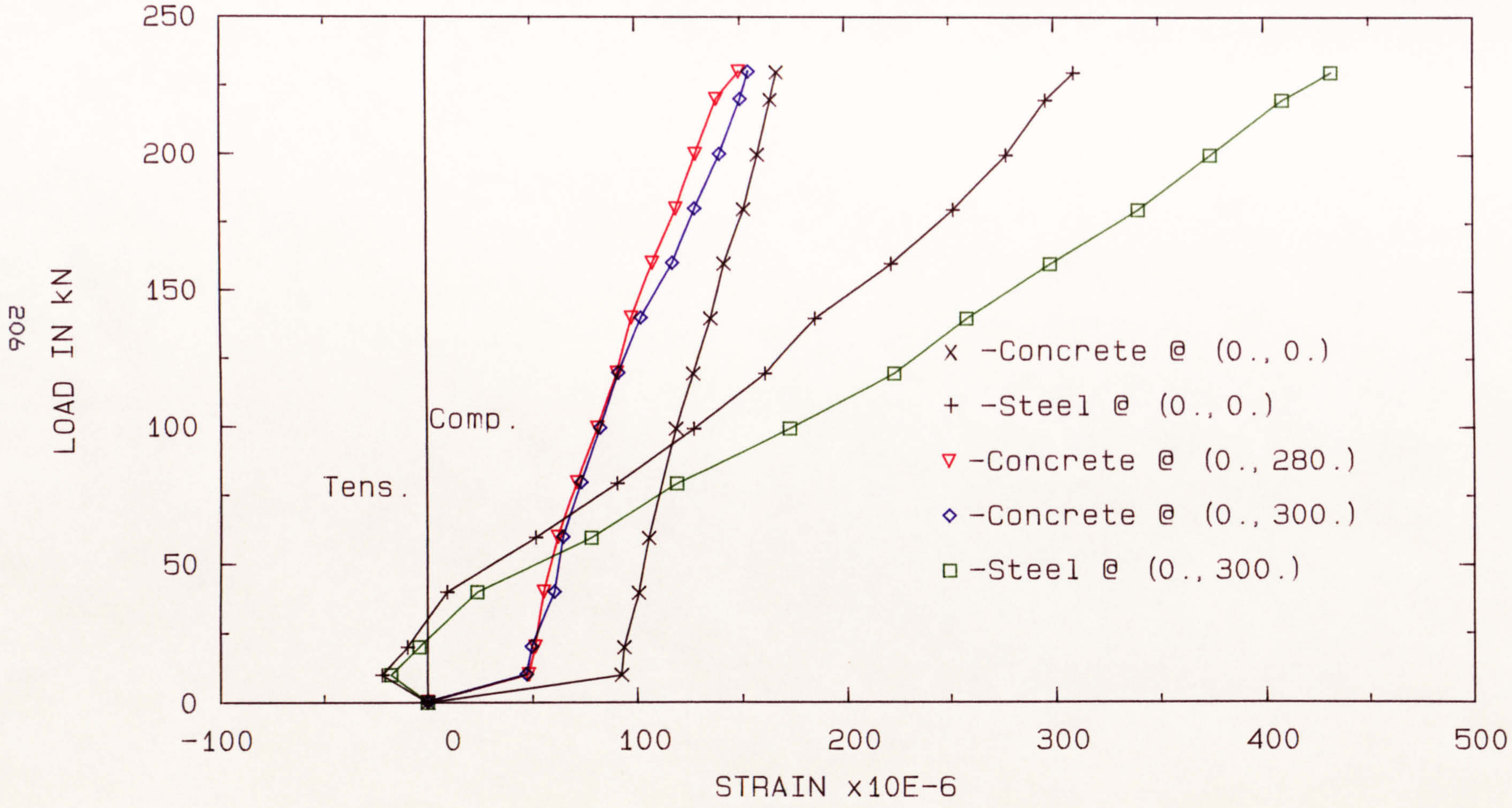

FIG.5.4 STRAIN VARIATION WITH HORIZONTAL LOAD (CSFU1/6)

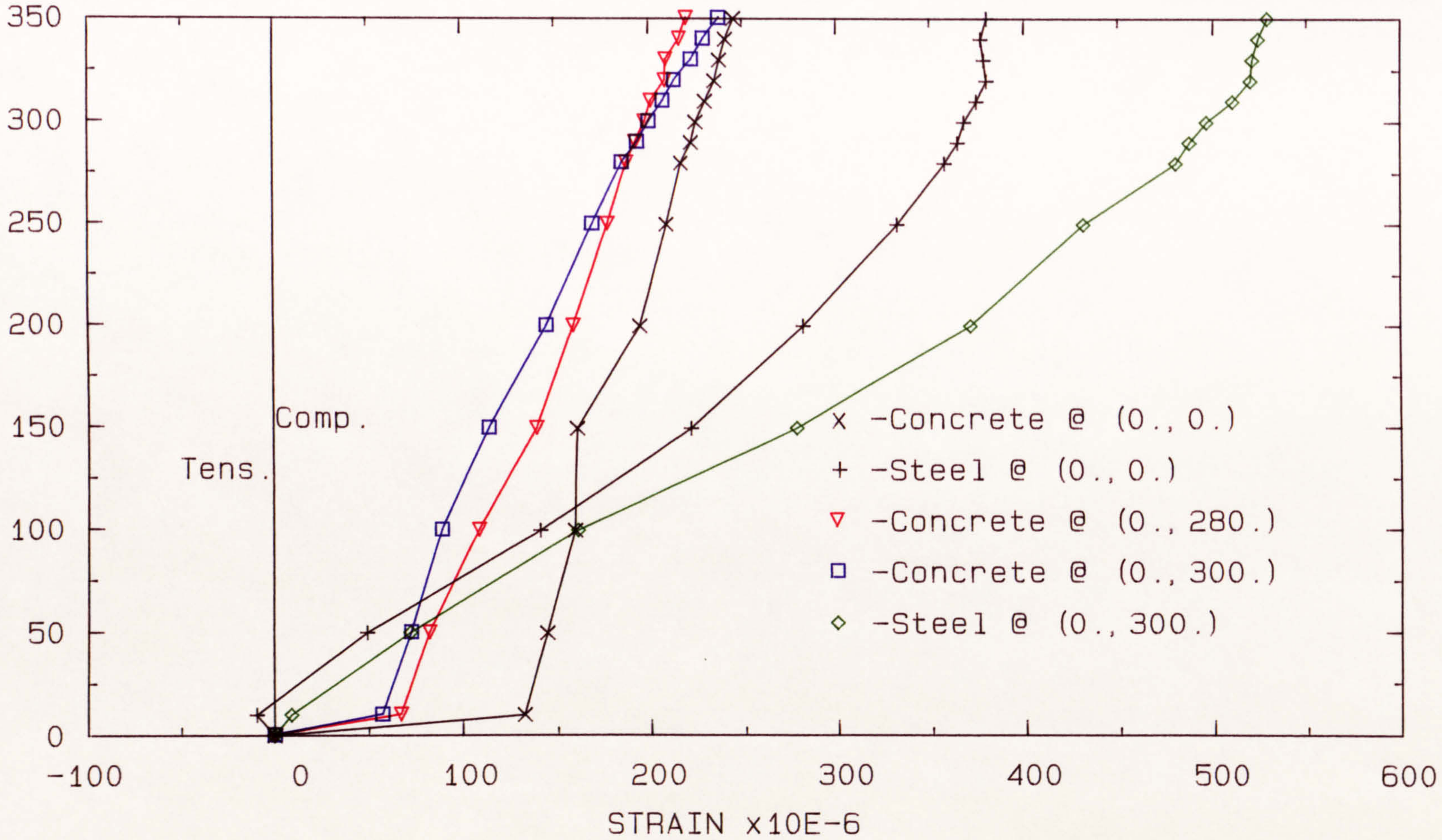

FIG.5.5 STRAIN VARIATION WITH HORIZONTAL LOAD (CSFU1/9)

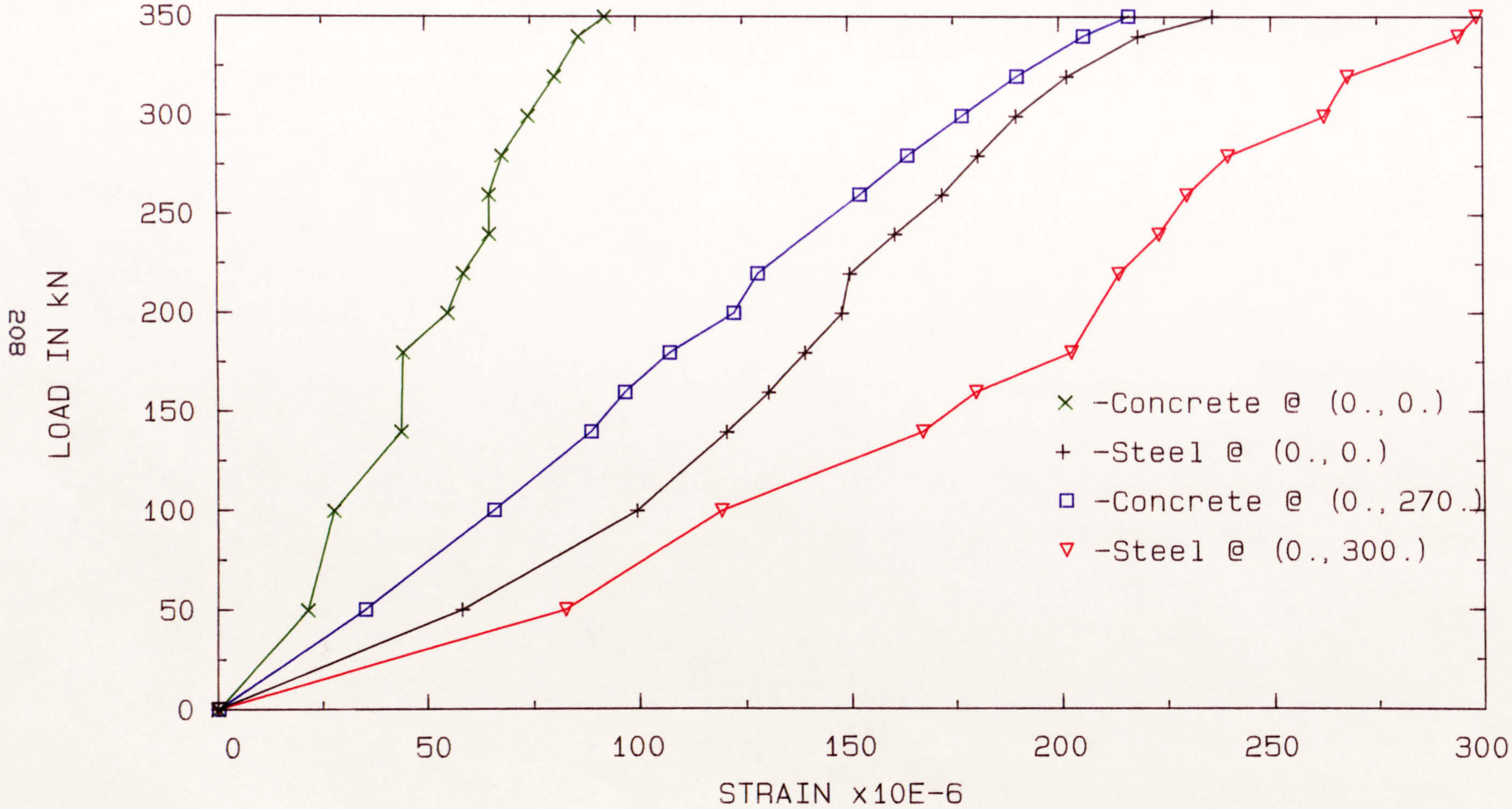

FIG.5.6 STRAIN VARIATION WITH HORIZONTAL LOAD (CSFU1/10)

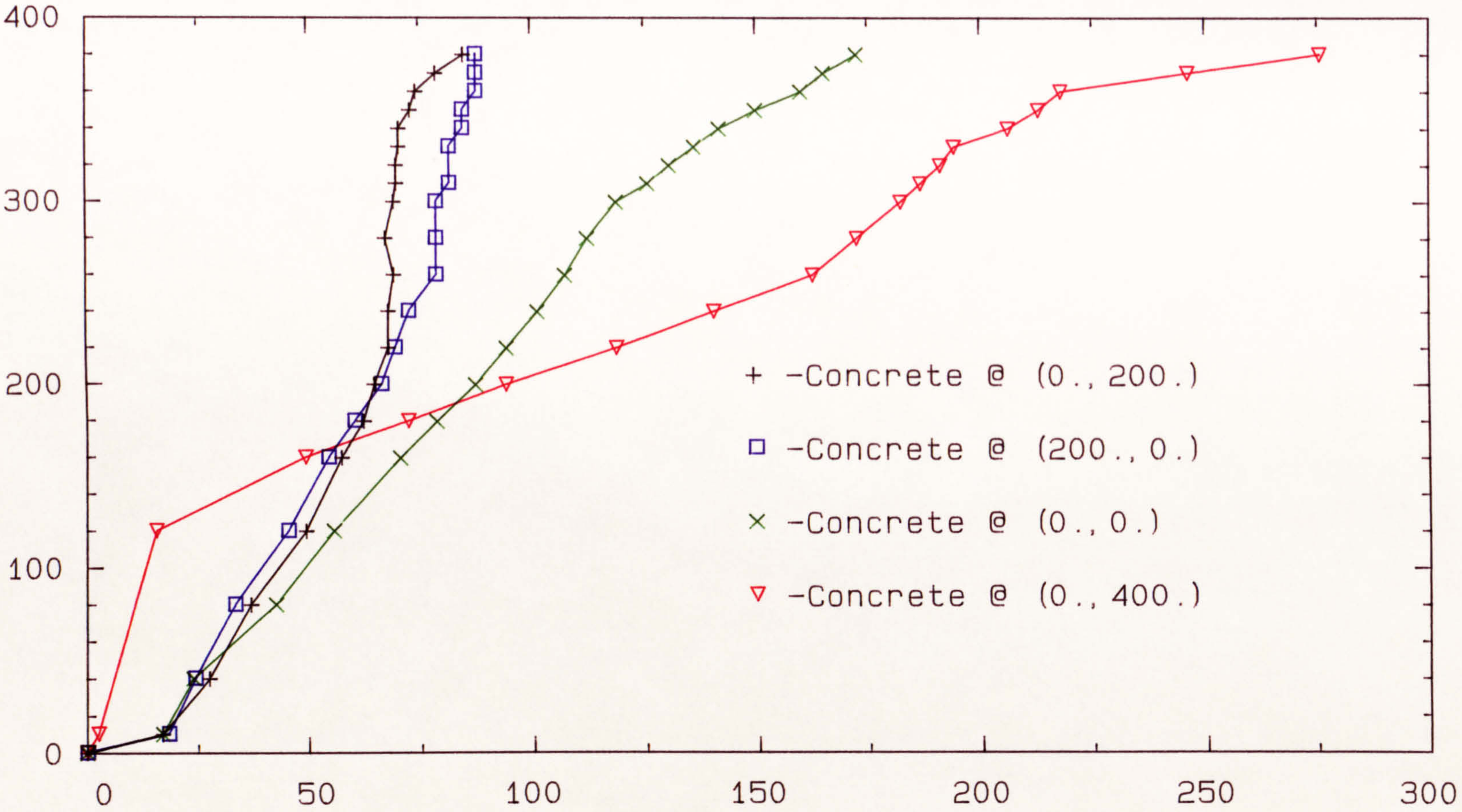

FIG.5.7 STRAIN VARAITION WITH HORIZONTAL LOAD (CU)

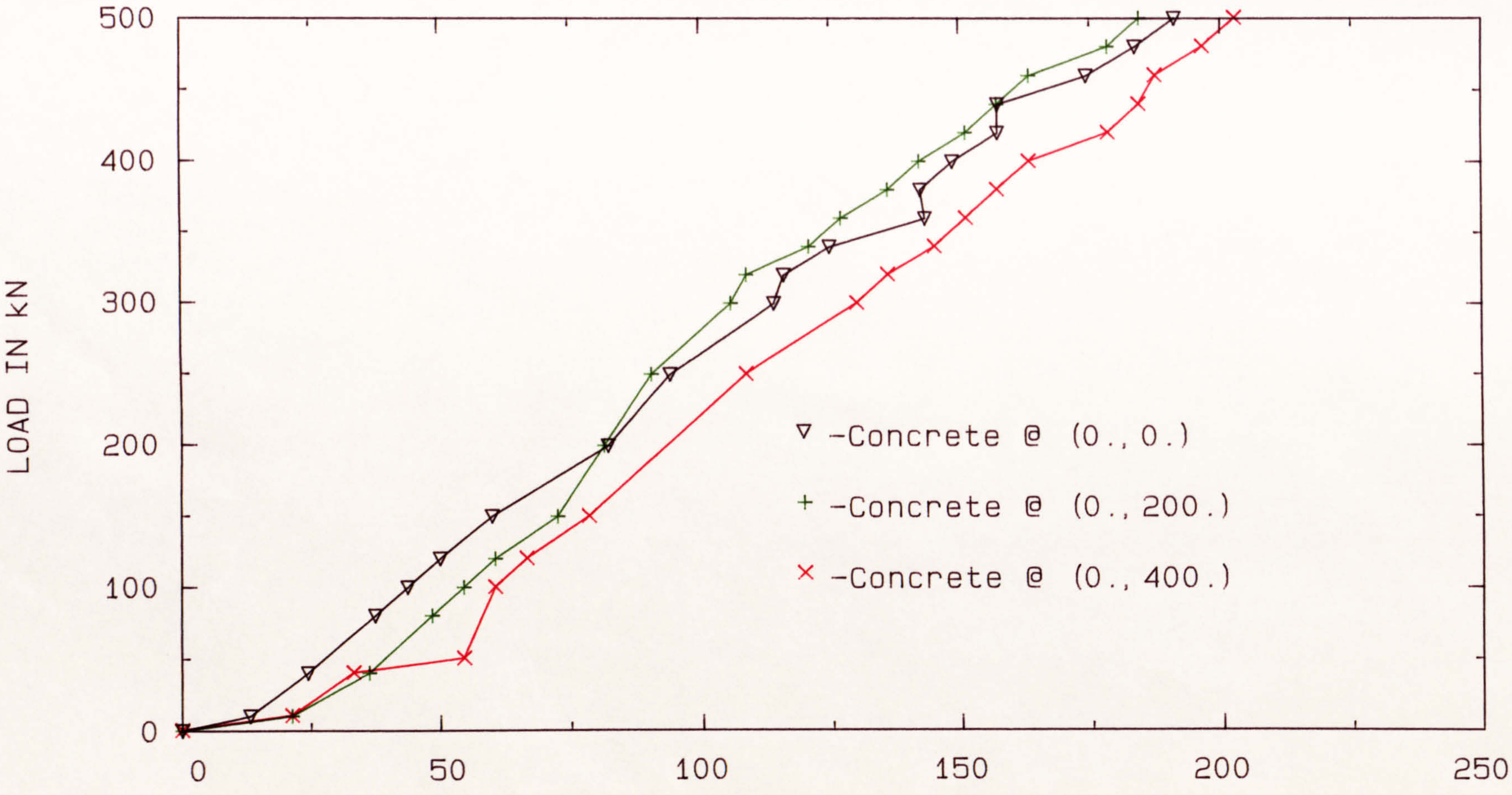

FIG.5.8 STRAIN VARIATION WITH HORIZONTAL LOAD (CS2)

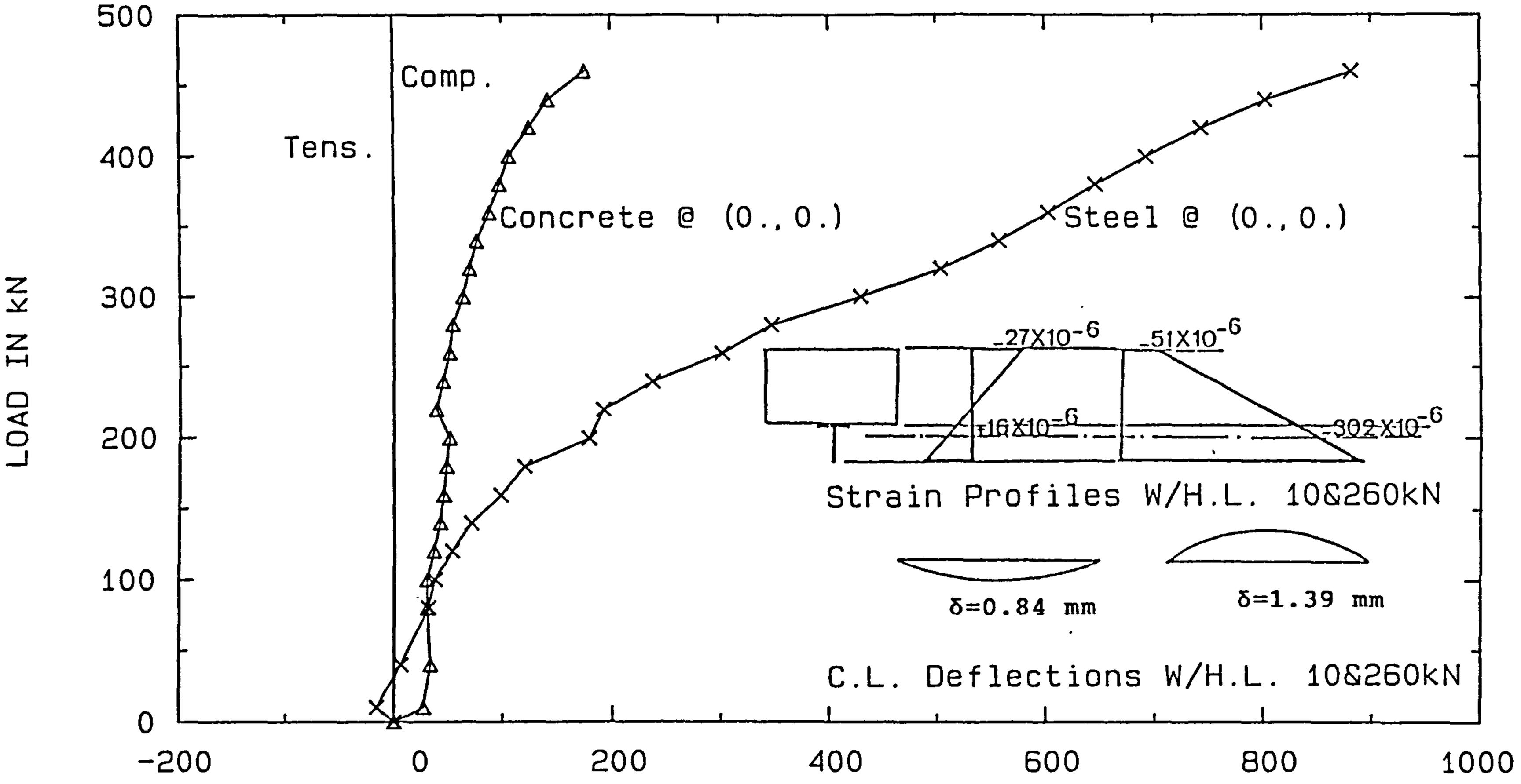

FIG.5.9 STRAIN VARIATION WITH HORIZONTAL LOAD (CSFU2)

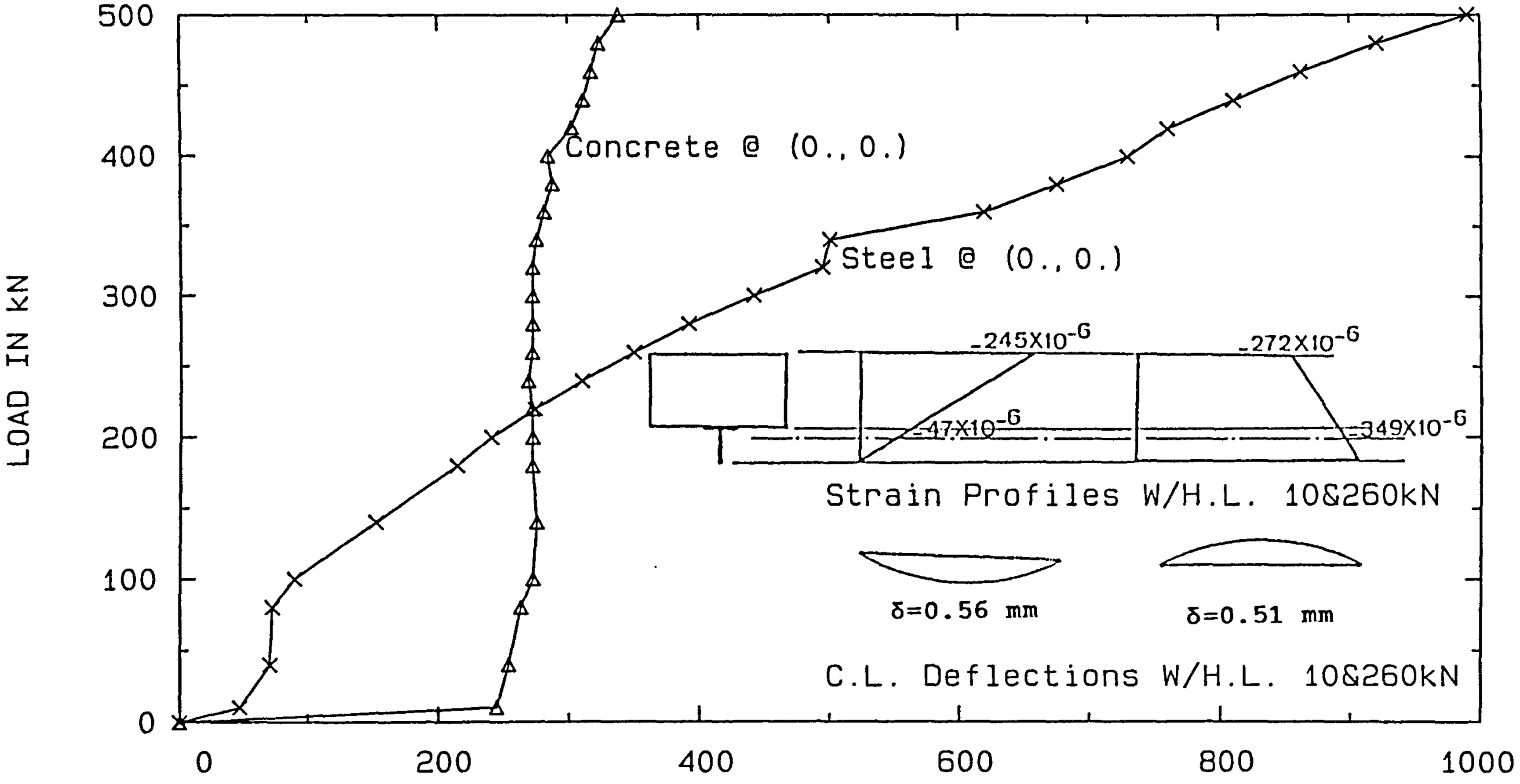

FIG.5.10 STRAIN VARIATION WITH HORIZONTAL LOAD (CSFU3)

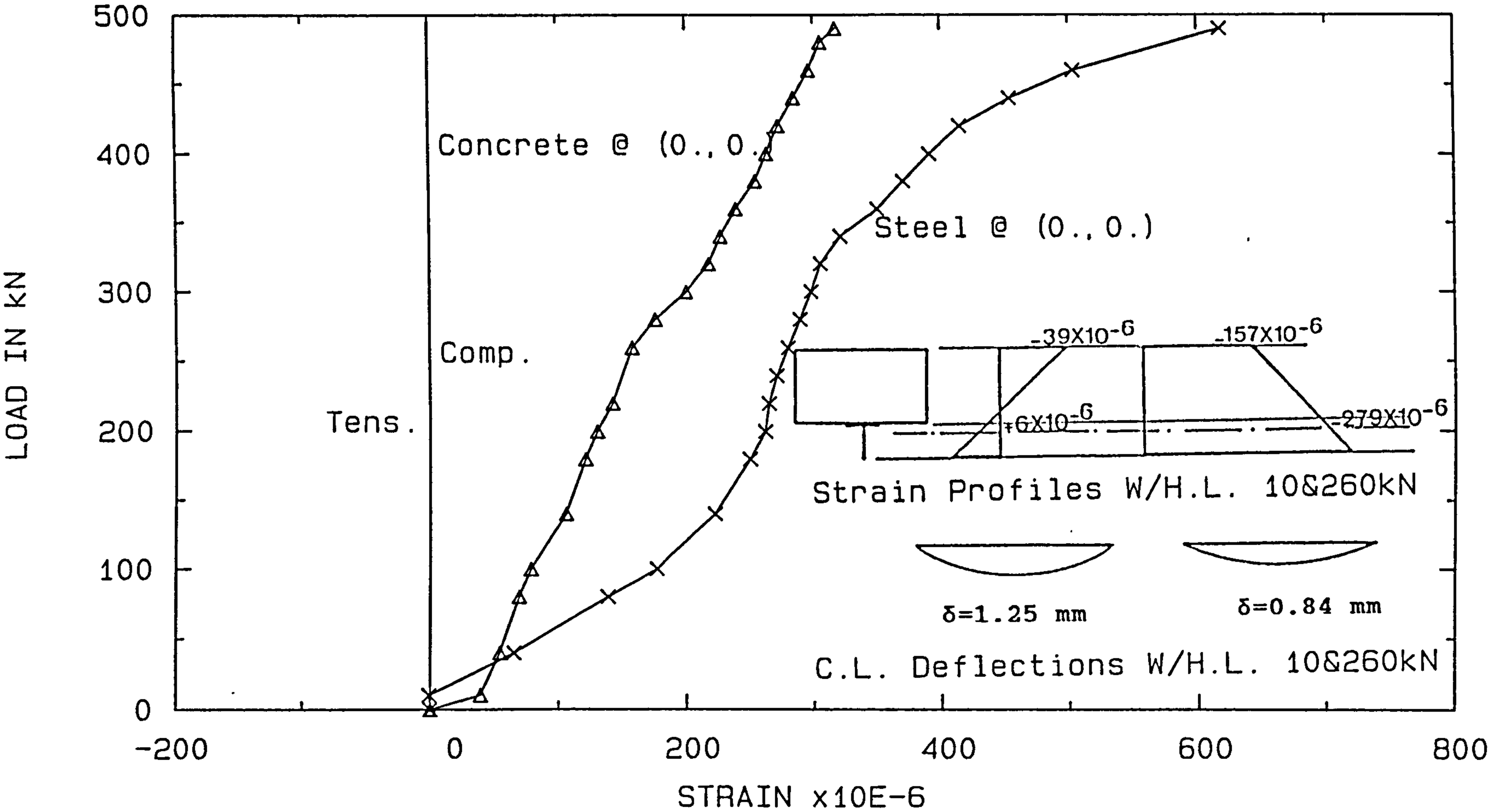

FIG.5.11 STRAIN VARIATION WITH HORIZONTAL LOAD (CSFU4)

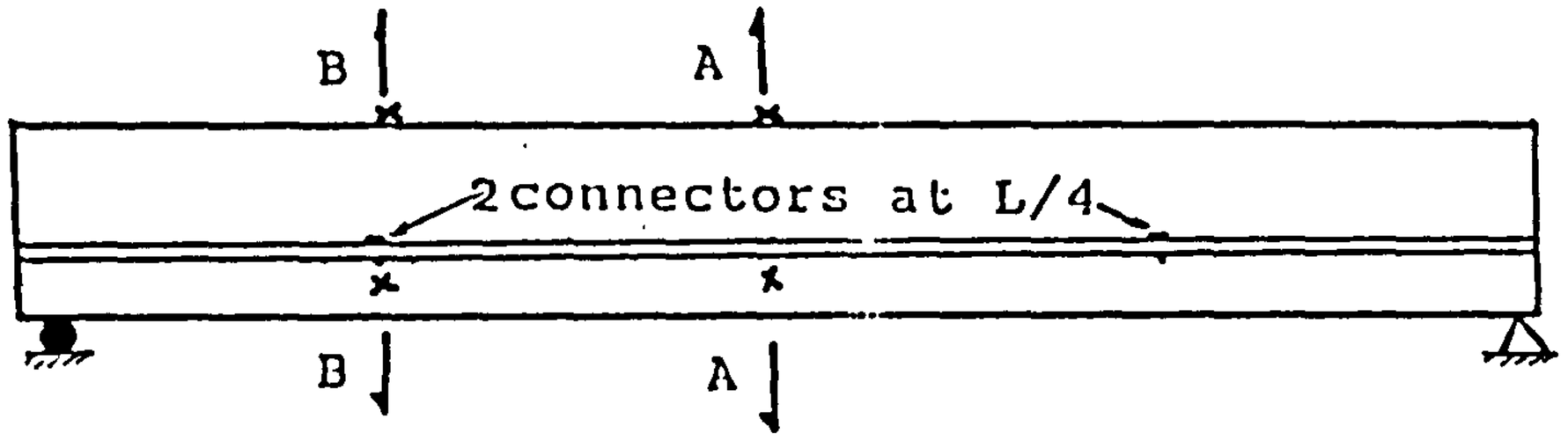

longitudinal section 1-1

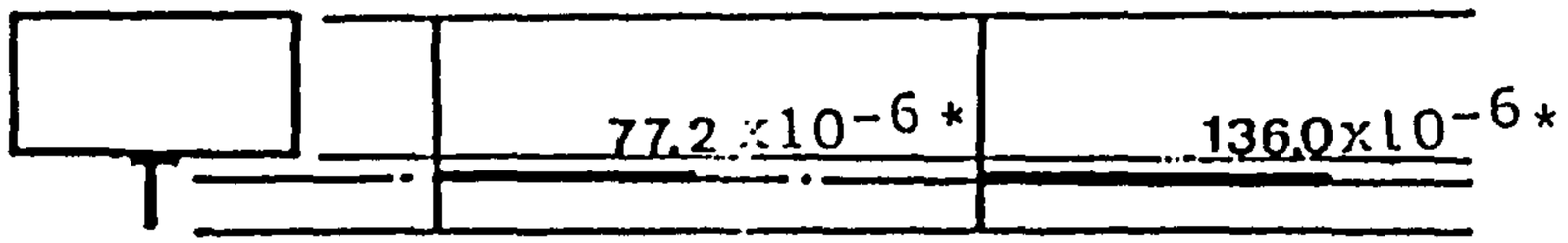

Section A-A Section B-B

Strain Profiles on C.G. of steel at (0,0) and (0,300) (V=8KN and H=80KN)

*Acoustic Gauge was at the C.G. of the stem

For further details see Table 4.1.1

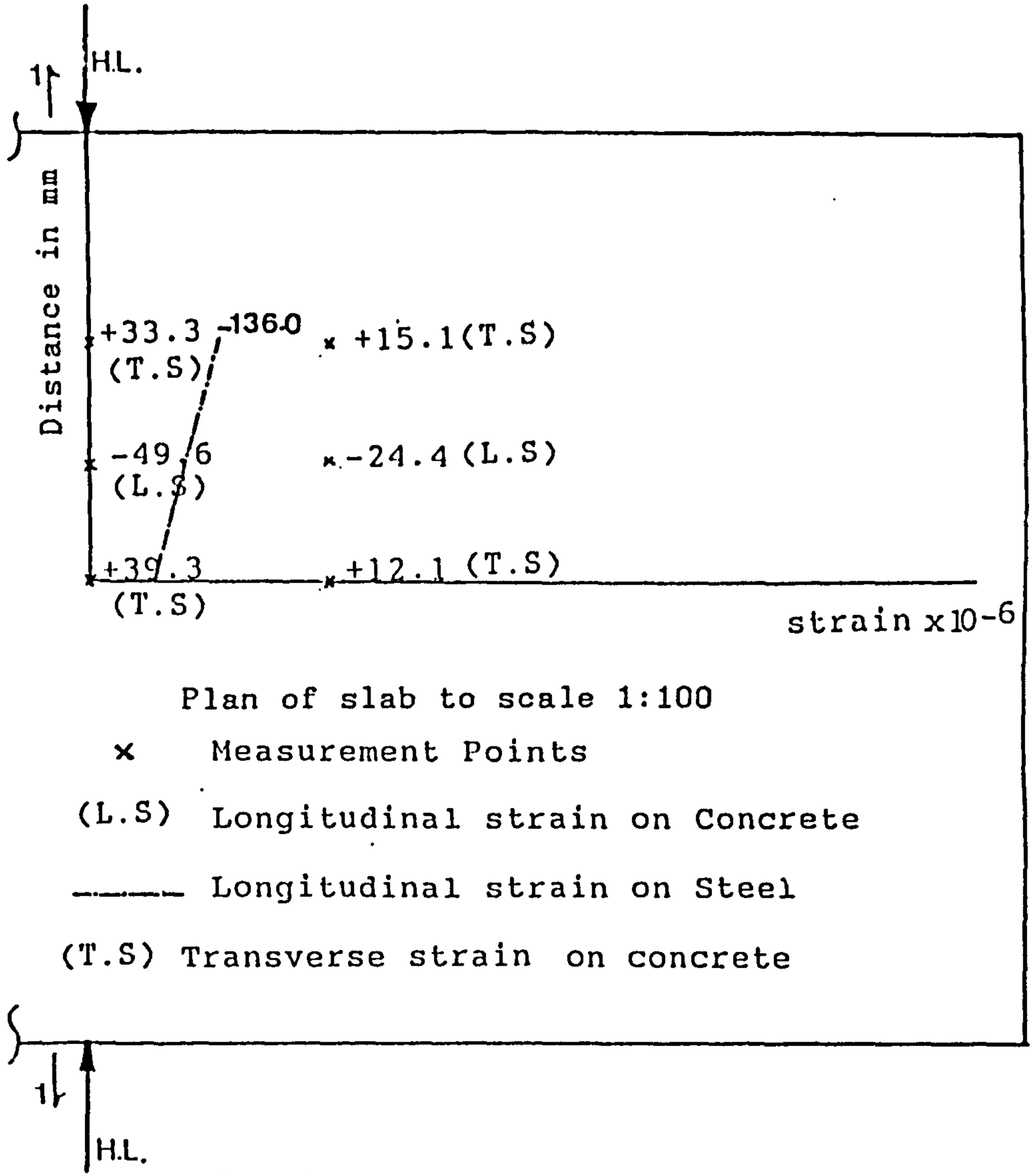

Fig. 5.12 Longitudinal and Transverse Strain Distribution for CSFU1 (Run1)

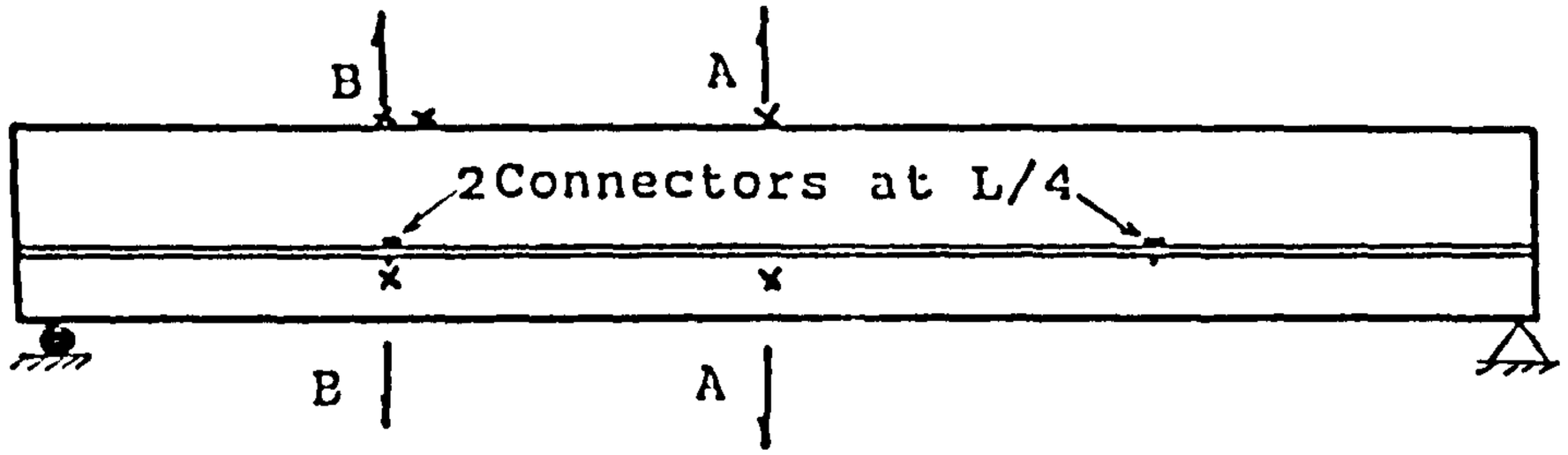

Long. Section 1-1

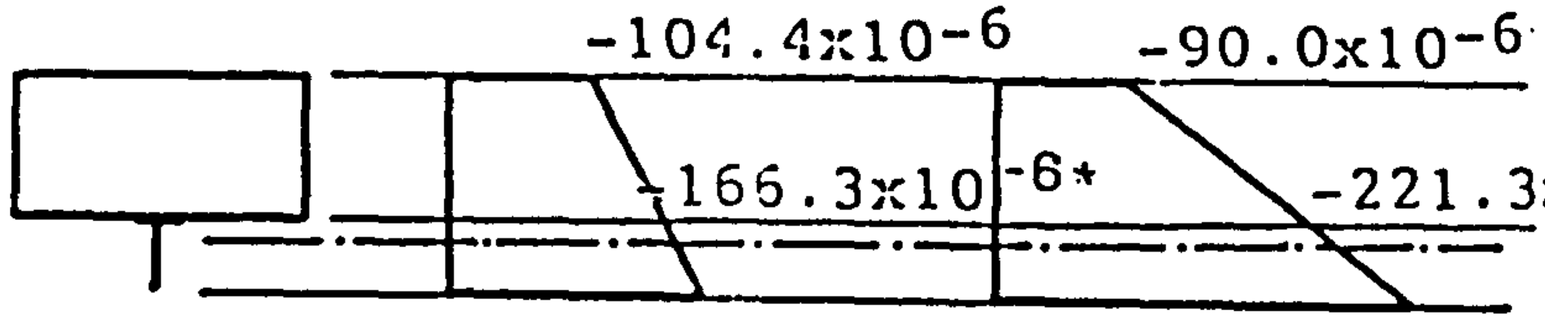

A-A
at(0,0)

B-B
at(0,300)

strain profiles at loading of
(V=12kN and H=120kN)

*Acoustic Gauge was the the C.G. of the stem

For further details see Table 4.1.2

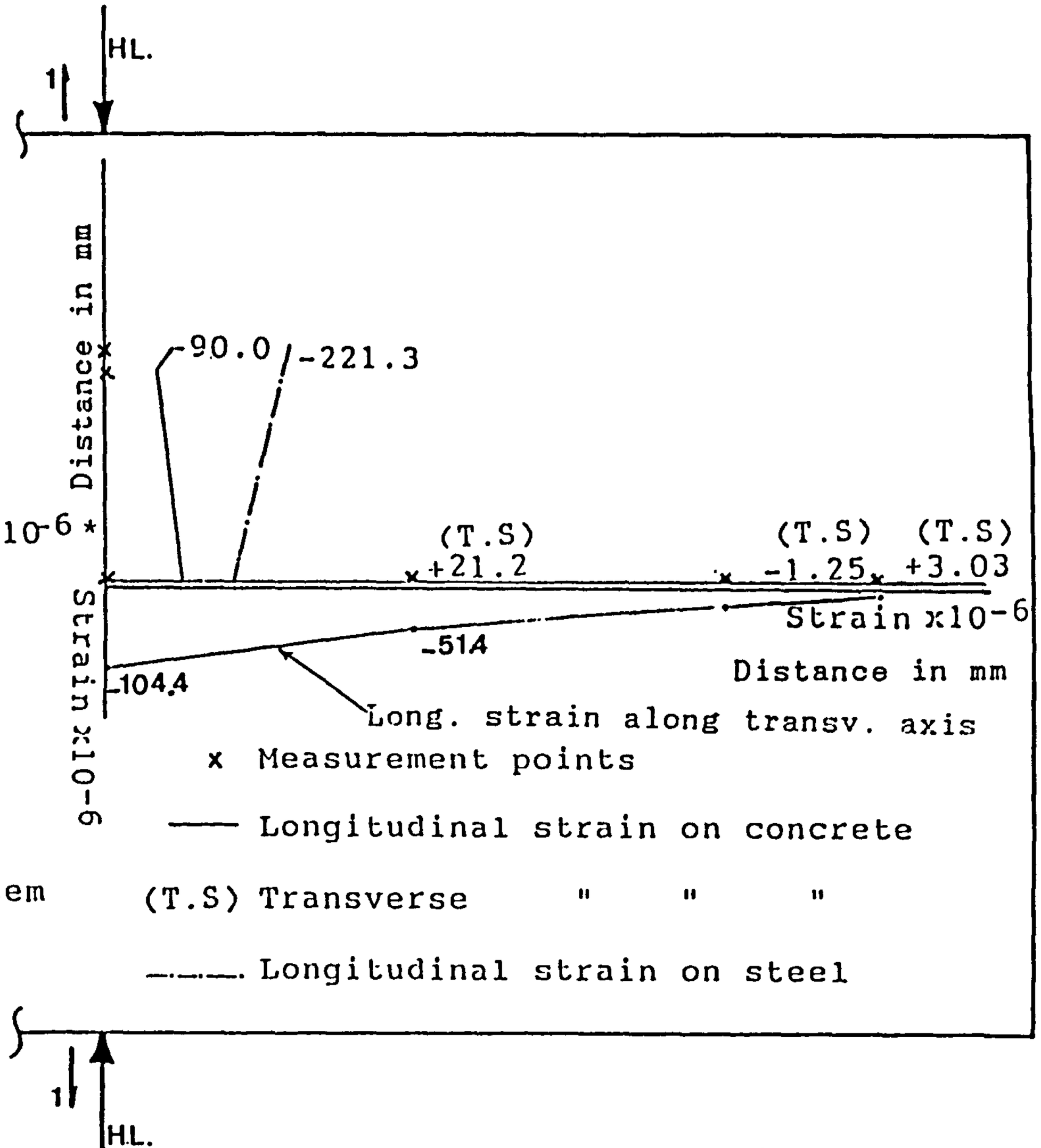

Fig. 5.13 Longitudinal and Transverse strain Distribution for CSFU1 (Run 3)

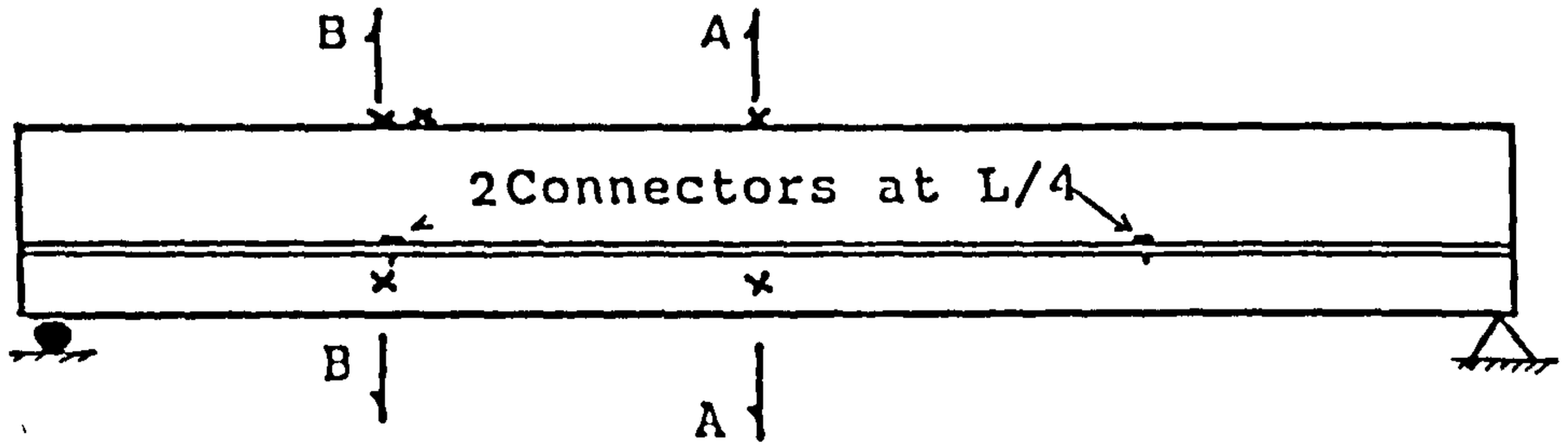

Long. section 1-1

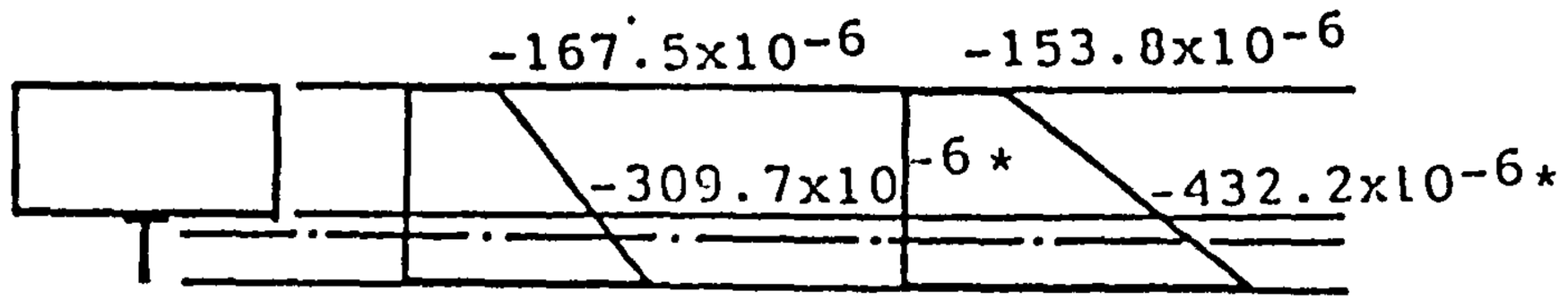

A-A
at (0,0)

B-B
at (0,300)

strain profiles at the loading of
(V=18kN and H=230kN)

*Acoustic Gauge was at the C.G. of the stem

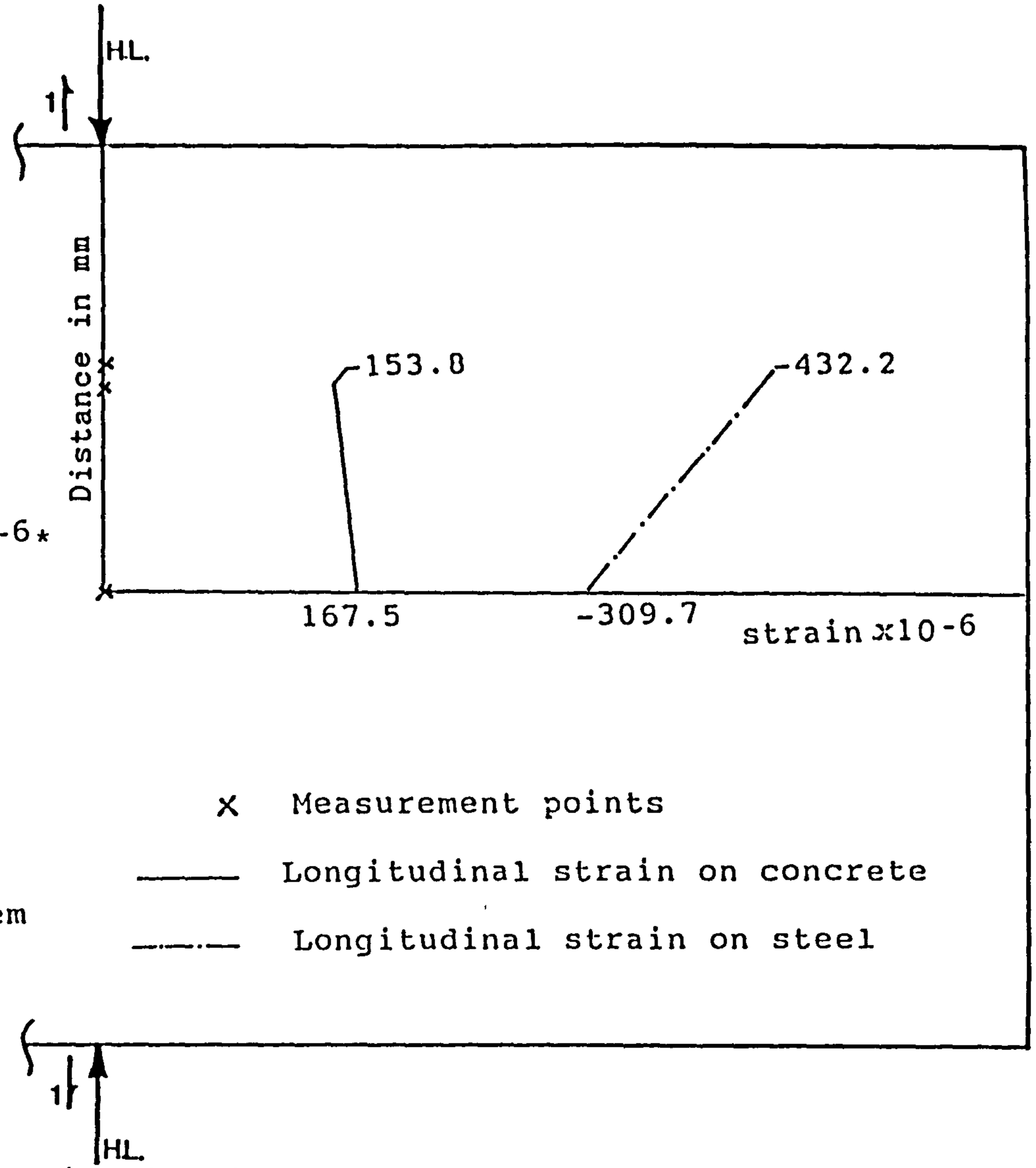

For further details see Table 4.1.3

Fig. 5.14 Longitudinal strain Distribution for CSFU1 (Run 6)

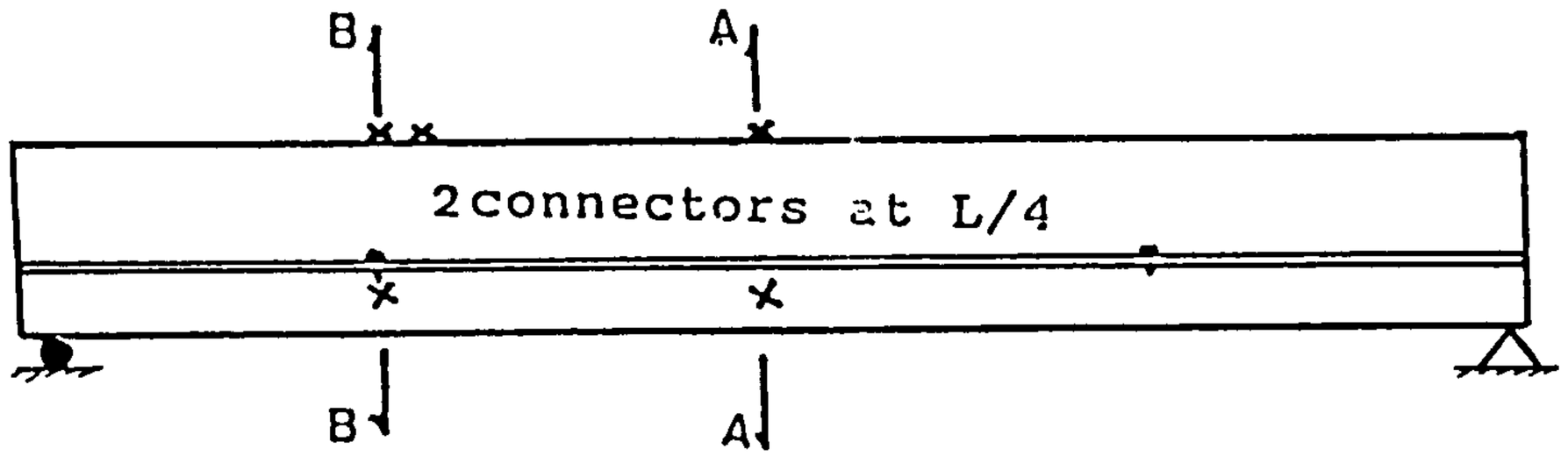

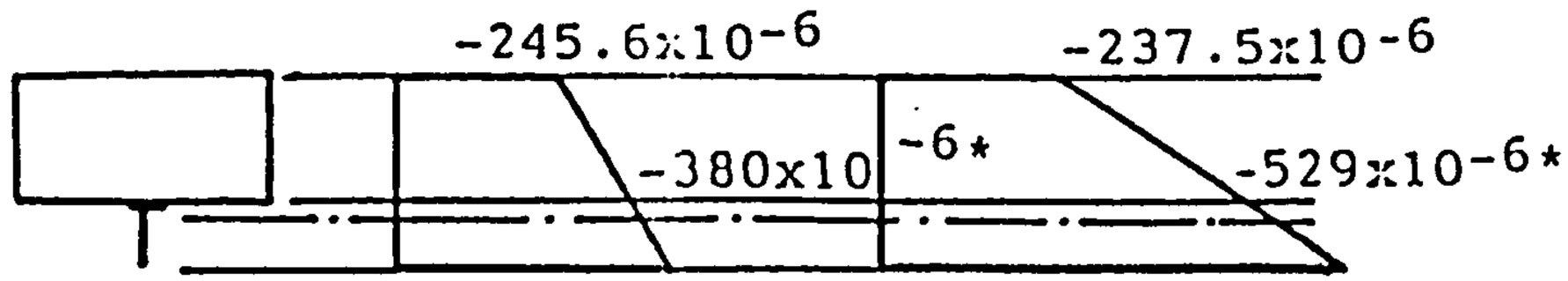

A-A
at (0,0)

B-B
at(0,300)

Strain Profiles (V=27KN an H=350KN)

*Acoustic Gauge was at the C.G. of the stem

For further details see Table 4.1.4

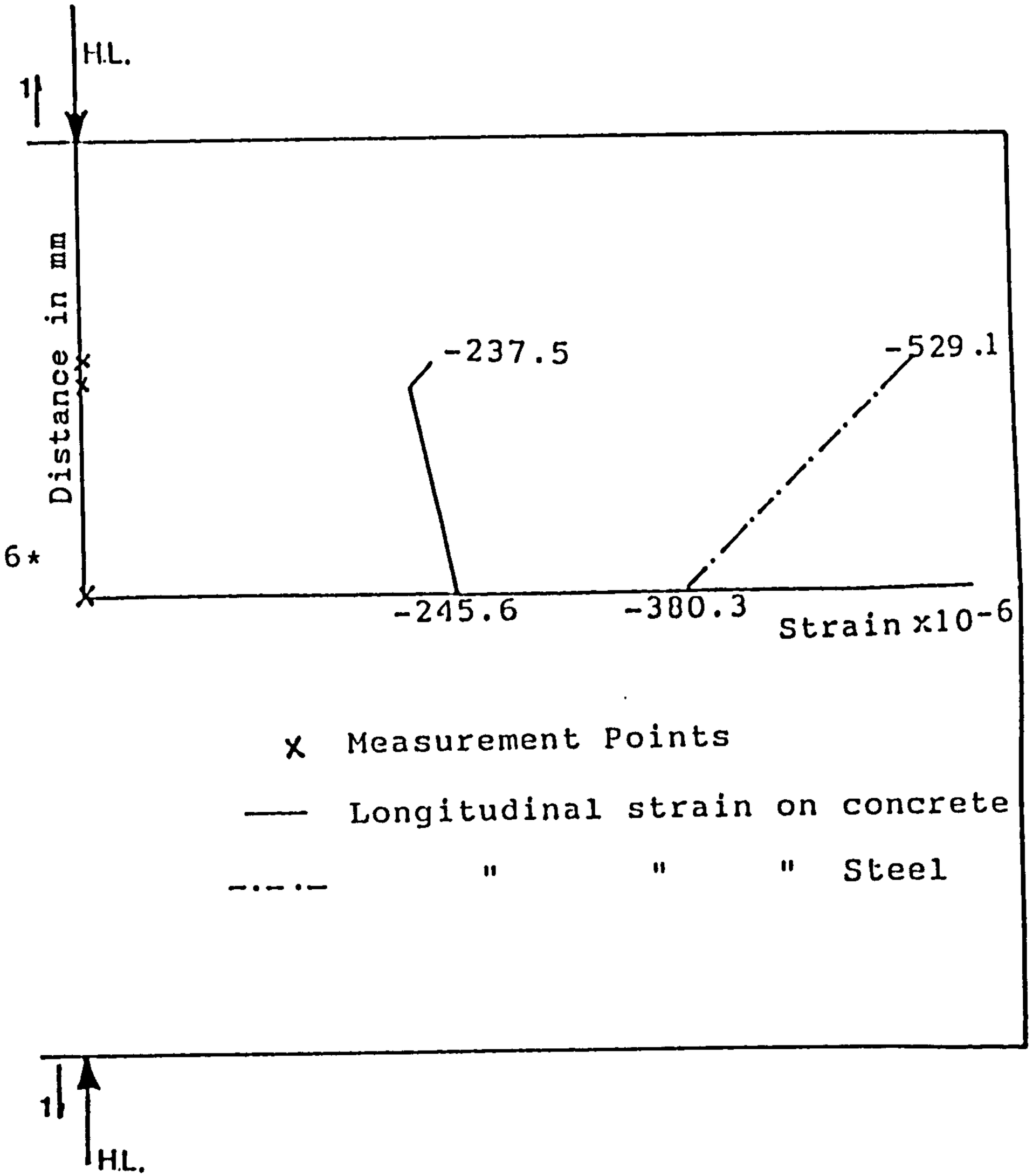

Fig. 5.15 Longitudinal strain Distribution for CSFU 1 (Run 9)

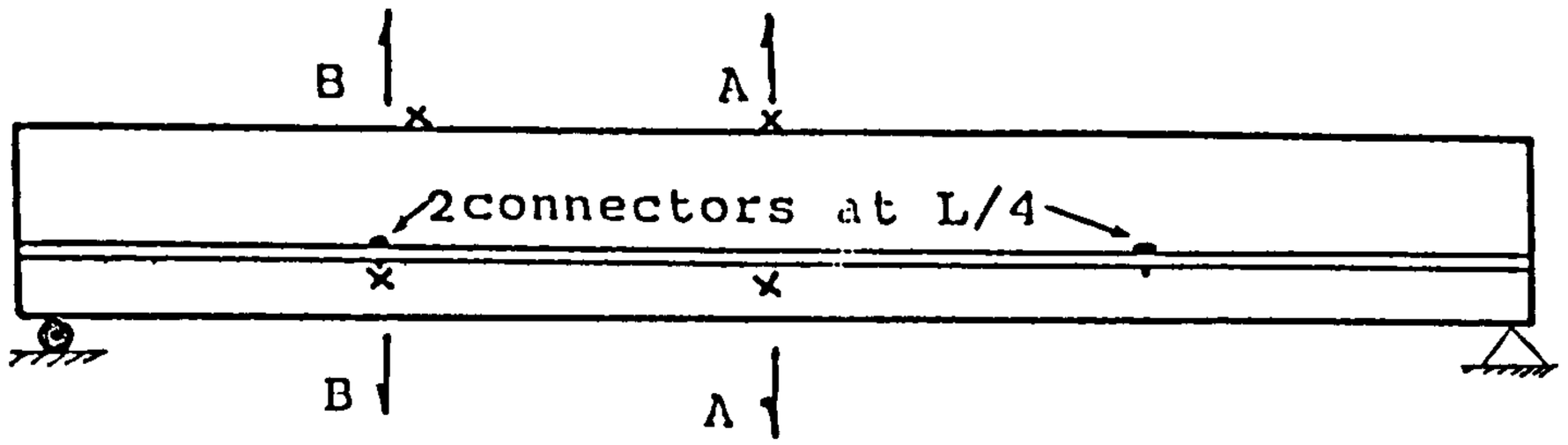

longitudinal section 1-1

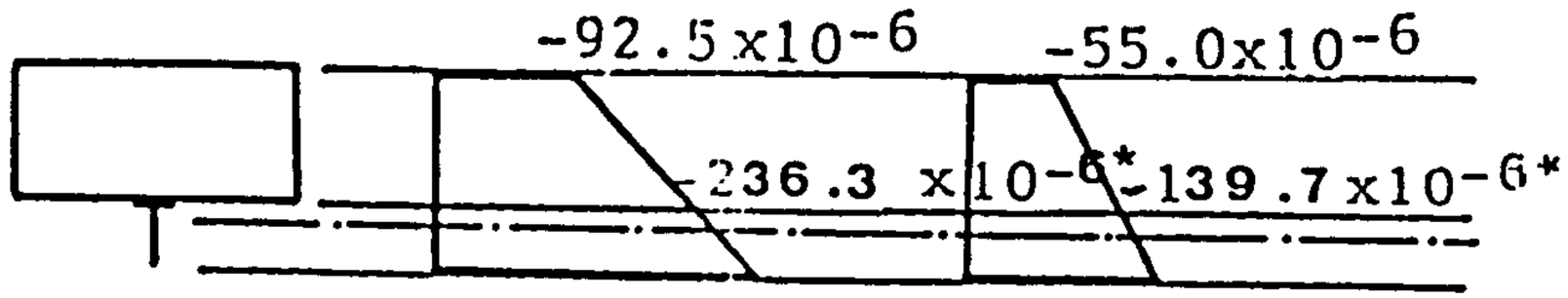

strain profiles at (0,0)

*Acoustics Gauge was at C.G. of the stem

For further details see Table 4.1.5

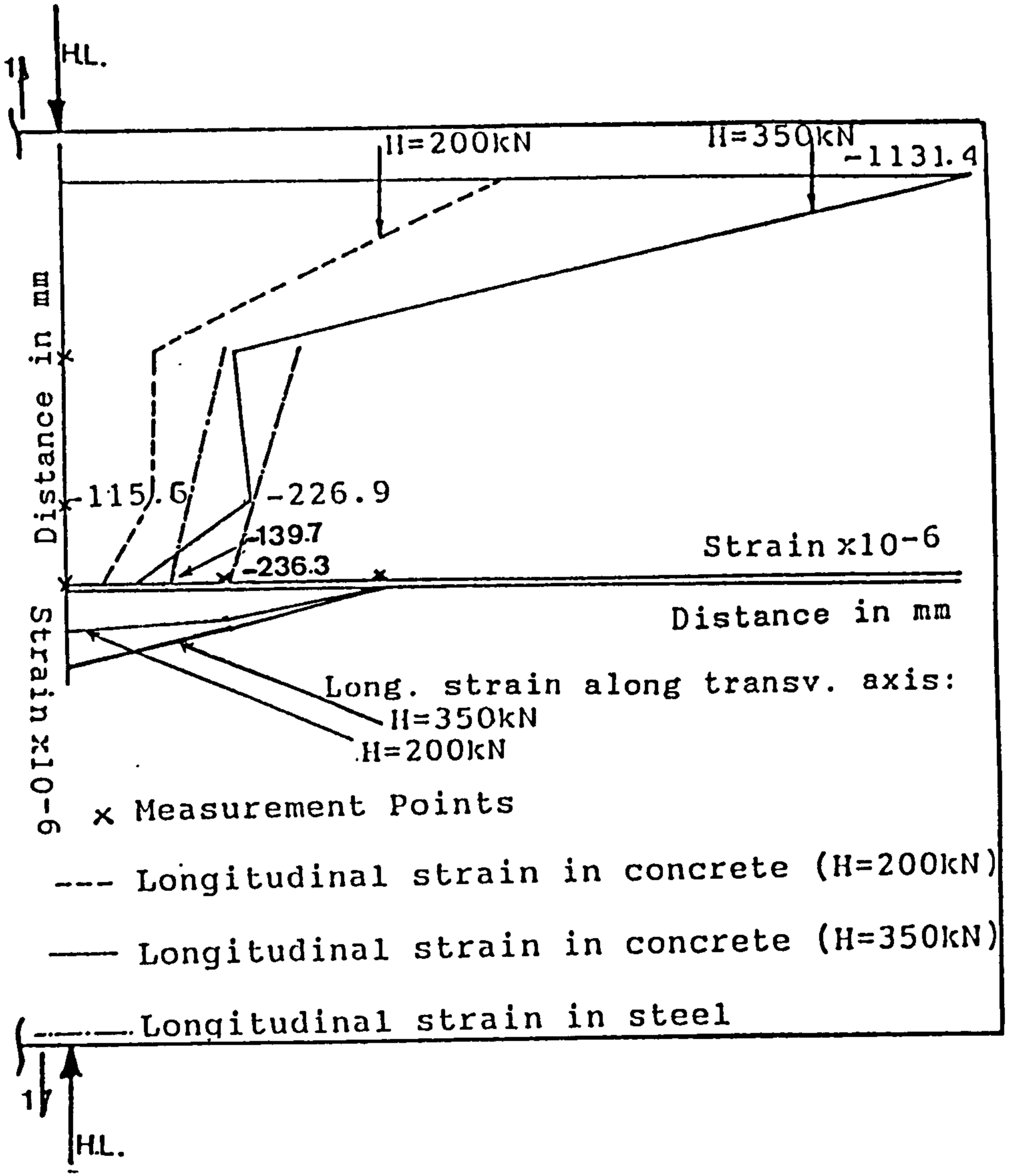

Fig. 5.16 Longitudinal strain Distribution for CSFU1 (Run 10)

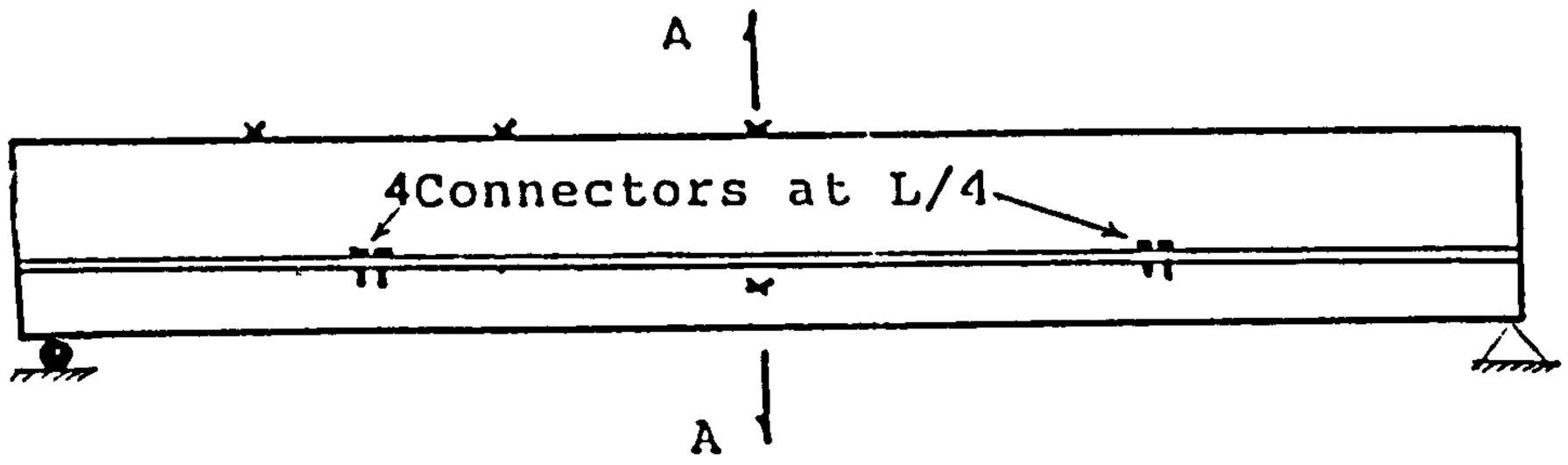

Longitudinal section 1-1

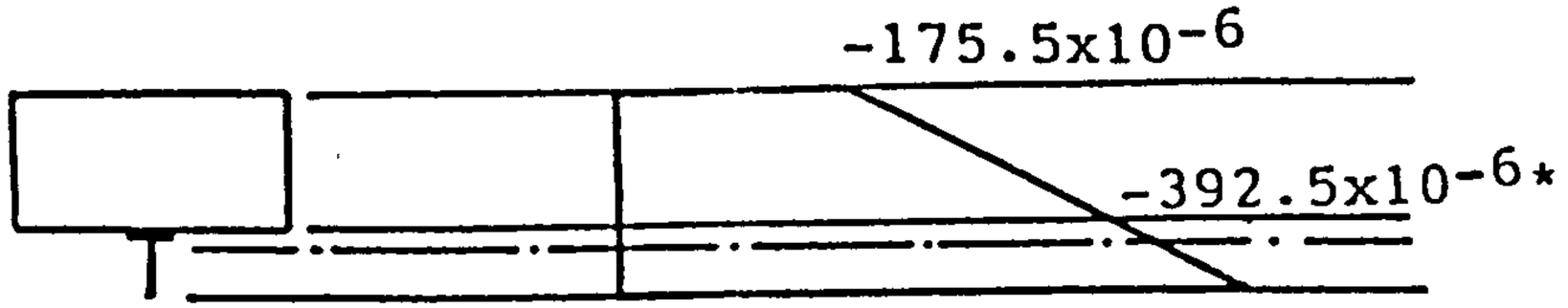

A-A

strain profile at (0,0)
(V=8kN and H=460kN)

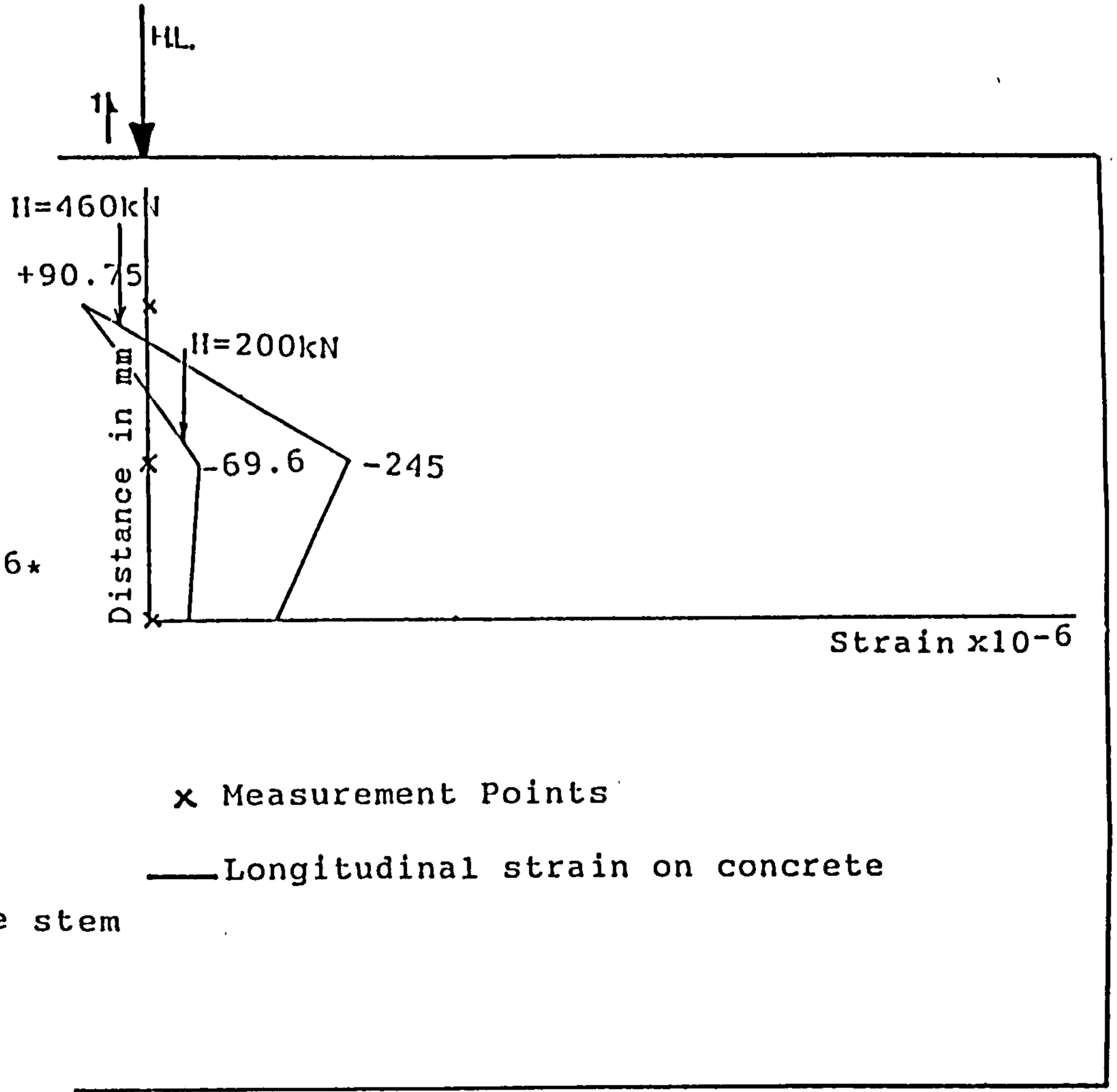

*Acoustic Gauge was at the C.G. of the stem

For further details see Table 4.4

Fig. 5.17 Longitudinal strain Distribution for CSFU2

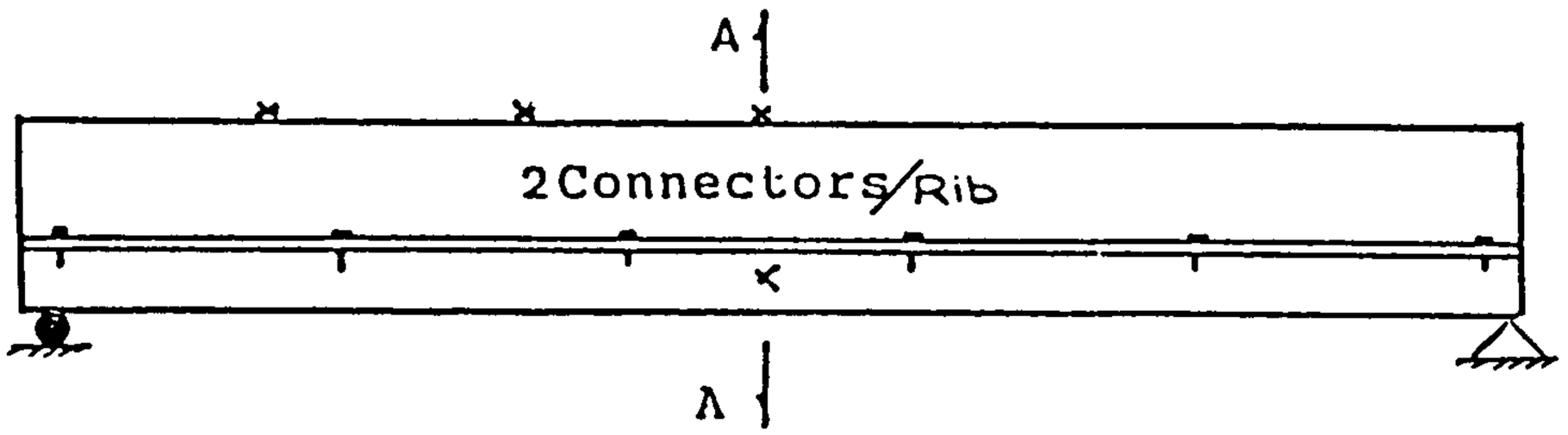

Longitudinal section 1-1

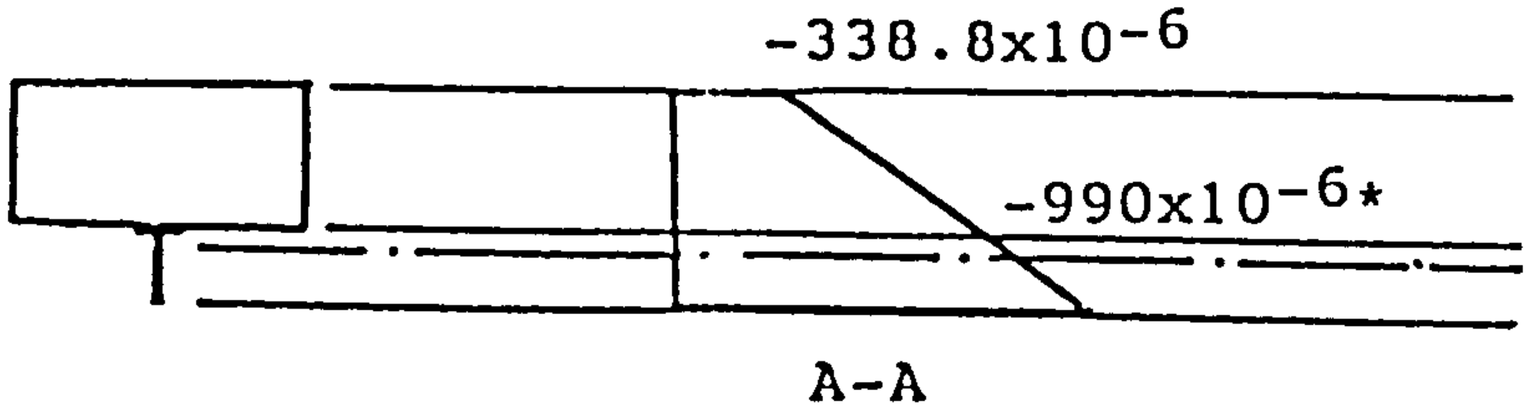

A-A

strain profile at (0,0)
(V=8kN and H=500kN)

*Acoustic Gauge was the C.G. of the stem

For further details see Table 4.5

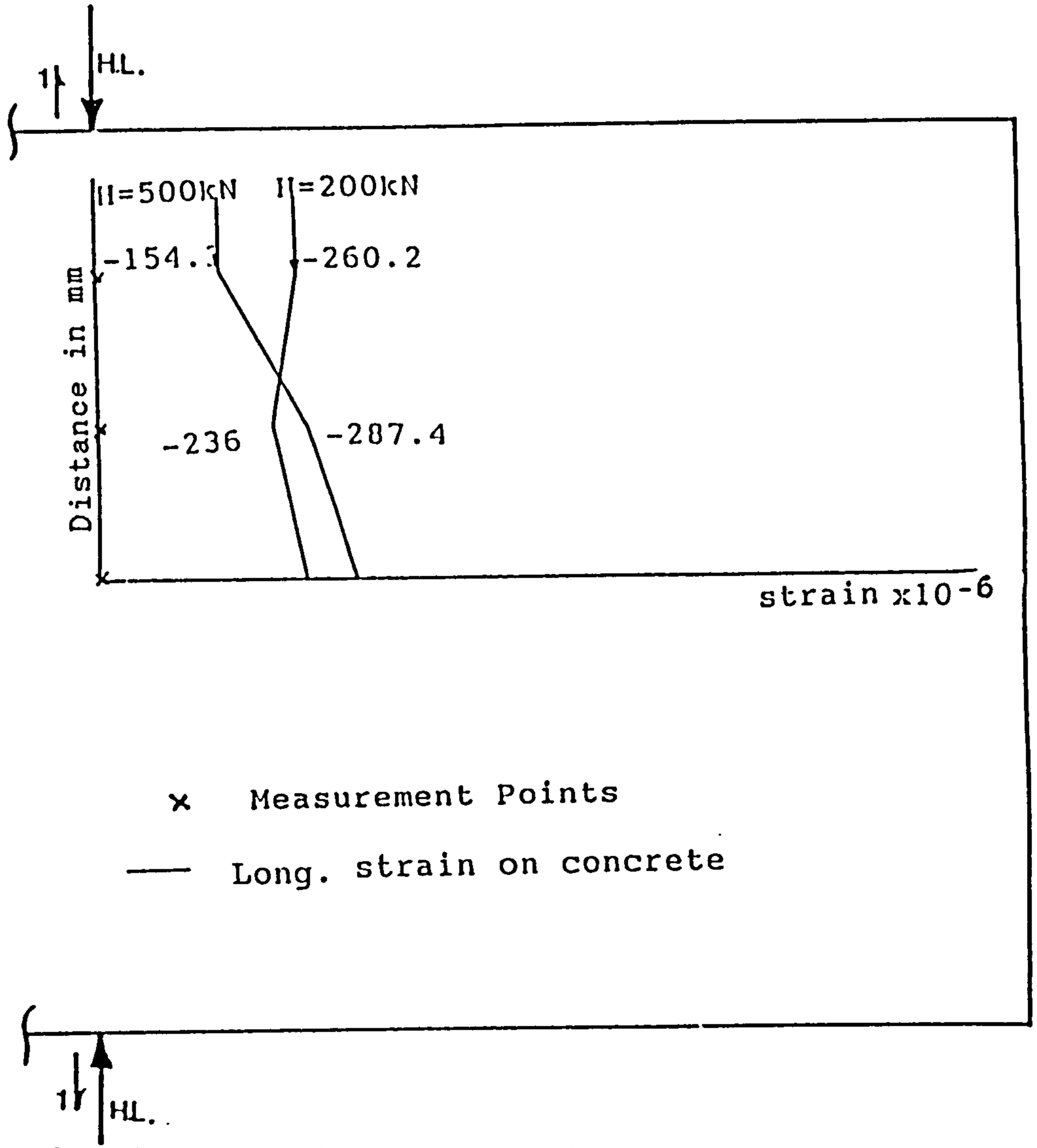

Fig. 5.18 longitudinal strain Distribution fo CSFU 3

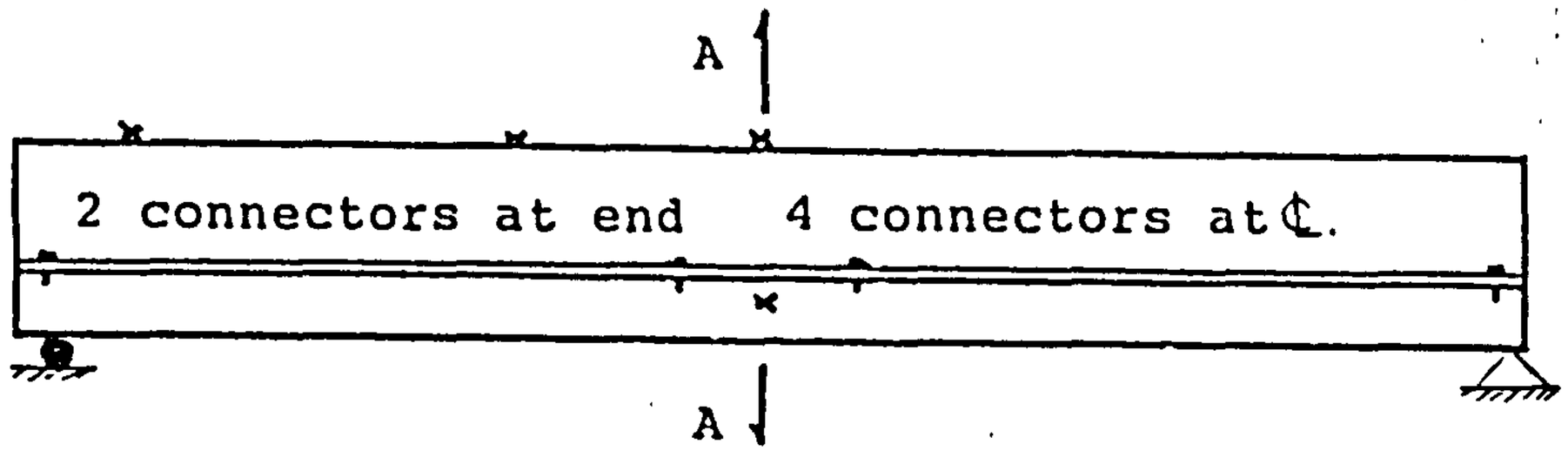

Longitudinal section 1-1

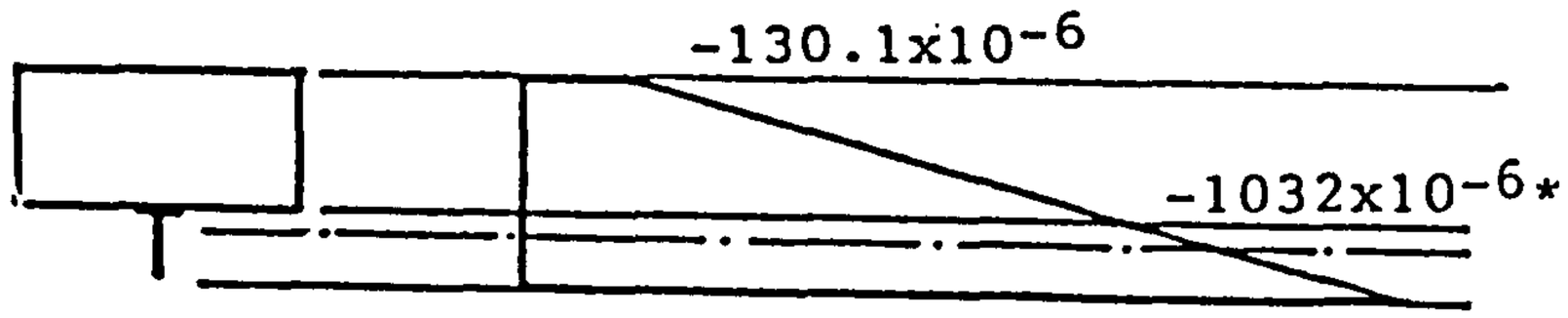

A-A

Strain Profile at (0,0)

(V=8kN and H=490kN)

*Acoustic Gauge was at the C.G. of the stem

For further details see Table 4.6

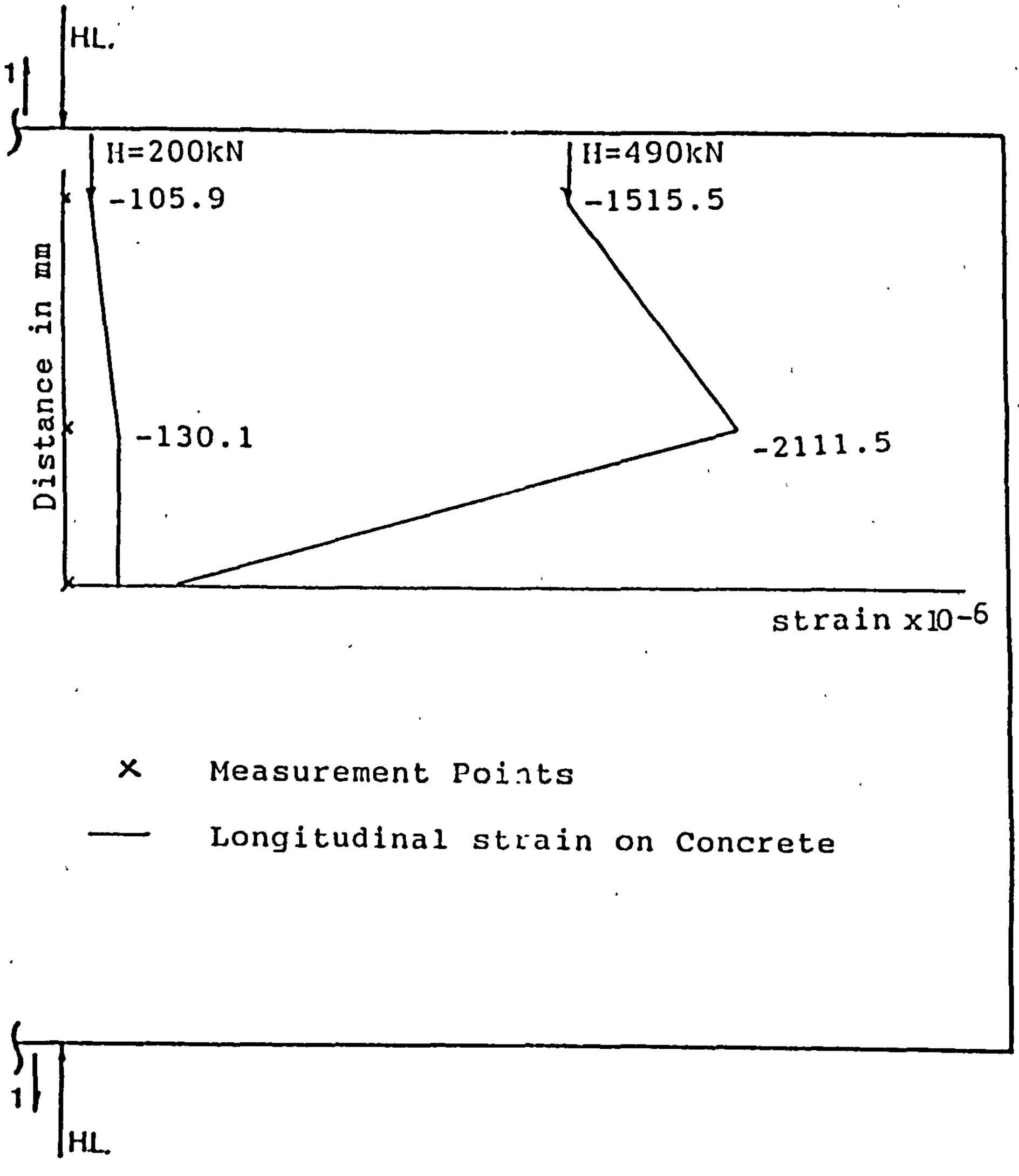

Fig. 5.19 Longitudinal Strain Distribution for CSFU4

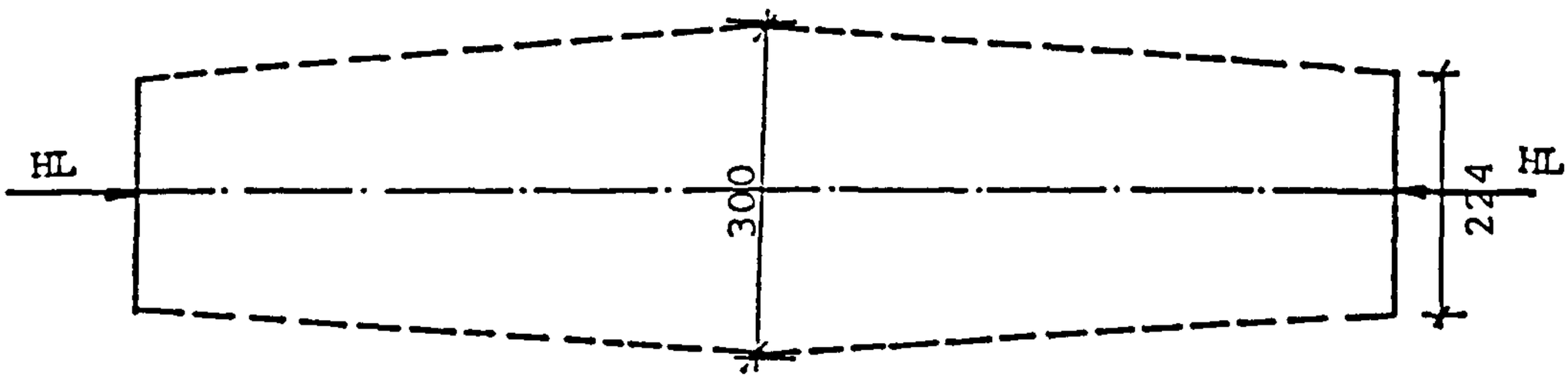

Fig. 5.20 Effective width of the comp. T-beam

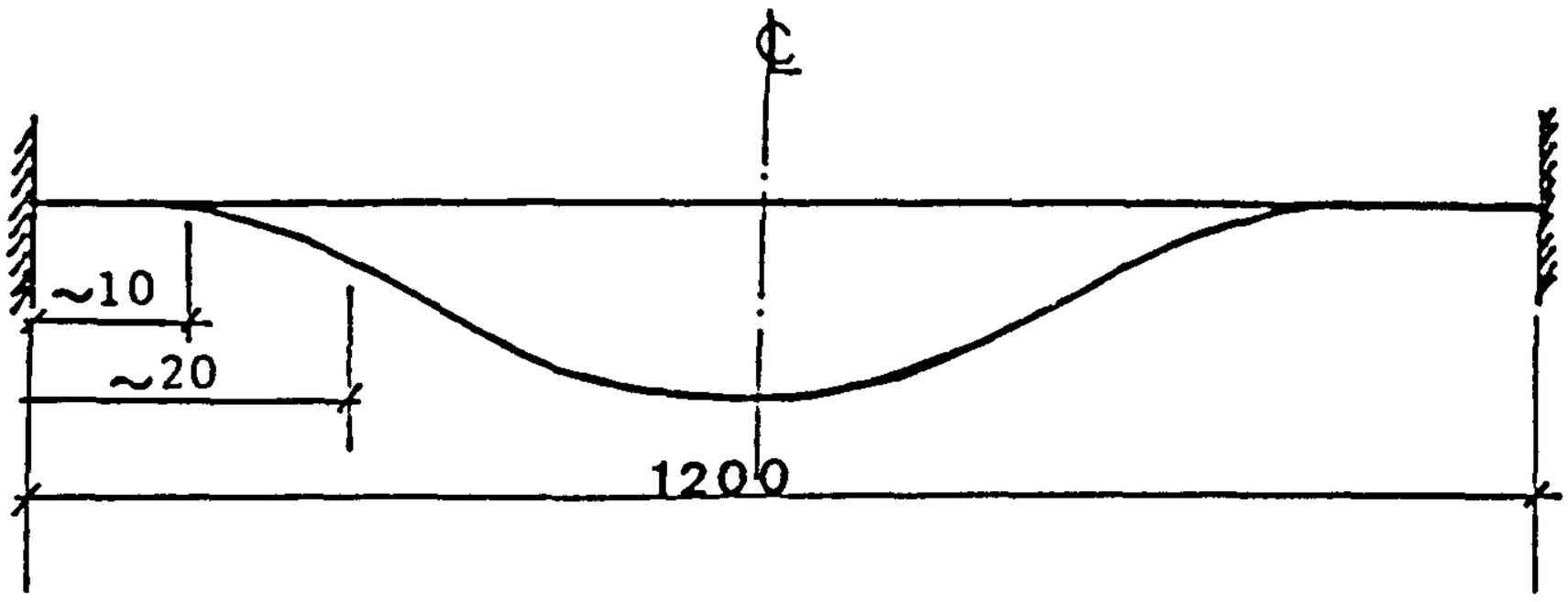

Fig. 5.21 Inflection Point on the comp. T-beam

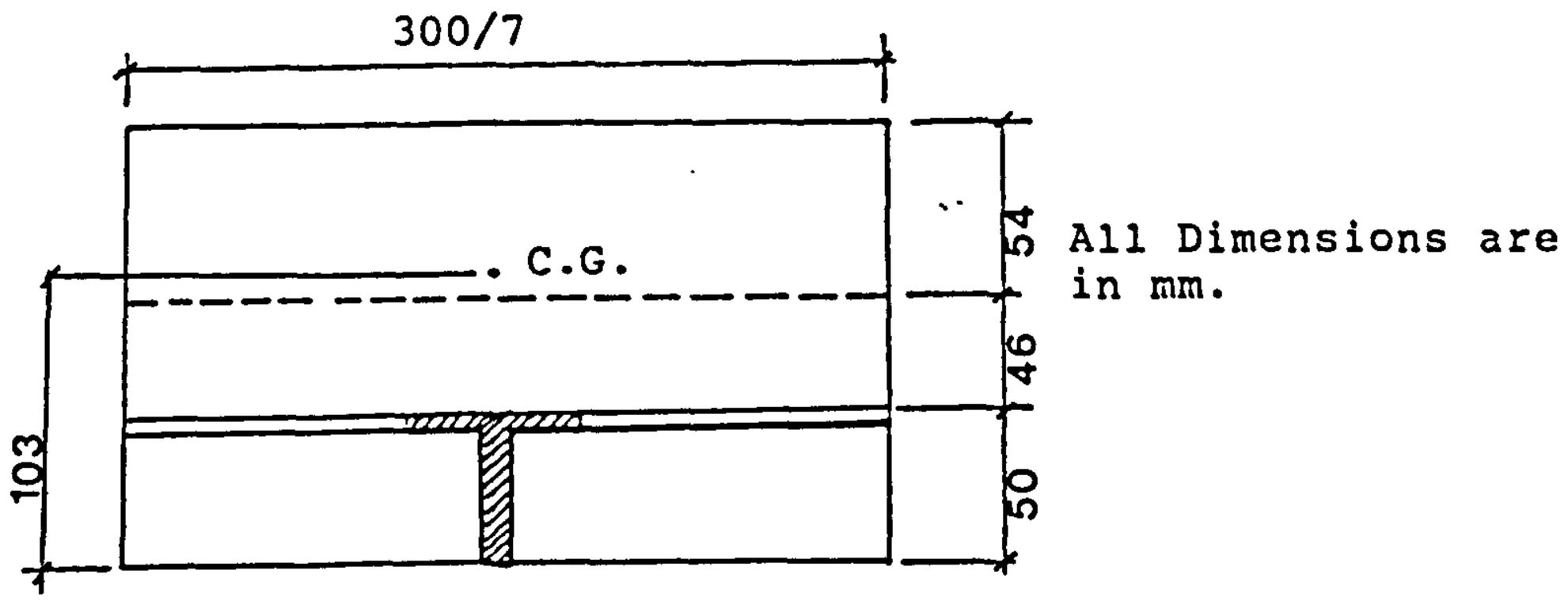

strains were measured at the C.L. on the concrete surface and at the C.G. of the stem

Fig. 5.22 Transformed cross section

CHAPTER SIX

CONCLUSIONS AND SUGGESTIONS FOR FUTURE WORK

6.1 CONCLUSIONS

The main objective of this work was to develop a method of analysis for composite space frames and to study the behaviour of the composite elements within the space frame. These objectives have generally been accomplished with the development of a computer program to analyse a composite space frame and the study of the behaviour of various composite units from the space frame with accompanying conclusions.

The main conclusions of the work are as follows:-

(1) The computer analysis of the system shows that the external ultimate limit state loading results in smaller internal forces and moments in the members compared to the capacity found experimentally.

(2) Higher rigidity, EI, and cross sectional area of the composite section compared to the non-composite section caused part of the load to transfer to the supports directly by shear which decreased the load transferred through the diagonals at the corners.

(3) Generally, the loads in the truss members at

the corners (diagonals) and along the edges (ties) are smaller in the composite space frame than in the space frame due to the higher rigidity of the composite members.

A decrease in deflection is also observed for the same reason. For the loading used in the same example (the service load on the structure), the maximum deflection decreases by more than 17%.

(4) Composite T-beams within a space frame test units can successfully resist higher loads axially and transversally compared to non-composite top-chord members.

(5) Self drilling, self tapping screws are satisfactory both as shear connectors and lateral restraints.

It could be said that there is no evidence of the need for bigger shear connectors, but that this should be investigated further.

(6) Shear connectors (lateral restraints) placed at each rib of the profiled steel sheet are found to be the best for the T-beam causing smaller centreline deflection and almost uniform strains along its longitudinal axis. The use of this arrangement of shear connectors (at each

rib) reduces the strain concentrations at the ends which enables the specimen to resist higher loads.

(7) Shear connectors (working also as lateral restraints) are found to be more effective if placed at the quarter points than if placed at the centreline and at the ends of the composite T-beam.

(8) The use of more connectors at the quarter points enhances both deflection and strain behaviour especially when accompanied with connectors in each rib.

(9) In all the cases tested, the composite T-beam width (along the transverse axis) within which the longitudinal strains are of significant value (compared to that at the centreline) is within ≈ 300 mm.

(10) Strains along both the longitudinal and the transverse axes are affected by the presence of shear connectors. They are relatively lower at sections at or close to shear connectors along the longitudinal axis. Along transverse sections the strains decreased with the increase of distance away from the centreline.

(11) As the maximum axial force is found on the

external edge of the structure, and in some of the experimental results show that there are high strains close to supports, it may be recommended that more connectors are used for the external members to minimise both stresses and slip.

6.2 Suggestions For Future Work

To cover all the aspects relevant to the present work, the following recommendations are made:

(1) The composite T-section should to be tested with strain measurements made at sufficient locations to enable the relationship between the strain values and their distances from the shear connectors to be established.

(2) By varying the numbers of connectors employed in tests, the most economic and efficient shear connectors spacing could be determined.

(3) The composite space frame units may be tested with the ribs of the profiled steel sheet running parallel to the top-chord member.

(4) The use of strain gauges to measure strains along the longitudinal axis of the T-beam on both the steel angles and the profiled steel sheet (where it is difficult to attach the acoustic strain gauges used in this work) at

required sections. This would help in finding the strain distribution at those cross section of the the T-beam especially at the mid-span.

(5) To investigate various parameters, concrete thickness, type of profiled sheet, other fasteners, shape and size of space frame elements...etc both by analysis and test.

(6) The testing of a full scale composite space frame would be the next logical step. The estimation of the failure loads using the author's program would be feasible. The experimental results obtained, would enable the computer program to be checked and improved.

(7) In addition to the notes stated in chapter 2 for the amendment of the computer program, the program could be used to analyse the studied structure (or similar) as thick plates (the concrete slab), thin plates (the profiled steel sheet), beams (the top-chord angles) in addition to the space truss elements. The remarks mentioned in chapter 2 (on the loading, the fixed end moments and the space truss rotated stiffness matrix) should also be considered with this method of analysis.

These conclusions and suggestions are proposed as a result of the work presented here. They will give useful

information for design purposes and future use of composite space frames.

APPENDIX A

A.1 Introduction

The two-unit space frame test specimen (see Figure A.1) considered in the present experimental work was loaded in as shown in Figure A1. That loading was considered during the preliminary testing. The following theorems (35) were applied here to show that with that loading, all members were of zero forces except the top-chord one. This point was to be verified experimentally. These theorems are:

Theorem 1: If all the bars meeting at a joint, with the exception of one bar n, lie in a plane, the component normal to the plane of the force in bar n is equal to the component normal to that plane of any external load or loads applied at that joint.

On the basis of the above theorem, the following two theorems may be stated:

Theorem 2: If all the bars meeting at a joint, with the exception of one bar n, lie in a plane and if no external load is applied at that joint, the force in bar n is zero.

Theorem 3: If all but two bars at a joint have no bar force and these two are not collinear, and if no external load acts at that joint, the bar force in each of these two bars is zero.

Refering to Figure A.1.

ad and ed are in a plane ade; cd is out of plane ade and

no external force at joint d. Therefore, force in membar cd is zero ($F_{cd} = 0$) (Theorem 2).

The theorem can also be applied to establish that forces are zero for the following bars:

ec, ed, ad, bc, bg, gh, gf, hf and ef.

Applying Theorem 3,

At joint e: $F_{ed} = F_{ec} = 0$; ea and eb are two bars meeting at joint e where no external load is applied. Therefore, $F_{ea} = F_{eb} = 0$.

The same approach could be followed to find that F_{fa} and F_{fb} are also zero.

Therefore, the only bar which carries the applied force is the top-chord member ab.

A1.1 Lateral Restraint Check

Lateral restraint was checked for the top-chord member as a beam according to the AISC (37). The member was assumed to be laterally supported at ends.

The braced length (l_b) of the member should satisfy the following two equations:

$l_b \leq 76\ b_f/\sqrt{F_y}$ and

$l_b \leq 20{,}000/((d/A_f)\ F_y)$

where (see Figure A.1a),

b_f = flange breadth,

F_y = steel yield stress,

d = cross-section depth and

A_f = area of the flangth

where the dimensions are in inches.

If the member is restrained at the ends, and its ends are pinned, then $kl_x = kl_y = 1200.$ mm

Substituting in to the two equations,

b_f = 80.0 mm (3.15 in.),

d = 50.0 mm (1.97 in.),

A_f = 100.0 mm^2 (0.155in^2) and

F_y = 40.0 ksi,

one lateral restraint is required within the length of the member (1200.0 mm).

A.2 Preliminary Testing

A.2.1 Load Transfer Test

This test was carried out to ensure that the axial load was mainly resisted by the top chord. The set-up for this test is shown in Figure A.1b. Three dial gauges were placed at the two ends near the supports and at the centreline of the top chord member, and their readings were recorded at zero loading. The end gauges were put to record any uplift while the dial gauge at mid-span was to record the mid-span deflection of the member at each load increment. Four acoustic gauges were placed at mid-span where two of them were on the flange and the other two were on the web. The acoustic gauges were adjusted and the strain readings at zero loading were recorded. The strains were recorded at each load increment by the data logger. The average reading of the four strain readings was taken as the strain at the section. The modulus of elasticity was taken as 200

kN/mm² to calculate stresses. Corresponding loads were calculated from these stresses and compared to the applied load. It was found as shown in Tables A.1 and A.2 that the applied load at the end is completely resisted by the member (see also Figure A.4).

A.2.2 Top-chord Capacity Tests

Some tests were carried out to find out the capacity of the top-chord member according to Southwell approach which simply states that if the ratio δ/p is plotted against the measured deflection δ, the points will fall on a straight line as shown in Figure A.2, and the resulted graph is usually called Southwell plot (27, 38, 39, 40, 41). The same graph could be obtained if the ratio ε/p is plotted against the measured strain ε (38,39), where p in both cases is the applied load. This line cuts the horizontal axis (δ or ε) at a distance a1 from the origin, and the inverse slope of the line gives the critical load.

The set-up for this test is shown in Figure A.1, and several tests were carried out. This set-up was checked for several times before recording any reading, and it was found satisfactory. However, a permanent deflection of nearly 5 mm occured at mid-span of the top chord of the first composite space frame unit at this stage of the experimental work. In addition to this permanent deflection, a lateral load of 6 kN in some cases and 8 kN in others was applied at the mid-span by the vertical

jack to produce an initial deflection on the member in order to use the Southwell technique. An axial load was applied by the horizontal jack simultaneously with the lateral load, and the deflection at mid-span was recorded at every 10 kN increment up to 150 kN. Results of these tests are shown in Tables A.3 to A.7. Horizontal loads versus mid-span deflections are shown in Figures A.5 to A.9. Southwell plots are also shown in Figures A.10 to A.14 and they were prepared using the Graphplot package which follow the least squares method recommended by Southwell.

A.3 Results Discussion

A.3.1 Load Transfer Test

Results (see Tables A.1 and 2) show to an acceptable percentage of error that the whole axial load applied through the C. G. of the top chord was mainly resisted by the member itself, and this goes with the three theorems mentioned in section A.1.

Stress versus strain graph shown in Figure A.4 shows that the member was tested in the elastic range.

A.3.2 Top chord Capacity Tests

The failure loads which were derived from the inverse of the slopes of the straight lines of Southwell plots fall between 193-221 kN (see Figures A.10 TO A.14). However, the failure loads found by tests were

found to fall between 190-210 kN (see Table 4.7a). The range of results found by Southwell method gave a good estimation of the capacity of the top chord member. It, therefore, could be said that the estimated failure load found by Southwell method for the top-chord member was found to be reliable for this type of structure.

The average failure load found by these tests was different than Euler load (334 kN) which was higher than test failure loads. This may be due to many reasons such as the two angles which composed the top chord differ in either length, width, thickness or straightness.

It should be noted that the load was to be applied at the centroid of the compound member. The deflections were very sensitive to any eccentricity with the presence of axial and lateral loadings, which in turn affected the result of failure load that was found from the deflection reading. It was found difficult to maintain the axial and the vertical loading the same in all the series of tests. This may show why these results were not as accurate as those accurate ones found for some ideal struts represented by Southwell or others works were all the points fell on straight lines.

TABLE A.1 PRELIMINARY TEST RESULTS

Applied Load (kN)	Average Strain $\times 10^{-6}$	Average Stress (kN/mm²)	Corresponding Load (kN)	Percentage Of Difference
0.0	0.0	0.0	0.0	0.0
10.0	46.57	9313.75	10.0	0.0
20.0	93.14	18627.5	20.1	0.50
30.0	144.2	28845.0	31.1	3.67
40.0	196.09	39218.75	42.3	5.75
50.0	246.26	49251.25	53.2	6.40
60.0	286.25	57250.0	61.8	3.00
70.0	337.51	67502.5	72.9	4.14
80.0	383.29	76657.5	82.8	3.50
90.0	434.86	86971.25	93.9	4.33
100.0	488.13	97626.25	105.4	5.40

TABLE A.2 PRELIMINARY TEST RESULTS

Applied Load (kN)	Average Strain $x10^{-6}$	Average Stress (kN/mm^2)	Corresponding Load (kN)	Percentage Of Difference
0.0	0.0	0.0	0.0	0.0
10.0	57.97	11593.75	12.5	2.5
20.0	105.78	21156.25	22.85	14.25
30.0	159.53	31906.25	34.46	14.9
40.0	214.06	42812.5	46.24	15.6
50.0	263.13	52625.0	56.84	13.7
60.0	312.34	62468.75	67.47	12.4
70.0	354.84	70968.75	76.65	9.49
80.0	397.66	97531.25	85.89	7.37
90.0	454.38	90875.0	98.15	9.05
100.0	507.97	101593.7	109.7	9.72

TABLE A.3 LOAD-DEFLECTION RESULT

Vertical Load (kN)	Axial Load p (kN)	Deflection δ (mm)	v=δ/p
6.0	30.0	-	-
	40.0	0.30	0.0075
	50.0	0.44	0.0088
	60.0	0.80	0.0133333
	70.0	1.02	0.0145714
	80.0	1.26	0.01575
	90.0	1.52	0.0168889
	100.0	1.95	0.01950
	110.0	2.21	0.02009091
	120.0	2.65	0.0220833
	130.0	2.98	0.0229231
	140.0	3.27	0.0233571
	150.0	3.50	0.023333

TABLE A.4 LOAD-DEFLECTION RESULTS

Vertical Load (kN)	Axial Load p (kN)	Deflection δ (mm)	$v=\delta/p$
6.0	30.0	-	-
	40.0	0.30	0.0075
	50.0	0.58	0.0116
	60.0	0.82	0.0136667
	70.0	1.02	0.0145714
	80.0	1.29	0.016125
	90.0	1.65	0.018333
	100.0	1.99	0.01990
	110.0	2.22	0.020182
	120.0	2.63	0.0219167
	130.0	2.96	0.0227692
	140.0	3.15	0.02250
	150.0	3.50	0.023333

TABLE A.5 LOAD-DEFLECTION RESULTS

Vertical Load (kN)	Axial Load p (kN)	Deflection δ (mm)	$v=\delta/p$
6.0	30.0	-	-
	40.0	0.21	0.00525
	50.0	0.45	0.0090
	60.0	0.67	0.0111667
	70.0	0.93	0.0132857
	80.0	1.20	0.0150
	90.0	1.47	0.016333
	100.0	1.82	0.01820
	110.0	2.25	0.0204545
	120.0	2.58	0.02150
	130.0	2.91	0.0223846
	140.0	3.09	0.0220714
	150.0	3.49	0.0232667

TABLE A.6 LOAD-DEFLECTION RESULTS

Vertical Load (kN)	Axial Load p (kN)	Deflection δ (mm)	δ=d/p
8.0	30.0	-	-
	40.0	0.21	0.00525
	50.0	0.47	0.0094
	60.0	0.67	0.0111667
	70.0	0.95	0.0135714
	80.0	1.17	0.014625
	90.0	1.53	0.0170
	100.0	1.93	0.0193
	110.0	2.27	0.0206364
	120.0	2.64	0.0220
	130.0	3.02	0.023231
	140.0	3.23	0.0230714
	150.0	3.63	0.0242

TABLE A.7 LOAD-DEFLECTION RESULTS

Vertical Load (kN)	Axial Load p (kN)	Deflection δ (mm)	δ=d/p
8.0	30.0	-	-
	40.0	0.22	0.0055
	50.0	0.44	0.0088
	60.0	0.64	0.0106667
	70.0	0.91	0.0130
	80.0	1.25	0.015625
	90.0	1.47	0.016333
	100.0	1.88	0.0188
	110.0	2.09	0.0190
	120.0	2.49	0.02075
	130.0	2.68	0.0206154
	140.0	3.08	0.0220
	150.0	3.42	0.0228

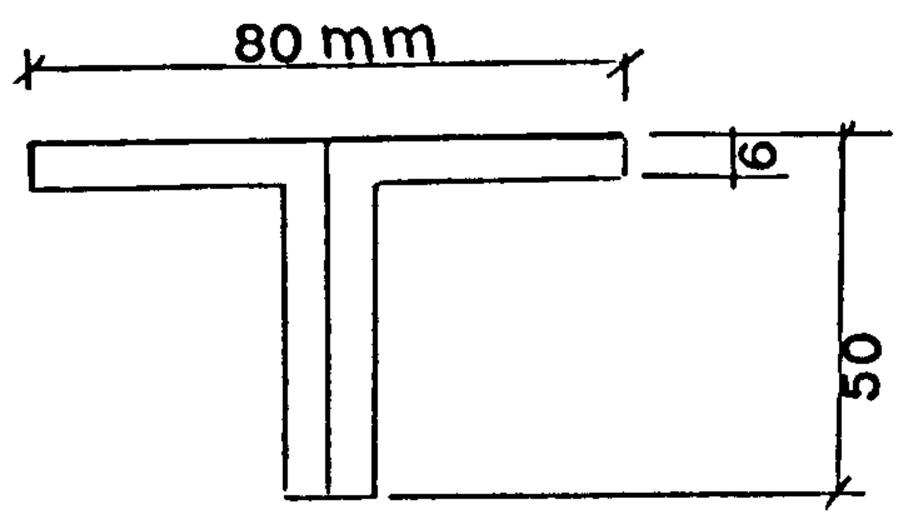

Fig. A.1a Top-chord cross-section

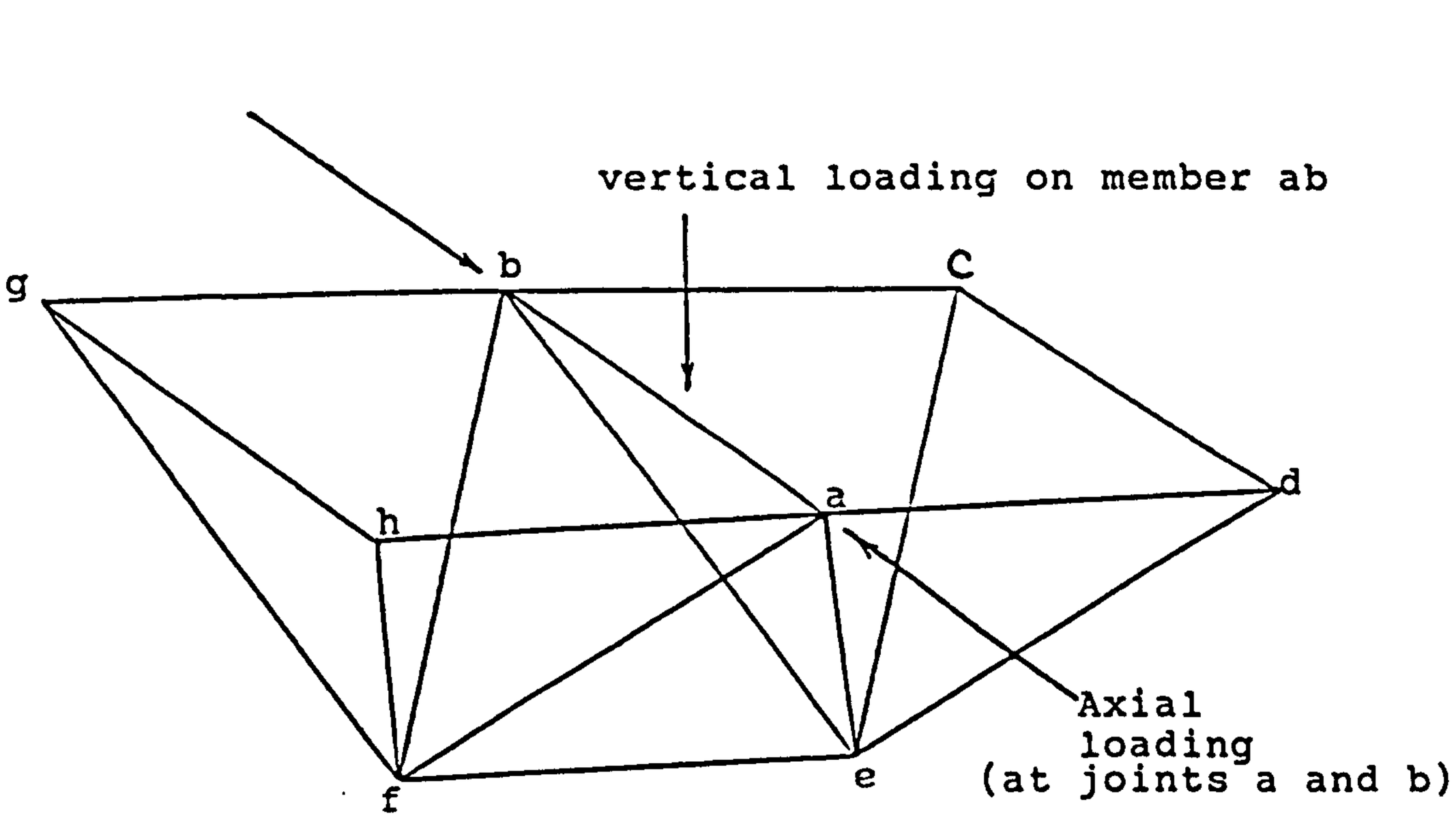

Fig. A1b A two-unit Space Deck w/vertical and Horizontal loadings.

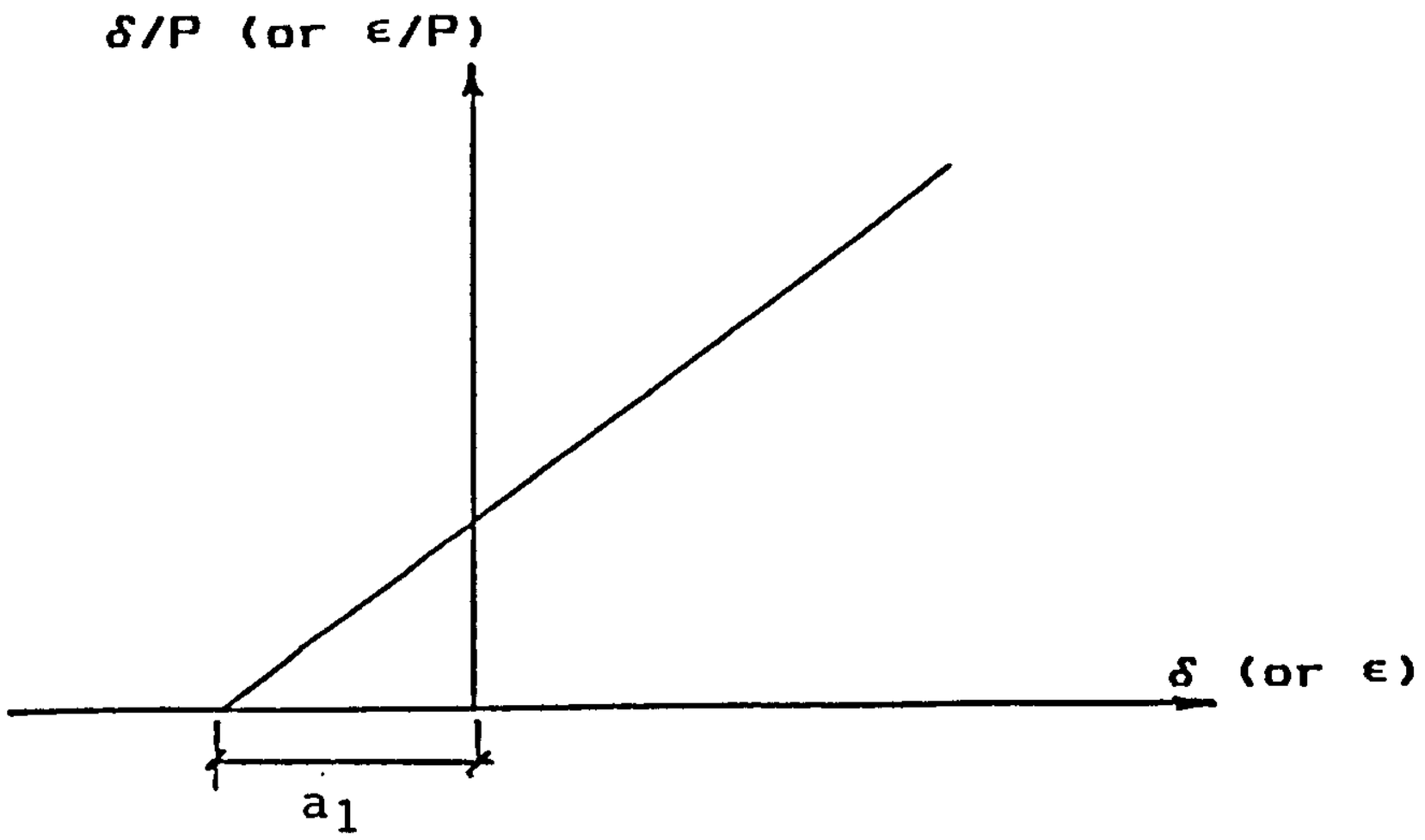

Fig A.2 Southwell Plot

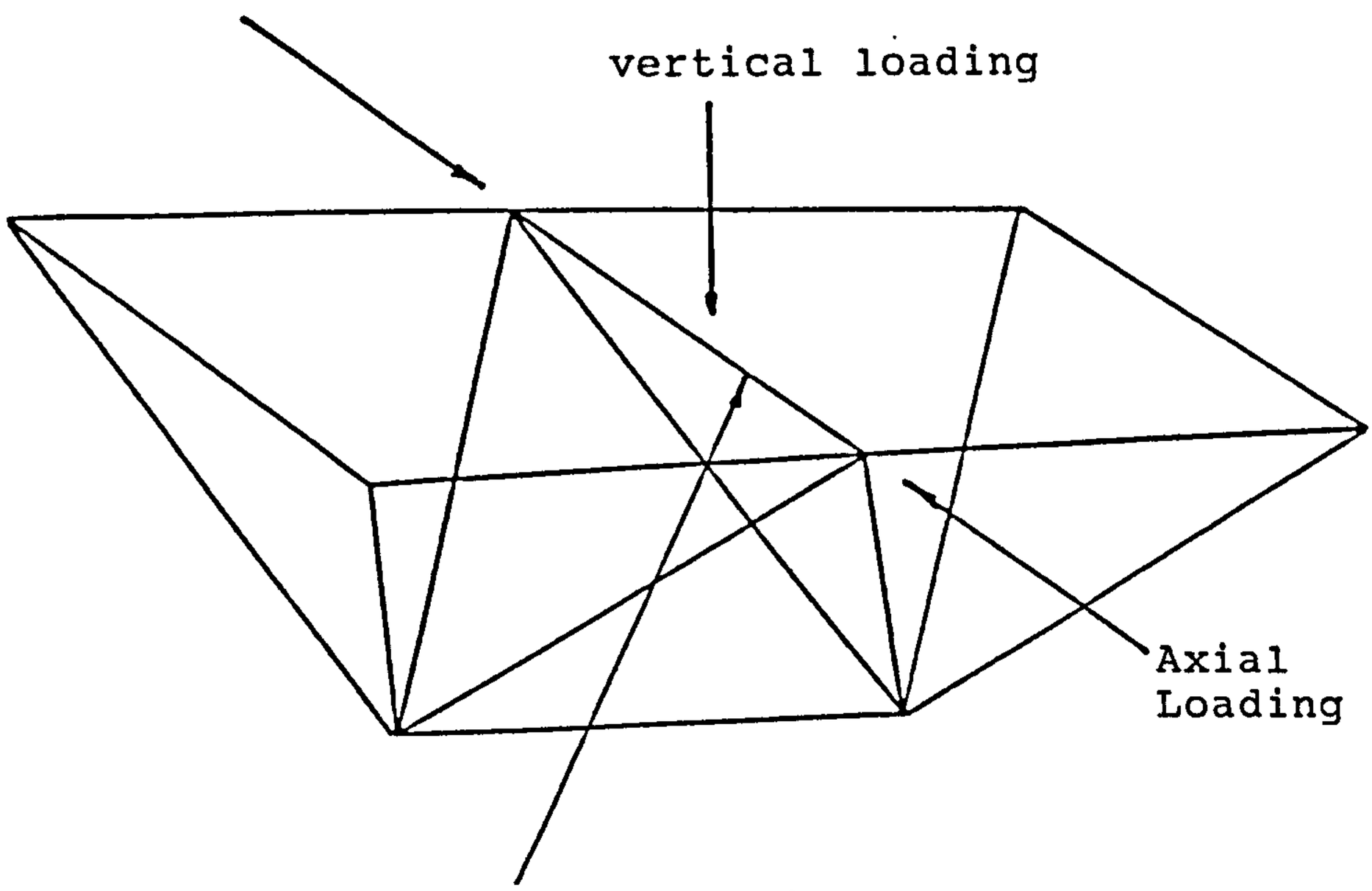

Fig. A.3 The top-chord Member considered within the two-unit Space Deck

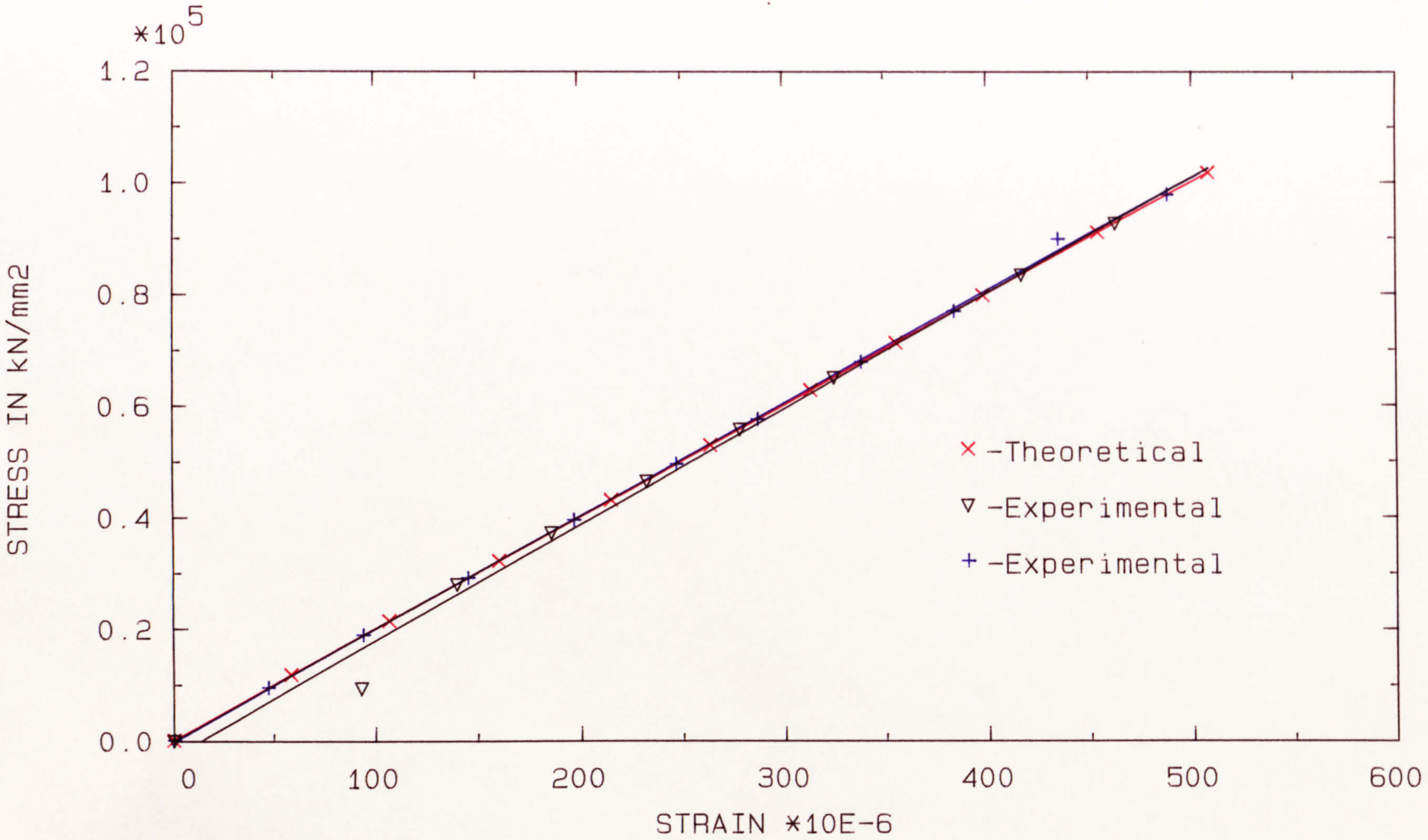

FIG.A.4 STRESS-STRAIN RELATION OF THE STEEL TOP-CHORD

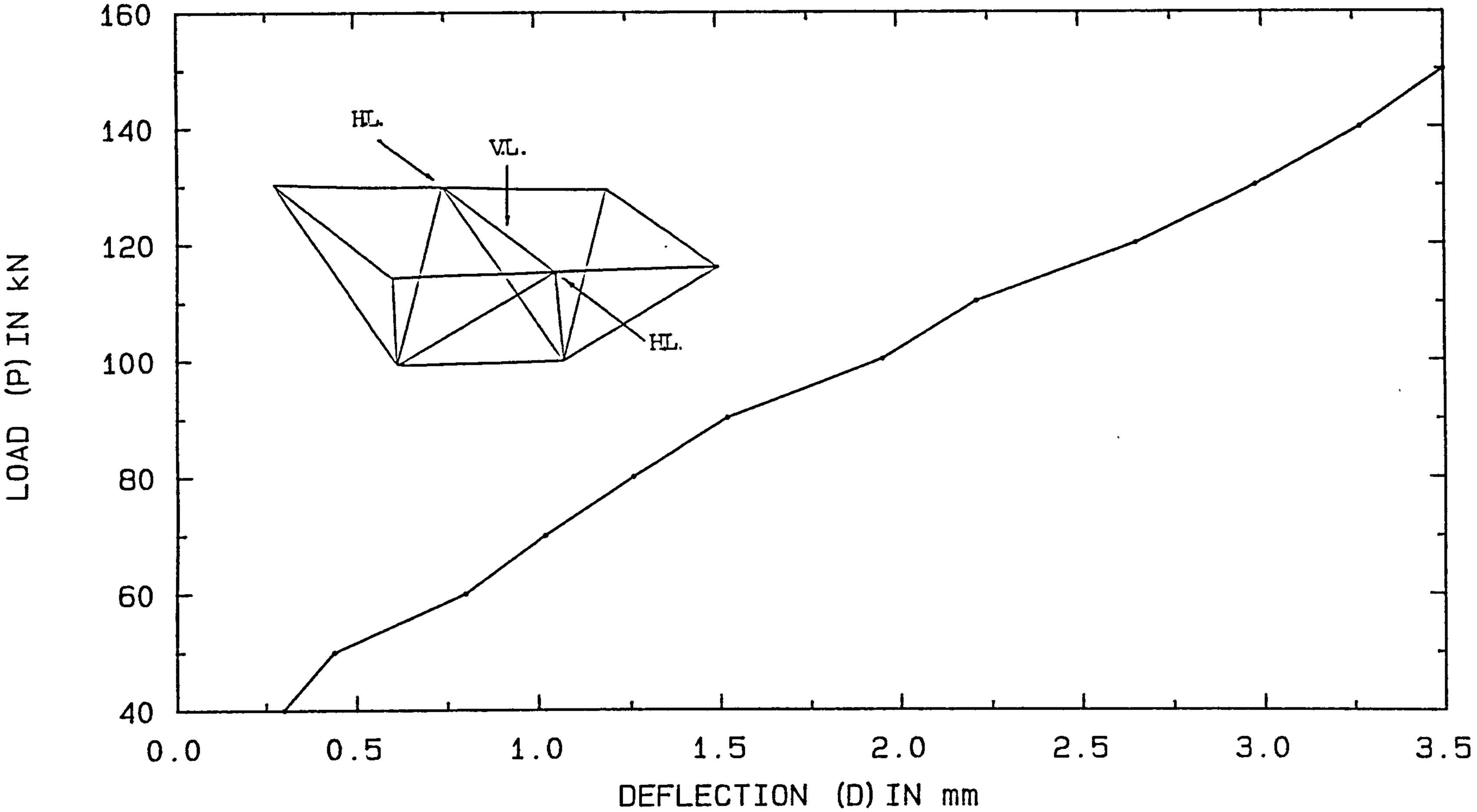

FIG.A.5 LOAD-DEFLECTION CURVE 1

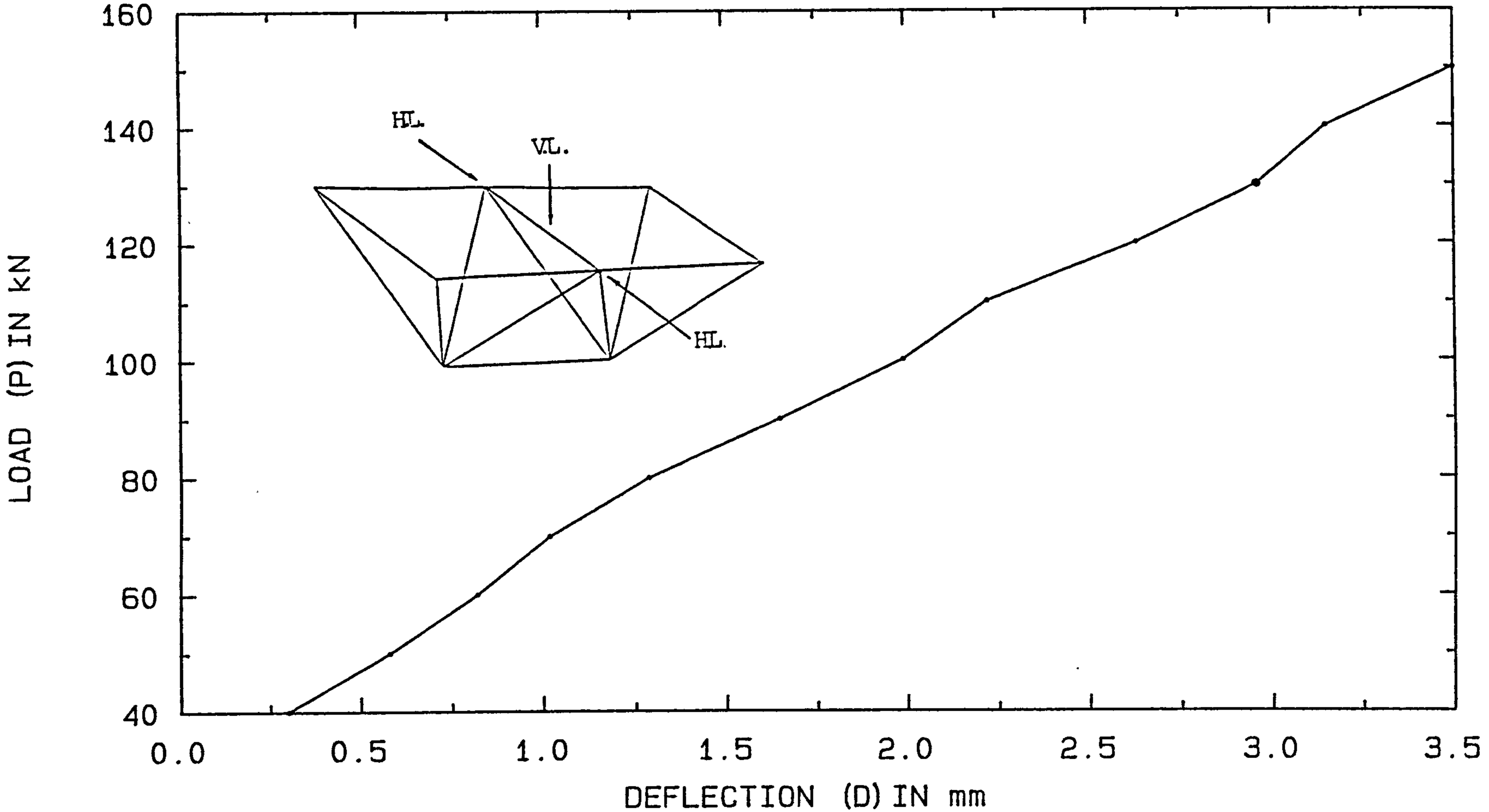

FIG.A.6 LOAD-DEFLECTION CURVE 2

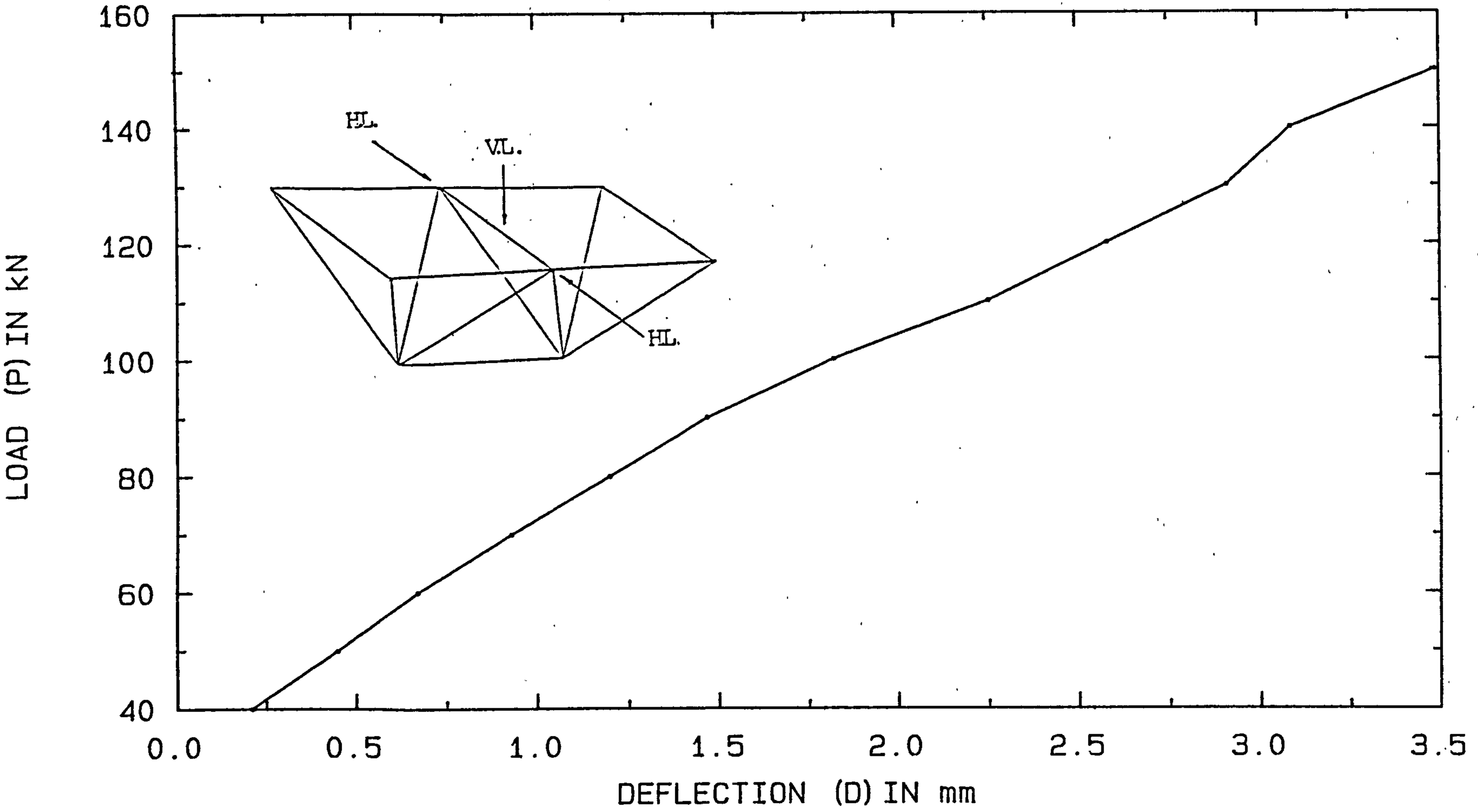

FIG.A.7 LOAD-DEFLECTION CURVE 3

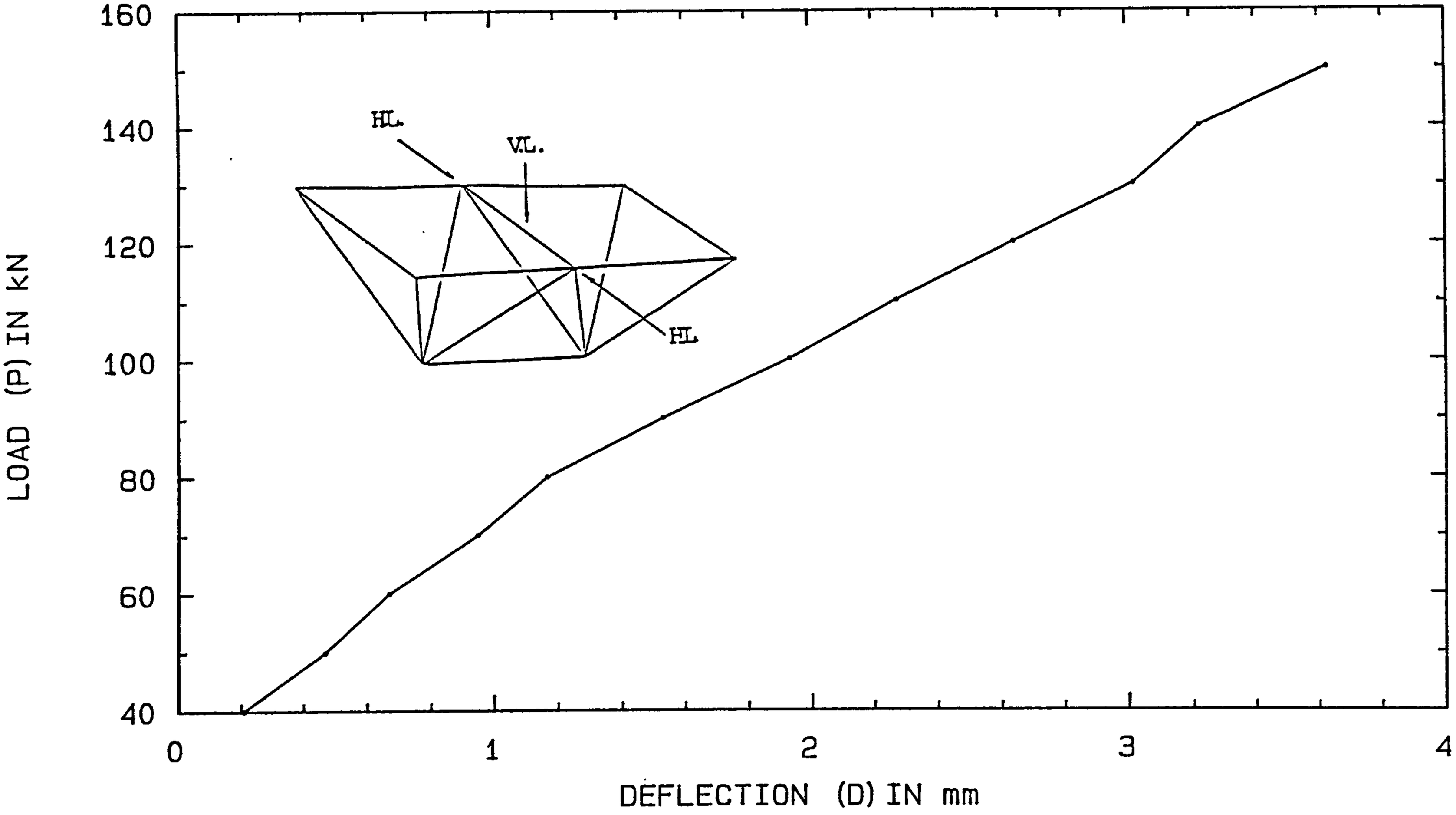

FIG.A.8 LOAD-DEFLECTION CURVE 4

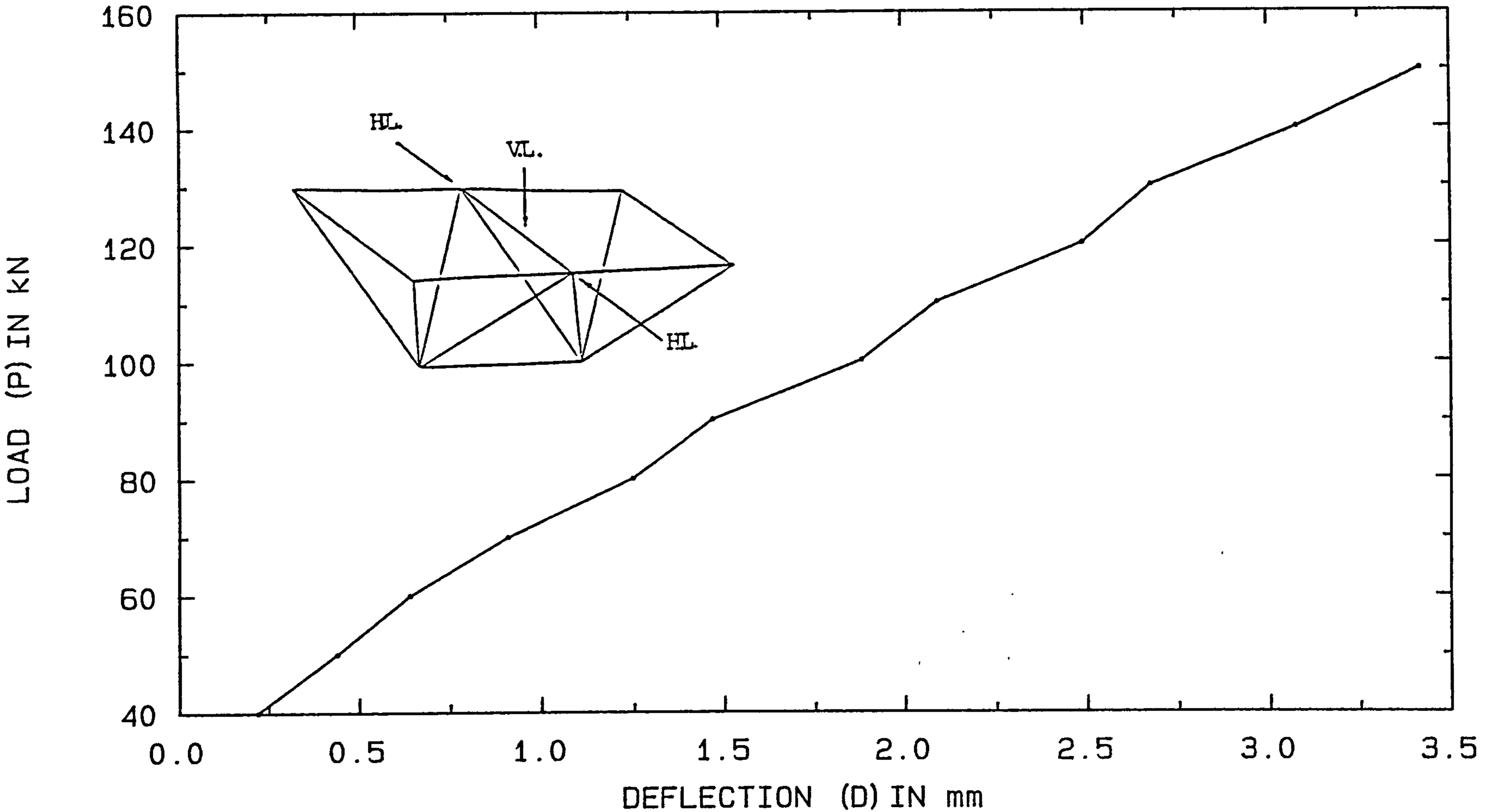

FIG.A.9 LOAD-DEFLECTION CURVE 5

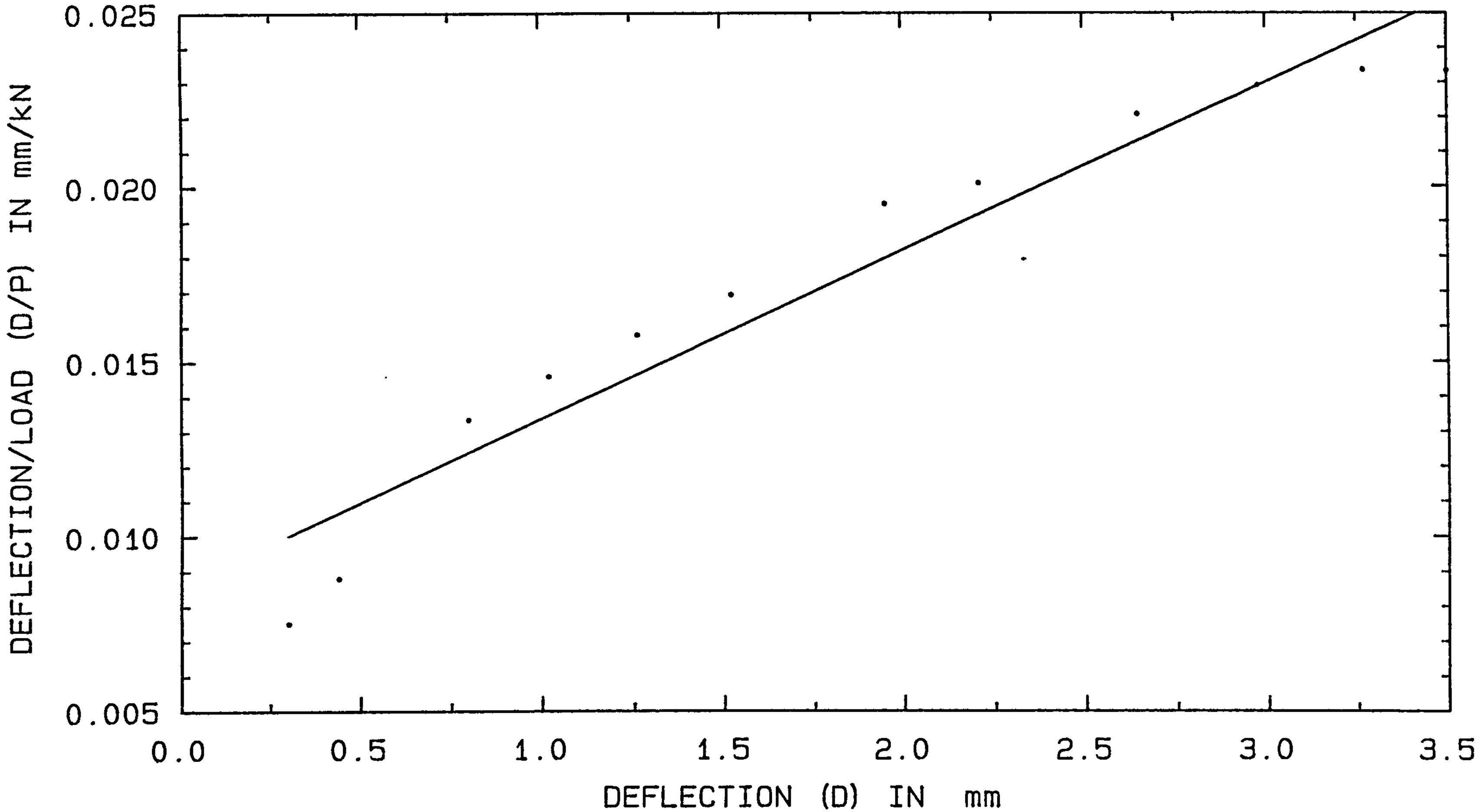

FIG.A.10 SOUTHWELL PLOT 1

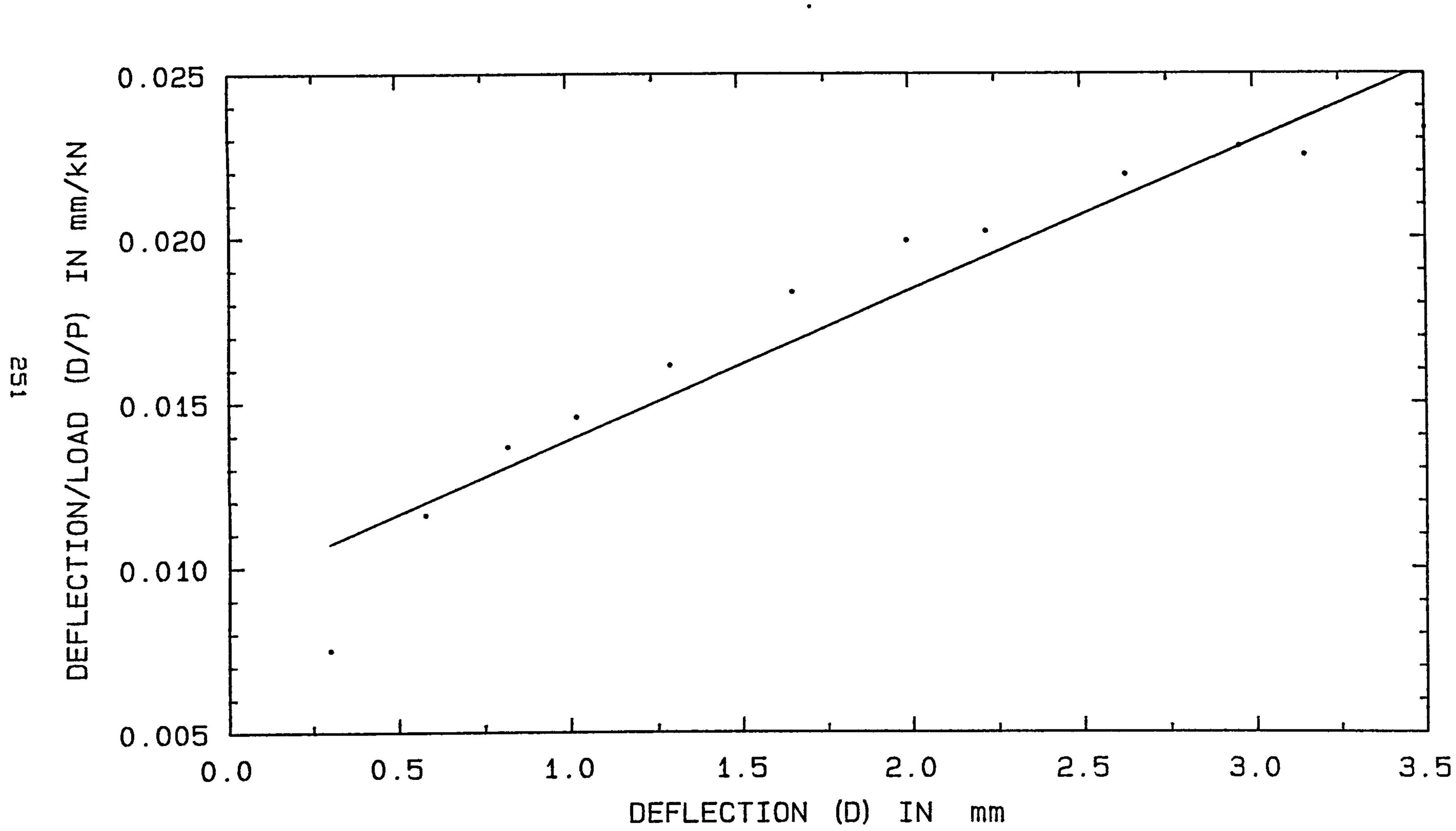

FIG.A.11 SOUTHWELL PLOT 2

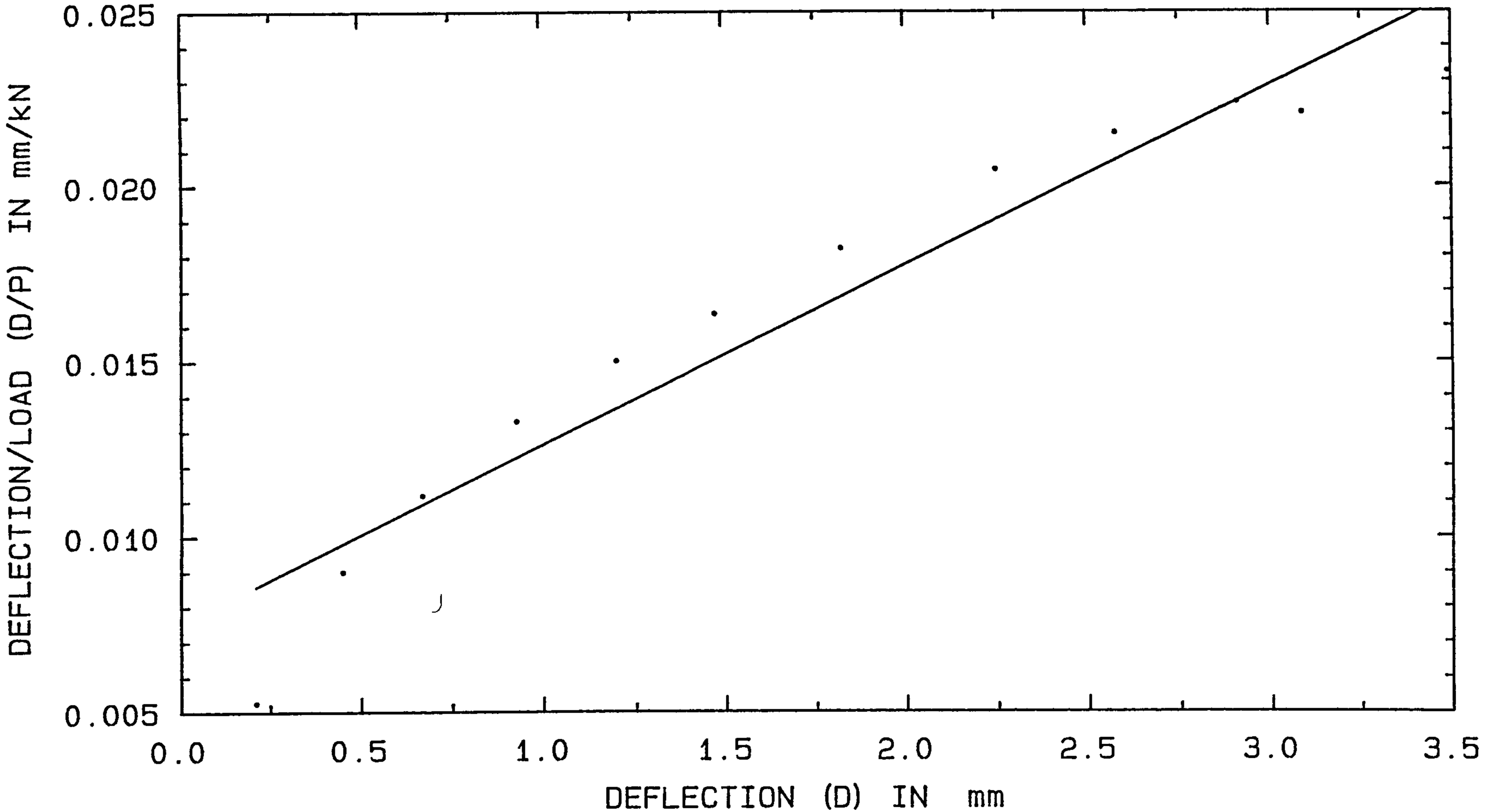

FIG.A.12 SOUTHWELL PLOT 3

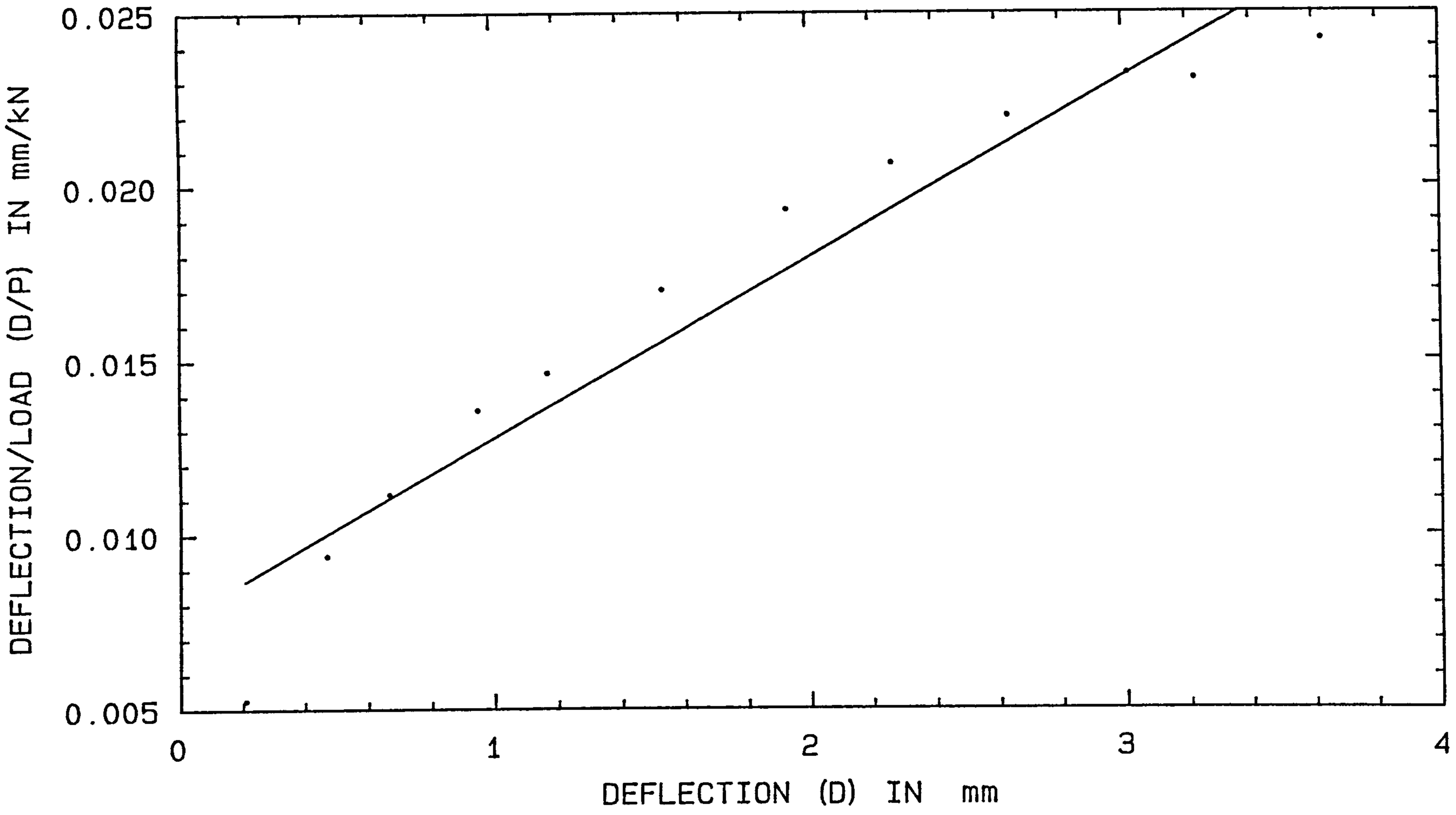

FIG.A.13 SOUTHWELL PLOT 4

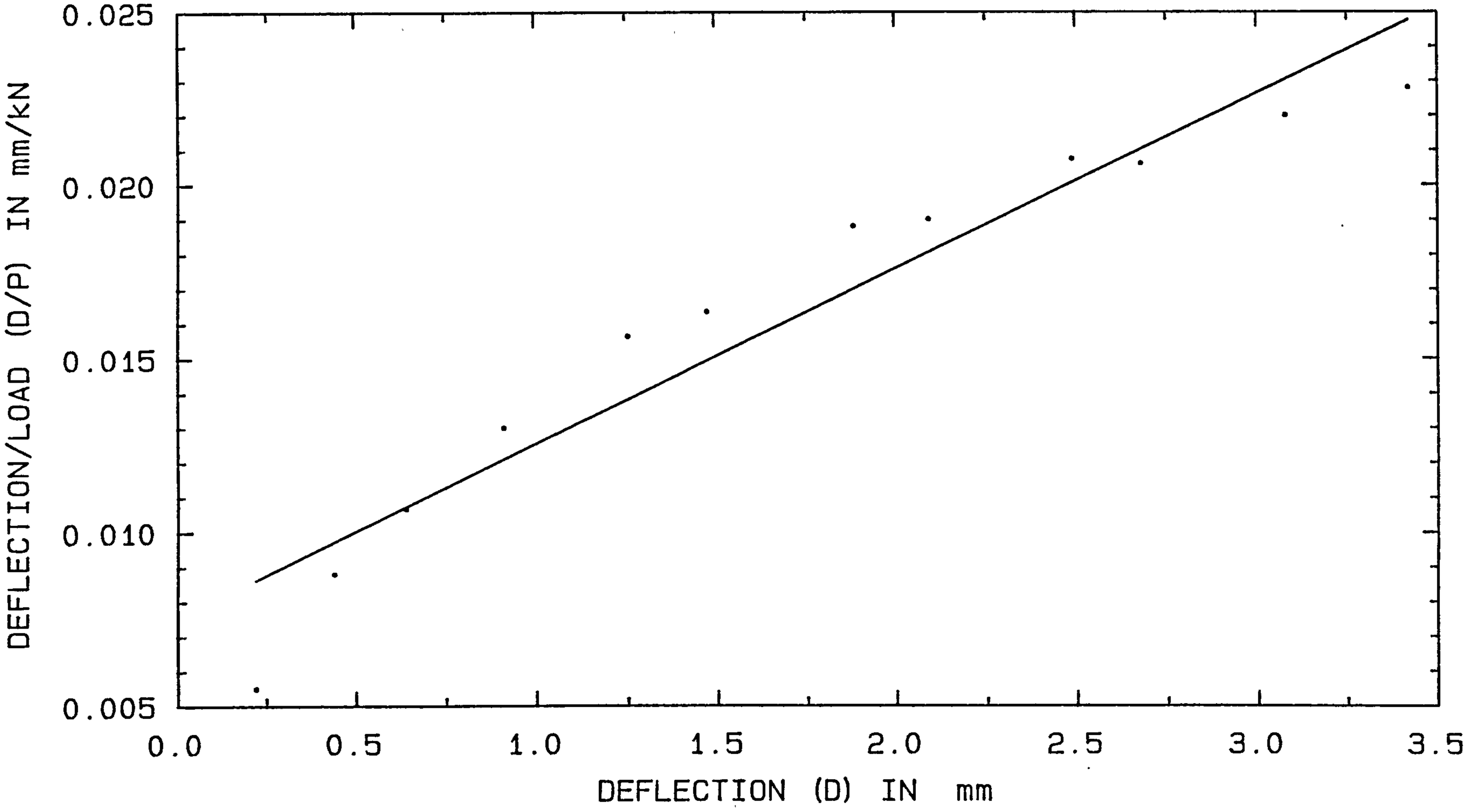

FIG.A.14 SOUTHWELL PLOT 5

APPENDIX B

B.1 Calculation of the Deflection

The following calculations are carried out for the deflection of the composite T-beams according to Johnson formula. The calculated deflection is to be compared to the experimental one as is mentioned in Chapter 5. The cross-section of the T-beams is shown below as well as its properties (see Figure B.1).

The shear strength of the connector was found as 5 kN/mm of the steel sheet when tested with no concrete (42). Shear strength of a similar connector (TEK) with concrete was found to be 14.3 kN (43). For the present work, the shear strength was assumed to be 15 kN per connector. The following deflection calculations are for CSFU3, CSFU2 and CSFU4 respectively.

Johnson formula is $\delta=\delta_1+\delta_f[1+\alpha(I_{bc}/I_s -1)(1-k/k_n)]$

where, δ_1 -deflection of strut alone (can be ignored).

δ_f -deflection for full interaction.

α = 0.3 for shot-fired connection, and 0.5 for welded studs (taken as 0.4).

I_{bc} -moment of inertia of the composite section.

I_s -moment of inertia for steel chords.

k/k_n -degree of connection.

δ_f=0.0630 x PL^3/EI (see Figure B.2)

δ_f= 0.0630x2x1200^3/210x6459651 =0.161 mm

I_{bc}/I_s=6459651/243767=26.5

k=12/20=0.75 (for CSFU3)

k=8/20=0.40 (for CSFU2 and CSFU4)

Substituting in to the formula,

δ=0.57 mm which is similar to that found experimentally (0.56 mm) for the case of CSFU3. It is 1.15 mm for the other two cases. However, the experimental values for these two cases are 0.48 mm (CSFU2) and 1.25 mm (CSFU4), hence, the formula may not be applicable for these two cases which are of the same number of connectors, but different in their arrangement.

B.2 Calculations of Stresses

The effective width was taken as 300 mm, and modular ratio (E_s/E_c) based on measured values was taken as 7 so that the centroid (Y), the area (A_t) and the moment of inertia (I_t) were calculated accordingly. The transformed cross-section is shown in figure B.1. These calculations are based on assumption of interaction which will apply overall to a composite beam/column with load variations due to the position of the shear connectors.

B.2.1 Cross-section Properties

A_s=1008.0 mm^2

A_c=2743.03 mm^2, and

A_t=3751. mm^2

I_s=243766.88 mm^4

I_c=936291.0 mm^4, and, therefore,

Y=103. mm

Although the centroid is calculated as 103 mm, it is taken as 100 mm similar to that considered during the experimental work). Hence,

d_s=66. mm

d_c=18. mm, and

I_t=6459651. mm^4

To calculate the flexural stresses at the top and bottom of the section, the distances c_1 and c_2 for concrete and steel (see figure B.1) are taken as 50 mm and 100 mm respectively.

B.2.2 Moment Due to Vertical Load

The vertical load (8kN) was applied through four spacers, as is discussed before, placed to each side of the composite T-beam. This load is assumed to be carried by the composite T-beam as shown in figure B.2 below, and the centreline moment is, then, 1.44 kN-m.

B.2.3 Numerical Illustration

The two moments in this calculation are that due the vertical load (P_1) and is named as M_1 and that due to the horizontal load (P_2) and is named as M_2. Therefore the stresses on concrete surface and on the stem of the double angles calculated as is mentioned in Chapter 5 are as follows:

$$\sigma_c = - P_2/A_t - M_1 \times C_1 / I_t + M_2 C_1 / I_t$$

$$\sigma_s = - P_2/A_t + M_1 \times C_2 / I_t - M_2 C_2 / I_t$$

B.2.4 Application

For the composite space frame unit 3, the following two numerical calculations at the horizontal loads of 40 and 180 kN (see Table 5.6).

At 40 kN:

σ_2= (-40/3751 -1.44x50/6459651 +40x0.51x50/6459651)10^3

= -10.5 N/mm² (for concrete in terms of steel based on short term loading modular ratio)

σ_2= (-40/3751 +1.44x100/6459651 -40x0.51x100/6459651)10^3

= -11.0 N/mm² (for steel)

At 180 kN:

σ_2=(-180/3751 -1.44x50/6459651 +180x0.28x50/6459651)10^3

= -47.6 N/mm² (for concrete in terms of steel based on short term loading modular ratio)

σ_2=(-180/3751 +1.44x100/6459651 -180x0.28x100/6459651)10^3

= -48.7 N/mm² (for steel)

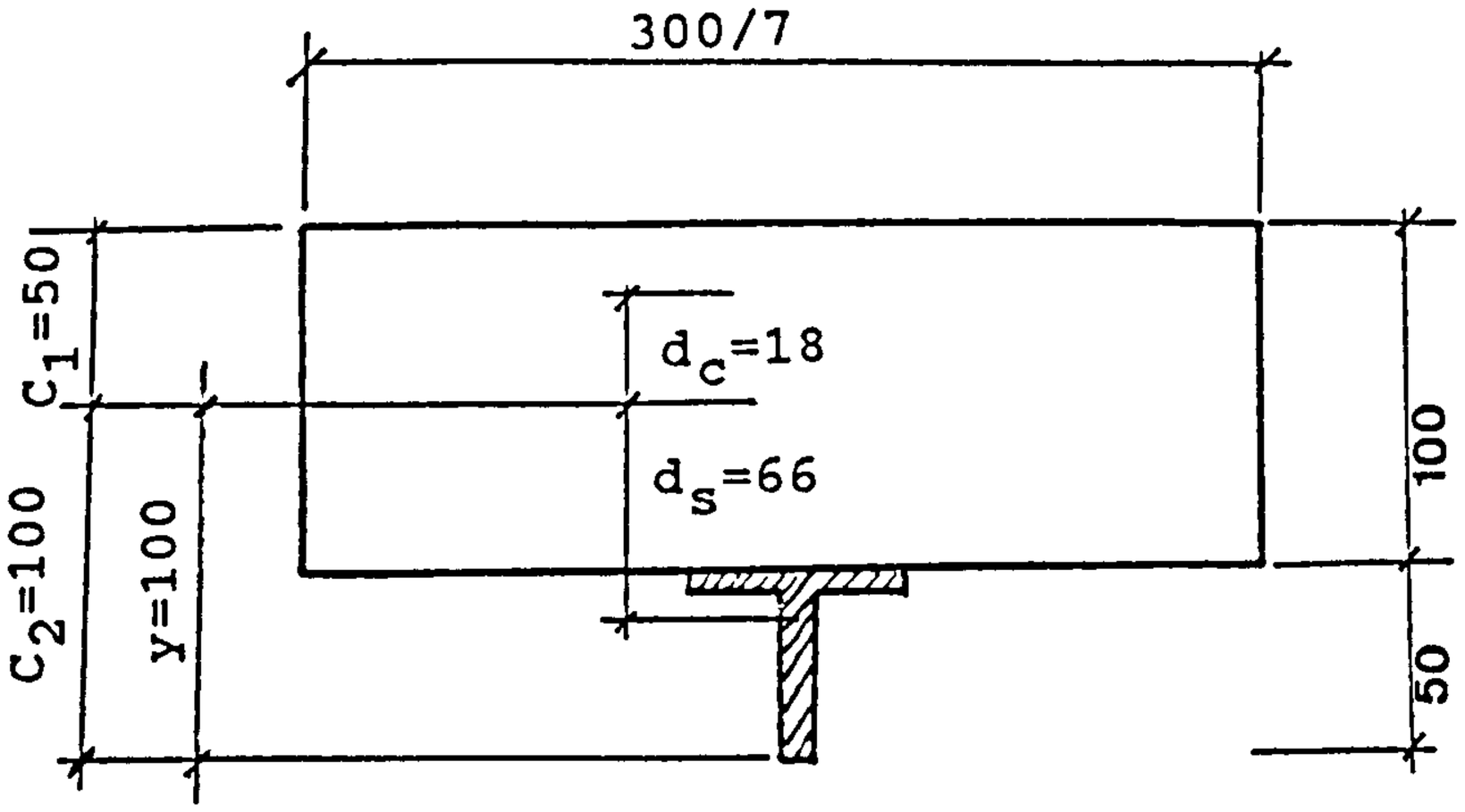

Fig. B.1 Transformed Cross-section

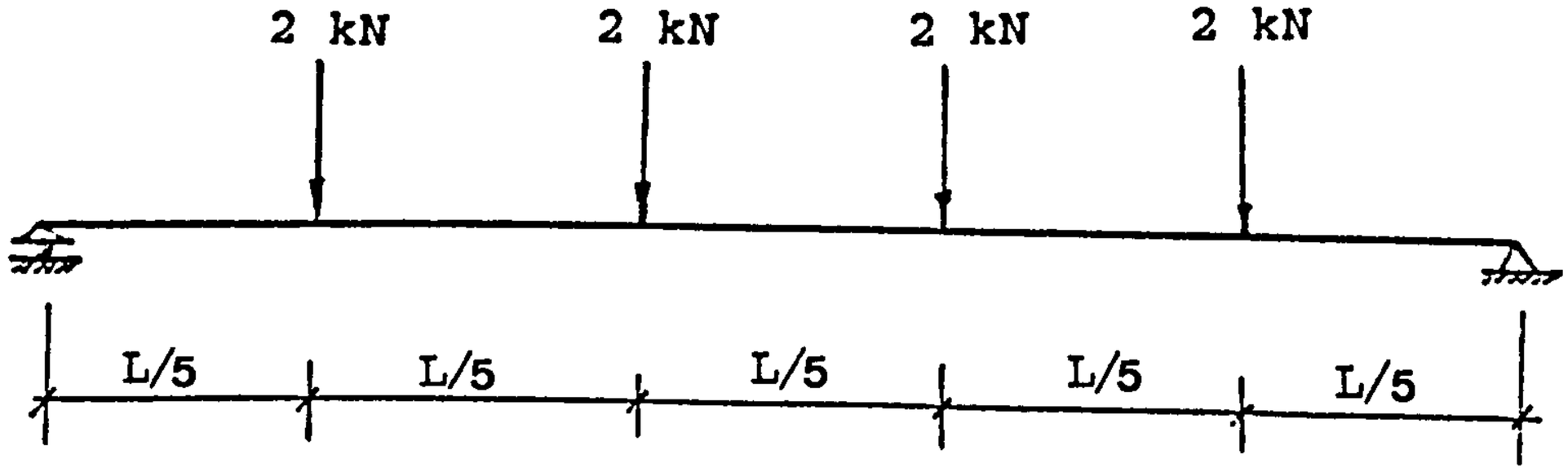

Fig. B.2 Composite T-beam with vertical loading

APPENDIX C

COMPOSITE SPACE FRAME PROGRAM

```
      OPTIONS (BIG,DREAL,CHECK)
      COMMON/FREMAT/B
      COMMON/FREMAT/D
      DIMENSION EK(20,20),D(459),KK(20),B(459,459),
     *X(459),Y(459),Z(459),ID(459,5),EK1(10,10),
     *KK1(10),TEK(10,10),GK(10,10),T(10,10),EK3(10,10),
     *KK3(10),D1(20),D2(10),D3(10),P(20),P1(10),P2(10)
C     EK AND EK1 ARE PLATE AND BEAM ELEMENTS STIFFNESS
C     MATRICES.
C     EK3 IS SPACE TRUSS ELEMENT TRANSFORMED MATRIX.
C     X,Y AND Z ARE JOINT CO-ORDINATE MATRICES.
C     D IS THE GLOBAL LOAD AND DEFLECTION MATRICES
C     FOR THE STRUCTURE.
C     B THE GLOBAL UNRESTRAINED STIFFNESS MATRIX FOR
C     THE STRUCTURE.
C     D1, D2 AND D3 ARE PLATE, BEAM AND SPACE TRUSS
C     ELEMENTS DEFLECTION MATRICES.
C     T IS BEAM ELEMENT ROTATION MATRIX.
C     P, P1 AND P2 ARE PLATE, BEAM AND SPACE TRUSS
C     ELEMENTS FORCE MATRICES.
      OPEN(UNIT=5,FILE='DT17/4',STATUS='OLD')
      OPEN(UNIT=6,FILE='RT17/4')
      OPEN(UNIT=7,FORM='UNFORMATTED')
      OPEN(UNIT=8,FORM='UNFORMATTED')
      REWIND 7
      REWIND 8
      READ(5,*)NJ
C     NJ=THE TOTAL NUMBER OF ACTIVE FREEDOMS FOR THE
C              COMPLETE SYSTEM.
      DO 20 I=1,NJ
      D(I)=0.
      DO 20 J=1,NJ
 20   B(I,J)=0.
      WRITE(6,*)
      WRITE(6,111)
 111  FORMAT(/,27X,'COMPOSITE SPACE FRAME ANALYSIS')
      WRITE(6,202)
 202  FORMAT(27X,'============================',/)
      WRITE(6,212)
 212  FORMAT(/,35X,'STRUCTURE DATA')
      WRITE(6,727)
 727  FORMAT(35X,'--------------',/)
C     GENERATE THE STIFFNESS MATRIX FOR THE PLATE.
      WRITE(6,313)
 313  FORMAT(/,33X,'(a) PLATE ELEMENTS',/)
      DO 10 I=1,20
      DO 10 J=1,20
 10   EK(I,J)=0.
      READ(5,*)NNP,M,A,V,TH,E,PI,SS,Q
C     NNP=NUMBER OF PLATE JOINTS.
```

```
C       M=NUMBER OF PLATE ELEMENTS.
C       A=SIDE LENGTH OF PLATE ELEMENTS.
C       V=POISON'S RATIO OF THE PLATE.
C       TH=PLATE ELEMENT THICKNESS.
C       E=MODULUS OF ELASTICITY OF THE PLATE.
C       PI=MOMENT OF INERTIA OF ONE REPEATING CROSS
C       SECTION OF THE PLATE.
C       SS=THE LENGTH OF ONE REPEATING CORRUGATION.
C       Q=WAVE LENGTH OF ONE REPEATING CORRUGATION.
        WRITE(6,515)
 515    FORMAT(/,13X,'NODE',5X,' GLOBAL FREEDOMS ',
       *9X,'X',9X,'Y',/)
        DO 12 I=1,NNP
        READ(5,*)L,ID(L,1),ID(L,2),ID(L,3),ID(L,4),
       *ID(L,5),X(L),Y(L)
C       ID(L,I) = THE GLOBAL FREEDOM NUMBERS.
   12   WRITE(6,3)L,ID(L,1),ID(L,2),ID(L,3),ID(L,4),
       *ID(L,5),X(L),Y(L)
    3   FORMAT(11X,6I5,2F12.6)
        WRITE(6,818)
  818   FORMAT(/,11X,' ELEMENT',2X,'ELEMENT NODES')
        DO 40 L=1,M
        READ(5,*)MN,IP,JP,KP,NP
C       IP, JP, KP AND NP ARE THE PLATE ELEMENT CORNERS.
        WRITE(6,22)MN,IP,JP,KP,NP
   22   FORMAT(11X,5I5)
        KK(1)=ID(IP,1)
        KK(2)=ID(IP,2)
        KK(3)=ID(IP,3)
        KK(4)=ID(IP,4)
        KK(5)=ID(IP,5)
        KK(6)=ID(JP,1)
        KK(7)=ID(JP,2)
        KK(8)=ID(JP,3)
        KK(9)=ID(JP,4)
        KK(10)=ID(JP,5)
        KK(11)=ID(KP,1)
        KK(12)=ID(KP,2)
        KK(13)=ID(KP,3)
        KK(14)=ID(KP,4)
        KK(15)=ID(KP,5)
        KK(16)=ID(NP,1)
        KK(17)=ID(NP,2)
        KK(18)=ID(NP,3)
        KK(19)=ID(NP,4)
        KK(20)=ID(NP,5)
        Hx=((Q/SS)*(E*TH**3))/(12.)
        Hy=E*PI/Q
        Hxy=(E*TH**3)*SS/(6.*(1.+V)*Q)
        H1=0.0
C       Hx=FLEXURAL RIGIDITY IN X-DIRECTION.
C       Hy=FLEXURAL RIGIDITY IN Y-DIRECTION.
C       Hxy=TORSIONAL RIGIDITY.
C       H1=V*(Hx*Hy)**0.5
        YA=(20.*A**2*Hy+8.*A**2*Hxy)/(15.*A**2)
```

```
YB=(15.*A**2*H1)/(15.*A**2)
YC=(20.*A**2*Hx+8.*A**2*Hxy)/(15.*A**2)
YD=(30.*A*Hy+15.*A*H1+6.*A*Hxy)/(15.*A**2)
YE=(30.*A*Hx+15.*A*H1+6.*A*Hxy)/(15.*A**2)
YF=(60.*Hx+60.*Hy+30.*H1+8.4*Hxy)/(15.*A**2)
YG=(10.*A**2*Hy-2.*A**2*Hxy)/(15.*A**2)
YH=(-30.*A*Hy-6.*A*Hxy)/(15.*A**2)
YI=(10.*A**2*Hx-8.*A**2*Hxy)/(15.*A**2)
YL=(15.*A*Hx-15.*A*H1-6.*A*Hxy)/(15.*A**2)
YM=(30.*Hx-60.*Hy-30.*H1-84.*Hxy)/(15.*A**2)
YN=(10.*A**2*Hy-8.*A**2*Hxy)/(15.*A**2)
YO=(-15.*A*Hy+15.*A*H1+6.*A*Hxy)/(15.*A**2)
YP=(5.*A**2*Hy+2.*A**2*Hxy)/(15.*A**2)
YQ=(15.*A*Hy-6.*A*Hxy)/(15.*A**2)
YR=(10.*A**2*Hx-2.*A**2*Hxy)/(15.*A**2)
YS=(30.*A*Hx+6.*A*Hxy)/(15.*A**2)
YT=(5.*A**2*Hx+2.*A**2*Hxy)/(15.*A**2)
YU=(15.*A*Hx-6.*A*Hxy)/(15.*A**2)
YX=(-60.*Hx+30.*Hy-30.*H1-84.*Hxy)/(15.*A**2)
YZ=(-30.*Hx-30.*Hy+30.*H1+84.*Hxy)/(15.*A**2)
d11=E/(1.-V**2)
d22=d11
d33=E/(2.*(1.+V))
d12=V*E/(1.-V**2)
d21=d12
F10=TH/12.
EK(1,1)=F10*(4.*d11+4.*d33)
EK(1,2)=F10*(3.*d21+3.*d33)
EK(1,6)=F10*(2.*d11-4.*d33)
EK(1,7)=F10*(-3.*d21+3.*d33)
EK(1,11)=F10*(-4.*d11+2.*d33)
EK(1,12)=F10*(3.*d21-3.*d33)
EK(1,16)=F10*(-2.*d11-2.*d33)
EK(1,17)=F10*(-3.*d21-3.*d33)
EK(2,2)=F10*(4.*d22+4.*d33)
EK(2,6)=F10*(3.*d21-3.*d33)
EK(2,7)=F10*(-4.*d22+2.*d33)
EK(2,11)=F10*(-3.*d21+3.*d33)
EK(2,12)=F10*(2.*d22-4.*d33)
EK(2,16)=F10*(-3.*d21-3.*d33)
EK(2,17)=F10*(-2.*d22-2.*d33)
EK(6,6)=F10*(4.*d11+4.*d33)
EK(6,7)=F10*(-3.*d21-3.*d33)
EK(6,11)=F10*(-2.*d11-2.*d33)
EK(6,12)=F10*(3.*d21+3.*d33)
EK(6,16)=F10*(-4.*d11+2.*d33)
EK(6,17)=F10*(-3.*d21+3.*d33)
EK(7,7)=F10*(4.*d22+4.*d33)
EK(7,11)=F10*(3.*d21+3.*d33)
EK(7,12)=F10*(-2.*d22-2.*d33)
EK(7,16)=F10*(3.*d21-3.*d33)
EK(7,17)=F10*(2.*d22-4.*d33)
EK(11,11)=F10*(4.*d11+4.*d33)
EK(11,12)=F10*(-3.*d21-3.*d33)
EK(11,16)=F10*(2.*d11-4.*d33)
```

```
EK(11,17)=F10*(3.*d21-3.*d33)
EK(12,12)=F10*(4.*d22+4.*d33)
EK(12,16)=F10*(-3.*d21+3.*d33)
EK(12,17)=F10*(-4.*d22+2.*d33)
EK(16,16)=F10*(4.*d11+4.*d33)
EK(16,17)=F10*(3.*d21+3.*d33)
EK(17,17)=F10*(4.*d22+4.*d33)
EK(3,3)=YA
EK(3,4)=-YB
EK(3,5)=-YD
EK(3,8)=YG
EK(3,9)=0.
EK(3,10)=-YH
EK(3,13)=YN
EK(3,14)=0.
EK(3,15)=YO
EK(3,18)=YP
EK(3,19)=0.
EK(3,20)=YQ
EK(4,4)=YC
EK(4,5)=YE
EK(4,8)=0.
EK(4,9)=YI
EK(4,10)=YL
EK(4,13)=0.
EK(4,14)=YR
EK(4,15)=-YS
EK(4,18)=0.
EK(4,19)=YT
EK(4,20)=-YU
EK(5,5)=YF
EK(5,8)=YH
EK(5,9)=YL
EK(5,10)=YM
EK(5,13)=YO
EK(5,14)=YS
EK(5,15)=YX
EK(5,18)=-YQ
EK(5,19)=YU
EK(5,20)=YZ
EK(8,8)=YA
EK(8,9)=YB
EK(8,10)=YD
EK(8,13)=YP
EK(8,14)=0.
EK(8,15)=-YQ
EK(8,18)=YN
EK(8,19)=0.
EK(8,20)=-YO
EK(9,9)=YC
EK(9,10)=YE
EK(9,13)=0.
EK(9,14)=YT
EK(9,15)=-YU
EK(9,18)=0.
```

```
      EK(9,19)=YR
      EK(9,20)=-YS
      EK(10,10)=YF
      EK(10,13)=YQ
      EK(10,14)=YU
      EK(10,15)=YZ
      EK(10,18)=-YO
      EK(10,19)=YS
      EK(10,20)=YX
      EK(13,13)=YA
      EK(13,14)=YB
      EK(13,15)=-YD
      EK(13,18)=YG
      EK(13,19)=0.
      EK(13,20)=-YH
      EK(14,14)=YC
      EK(14,15)=-YE
      EK(14,18)=0.
      EK(14,19)=YI
      EK(14,20)=-YL
      EK(15,15)=YF
      EK(15,18)=YH
      EK(15,19)=-YL
      EK(15,20)=YM
      EK(18,18)=YA
      EK(18,19)=-YB
      EK(18,20)=YD
      EK(19,19)=YC
      EK(19,20)=-YE
      EK(20,20)=YF
      DO 15 I=1,20
      DO 15 J=1,20
 15   EK(J,I)=EK(I,J)
      WRITE(7)KK,EK,IP,JP,KP,NP
      DO 35 I=1,20
      II=KK(I)
      IF(II.LT.0)GO TO 35
      DO 30 J=1,20
      JJ=KK(J)
      IF(JJ.LT.0)GO TO 30
      B(II,JJ)=B(II,JJ)+EK(I,J)
 30   CONTINUE
 35   CONTINUE
 40   CONTINUE
C     GENERATE THE STIFFNESS MATRIX FOR THE
C     COMPOSITE  BEAM.
      WRITE(6,414)
 414  FORMAT(/,35X,'(b) BEAM ELEMENTS',/)
      DO 101 I=1,10
      DO 101 J=1,10
      EK1(I,J)=0.
 101  T(I,J)=0.
      READ(5,*)NNP,M1,E,V
C     NNP=NUMBER OF BEAM JOINTS.
C     M1=NUMBER OF BEAM ELEMENTS.
```

```
      WRITE(6,515)
      DO 121 I=1,NNP
      READ(5,*)L,ID(L,1),ID(L,2),ID(L,3),ID(L,4),
     *ID(L,5),X(L),Y(L)
  121 WRITE(6,31)L,ID(L,1),ID(L,2),ID(L,3),ID(L,4),
     *ID(L,5),X(L),Y(L)
   31 FORMAT(11X,6I5,2F12.6)
      WRITE(6,919)
  919 FORMAT(/,13X,'ELEMENT',1X,'ELEMENT NODES',
     *5X,'LENGTH',/)
      DO 401 L=1,M1
      READ(5,*)MN,IB,JB,AS,SI,SJ
C     MN=ELEMENT NO.
C     IB AND JB ARE MEAM JOINTS.
C     AS=CROSS-SECTIONAL AREA OF BEAM ELEMENT.
C     SI IS M.O.I. OF THE COMPOSITE BEAM
C     SJ IS THE TORSIONAL CONSTANT OF THE
C     COMPOSITEL BEAM
      XL=((X(JB)-X(IB))**2+(Y(JB)-Y(IB))**2)**0.5
      CX=(X(JB)-X(IB))/XL
      CY=(Y(JB)-Y(IB))/XL
C     XL=ELEMENT LENGTH.
C     CX=COSINE ALPHA.
C     CY=SINE ALPHA.
C     ALPHA IS THE ANGLE BETWEEN THE ELEMENT AND THE
C     X-AXIS.
      WRITE(6,221)MN,IB,JB,XL,CX,CY
  221 FORMAT(14X,I3,5X,I3,3X,I3,6X,3F9.2)
      KK1(1)=ID(IB,1)
      KK1(2)=ID(IB,2)
      KK1(3)=ID(IB,3)
      KK1(4)=ID(IB,4)
      KK1(5)=ID(IB,5)
      KK1(6)=ID(JB,1)
      KK1(7)=ID(JB,2)
      KK1(8)=ID(JB,3)
      KK1(9)=ID(JB,4)
      KK1(10)=ID(JB,5)
      C=E*SI/XL
      C1=6.*C/XL
      C2=12.*C/XL**2
      G=E/(2.*(1.+V))
C     G=SHEAR MODULUS.
      EK1(1,1)=E*AS/XL
      EK1(1,6)=-E*AS/XL
      EK1(2,2)=C2
      EK1(2,7)=-C2
      EK1(3,3)=G*SJ/XL
      EK1(3,8)=-G*SJ/XL
      EK1(4,4)=4.*C
      EK1(4,5)=C1
      EK1(4,9)=2.*C
      EK1(4,10)=-C1
      EK1(5,5)=C2
      EK1(5,9)=C1
```

```
      EK1(5,10)=-C2
      EK1(6,6)=E*AS/XL
      EK1(7,7)=C2
      EK1(8,8)=G*SJ/XL
      EK1(9,9)=4.*C
      EK1(9,10)=-C1
      EK1(10,10)=C2
      DO 201 I=1,10
      DO 201 J=1,10
201   EK1(J,I)=EK1(I,J)
      T(1,1)=CX
      T(1,2)=-CY
      T(2,1)=CY
      T(2,2)=CX
      T(3,3)=CX
      T(3,4)=-CY
      T(4,3)=CY
      T(4,4)=CX
      T(5,5)=1.
      T(6,6)=CX
      T(6,7)=-CY
      T(7,6)=CY
      T(7,7)=CX
      T(8,8)=CX
      T(8,9)=-CY
      T(9,8)=CY
      T(9,9)=CX
      T(10,10)=1.
      DO 70 II=1,10
      DO 70 JJ=1,10
      TEK(II,JJ)=0.
      DO 70 KV=1,10
70    TEK(II,JJ)=TEK(II,JJ)+T(II,KV)*EK1(KV,JJ)
      DO 71 II=1,10
      DO 71 JJ=1,10
      GK(II,JJ)=0.
      DO 71 KV=1,10
71    GK(II,JJ)=GK(II,JJ)+TEK(II,KV)*T(JJ,KV)
      WRITE(7)KK1,GK,IB,JB
      DO 351 I=1,10
      II=KK1(I)
      IF(II.LT.0)GO TO 351
      DO 301 J=1,10
      JJ=KK1(J)
      IF(JJ.LT.0)GO TO 301
      B(II,JJ)=B(II,JJ)+GK(I,J)
301   CONTINUE
351   CONTINUE
 401  CONTINUE
C     GENERATE THE STIFFNESS MATRIX FOR THE TRUSS
      DO 1011 I=1,10
      DO 1011 J=1,10
 1011 EK3(I,J)=0.
      READ(5,*)NNP,M3,E
C     NNP=NUMBER OF TRUSS JOINTS.
```

```
C       M3=NUMBER OF TRUSS MEMBERS.
        WRITE(6,616)
 616    FORMAT(/,40X,'(c) TRUSS ELEMENTS',/)
        WRITE(6,717)
 717    FORMAT(/,13X,'NODE',4X,'GLOBAL FREEDOMS',
       *11X,'X',10X,'Y',13X,'Z',/)
        DO 1211 I=1,NNP
        READ(5,*)L,ID(L,1),ID(L,2),ID(L,3),ID(L,4),
       *ID(L,5),X(L),Y(L),Z(L)
 1211   WRITE(6,311)L,ID(L,1),ID(L,2),ID(L,3),ID(L,4),
       *ID(L,5),X(L),Y(L),Z(L)
 311    FORMAT(11X,6I5,3F12.6)
        WRITE(6,919)
        DO 4011 L=1,M3
        READ(5,*)MN,IT,JT,AT
C       MN=ELEMENT NO.
C       IT AND JT ARE TRUSS JOINTS.
C       AT=CROSS SECTIONAL AREA OF TRUSS ELEMENT.
        XL=((X(JT)-X(IT))**2+(Y(JT)-Y(IT))**2+(Z(JT)-
       *Z(IT))**2)**.5
        CX=(X(JT)-X(IT))/XL
        CY=(Y(JT)-Y(IT))/XL
        CZ=(Z(JT)-Z(IT))/XL
C       DIRECTIONAL COSINES.
        WRITE(6,2211)MN,IT,JT,XL,AT,CX,CY,CZ
 2211   FORMAT(14X,I3,5X,I3,3X,I3,6X,5F9.2)
        KK3(1)=ID(IT,1)
        KK3(2)=ID(IT,2)
        KK3(3)=ID(IT,3)
        KK3(4)=ID(IT,4)
        KK3(5)=ID(IT,5)
        KK3(6)=ID(JT,1)
        KK3(7)=ID(JT,2)
        KK3(8)=ID(JT,3)
        KK3(9)=ID(JT,4)
        KK3(10)=ID(JT,5)
        C11=AT*E/XL
        C12=C11*CX*CY
        C13=C11*CX*CZ
        C15=C11*CY*CZ
        EK3(1,1)=C11*CX**2
        EK3(1,2)=C12
        EK3(1,5)=C13
        EK3(1,6)=-C11*CX**2
        EK3(1,7)=-C12
        EK3(1,10)=-C13
        EK3(2,2)=C11*CY**2
        EK3(2,5)=C15
        EK3(2,6)=-C12
        EK3(2,7)=-C11*CY**2
        EK3(2,10)=-C15
        EK3(5,5)=C11*CZ**2
        EK3(5,6)=-C13
        EK3(5,7)=-C15
        EK3(5,10)=-C11*CZ**2
```

```
      EK3(6,6)=C11*CX**2
      EK3(6,7)=C12
      EK3(6,10)=C13
      EK3(7,7)=C11*CY**2
      EK3(7,10)=C15
      EK3(10,10)=C11*CZ**2
      DO 2011 I=1,10
      DO 2011 J=1,10
2011  EK3(J,I)=EK3(I,J)
      WRITE(7)KK3,EK3,IT,JT,CX,CY,CZ
      DO 3511 I=1,10
      II=KK3(I)
      IF(II.LT.0)GO TO 3511
      DO 3011 J=1,10
      JJ=KK3(J)
      IF(JJ.LT.0)GO TO 3011
      B(II,JJ)=B(II,JJ)+EK3(I,J)
 3011 CONTINUE
 3511 CONTINUE
 4011 CONTINUE
      WRITE(6,9191)
 9191 FORMAT(/,12X,'NODE',5X,'FORCE DIRECTION',8X,
     *'FORCE (kN)',/)
 45   READ(5,*)NN,IDIR,F1
      WRITE(6,3000)NN,IDIR,F1
C     F1=THE APPLIED EXTERNAL FORCE
 3000 FORMAT(/,10X,I4,12X,I4,14X,E12.6)
      IF(NN.GT.NJ)GO TO 50
      N1=ID(NN,IDIR)
      D(N1)=D(N1)+F1
      GO TO 45
 50   CONTINUE
      CALL DECOMP(B,459,459)
      CALL BACSUB(B,D,459,459)
      WRITE(6,505)
505   FORMAT(///,25X,'STRUCTURE RESULTS')
      WRITE(6,828)
828   FORMAT(25X,'-----------------',//)
      WRITE(6,323)
323   FORMAT(/,24X,'(a) PLATE ELEMENTS',/)
      REWIND 7
      DO 24 L=1,M
      WRITE(6,59)L
59    FORMAT(/,26X,'PLATE ELEMENT',I3)
      DO 28 I=1,20
      P(I)=0.
28    D1(I)=0.
      READ(7)KK,EK,IP,JP,KP,NP
      DO 26 I=1,20
      II=KK(I)
      IF(II.LT.0)GO TO 29
      D1(I)=D(II)
      GO TO 26
29    D1(I)=0.
26    CONTINUE
```

```
      DO 69 I=1,20
      DO 69 J=1,20
69    P(I)=P(I)+EK(I,J)*D1(J)
      WRITE(6,1016)
1016 FORMAT(/,11X,'NODE',3X,'FREEDOM NO.',3X,
     *'DEFORMATIONS',7X,'END ACTIONS',/)
      DO 79 MP=1,20,5
      LL=0
      IF (MP.EQ.1) GO TO 789
      IF (MP.EQ.6) GO TO 791
      IF (MP.EQ.11)GO TO 792
      IF (MP.EQ.16)GO TO 793
      GO TO 79
789   WRITE(6,1014)IP,KK(MP),D1(MP),P(MP)
      WRITE(6,1015)(KK(LL),D1(LL),P(LL),LL=2,5)
      GO TO 79
791   WRITE(6,1014)JP,KK(MP),D1(MP),P(MP)
      WRITE(6,1015)(KK(LL),D1(LL),P(LL),LL=7,10)
      GO TO 79
792   WRITE(6,1014)KP,KK(MP),D1(MP),P(MP)
      WRITE(6,1015)(KK(LL),D1(LL),P(LL),LL=12,15)
      GO TO 79
793   WRITE(6,1014)NP,KK(MP),D1(MP),P(MP)
      WRITE(6,1015)(KK(LL),D1(LL),P(LL),LL=17,20)
79    CONTINUE
1014 FORMAT(11X,I3,7X,I3,4X,E16.6,3X,E16.6)
1015 FORMAT(21X,I3,4X,E16.6,3X,E16.6)
24    CONTINUE
      WRITE(6,424)
424   FORMAT(//,25X,'(b) BEAM ELEMENTS',/)
      DO 240 L1=1,M1
      WRITE(6,590)L1
590   FORMAT(/,26X,'BEAM ELEMENT',I4)
      DO 280 I1=1,10
      P1(I1)=0.
280   D2(I1)=0.
      READ(7)KK1,GK,IB,JB
      DO 260 I1=1,10
      II=KK1(I1)
      IF(II.LT.0)GO TO 290
      D2(I1)=D(II)
      GO TO 260
290   D2(I1)=0.
260   CONTINUE
      DO 690 I=1,10
      DO 690 J=1,10
690   P1(I)=P1(I)+GK(I,J)*D2(J)
      WRITE(6,1016)
      DO 790 MB=1,10,5
      LL=0
      IF(MB.EQ.1)GO TO 777
      IF(MB.EQ.6)GO TO 776
777   WRITE(6,1014)IB,KK1(MB),D2(MB),P1(MB)
      WRITE(6,1015)(KK1(LL),D2(LL),P1(LL),LL=2,5)
      GO TO 790
```

```
776   WRITE(6,1014)JB,KK1(MB),D2(MB),P1(MB)
      WRITE(6,1015)(KK1(LL),D2(LL),P1(LL),LL=7,10)
790   CONTINUE
240   CONTINUE
      WRITE(6,626)
626   FORMAT(//,25X,'(c) TRUSS ELEMENTS',/)
      DO 2400 L2=1,M3
      WRITE(6,5900)L2
5900  FORMAT(/,26X,'TRUSS ELEMENT',I4)
      DO 2800 I1=1,10
      P2(I1)=0.
2800  D3(I1)=0.
      READ(7)KK3,EK3,IT,JT,CX,CY,CZ
      DO 2600 I1=1,10
      II=KK3(I1)
      IF(II.LT.0)GO TO 2900
      D3(I1)=D(II)
      GO TO 2600
 2900 D3(I1)=0.
 2600 CONTINUE
      DO 6900 I=1,10
      DO 6900 J=1,10
 6900 P2(I)=P2(I)+EK3(I,J)*D3(J)
      P3=P2(1)*CX+P2(2)*CY+P2(5)*CZ
      P4=P2(6)*CX+P2(7)*CY+P2(10)*CZ
C     P3 AND P4 ARE THE AXIAL END FORCES OF THE SPACE
C     TRUSS MEMBERS.
      WRITE(8)L2,P3,P4
      WRITE(6,1016)
      DO 7900 MT=1,10,5
      LL=0
      IF(MT.EQ.1)GO TO 775
      IF(MT.EQ.6)GO TO 774
 775  WRITE(6,1014)IT,KK3(MT),D3(MT),P2(MT)
      WRITE(6,1015)(KK3(LL),D3(LL),P2(LL),LL=2,5)
      GO TO 7900
 774  WRITE(6,1014)JT,KK3(MT),D3(MT),P2(MT)
      WRITE(6,1015)(KK3(LL),D3(LL),P2(LL),LL=7,10)
7900  CONTINUE
2400  CONTINUE
      WRITE(6,7989)
7989  FORMAT(/,16X,'MEMBER',12X,'J-END FORCE',7X,
     *'K-END FORCE',/)
      REWIND (8)
      DO 7990 IA=1,M3
      READ(8) L2,P3,P4
7990  WRITE(6,7991)L2,P3,P4
7991  FORMAT(16X,I3,15X,E11.5,8X,E11.5)
      CLOSE(5)
      CLOSE(6)
      CLOSE(7)
      STOP
      END

      SUBROUTINE DECOMP(S,N,ND)
```

```
      DIMENSION S(ND,ND)
      DO 160 I=1,N
      S1=0.
      KK1=I-1
      IF (KK1.LT.1)GO TO 51
      DO 50 K=1,KK1
      S1=S1+S(K,I)**2*S(K,K)
50    CONTINUE
51    S(I,I)=S(I,I)-S1
      JJ=I+1
      IF(JJ.GT.N)GO TO 160
      DO 150 J=JJ,N
      S2=0.
      K1=I-1
      IF(K1.LT.1)GO TO 141
      DO 140 K=1,K1
      S2=S2+S(K,I)*S(K,K)*S(K,J)
140   CONTINUE
141   S(I,J)=(S(I,J)-S2)/S(I,I)
150   CONTINUE
160   CONTINUE
      RETURN
      END


      SUBROUTINE BACSUB(S,F,N,ND)
      DIMENSION S(ND,ND),F(ND)
C     FORWARD PASS
      DO 60 I=1,N
      S1=0.
      KK1=I-1
      IF(KK1.LT.1)GO TO 51
      DO 50 K=1,KK1
      S1=S1+S(K,I)*F(K)
50    CONTINUE
51    F(I)=F(I)-S1
60    CONTINUE
C     BACKWARD PASS
      DO 110 I1=1,N
      I=N+1-I1
      S1=0.
      J1=I+1
      IF(J1.GT.N)GO TO 101
      DO 100 JJ=J1,N
      S1=S1+S(I,I)*S(I,JJ)*F(JJ)
100   CONTINUE
101   CONTINUE
      F(I)=(F(I)-S1)/S(I,I)
110   CONTINUE
      RETURN
      END
```

REFERENCES

(1) H. R. Evans and H. D. Wright 'Steel-Concrete Composite Flooring Deck Structures', 'Steel Concrete Composite Structures Stability and Strength', Ed.R. Narayanan, Elsevier Applied Science, London and New York,1988.

(2) A. A. G. El Dharat 'The structural Behaviour of Composite Reinforced Concrete Trough Floors',Ph.D. Thesis, University of Salford, Salford, 1985.

(3) David O'Leary and David Thomas 'Composite Beams with Profiled-Steel Sheeting and Non-welded Shear Connectors', Steel Construction Today, 1988, Vol.2, No.4, pp117-121.

(4) G. M. Sabnis 'Hand Book of Composite Construction Engineering', Van Nostrand Reinhold Company, New York,1979.

(5) CONSTRADO 'Steel Designers Manual', Fourth Edition (Revised), Collins Professional and Technical Books, 1987.

(6) Z. S. Makowski 'Review of The Development of Various Types of Double-layer Grids', 'Analysis, Design And Construction Of Double-Layer Grids', Ed. Z. S. Makowski, Applied Science Publishers, London, 1981.

(7) V. P. Whitworth, 'Space Deck System', 'Analysis, Design And Construction Of Double-Layer Grids', Ed. Z. S. Makowski, London, 1981.

(8) Space Decks Ltd.,'Manufacturers Brochure', Space Decks Ltd., Chard, Somerset, England TA20 2AA,1986.

(9) Space Decks Limited, 'E1515 Series', Space Decks Ltd., Chad, Somerset, England TA20 2AA, 1982.

(10) Space Decks Limited, 'E1212 Series', Space Decks Ltd., Chad, Somerset, England TA20 2AA, 1984.

(11) D. C. O'Leary and C. T. Duffy, 'Feasibility Study-Composite Space Deck', Report No. 83/193, Civil Engineering Department, University of Salford, December, 1984.

(12) H. W. Lee, 'The Elastic And Inelastic Buckling of Single Angle, Tee And Double Angle Struts', Master Thesis, The University Of Queensland, St. Lucia, Australia, 1984.

(13) J. Kennedy and M. Murty, 'Buckling of Steel Angle and T-Struts',ASCE Vol.98, No.ST11, November 1972.

(14) Dong Shilin and Yang Yangge, 'Simplified Calculation For Analysing Space Truss and Plate Composite Structures', Jian Zhu Jie Gou Xue Bao/Journal of Building Structures, Vol.6, No.4, 1985, pp 10-20.

(15) F. W. Beaufait, W. H. Rowan, P. G. Hoadly and R. M.

Hackett, 'Computer Methods Of Structural Analysis', Department of Civil Engineering, Vanderbilt University, Tennessee, 1982.

(16) K. C. Rocky, H. R. Evans, D. W. Griffths and D. A. Nethercot, 'The Finite Element Method', Collins Professional and Technical Books, Second Edition, 1985.

(17) R. Szilard, 'Theory and Analysis of Plates', Prentice-Hall International, New Jersey, 1974.

(18) J. T. Easley and D. E. McFarland, 'Buckling of Light-gauge Corrugated Metal Sheet Diaphragms', Journal of the structural Division, ASCE Proceedings, Vol.95, No. ST7, July 1969, pp 1497-1516.

(19) O. C. Zienkiewicz, 'The Finite Element Method', McGraw-Hill, London, 1977.

(20) A. Ghali and A. M. Neville, 'Structural Analysis', Second Edition, Chapman Hall, London, 1983.

(21) B. Nath, 'Fundamentals of Finite Elements for Engineers', The Athlone Press of The University of London, 1974.

(22) A course on Matrix Methods of Structures, Civil Engineering Department, Tennessee Tecknological University, 1984.

(23) O. C. Zienkiewicz and Y. K. Cheung, 'The Finite Element Method For Analysis of Elastic Isotropic and

Orthotropic Slabs', Proceedings of the Institute of Civil Engineers (London), Vol.28, 1964, pp 471-488.

(24) M. Kuleib, 'Composite Space Frame Analysis: Computer Program, Data and Results Listing', Report No. 89/228,Civil Engineering Department, University of Salford, August, 1989.

(25) S. Timoshinko and S. Woinowsk-Krieger' 'Theory of Plates and Shells', Second Edition, McGraw-Hill, New York, 1959.

(26) Y. K. Cheung and H. C. chan, 'A family of Rectangular Bending Elements', Computers & Structures, Vol.10, 1979, pp 613-619.

(27) S. L. Leė and Ballesteros, 'Uniformly Loaded Rectangular Plate Supported at Corners', International Journal of Mech. Sci., Vol.2, No.3, 1960, pp 206-211.

(28) R. V. Southwell, 'On The Analysis of Experimental Observations in Problems of Elastic Stability', Proc. Royal Soc., London, Series A, Vol.135, 1932, p601.

(29) British Standards Institution, 'Tensile Testing of Metals', BS18: Part 3: Steel Sheet and Strip (less than 3mm and not less than 0.5mm thick), London, 1971.

(30) British Standards Institution, 'Tensile Testing of Metals'.BS18: Part 2: Steel (general), London, 1971.

(31) British Standards Institution, 'Methods of Testing

Concrete', BS1881: Parts 1, 2, 3, 4 and 5, London, 1970.

(32) S. Kitipornchai and H. W. Lee 'Inelastic Experiments on Angle and Tee Struts', Research Report No. CE 54, Department of Civil Engineering, University of Queensland, Australia, 1984.

(33) R. B. Johnson and I. M. May, 'Partial-Interaction Design of Composite Beams', The Structural Engineer, Vol.53, No.8 August 1975.

(34) R. B. Johnson, 'Composite Structures of Steel and Concrete', VOL.1: Beams, Columns, Frames and Applications in Buildings, Constrado Monographs, Granada Publishing, 1982.

(35) J. J. Azar, 'Bending Theory of Multilayer Orthotropic Sandwich Plates', AIAA Journal, Vol.6, No.11, November 1968, pp 2166-2169.

(36) J. J. Azar and P. Johnson, 'Deflection of Orthotropic Sandwich Plates', AIAA journal, Vol.10, No.8, August 1972, pp 981-982.

(37) C. H. Norris, J. B. Wilbur and S. Utku, 'Elementary Structural Analysis', Mcgraw-Hill, Singpore, Third Edition, 1984.

(38) American Institute of Steel Construction, Inc., 'Steel Construction Manual', Eigth Edition, Chicago, Illinois, 1980.

(39) B. E. Gregory, 'The Use of Measured Strains to Obtain Critical Loads', Australian Journal of Applied Science, 1959.

(40) B. E. Gregory, 'The Buckling of Structures', Civil Engineer (London), Vol.55, No. 650, September 1960.

(41) J. Roorda, 'Some Thoughts on Southwell Plot', Proc. A.S.C.E., EM6, Vol.93, 1967.

(42) J. Grimshaw, 'Tests on Sheeting Connections', Report No. 77/99, Civil Engineering Department, University of Salford, October, 1977.

(43) Stuart Moy, Colin Jolly and Ashraf El-Shihy, 'Unwelded Shear Connectors for Composite Beams', Composite Steel Structures, Ed. R. Narayanan, Elsevier Applied Science Publishers LTD, 1987.

(44) Ashraf M. El-Shihy 'Unwelded Shear Connectors in Composite Steel and Concrete Structures', Ph.D. Thesis, University of Southampton, September, 1986.